eman ta zabal zazu

Universidad del País Vasco
Euskal Herriko Unibertsitatea

New Neuroimaging methods for clinical neuroscience and neurological disorders

Thesis
for obtaining the PhD degree in Biomedical Research program of Cell Biology and Histology Department, University of Basque Country

September 2015

Ibai Diez Palacio

PhD Supervisor
Jesus M. Cortes Diaz

Laburpena

2006garren urtean, Munduko Osasun Erakundeak egindako estimazioaren arabera, gaitz neurologikoek eta haien ondorioek milaka milioi gizakiengan eragiten dute. Munduan, 6.8 milioi pertsona inguru hil egiten dira urtero gaitz neurologikoak direla eta, 50 milioi pertsona baino gehiagok epilepsia daukate, 35.6 milioi pertsonek dementzia jasaten dute (7.7 milioi kasu berri agertzen direlarik urtero eta Alzheimer gaitza ohikoena izanik) eta populazioaren ehuneko hamarrak baino gehiagok buruko mina jasaten dute; hauek denak, gaixotasun neurologikoen ondorioak dira. Europan bakarrik, gaitz neurologikoen inguruko gastu ekonomikoa 139 mila milioi eurokoa izan zen 2004ean eta hirugarren milurteko hasieran eskuratutako datuek ez dute adierazten egoera hobetuko denik. Populazioa zaharkitzearekin batera, garun arazoen pertsonen ehunekoak gora egiten jarraitzen du, eta ondorioz, tratamendu berri eta eraginkorrak lortzeko asmoarekin, burmuinaren ezagupen sakonagoak sustatzen duten ikerketak bultzatu behar dira.

Gaur egun, ikerketa ugarik gaixotasun zehatz batzuek garunean eragiten dituzten aldaketei azalpena ematen hasi dira burmuin egituran, funtzionamenduan edo bien arteko korrelazioan oinarrituta. Nahiz eta zientziaren aurrerapenak azkar doazen, garunaren funtzionamenduaren inguruan ezjakintasun handia dago oraindik.

Tesi honetan, gaitz neurologiko desberdinek garunaren estruktura eta funtzionamenduan duten eragina aztertzeko metodo berriak garatu dira. Metodo hauek, garuneko lesio traumatiko hedatsuak, Alzheimer eta kontzientzia gaitzak ikertzeko erabili dira. Hain zuzen ere, erresonantzia magnetiko bidezko irudigintza (MRI- *Magnetic*

Resonace Imaginig) delakoarekin lortutako datuekin lan egin da. Honek, burmuinaren ezaugarri funtzionalak eta estrukturalak argitzeko trebetasuna duela erakutsi du. Irudi hauen bidez garun kaltetuetan aurkitutako aldaketak biomarkatzaile bezala proposatu dira gaitz neurologiko desberdinetan diagnostiko espezifikoagoa eta azkarragoa sustatzeko, pronostiko zehatzagoa emateko eta terapia neurobabesle berriak garatzeko. Tesi honetan egindako ikerketetan hiru irudi mota desberdin erabili dira: irudi estrukturalak, difusio irudiak eta irudi funtzionalak. Irudi funtzionalak eskuratzeko, gaixoen seinaleak neurtu egiten dira jarduerarik egiten ez dagoenen edota estimulurik jasotzen ez duenean.

Konektibitatea aztertzeko garuna sare bat bezala erabiltzen da normalean. Sareek sistema biologiko konplexuak (garuna barne) aztertzeko potentzial izugarria dute eta hauek erabiliz, garunaren oinarrizko arkitektura eta funtzio nagusiak azaltzen hasi dira. Sareak deskribatzen eta kuantifikatzen dituen hizkuntza matematikoari Grafo teoria deritzogu. Tesi honetan sare estrukturalak (garun erregio desberdinak lotzen dituzten zuntz kopuruak deskribatzen duen grafoa) eta funtzionalak (populazio neuronal desberdin artean azaltzen diren aktibazioak eta mendekotasunak deskribatzen dituena) erabili dira.

Lehenik eta behin, kontzientzia gaitzak grafo funtzionalak nola aldatzen dituzten ikertu egin da. Azken urteotan frogaturik geratu da fMRI-ren bidez eskuratutako irudiak erabiliz lortzen diren garun sareak kontzientzia gaitzen (DOC) ondorioz aldatu egiten direla [113, 76]. DOC-a, burmuinaren lesio larri baten ondorioz gerta daiteke eta gaitz hau duten gaixoek, bi ezaugarri desberdin izan ditzakete: alde batetik loaren zikloa eten egin daiteke eta beste aldetik, norberaren eta bere ingurunearen ezaguera galdu dezakete.

Hamazazpi heldu osasuntsu (Kontrol Taldea) eta 9 DOC gaixok (DOC taldea) parte hartu zuten ikerketa honetan. Gaixo bakoitzaren koma eskala *Revised Coma Recovery Scale* (CRS-R, [64]) erabiliz neurtu zen. Gaixoak bi aldiz eskaneatu ziren: lehenengoa, burmuinaren lesioa gertatzetik 2-6 hilabete igaro ondoren eta bigarrena 3-6 hilabetera. 4 DOC gaixok (Berreskurapen Taldea) kontzientzia be-

rreskuratu zuten bigarren eskanerra egin baino lehen.

Lan honetan, fMRI seinaletatik lortutako konektibitate funtzionala (korrelazio partziala erabiliz) eta efektiboa (entropia transferentzia erabiliz) kontzientzia gaitzen ondorioz aldatzen den aztertu da.

90 interes erregio (ROI) definitu ziren *Automatic Anatomical Labeling atlas*-ean (AAL) oinarrituz [161]. AAL atlasa zati kortikalak eta subkortikalak hartzen ditu bere barne, eta horregatik DOC gaixoak ikertzeko aukeratua izan zen. Grafo konexioak aztertu ondoren 2 biomarkatzaile aurkitu ziren: hemisferio desberdinen arteko erregio homologoen PC (Partial Correlation) balioak eta ezkerreko hemisferio barruko TE (Transferentzia Entropia) balioak.

Hemisferio desberdinen arteko erregio homologoen arteko PC balioak kontrol taldean handiagoak direla ikusi da (DOC eta berreskuratutako gaixoen kasuan ematen direnak baino handiagoak). Erregio homologoen arteko PC balio handiek bi hemisferioen arteko informazio-fluxua isolatzen dute. Garun osoko TE batezbesteko balioa kalkulatzen bada ez da DOC eta kontrolen artean desberdintasunik ikusten,baina hemisferio bakoitzeko barruko konexioak begiratzen badira desberdintasun nabarmenak antzeman daitezke. Berreskuratutako taldean, ezker hemisferioko TE konexioak kontrolak baino handiagoak ziren.

Emaitza hauetan oinarrituta DOC gaixoak ebaluatzeko biomarkatzaile hoberenak hemisferio desberdinen arteko erregio homologoen arteko PC-ak (8.5 Irudia) eta ezkerreko hemisferio barruko TE konexioak (8.7 Irudia) direla esan daiteke. Biomarkatzaile hauek jokabidearen eskalarekin eta eskala nerologikoekin (CRS-S eskala) korrelazioak dituzten edo ez kalkulatu da. Emaitzak 8.8 irudian ikusi daitezke. Hemisferio desberdinen arteko konexio homologoetako TE balioak, korrelazio handia du komunikazio eskalarekin. Ezkerreko hemisferio barruko TE konexioak 0.73-ko korrelazioa du hitzezko eskalarekin, komunikazio eskalarekin eta guztien batuketarekin (8.8 irudian JFK).

Konexio inter-hemisferiko homologoen artean, konektibitate patroi desberdinak ikus daitezke; hurbilago dauden konexioek korrelazio balio handiagoak dituzte urrunago daudenak baino. 20mm baino hur-

bilago dauden garun zatietan ez dira kontrol eta DOC taldeen arteko konexio inter-hemisferiko homologoetan desberdintasunik ikusi. Distantzia hau handitzerakoan desberdintasunak handiagoak egiten dira. Koma batetik berreskuratu diren subjektuetan urrun dauden konexioek DOC gaixoek dituztenak baino balio altuagoak dituzte (e8.6 Irudia).

Ondoren egin zen ikerketa lanean, datu estrukturalak eta funtzionalak erabiliz atlas berri bat sortu zen. Literaturan aurkitutako lan desberdinek garunaren estruktura eta funtzio konektibitateek (SC eta FC) antolamendu hierarkikoa dutela frogatu dute. Honela, garuna, modulu (edo area) desberdinetan banatzen da eta *hub* konektoreen bidez modulu hauek komunikatu egiten dira elkarren artean [150, 152, 73].

12 pertsona osasuntsuk osatutako talde batetik datu funtzionalak eta estrukturalak lortu ziren eta 2514 erregioko sare funtzionalak eta estrukturalak kalkulatu ziren. Lan honetan 12 subjektuen batezbesteko sareekin lan egin da, subjektu bakoitzaren aldakortasuna murrizteko.

Sare hauetan moduluak (antzekoak diren erpin taldeak) aurkitzeko, *Hierarchical Agglomerative Clustering* (HAC) multzokatze teknikak erabili zen [133, 107, 50]. Prozesu honen ondorioz zuhaitz hierarkikoa edo dendrograma bat sortzen da non pausu bakoitzean bi erregio batzen diren modulu berri bat osatuz. FC eta SC sareek modularitate handia dute (jadanik frogatu egin den bezala) eta hauen artean antzekotasun izugarri handia dagoela ikusi dugu (orain arte ikusi ez dena).

Garun zatiketa baten moduluak konexio funtzionalak eta estrukturalak ondo deskribatzen dituela ziurtatzeko (9.5 irudia) *cross-modularity* X indizea garatu dugu. Garun zatiketa batek *cross-modularity* balio handia izango du baldin eta SC eta FC moduluek antzekotasun handia badute eta sareen moduluak osatzen dituzten konexio ugari badaude eta moduluen artean konexio gutxi badituzte. 20 modulu funtzionaletan zatitutako garunak cross-modularity balio handiena lortu duela aurkitu dugu (9.5era 9.8 irudiak). Zatiketa hau SFM deitu da.

Lortutako garun zatiketak beste garun atlas desberdinekin antzekotasun handiak ditu. Normalean literaturan aurkitutako atlas desberdinak garunaren anatomian edo funtzioan oinarrituta daude. Lan honetan sortutako atlas berria garunaren anatomian eta funtzioan batera oinarrituta dago.

Hurrengo lanean, erregio desberdinen artean informazio fluxua kalkulatzeko metodo berri bat garatu da. Garun erregio desberdinetatik aktibitate funtzionala ateratzeko normalean erregio honetan dauden *voxel* guztien denbora seinaleen batezbestekoa kalkulatzen da. Seinale guzti hauen batezbestekoa kalkulatzean erregio honek egiten dituen aktibitate batzuen informazioa galdu dezakegu. Hori dela eta, Osagai Nagusien Analisia (PCA) erabili da garun erregio bakoitzetik osagai garrantzitsu gehiago ateratzeko. Seinale guzti hauen batezbestekoa erabiltzeak erregio hauetan gertatzen den aktibitatearen %12 bariantza besterik ez du azaltzen(erregio honetan gertatzen ari den beste %88 galdu egiten da). Kasu honetan, PCA erabiltzerakoan lehen 10 osagaiek datuen %60 bariantza azaltzen dute eta lehen 72 osagaiek %99.

Osagai hauek erabili dira informazio-fluxua kalkulatzeko metodo berrian. Metodo hau informazio fluxua kalkulatzeko Transferentzia Entropian (TE) oinarrituta dago.

Metodo honen balioa frogatzeko Alzheimer gaixoen RSN erregioen (garunean atseden egoeran sortutako dinamikak deskonposatzerakoan lortzen diren aktibazio patroiak) arteko komunikazio ikertu egin da. Normalean erabiltzen diren 8 RSN osagaiak kontuan izan dira [10] (ez dira RSN osagaiak bakarrik erabili, osagai hauek osatzen dituzten garun erregioak erabiliz, *voxel* guztien seinaleak baizik).

Analisia ADNI ekimena dituzten datuetatik, n = 10 subjektu osasuntsu (5 gizon eta 5 emakume, 73.70 $\pm$ 1.16 urtekoak) eta n = 10 Alzheimer gaixo (5 gizon eta 5 emakume, 73.40 $\pm$1.08 urtekoak) erabili ziren.

Metodo hau erabiltzeko lehenengo seinale hemodinamikoak aktibitate neuronalera bihurtu ziren, *HRD blind deconvolution* metodoa erabiliz. Gero, garatutako metodo berriaren bitartez osagai kopuru desberdinak erabiliz informazio fluxua kalkulatu zen.

RSN-en arteko komunikazioa Alzheimer gaixoetan handiago zela ikusi zen. Baina Alzheimer gaixoen eta kontrolen arteko desberdintasunak nabariagoak ziren bigarren eta hirugarren osagaiak erabiltzen zirenean. Normalean batezbesteko seinalea lehen osagaiak adierazten du. Beraz, teknika honek teknika arruntak erabiliz ikusten ez diren desberdintasunak ateratzen ditu. Beste lan batzuetan osagai kopuru hauek erregio honek azaltzen duen bariantzaren arabera sailkatzen dira. Kasu honetan, osagai kopuru desberdinekin frogatzen da eta osagai kopuru egokiena zein den bilatzen da (gaixoen eta kontrolen artean desberdintasun handiagoa duen osagai kopurua).

Azkenik, egindako ikerketan axoietan kalteak dituzten gaixoen burmuin berrantolaketa azaltzeko (berrantolaketa funtzionala eta estrukturala) SFM moduluak erabili dira. Kasu honetan ere, garun erregio bakoitzetik osagai ugari erabili dira erregio bakoitzean aktibazio ezberdinak ondo azalduta izateko.

Trauma batean buruaren mugimendu azkarrak direla medio axoiak kaltetu daitezke. Axoietan aurkitutako kalteek garuneko sare estrukturalak osatzen dituzten konexio ugari moztu ditzakete. Plastikotasuna dela eta, burmuinak kalteak eragin duten arazoak konpontzeko, konexioak berrantolatuko ditu. Kasu honetan, trauma ondorengo urteetan garunak eduki duen berrantolaketa estrukturala eta berrantolaketa estruktural honek burmuineko sare funtzionalak nola aldatzen dituen ikertu da.

Lan honetan 41 subjektu ikertu ziren. Hauetako 14 subjektuk axoietan kaltea zuten (TAI) (13.14 $\pm$ 3.25 urtetakoak, 6 mutil eta 9 neska) eta beste 27 subjektuak kontrol moduan erabili ziren (15.04 $\pm$ 2.26 urtekoak, 12 gizon eta 15 neska). Trauma 10 $\pm$ 2.26 urte zituztela gertatu zen eta gutxi gora behera trauma ondoren 3.5 urte pasatzerakoan erresonantzia analisia egin zitzaien.

Sare estrukturalak erabiliz erregioen barneko konexioak eta erregioen arteko konexioak aztertu ziren. Konkretuki, erregioen maila kalkulatu zen (mailak, erregio bakoitzak zenbat konexio dituen neurtzen du). TAI gaixoek kontrolek baino konexio gutxiago dituzte; garuneko motor erregioan, garun enborrean, garuntxoan, zinguluan, polo tenporalean eta erregio subkortikaletan konkretuki. Erregio haue-

tako kalteak normalean arazo motorrekin, oreka kontrol arazoekin eta memoria arazoekin identifikatu dira. TAI gaixoek burmuinaren aurreko partean kontrolek baino konexio gehiago zituzten.

Garuneko 20 moduluetako aktibitatea ateratzerakoan, TAI gaixoek burmuineko aurreko partean aktibitate gehiago zutela ikusi zen. Garuneko aurreko erregioek zergatik konektibitate estruktural eta aktibitate funtzional handiago zuten aztertzeko metodo berri bat garatu zen. Metodo honek SFM-k osatutako 20 modulu bakoitzetik erregio garrantzitsuenekin elkar lan egiten zuten 5 burmuinak kalkulatu zen. Kontrolen eta TAI gaixoen arteko sare funtzionala konparatzerakoan, TAI gaixoek garuneko erregio subkortikalak erabiltzen dituztenean aurreko partean konektibitatea handitzen dutela ikusi zen. Horrela, garuneko aurreko parteak erregio subkortikalek dituzten atrofiaren ondorioz gehiago aktibatzen dira hau konpentsatzeko etaberdina gertatzen zen garuneko arreta erregioak aktibatzen zirenean.

Acknowledgments

I would like to thank all the people without whose help and support this thesis would not have been possible. First of all, I want to thank to Biocruces, who has supported me financially during this time. I am deeply grateful to Jesus M. Cortes who gave me the opportunity to work in BioCruces Institute and who introduce me to the neuroscience field. During these years I have learned a lot of things and work in amazing projects. I also want to thank all people that help and support me in BioCruces Research Institute, specially to Asier Erramuze, Iñigo Gabilondo, Paolo Bonifazzi, Iñaki Escudero and Beatriz Mateos.

It was also a enormous privilege to work with Sebastiano Stramaglia and I appreciate a lot his help, valuable guidance and support.

I also greatly appreciate all the help, support and advices of Daniele Marinazzo. I want to thank the opportunity to work in Daniele's lab in the University of Ghent, it has been a great experience where I have enjoyed and learned a lot. I also want to express my sincere gratitude to Stephan P. Swinnen from KU Leuven for our collaboration and to thank Basque Health Department for the funding for this internship.

I especially thank all the services of Cruces University Hospital who have collaborated in this work and to Dante R. Chialvo for his suggestions and guidance.

I would also like to thank Carlos for your patience, love and understanding. Today we have reached a new goal, my achievements are your achievements.

Finally, I want to thank to my family for their unconditional love

and all the work and sacrifices they did in all these years. Without you, I would not be the person I am today.

Contents

Chapter 1

Introduction

The brain, smaller than most desktop computers, is the most complex and elegant existing device than most of the advanced High Performance Computing Laboratories have not been able to reproduce it so far [71][96][105]. The brain receives and interprets a vast amount of sensory information, controls simple and complex motor behaviours and makes us to take complex decisions, think creatively and feel emotions [164].

Neurological disorders, malfunctioning of the brain operations, and their sequelae affect as many as one thousand millions human beings worldwide (2006 year estimation by The World Health Organization). The specific causes of neurological problems vary, but they can include genetic disorders, congenital abnormalities or disorders, infections, lifestyle or environmental health problems (including malnutrition), brain/spinal/nerve injury, cerebrovascular disorders evolving to brain injury, etc. An estimated 6.8 million people die every year as a result of neurological disorders, more than 50 million people have epilepsy, 35.6 million people suffer dementia with 7.7 million new cases every year (Alzheimer's disease is the most common cause, 60 - 70% of cases), more than 10% of people have migraine etc. Only in Europe, the economic cost of neurological diseases was estimated to be about 139 thousand millions euros in 2004. Even more pessimistic, the beginning of the third millennium will be worse, due to prolonged ageing, as neurodevelopmental disorders are growing more and more.

A much deeper knowledge of the brain is necessary to design new and effective treatments.

Many studies have begun to provide an understanding on the alterations in brain function that occur in various diseases based on the brain structure, their function or in the intercorrelation between structure and function. Despite rapid scientific progress, much about how the brain networks are altered across different diseases is not yet known.

In this thesis, I developed different methods for a deeper understanding of how brain function and structure is altered with different neurological disorders. These methods have been applied to health subjects, traumatic brain injury patients, Alzheimer patients and patients with a deficit of consciousness. Because neuroscience is highly interdisciplinary where neurologists, engineers, biologists and physicists work together, I will try to keep this thesis simple for everyone, avoiding a lot of mathematical and methodological details. But for more detailed information you can refer to Appendix A. This information can also be found in the articles resulting from this work and listed in the List of publications at the end of the thesis (page 231).

1.1 Basic Brain Anatomy – for non neurologists –

The brain is an efficient computing device resulting from the structural and functional properties of interconnected neurons. At the cellular level neurons are the basic working unit of the brain: specialized cells designed to process and transmit information through electrical and chemical signals.

Figure 1.1 shows a typical mammalian neuron consisting of:

- **Cell body**: This is the factory of the neuron, containing the cell nucleus and cytoplasm.
- **Axons**: The axon extends from the cell body to transmit messages to other neurons. The neurons transmit electrical impulses along their axons, which can range in length from a tiny

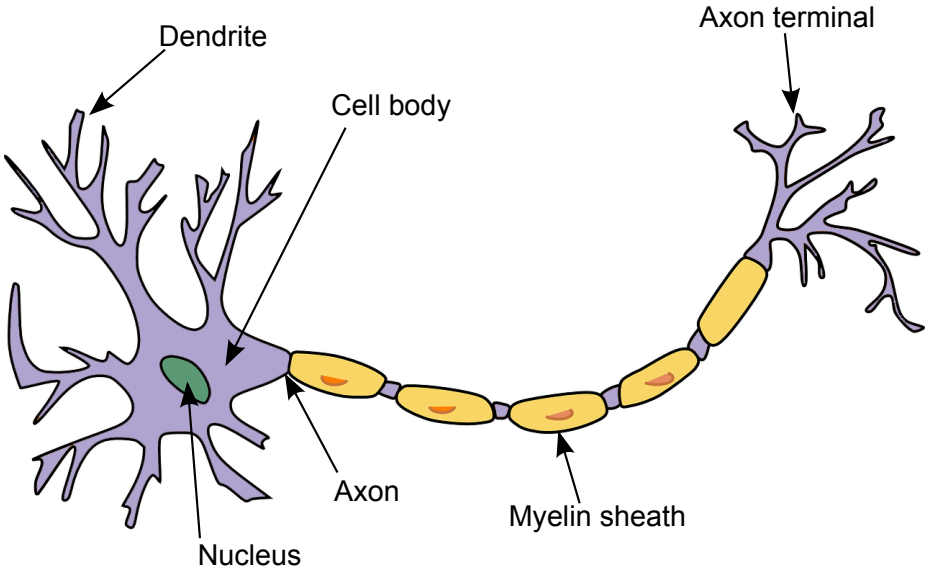

Figure 1.1: Morphology of a typical mammalian neuron.

fraction of a centimeter to about one meter or more. A cell body only gives rise to one axon, although the axon may branch hundreds of times before it terminates. Many axons are covered with a layered myelin sheath, which accelerates the transmission of electrical signals along the axon. This sheath is made by specialized cells called glia.

- **Dendrites**: These are the branched projections of a neuron that receives messages from other neural cells to the cell body. A cell body give rises to multiple dendrites to receive messages from many other neurons. The contact points where a neuron communicates with another neuron is called a synapse. The axons from other neurons form synapses with neuron dendrites.

The main objective of axons and dendrites is to connect neurons and form neural networks. These neurons are organized into grey and white matter. Grey matter contains numerous cell bodies and relatively few myelinated axons, while white matter is composed mainly

of long-range myelinated axon tracts and contains relatively few cell bodies (Figure 1.2). In the brain we can also find cerebrospinal fluid, acting as a cushion or buffer for the brain's cortex. It provides basic mechanical and immunological protection to the brain inside the skull and serves a vital function in cerebral autoregulation of cerebral blood flow.

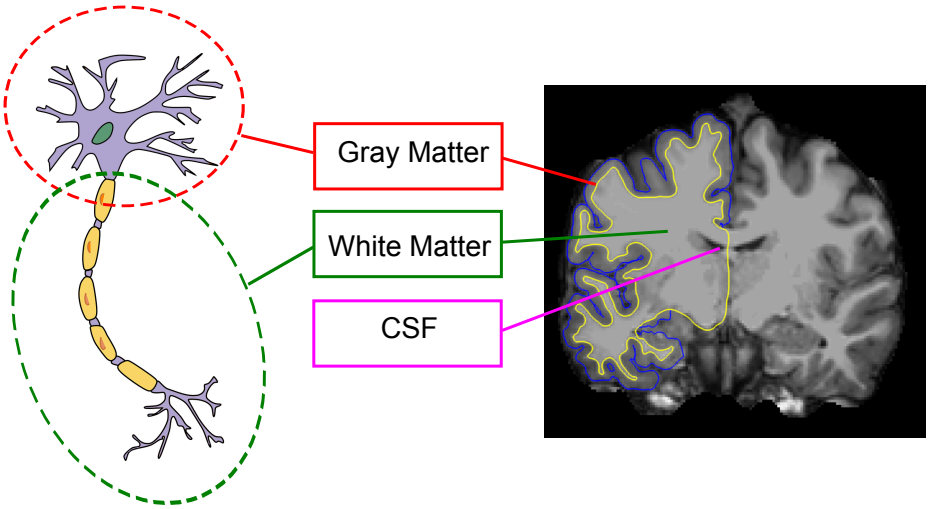

Figure 1.2: Coronal slice of the brain illustrating gray matter, white matter and cerebrospinal fluid (CSF).

The human brain is composed of about 10^{11} neurons and about 10^4 synapses per neuron that are compressed within a volume of around 1,400 cm^3, forming a dense web of cellular connections that is yet to be completely mapped [153]. The human brain, representing only the 2% of the body weight, requires 20% of the body's total energy and it is estimated that the 60 to 80% of the brain energy is used to support communication among neurons and their supporting cells, while momentary demands (task evoked activity) accounts for 0.5 to 1% of the total energy budget [125].

1.2 Brain data acquisition – for non radiologists –

There are different techniques that allow us to acquire data to study the brain. These techniques can be classified in different levels based on their spatial resolution [151]:

- **Microscale**: corresponds to single neuron and synaptic connectivity measures.
- **Mesoscale**: measures neuronal groups or populations with a spatial resolution of hundreds of micrometers.
- **Macroscale**: represents a very large number of neuronal populations forming distinct brain regions that are interconnected by inter-regional pathways.

In this thesis I will focus neuroimaging techniques for Magnetic Resonance Imaging (MRI) data (macroscale acquisitions).

MRI has demonstrated its ability to unveil non-invasively functional and structural properties of the brain in healthy populations, a knowledge that has been extremely useful to characterize the abnormal structural-functional brain patterns in several neurological disorders. These specific patterns of brain damage, in turn, have been proposed as biomarkers in neurological disorders to promote earlier and more specific diagnosis, a more precise prognosis and to design clinical trials for the development of neuroprotective therapies.

MRI has a wide range of applications in medical diagnosis and it can acquire different type of images of the brain. For the different studies carried out in this thesis we focused on the combination of three different types of acquisitions: structural, diffusion and functional scans (Figure 1.3). These scans are 3-dimensional images, composed by voxels, a value on a regular grid in three-dimensional space (the equivalent to a pixel in 2-dimensional images). The typical voxel size of these images is between 1mm - 5mm in each view (sagital, coronal and axial).

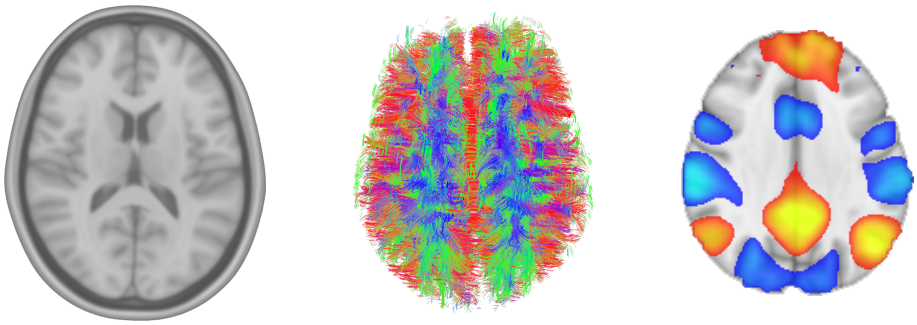

Figure 1.3: Axial slice of the brain structural scan, fibre tracts and functional network.

1.2.1 Structural data

High-resolution structural images are best suited to qualitatively and quantitatively describe the shape, size, and integrity of gray and white matter structures in the brain. In most of the neuroimaging studies a structural image is used to provide an anatomical reference for visualization, localization of the regions of interest, fusion of different image modalities and to make group analysis. Since brain function depends to some extent on the integrity of brain structure, structural images allow one to examine the impact of tissue loss or damage on functional signals.

1.2.2 Diffusion data

Diffusion MRI measures the magnitude and direction of the ther-mal motion of water molecules in each voxel. Water molecules move freely in all directions at temperatures greater than absolute zero ($>-273^{\circ}$) if there is no structure preventing movement. In the gray matter and cerebrospinal fluid we can find isotropic diffusion, i.e. water molecules diffusing equally in all directions, but in white matter the diffusion is restricted by the physical medium and water molecules follow the direction of the axons (anisotropic diffusion) as illustrated in Figure

1.4.

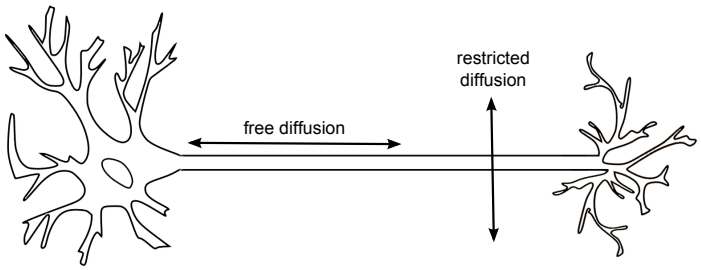

Figure 1.4: Water molecules diffusion is restricted in axons.

Water molecules diffusion is a 3-dimensional process where molecules move differently in each of the directions. An efficient way to describe this movement is to use a tensor that characterises this movement (Figure 1.5): 3 vectors describing the directions of the tensor and 3 diffusion strength rates, one for each direction.

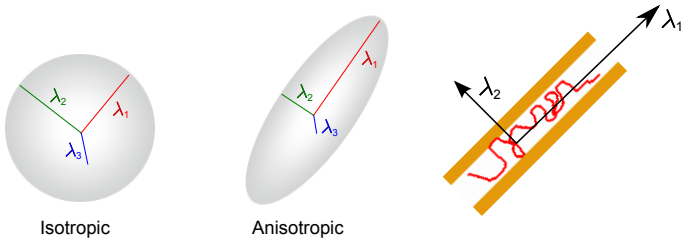

Figure 1.5: Spherical shape tensor describing isotropic and anisotropic diffusion and a 2D projection of a fibre and the diffusion propagation.

Once we know the orientation of fibres at every voxel within the brain, it is possible to join and follow these directions, reconstruct entire pathways and brain connections in a process called tractography. In its simplest form, we start at a seed location and follow the preferred direction until reaching gray matter or a limit for the

curvature(typically at 45°). This simplest technique is called streamline or deterministic tractography and is illustrated in Figure 1.6.

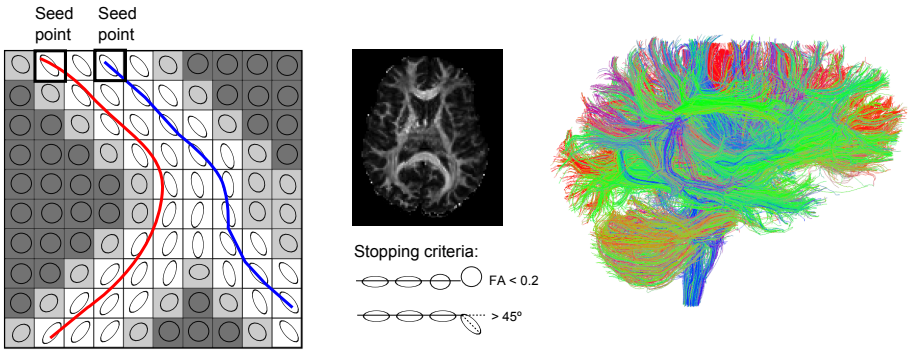

Figure 1.6: Tracking of fibres starting at different seed regions. As shown in the fractional anisotropy axial slice, each grey matter voxel has low intensity values <0.2 (where fibres end). Fibres are not allowed to have a curvature greater than 45°.

The fibres from the tractography are not real axons. Axons have a diameter on the order of 1μm, but our voxels are typically in a scale of approximately 1-5 mm. We may have tens of thousands of axons in each voxel, not having all of them the same direction. Fortunately inter-areal connections are organized in large bundles where hundreds of thousands of axons are coherently organized. It is important to emphasize that we are not obtaining the routes of individual axons, rather extracting the macroscopic structural connectivity of the brain.

Furthermore, one voxel can have many connections and some of the fibre bundles can cross each other. This usually causes problems when dealing with deterministic tractography where each voxel only is allowed to have one possible connection, but new techniques are providing improved results. Probabilistic tractography techniques estimate the most likely fibre orientation at each voxel and a distribution representing how likely each of the other orientations lie along a fibre. Then, tracing the connections thousands of times, each time using a slightly different orientation (according to their likelihood)

we obtain a set of probable fibres passing through each voxel.

Tractography is to the date the only available tool for identifying and measuring these pathways non-invasively and in-vivo. The diffusion tensor at each voxel is computed using different weighted acquisitions and applying different gradient orientations in the scanner. To compute the tensor, we need to acquire at least six gradient directions, but it is preferable to use more for a better resolution of the fibre tracts curvature, the more gradient directions the longer the time acquisition will be. This acquisition is called Diffusion Tensor Imaging (DTI). Importantly, DTI performance has been validated by replicating the structural connectivity extracted with other invasive methods; see e.g. a validation by post-mortem dissections of human brain [32], although the latter gave a much higher resolution than DTI.

For more details on the data processing of diffusion images refer to Appendix A.

1.2.3 Functional data

Functional Magnetic Resonance Imaging (fMRI) is a noninvasive way to measure hemodynamic response within the brain. Thus fMRI is an indirect measure for neuronal activity. Increased neural activity (increased firing of neurons) causes more energy demand, through a process called hemodynamic response where blood releases oxygen to the fired neurons at a greater rate in comparison to inactive neurons. This causes a change of the relative levels of oxyhemoglobin and deoxyhemoglobin (oxygenated or deoxygenated blood) and this leads to magnetic signal variation which can be detected using an MRI scanner.

While neural activity occurs in milliseconds, hemodynamic response is a slower mechanism and takes about 5 seconds to reach its maximum value followed by an undershoot at 15 seconds from the beginning. Figure 1.7 represents a typical hemodynamic response caused by neural activity. This hemodynamic response shape can slightly variate between individuals and brain regions.

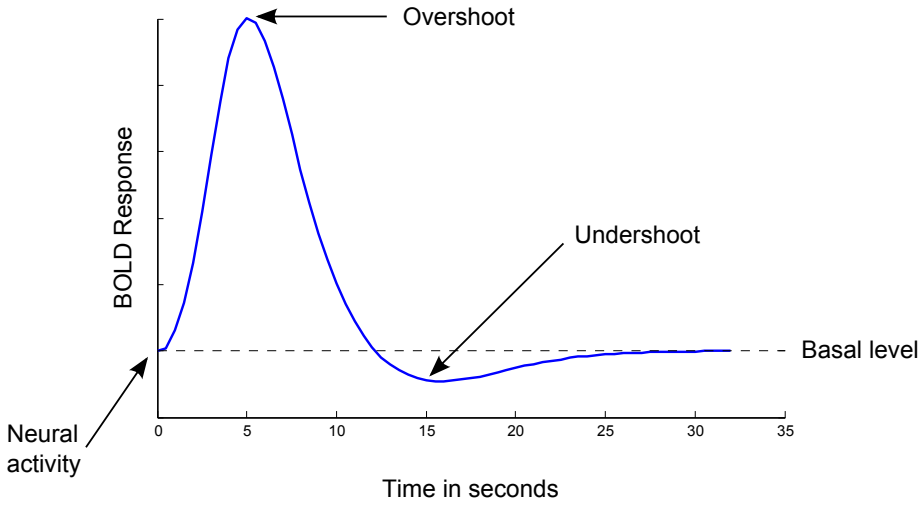

Figure 1.7: Hemodynamic Response Function.

Hemodynamic response can be treated as a linear and time invariant system as the response to a continuous neural activity is the sum of the hemodynamic signal translated in time.

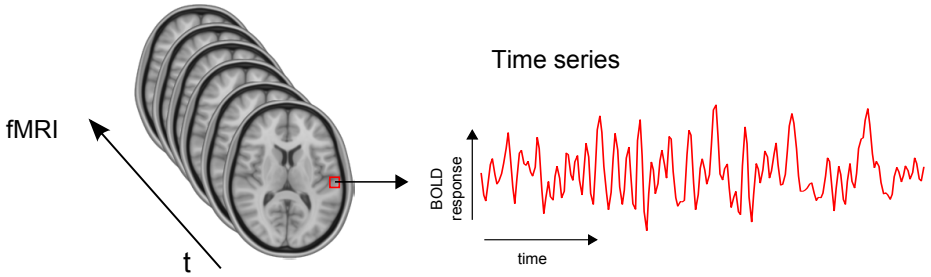

Figure 1.8: A BOLD time-series is extracted for each voxel in the brain.

fMRI acquisition produces time-series, with the blood oxygenation level-dependent (BOLD) signal, for each voxel of the brain, typically of 1-5 mm size in each direction (Figure 1.8). Each time point in a

fMRI signal is acquired every 1-3 seconds (low time resolution) and one typically acquires 200 time points (10 minutes acquisition) for studying the resting brain.

In general, fMRI can be used mainly in two modalities: task-fMRI and resting-state fMRI (rs-fMRI). During task-fMRI the subject/patient is monitored while responding to a specific stimuli or performing a specific task inside the scanner to study the functional behaviour or alterations at different brain circuitries in defined paradigms. On the other hand, brain activity is also present even in the absence of an externally prompted task, the so called resting brain, making it attractive for clinical studies. The resting fMRI monitors the subject/patient brain activity in the absence of goal-directed behavior or salient stimuli, while the patient does not think of anything in particular but not falling asleep.

It is important to remember that these time-series, based on the BOLD signal, do not measure electrical or metabolic activity in the brain, they provide an indirect measure of brain neuronal activity. The obtained time-series are very noisy and need different preprocessing stages to clean the data before further analysis. For more details on the data processing, see Appendix A.

Using Independent Component Analysis (ICA) on the extracted time-series, the overall brain dynamics generated at rest can be decomposed as a superposition of multiple activation patterns, the so-called Resting State Networks (RSNs). Becoming a fundamental characteristic of brain function, RSNs are a pivotal element for understanding the dynamics and organization of the brain basal activity in health and disease [127, 52, 123, 124]. RSNs emerge from the correlation in signal fluctuations across brain regions during resting state. Despite the simplicity of the context in which these brain activity patterns are generated, RSNs dynamics is rich and complex. Different RSNs have been associated to specific cognitive networks e.g. there are visual networks, sensory-motor networks, auditory networks, default mode networks, executive control networks, and some others [10] (for further details see Chapter 4. These same RSNs do appear in all healthy subjects and have been reported to be altered with

different neurological disorders.

1.3 Brain networks – for non engineers–

To study neurological dysfunction, it is of great interest to treat the brain as a network. Networks have shown an incredible potential to study complex biological systems, including the brain, and are beginning to reveal fundamental principles of brain architecture and function. The mathematical language that describes and quantifies networks is called graph theory.

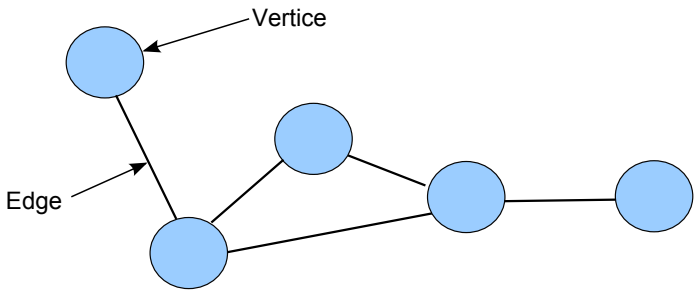

Figure 1.9: A graph is composed of vertices and edges.

Graphs offer a proper language to describe whole-brain patterns and interregional interactions (Figure 1.9). A graph is a mathematical representation of a network and it consists of a finite set of:

- **Vertices (nodes)**: They represent the brain regions of interest. Choosing them correctly will have a large influence on the resulting graph.
- **Edges (links)**: These represents the connectivity between the brain regions.

Combining graph theory and the predictive nature of machine-learning in brain data is opening new possibilities for diagnosis and

prognosis of neurological disorders because these networks are affected during disease. Although graphs offer a great potential to characterise the diseases, nowadays brain graphs are not a recognized tool in clinical practice.

The first step towards constructing a brain graph is to select the vertices or brain regions of interest. There exist different choices for mapping voxels to graph vertices:

- **Voxel-based**: Each voxel of the image is used as a vertex of the graph. Depending on the analysis to be done with the resulting graph, this option can be computationally very expensive. State-of-the-art graph algorithms can deal only with graphs including some hundred up to a few thousand nodes at maximum. This is the reason why this option is not usually used.

- **Atlas-based**: Anatomical knowledge generated from post-mortem studies have led to many atlases that divide the brain into different anatomical regions (one vertex per region). This is the most used approach for brain graph analysis.

- **Data-based**: Data driven approaches like Independent Component Analysis or clustering could be used to generate subject specific functional or structural regions (one vertex per region, but in this case a voxel can belong to various regions). We will provide more details on this approach in Chapter 3.

Once the vertices are selected the next step is to define the connectivity between these vertices. There are three main types of connectivity [151, 19]:

- **Structural connectivity**: encodes anatomical connections between brain regions [149], typically white matter tracts computed from DTI [38]. White matter (dys)connectivity is thought to form the substrate for many different neurological and psychiatric disorders.

- **Functional connectivity**: defines the activation profiles and dependencies among distinct neuronal populations [56]. If two regions have a similar functional activation profile they will have a strong connectivity index between these regions (cf. Figure 1.10). Estimation of dependencies is difficult when the number of vertices is large in comparison to the number of time points.

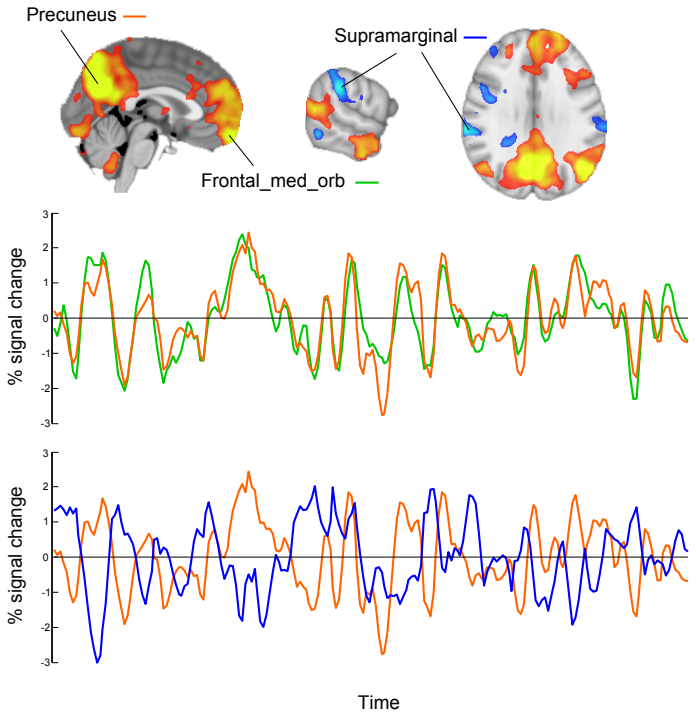

Figure 1.10: The time-series extracted from a voxel of the precuneus was correlated with all the voxels time-series of the brain. Red-yellow colors represent regions with positive correlation and blue regions negative ones. Precuneus voxel time-series is colored in orange and the frontal medial orbital time-series in green (observe high similarity between these activation profiles so they have a strong functional connectivity value). Supramarginal voxel time-series is shown in blue to show that when the precuneus is active this region is not and vice versa (i.e. they are anti correlated areas).

- **Effective connectivity**: identifies causal interactions underlying temporally ordered activation or information flow [58].

These connections, from the structural data to information transfer between remote brain regions, are essential to understanding brain function. Instead of a univariate analysis of each voxel, brain networks are becoming popular for the study of the interactions between brain regions.

Edges connecting vertices can be directed or undirected. Directed edges represent the fact that one vertex exerts some influence on its neighbor (two vertices are called neighbors if they are connected by an edge) but not the other way around. On the other hand, on undirected edges the influence between vertices A-B is the same as the influence between vertices B-A. When we generate the graph from structural or functional connectivity we obtain undirected networks, while effective connectivity generates a directed network. Table 1.1 illustrates different networks that can be generated from this connectivity data.

In Chapter 2 we will see more details about graph generation and how to use them to find differences in disease.

1.4 Thesis overview

In this thesis I used brain network analysis to unveil functional and structural patterns in healthy brain and study alterations in different pathologies.

In Chapter 2 more details about graph generation are explained. In particular, functional and effective networks are used to find image-biomarkers for patients with disorder of consciousness. Finally these biomarkers are compared with different clinical practice scores.

In Chapter 3 functional and structural networks are combined to generate a new data driven brain atlas that accounts for both structure and function. We also described crossmodularity, a new method to choose the best brain partition. The obtained brain partition is compared with different anatomical and functional atlases.

Table 1.1: Different types of brain connectivity networks based on the measured feature connecting each pair of nodes.

Structural connectivity	**Functional connectivity**	**Effective connectivity**
Number of Fibres	Pearson Correlation	Granger-causality
Volume	Partial Correlation	Transfer entropy
Density	Mutual Information	Direct Causal Modelling
Fibre Length	Coherence	Structural Equation Modelling
Fractional Anisotropy	Phase synchronization	
Mean Diffusivity	Generalized nonlinear synchronization	
Radial Diffusivity		
Axial Diffusivity		

In Chapter 4 we use Principal Component Analysis to extract more information from the Resting State Networks of the brain and compute a new information flow measures using many brain components. We used this method to find differences in the communication of Resting State Networks in Alzheimer's disease and we demonstrate that the differences are not always shown in the principal component (the one usually used for information flow analyses).

In Chapter 5 we will use the atlas derived in Chapter 3 to study the functional and structural reorganization of the brain of patients with traumatic axonal injury. Extracting more components from each region, as done in Chapter 4, we developed a new technique to find differences in pathological brain when specific interactions occur between different brain regions.

To finish this thesis, in Chapter 6 a general conclusion is provided.

As a result of the work done in BioCruces Research Institute we created a platform for performing automatic neuroimage processing for the images acquired at Cruces University Hospital. The available algorithms have been implemented based on real needs of clinicians

in the hospital. For more details refer to Appendix B.

Chapter 2

Functional alterations in patients with disorder of consciousness

In the previous chapter we make an introduction to brain networks. In this chapter we will see how to construct functional and effective connectivity networks and we are going to use them to search for biomarkers of patients with disorders of consciousness.

Recent studies have shown that brain networks obtained from the functional Magnetic Resonance Imaging (fMRI) are altered in patients with severe disorder of consciousness (DOC)[113, 76]. A DOC can result from severe brain injury and is characterized by an absence of awareness of the self and the environment, either with preserved or disrupted sleep-awake cycle. DOC encompasses a wide spectrum of clinical conditions with different levels in the content of conscious awareness, ranging from the coma state (CS, patients who have a disrupted sleep-awake cycle and don't wake up), vegetative state (VS, who preserve sleep-awake cycle but are unaware of themselves and the environment), minimally consciousness state (MCS, patients who are unable to reliably communicate but show reproducible albeit fluctuating behavioral evidence of awareness), to finally lock-in syndrome (LI, patients who are fully conscious but are completely paralyzed except for small movements of the eyes or eyelids).

For the prognosis of these patients, the clinical practice scores this graduation in DOC response by the Glasgow Coma Scale (GCS) [158], or as we use in this work, by an alternative scale such as the JFK Coma Recovery Scale-Revised (CSR-R) [64]. This scale outputs the neurological and behavioural state of the DOC patient providing a number ranging from 0 to 23, 0 for the deepest coma state, 23 for the fully recovered one.

Despite the existence of such scales, we need more reliable methods that – based on brain neuroimaging – can provide better characterization of the large-scale disturbances of brain function in DOC, which is fundamental for the understanding and eventual prediction of coma outcome. In this case, the resting state paradigm is a very meaningful one as DOC patients are not able to efficiently perform any other specific task.

This chapter addresses the question of whether the functional and effective connectivity obtained from the rs-fMRI is altered as a consequence of consciousness disturbances. We have analyzed data belonging to two different groups, healthy adults and DOC patients, and found significant differences between the two groups.

2.1 Subjects and data pre-processing

Seventeen healthy subjects (Group 1) aged 25 $\pm$ 5 year old, with no history of neurological or psychiatric problems, participated in this study as a control group. The Edinburgh Handedness Inventory was used to assess handedness [114]. Thirteen subjects were right-handed and four left-handed. Eleven DOC patients (Group 2) were scanned (age range, 17- 44 years; 6 men). Data from two patients were subsequently excluded because of unacceptable degrees of head and body movement. The coma severity for each patient was clinically assessed using the Revised Coma Recovery Scale (CRS-R, [64]): scores range from 0 (meaning deep coma state) to 23 (full recovery). The patients were scanned a first time between 2 and 6 months after major acute brain injury, and a second time between 3 and 6 months after the first scan (Table 2.1). 4 DOC patients (Recovery Group) recovered con-

Table 2.1: Clinical characteristics of DOC patients. TSI: Time Since Injury; VS: Vegetative State; MCS: Minimally Consciousness State; C: Conscious; EMCS: Emergence from MCS (an intermediate state between MCS and C); *: Patients who recovered consciousness before the second session

Patient code	Age	TSI (months)	Assessment scan 1	Time between scans (months)	Assessment scan 2
P1	34	2	VS	5	VS
P2*	18	4	MCS	4	C
P3*	44	2	MCS	3	C
P4	17	6	VS	6	MCS
P5	26	4	VS	3	MCS
P6*	26	4	EMCS	4	C
P7	29	4	MCS	3	MCS
P8	41	2	VS	6	VS
P9*	34	5	VS	5	C

sciousness before the second session (marked with asterisk in Table 2.1).

The study protocol was approved by the Institutional Review Board of the Institute of Neurological Research FLENI. Informed consent was directly obtained from healthy participants and from the next kin of each of the patients.

The fMRI measurements were carried out on a 3T Signa HDxt GE scanner using an 8 channel head coil. Resting State Functional Magnetic Resonance and anatomical scans were acquired (for more information about scanning protocol refer to [97]). For the resting state acquisition, subjects lied quietly for a period of 7 minutes.

The functional images were subjected to temporal alignment and volumes were corrected for movement using a six-parameter automated algorithm. The realigned volumes were spatially normalized to fit to the template created using the Montreal Neurological Institute reference brain based on Talairach and Tournoux's sterotaxic

coordinate system [6]. The spatially normalized volumes consisting of 4 x 4 x 4 mm^3 voxels were smoothed with a 8-mm FWHM isotropic Gaussian kernel. Additionally, a linear trend removal and band pass filtering between 0.01 and 0.08 Hz was applied to the data. For more details on the pre-processing steps refer to Appendix A

2.2 Alterations in Functional Connectivity

Using network theory to infer the functional structure of a network from the analysis of its spontaneous dynamics, it is possible to identify and characterize key synchronization mechanisms and nodes that are essential for its functional operation. As defined in Chapter 1, the activation profiles and dependencies among distinct neuronal populations defines functional connectivity graphs.

90 Regions of Interest (ROI) were defined based on the Automatic Anatomical Labeling (AAL) atlas [161], Figs. 2.1a, 2.1b and 2.1d. Each brain area is represented by two ROIs, one on the left hemisphere and the other one in the right hemisphere (eg. hippocampusLeft, hippocampusRight, amygdalaLeft, amygdalaRight, insulaLeft, insulaRight, etc.). Thus, the AAL atlas has 45 brain areas forming a total of 90 different ROIs. Importantly for the study of DOC patients, the AAL atlas includes both cortical and subcortical components (eg., hippocampus, thalamus and amygdala).

Per each ROI we have extracted a mesoscopic (multi-voxel) fMRI time-series resulting from averaging over all fMRI time-series corresponding to all voxels within a ROI (Fig. 2.1b is showing the ROI size distribution among all areas). The MNI coordinates of the centroids in each ROI are used to calculate the Euclidean distance between each pair of regions (Fig. 2.1b). There exist different ways to extract time-series from regions of interest. For more information refer to Appendix A.

If we look to the functional activity of different voxels of the brain we can find regions with very similar behaviour (Figure 1.10). If two

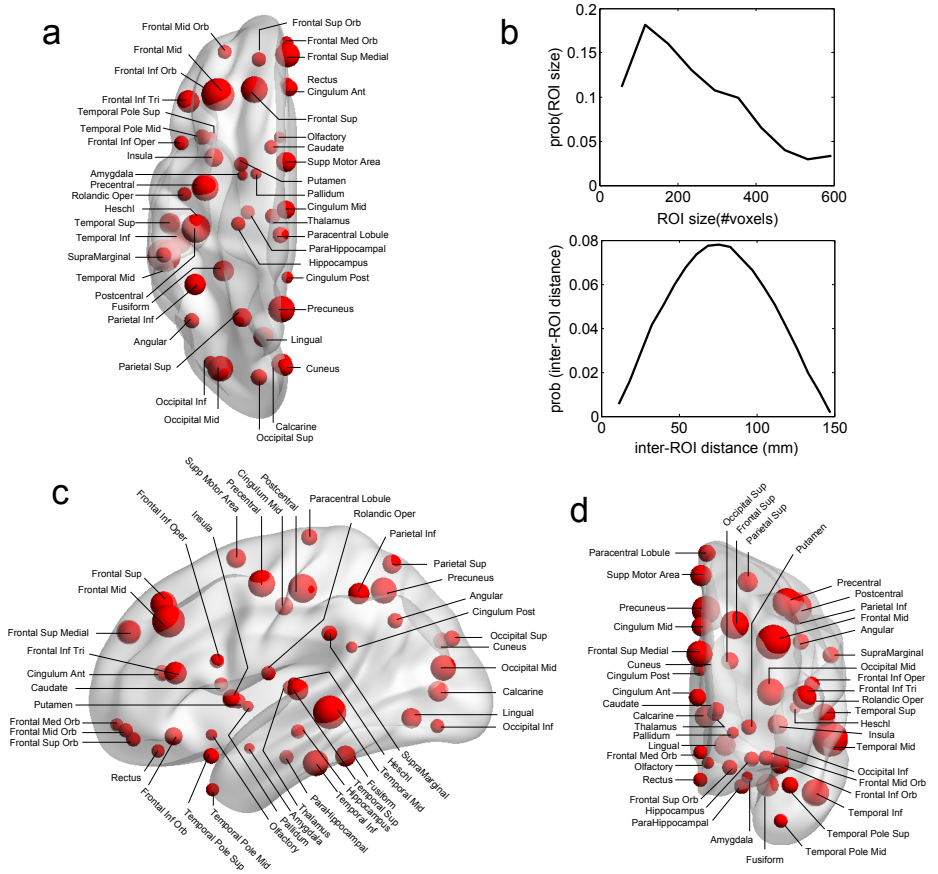

Figure 2.1: **Anatomical Brain parcellation and Regions of Interest (ROI). a**: Axial, **c**: Saggital , **d**: Coronoal views. Red spheres representing specific ROIs. Sphere diameter is proportional to ROI size (the number of voxels). Notice that the atlas has both cortical and subcortical components. **b**: ROI size distribution and inter-ROI distance distribution. To give an estimation, as each voxel is about 4 cubic millimeters, the ROI average size ($\approx$ 150 voxels) is equivalent to a 3D cube of 21mm edge. Biggest ROI ($\approx$ 600 voxels) corresponds to 3D cubes of 34mm edge.

regions are activated at the same time this suggest that they might collaborate in the same task and that they should be somehow connected. Based on how similar the activity is in two different regions, we can compute a measure defining a weight of the connection between these 2 regions. It is also interesting to mention that there also exist anticorrelated regions in the brain, when one region is active and the other is not active and vice versa (Figure 1.10).

A functional connectivity is usually represented as a matrix where each entry of the matrix represent the connection between 2 regions. We can observe two 90x90 regions connectivity matrices in Figure 2.3. The first row of the matrix represent the functional connectivity of the first AAL region (Precentral Left) with the rest of 90 regions of the brain. The color represents the connectivity weight (negative values represent anticorrelations). The principal diagonal with "1" values means that each region activity is (obviously) correlated with itself. For functional connectivity measures this matrix is symmetric, A connects with B in the same way B connects with A.

The most common method to define Functional Connectivity (FC) is computing the correlation in the rs-fMRI time-series [17]. This correlation between time-series can arise from a number of reasons (Figure 2.2). When two regions of the brain have similar activation patterns, it could be because they are directly connected, indirectly connected or because they are not connected but they have a common input (neighbour).

After calculating a standard correlation measure, it is typical to observe that almost all brain regions are correlated (Figure 2.3), because standard Correlation does not differentiate between direct, indirect or shared influence.

In this study we have used Partial Correlation (PC) to construct the functional networks from the time-series of the regions of interest. PC removes the indirect effects of the data. For more details on how to compute correlation and partial correlation see Appendix A. In a previous study [3] we reported how partial correlation better predicts the structural connectivity (computed with tractography) than the standard correlation.

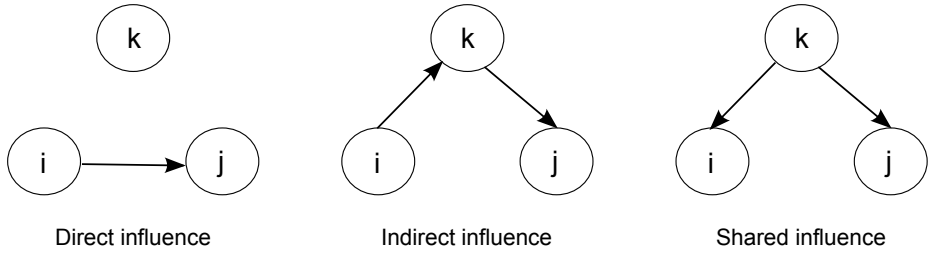

Figure 2.2: Two brain regions correlation can arise from direct influence between two regions (left panel), indirect influence via another region (center panel) or shared influence from a common input region (right panel).

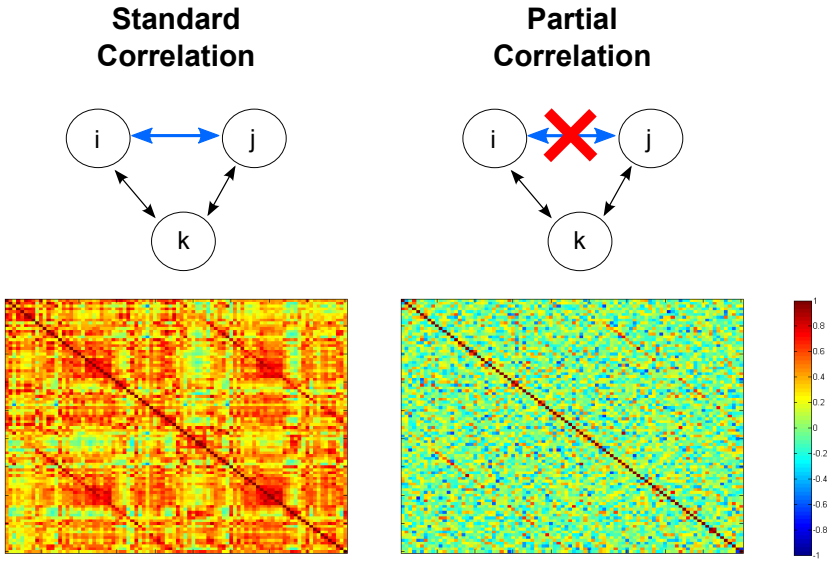

Figure 2.3: Standard correlation computes direct and indirect (blue line) effects. If i is connected to k and k is connected to j, standard correlation will give a high correlation value between i and j. Partial correlation removes the indirect effect and shows just the direct connections.

Figure 2.4 shows a control subject connectivity matrix and a DOC patient connectivity matrix. We can observe how 2 straight lines, parallel to the principal diagonal, appearing in the control matrix disappeared in the DOC matrix. These two lines represent the connectivity of inter hemispheric homologous areas in the brain (e.g. hippocampus left with hippocampus right ...). This difference between the 2 groups suggests a possible biomarker for DOC patients.

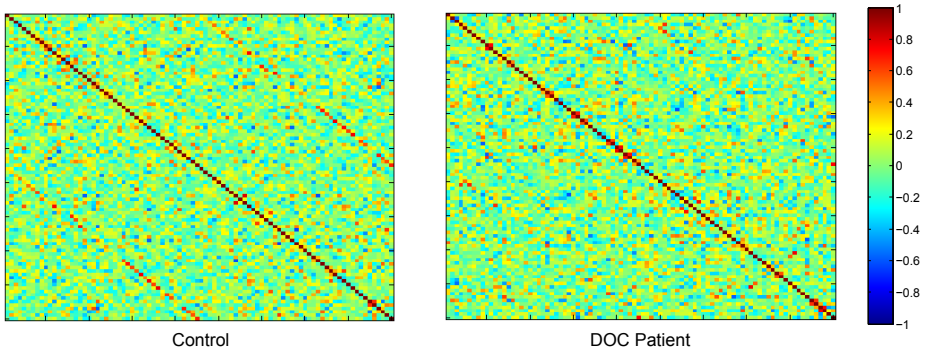

Figure 2.4: Control and DOC patients functional connectivity matrix. The inter hemispheric homologous connections disappears in DOC patients, the two straight lines parallel to the principal diagonal.

We also have computed the *standard* correlation C, and although C is more noisy than PC, the results we are showing here for the PC are also valid for the standard correlation.

PC matrices were calculated for each subject. PC values have been grouped into the following categories: inter-hemispheric (between one area on the left and all the other areas in the right hemisphere, or vice versa), between-homologous inter-hemispheric (one area on the left hemisphere and its homologous area on the right hemisphere, or vice versa), right intra-hemispheric, left intra-hemispheric, and total.

First we looked into the neural partial correlation patterns (Table 2.2). ANOVA between Controls and DOC shows a significant effect of categories ($p<0.001$), and a significant interaction between categories and groups ($p<0.001$). Controls have a significantly smaller

Table 2.2: Summary of PC average values ± standard deviation. **significantly different from Controls; p<0.05.*

Partial Correlation	Controls	DOC	Recovey
inter-hemispheric	0.11±0.01	0.12±0.01	0.12±0.01
homologue inter-hemispheric	0.4±0.03	0.24±0.03*	0.26±0.04*
left intra-hemispheric	0.13±0.01	0.15±0.01	0.15±0.01
right intra-hemispheric	0.13±0.01	0.15±0.01	0.15±0.01
Total	0.12±0.01	0.13±0.01*	0.13±0.01*

PC mean value than patients ($p<0.001$). When looking to categories, inter hemispheric homologous PCs are significantly higher than intra hemispheric and all the inter hemispheric PCs ($p<0.001$). In addition, intra hemisphere connectivity values are significantly higher than inter hemispheric ones ($p<0.001$). To further inspect the interaction, we performed *post-hoc* multiple comparison tests between groups for the different categories. Inter hemispheric homologous PCs are significantly higher in Controls ($p<0.001$).

Interestingly to remark, it has been shown before that the interhemispheric correlations in the rs-fMRI dynamics correlate with the interhemispheric coherence existing in electrophysiological data in human sensory cortex [112], mainly correlated with the gamma rhythms in Local Field Potentials. Thus, at the functional level, a breakdown in the interhemispheric rs-fMRI correlations in DOC patients is indicating a breakdown in the electrophysiological gamma power coherence.

When comparing Controls and patients that recovered from DOC, the effect of group still holds but is smaller than that between Controls and DOC ($p=0.002$). The effect of categories is the same as in Control vs. DOC comparison. Post-hoc tests show that homologous inter hemispheric PCs are significantly smaller in patients that recovered from DOC with respect to Controls ($p<0.001$). Finally, the comparison including all brain categories (total) was significant

between Control vs. DOC(P=0.018). Results can be seen in Table 2.2 and Figure 2.5.

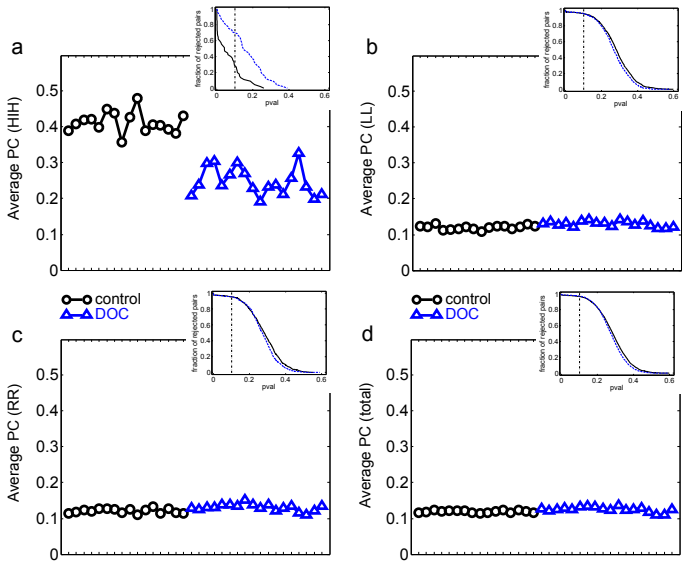

Figure 2.5: **Average PC values per subject**. **a**: HIH (homologue inter-hemispheric areas); **b**: LL (left intra-hemispheric); **c**: RR (right intra-hemispheric); **d**: total. Insets depict the fraction of rejected pairs of areas for a given probability level. PC values were thresholded at a probability value of 0.1 (dashed lines in the insets) . Black circle: Control; Blue triangles: DOC. Observe the huge differences beween Controls and DOC for HIH compared to LL and RR. For detailed values, see Table 2.2.

For PC there is a manifest anatomical disparity in the correlations pattern: it can be observed that homologue areas that are closer to each other show stronger correlations than further ones. To disentangle the behavior of the neural correlations regarding to a spatial factor, we brought up the Euclidean distances between the centroids of homologue areas. For Controls the areas close to each other presented a high correlation, and beyond a threshold distance of 20 mm, correlations decreased, although the values remained high. Interest-

ingly, this same behavior was found in DOC patients. However, the correlation values there were shifted down, with lower mean values for areas closer than 20 mm, and decreasing for increasing distances. Thus, for ROIs areas distance-separated smaller than 20mm, differences between Controls and DOC were smaller compared to areas separated at long distances, distance separation < 20mm pval=10^{-6}, distance >40mm pval=10^{-14}. When inspecting DOC patients with the patients recovered form DOC, there were no observable differences for anatomically closer areas, while a higher correlation of some of the anatomically further areas for recovered patients could be detected (Figure 2.6).

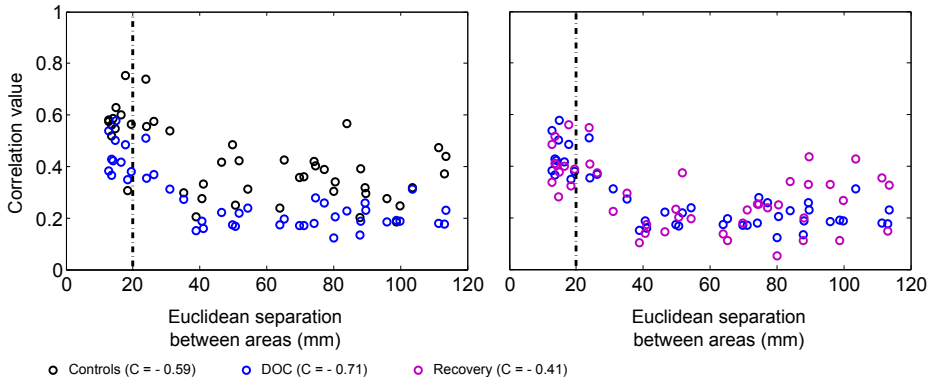

Figure 2.6: **Sum of Inter-hemispheric homologous PC**. Correlations between areas decreases as Euclidean distance between them increases for Controls, DOC and recovered patients.

In summary, the partial correlation approach allows to expose a differential functional connectivity in a healthy conscious brain in comparison with DOC state and one recently recovered from it. A reduced inter-hemispher-ic connectivity and an increased intra-hemispheric connectivity are evident in DOC patients.

2.3 Alterations in Effective Connectivity

Effective connectivity is defined as the direct influence that one neural system exerts on another. Techniques based on information theory can be used to compute effective connectivity.

Information theory is a consolidated field in which different measures, typically built as extensions of the Shanon Entropy (the average uncertainty in a random variable) are used for quantification of interactions between variables, e.g. by measuring the uncertainty reduction (information) which is shared or transferred between two variables [82, 34]. In the last decade, the transfer entropy (TE) method is growing in popularity as it can account for directed interactions between time-series variables [137]; when applied to neuroimaging time-series (any modality), TE is a data-driven measure that assesses the functional connectivity (FC) between brain areas even for non-linear interactions. Unlike the correlations, TE reveals directionality in the interactions, thus allowing to determine a *directed* FC between areas. The TE is a non-symmetrical measure, i.e. the interaction between A and B is different to the one from B to A . More details on how to compute TE can be found in Appendix A.

Specifically, TE quantifies the mutual information between the future activity in one ROI and the activity of another ROI conditionated on the activity of the former ROI. For the case of Gaussian data, the information bits measured by the TE coincide with the Granger causality measured from time-series [8]; for non Gaussian data, TE and Granger causality might provide different measures.

Regarding the calculation of TE, it is well-known that the calculation of the entropies with small data sets introduces a bias [117, 116, 18]. Because we are performing groups comparison with the same data size in each group (i.e. the time-series in each subject have the same data points), such a bias will be preserve in the two groups, and the groups comparison keeps still going.

TE matrices were calculated for each subject. TE values were grouped into the following categories: inter-hemispheric (from one area on the left to all the other areas at the right hemisphere, and from one area on the right to all other areas at the left hemisphere),

between-homologous inter-hemispheric (one area on the left hemisphere to its homologous area on the right hemisphere and vice versa), right intra-hemispheric, left intra-hemispheric, and total.

ANOVA on TE values for Control and DOC shows a significant effect of group ($p=0.0025$) and categories ($p<0.001$). Particularly there were significant differences between homologue inter-hemispheric TEs and the TE values for the other categories. In the case of homologous inter-hemispheric from left to right, TEs were significantly lower than left intra-hemispheric, right intra-hemispheric and inter-hemisferic (left to right and right to left) TEs ($p<0.005$), whereas homologous inter-hemispheric from right to left TEs were significantly lower than right intra-hemispheric and inter-hemispheric right to left TEs ($p<0.025$). There was no interaction effect between group and category. The post-hoc analysis showed that left intra-hemispheric, inter-hemispheric from left to right and total TE values differ between controls and patients.

However, when performing the ANOVA for Control and DOC there was a significant effect of group ($p<0.001$) and categories ($p<0.001$). Post-hoc tests showed that intra-hemispheric left and right TEs were significantly higher in Controls than in DOC ($p<0.05$). In addition, TE for inter-hemispheric from left to right was also significantly higher in Controls ($p=0.001$).

When comparing Controls and DOC, there was significant effect of group ($p=0.042$) and categories ($p<0.001$). Additionally, when looking into the main effect of brain sections, inter-hemispheric homologous TE values were significantly smaller than inter-hemispheric values ($p<0.05$).

The results can be seen in Table 2.3. If two time-series are highly correlated, their TE is close to zero in both directions; if they are not correlated but one influences the other's behavior, TE is high in that direction and very low in the opposite direction. In our results, the significant smaller TE between homologue areas with respect to the other TE values is consistent to the fact that they are highly correlated.

The differences found within hemispheres between the groups par-

Table 2.3: Summary of TE average values ± standard deviation. **significantly different from G1; p<0.05.* HLR: homologous inter-hemispheric from left to right; HRL: homologous inter-hemispheric from right to left; LL: left intra-hemispheric; RR: right intra-hemispheric; LR: inter-hemispheric left to right; RL: inter-hemispheric right to left.

TE	Controls	DOC	Recovery
HLR	0.009±0.027	0.006±0.015	0.017±0.030
HRL	0.011±0.020	0.02±0.049	0.019± 0.032
LL	0.04±0.021	0.017±0.016*	0.04±0.003
RR	0.039±0.020	0.027±0.039	0.065±0.050
LR	0.043±0.024	0.021±0.021*	0.047±0.017
RL	0.043±0.021	0.031±0.045	0.066±0.049
Total	0.041±0.018	0.024±0.026*	0.054±0.028

allelize the increased intra-hemispheric correlations in DOC patients. When looking at recovered patients, their averages are also biased by one patient that presented extremely high TE values.

Regarding the TE, not only the mean values of TE in intra-hemispheric left areas were different between groups (Table 2.3), but the number of significant values of TE, i.e. the number of arrows plotted in Figs. 2.7, varies across different groups. This number was more than 9 times bigger in Controls compared with DOC (Controls # links=47, DOC # links=5). When comparing with Recovery group (the patients that awaked and became fully conscious at the second fMRI acquisition), this number doubled the one in Control (# links=99), possibly indicating a "transitory" brain state in the pattern of information flows in recovered patients in comparison with control. In a similar spirit, Anil Seth and colleagues defined the causal density for measuring consciousness in brain states as the number of Granger-causality connections flowing in and out per each specific area (for review see [140]). Interestingly, a similar behavior has been reported during recovery from anesthesia, where an incre-

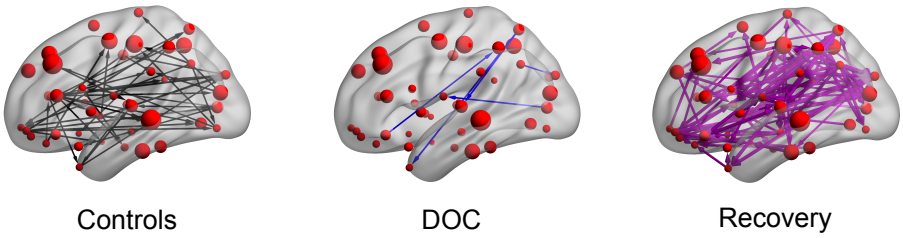

Figure 2.7: **Left intra-hemispheric TE**. Intra-hemispheric left (and to a lesser extent, the right TE) TE values for the 3 different groups. The thickness of links and arrows are proportional to the TE values; the thickness normalization factor is common among all the 3 groups. For clarity in the visualization, links have been thresholded and only TE values bigger than TE = 0.2 are depicted.

ment in functional connectivity above the normal wakeful baseline is found [80].

In summary, TE analysis allows for detecting an altered FC in DOC patients. For instance, TE within hemispheres and between hemispheres is smaller, although no difference was found when looking at homologue areas. In contrast to the results obtained in the PC analysis, the differences found uphold irrespective of the Euclidean distance separating ROIs pairs, although when considering intra-hemispheric left TE, a slight decrease in the statistical p value was observed.

2.4 DOC image biomarkers and correlation with CRS-R scores

In this study we have investigated whether the functional connectivity (FC) is altered as a consequence of consciousness disturbances. We have applied the Partial Correlation (PC) and the Transfer Entropy (TE) approaches to analyze the FC from resting-state fMRI

data. We have compared two groups, healthy subjects (control) and Disorder of Consciousness (DOC) patients. The analysis was done over the 90 anatomical brain areas, defining regions of interest (ROI) from the AAL atlas. We have grouped the different pairs of ROIs in inter-hemispheric homologue regions, inter-hemispheric , left intra-hemispheric, right intra-hemispheric and total (all regions). We have found two particular markers that account for the large-scale disturbance of patients brain function: the PC calculated over homologue inter-hemispheric (HIH) regions and the TE calculated over the left intra-hemispheric (LL) ROIs.

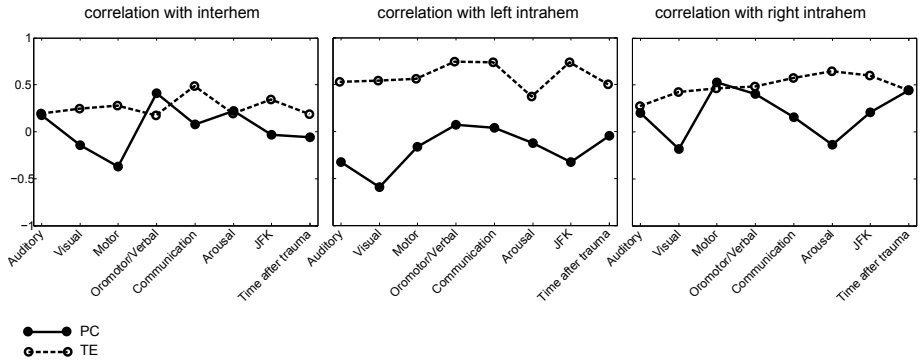

Figure 2.8: **Inter-hemispheric PC and left intra-hemispheric TE**. Correlation between PC (solid line) and TE (dashed) with the CRS-R scores at the different functional scales: Auditory, Visual,Motor, Oromotor/Verbal, Communication, Arousal and the total sum over all the function scales (JFK) as well as with the acquisition time after trauma. The correlation has been calculated over pairs which are (I) inter-hemispheric (HIH for PC and (HLR+HRL)/2 for TE, (J) left intra-hemispheric (LL) and (K) right intra-hemispheric (RR).

The PC in HIH regions was found to be notably larger for control compared to DOC patients. These results hold also when comparing Controls with the recovered group. The same comparison but done

over the total average of the 90 regions did not show significant differences. Thus, one relevant point of our analysis is the finding that only by the calculation of the PC in the proposed grouping of brain regions, it was possible to detect a significant marker for the patient's disturbance, results that are hidden when we looked at the PC of the total AAL brain regions.

In the case of TE, the total score did not show any significant difference either, but the brain subdivision revealed that the left intrahemispheric influences were different in control respect to DOC.

To have high correlations is different from having high TE between two time-series. Two fully correlated time-series have zero TE because 2 equal time-series are not adding any further information to the situation of only having one. As a consequence of this, the observation of having high PC for HIH pairs in healthy subjects achieves high isolation of the information within hemispheres; thus, the TE values in both LL and RR are significantly higher than the corresponding values in HLR and HRL.

Based on these results the best two discriminators are the between-homologue inter-hemispheric PC (Figure 2.5) and the left intra-hemispheric TE (Figure 2.7).

We then asked if the two fMRI measures, between homologue inter-hemispheric PC and left intra-hemispheric TE, were correlated with the neurological and behavioural scale given by the CRS-S. This is represented in Figure 2.8. For homologue inter-hemispheric pairs we found that TE gave the bigger correlation with the corresponding value in the communication function scale. For left intra-hemispheric pairs, TE had 0.73 correlations with oromotor/verbal function scale, 0.73 with the communication function scale and 0.73 with the total CRS-R (marked as "JFK" in Figure 2.8).

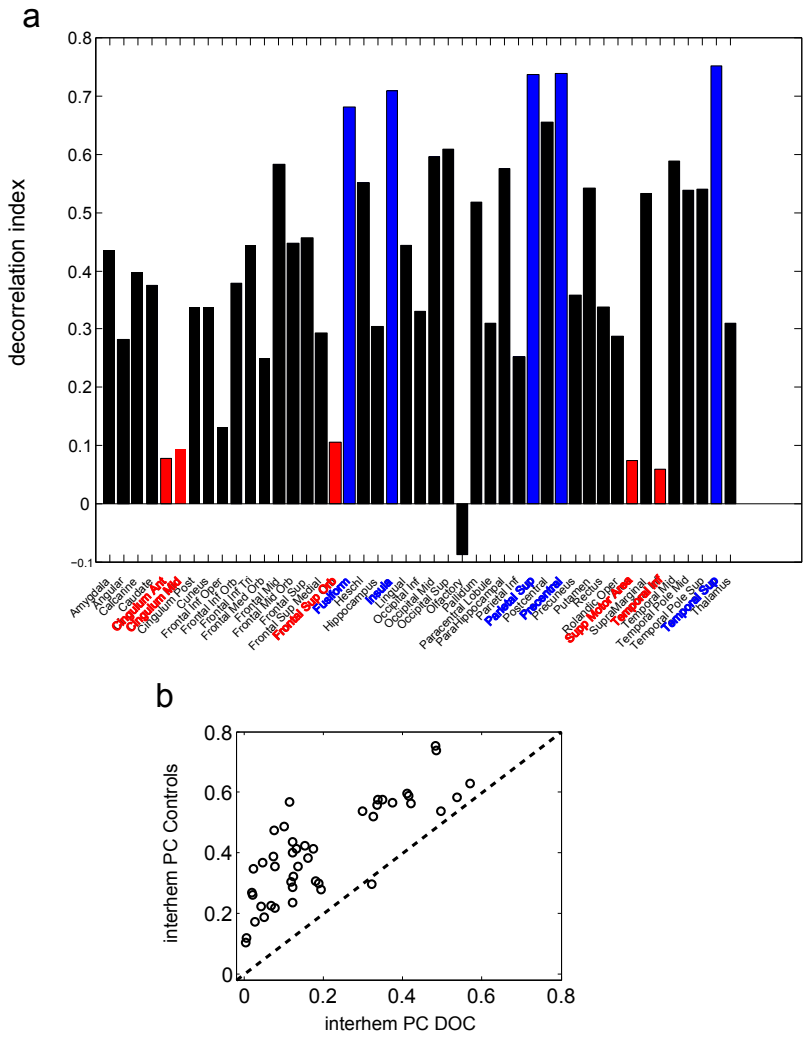

Figure 2.9: Decorrelation index indicating differences between Controls and DOC in the AAL regions. Blue bars indicate the most affected areas and red the less affected ones. Panel b represents the correlation between Control and DOC measures. Regions close to the diagonal are less affected than the furthest ones.

2.5 Future Work: DOC impairment at specific brain areas

The aim of this analysis is not to work at the level of an individual DOC patient but to search for rs-fMRI markers that can account for groups differences in DOC patients. We have not studied yet any measure that can account for DOC impairment at specific brain areas. To this end, one could analyze in principle the FC graphs obtained by either PC or TE using complex networks analysis, or any other kind of graph exploration methods. In a much simpler spirit (just to illustrate that this approach is plausible), we have chosen to plot the PC values per area comparing DOC versus Controls. This is illustrated in Figure 2.9. The decorrelation index per area is plotted, (corrG1-corrG2)/corrG1. Colored in blue, the top-five bigger decorrelation index corresponded with the following areas: Fusiform, Insula, Parietal Superior, Precentral and Temporal Superior. Consequently, this analysis revealed that those areas had a major DOC impairment. The areas with less DOC impairment, colored in red, were: Cingulum Anterior, Cingulum Middle, Frontal Superior Orbital, Superior Motor Area and Temporal Inferior.

Chapter 3

Modular skeleton shared by structure and function

In previous chapters we saw how to create functional connectivity networks and how to use them to find differences between Control and patients. Instead of using a defined anatomical or functional atlas, in this chapter we will use both functional and structural networks to find a brain partition that accounts for both structure and function. We will also study the similarities between the data-driven atlas we obtained and other existing anatomical and functional atlases. In the next chapters we will make use of this atlas to study brain reorganization after disease.

Two complementary principles underlie human brain functioning, segregation and integration [160]:

- **Segregation** refers to the need of functionally specialized brain areas to process incoming information and to perform distinct tasks separately.
- **Integration** or binding is required for the coordinated activation of neuronal populations across brain areas that result in coherent cognitive and behavioral states [68, 25].

Elucidating the wiring architecture of brain networks is essential to understanding how an optimal balance between segregation and

integration might be achieved, and it constitutes a key challenge in contemporary neuroscience.

Different complex networks analyses have been used to study brain architecture and the relevant features of its emergent dynamic or functional states[153], rapidly revealing that both structural connectivity (SC) and functional connectivity (FC) networks exhibit a hierarchical organization of distinct brain modules (or areas) that communicate through connector hubs [150, 152, 73]. Hence, it was proposed that such a hierarchically compartmentalized organization is essential for segregation, while the existence of connector hubs and the presence of weak links between otherwise separated moduli facilitate the optimal balance between integration and segregation [152, 61] (Figure 3.1).

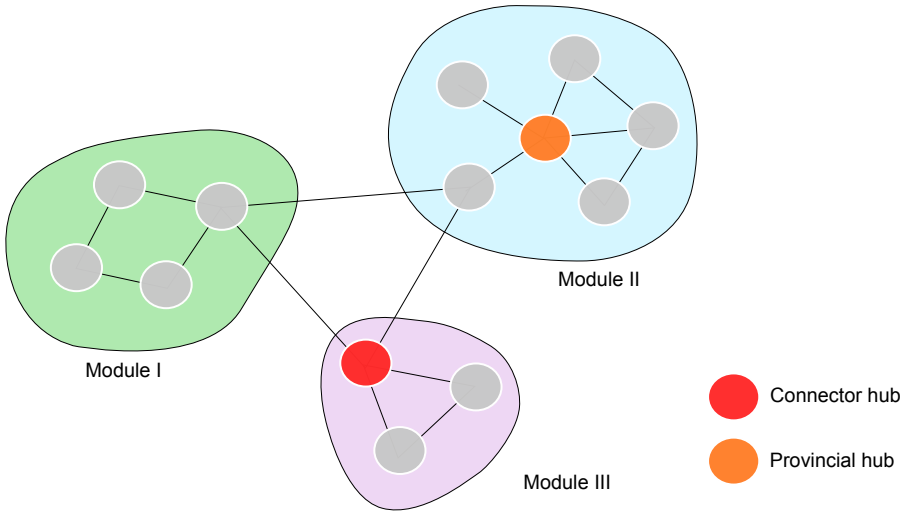

Figure 3.1: The modules in the network represent subsets of nodes with a high within-module connectivity and relatively low intermodule connectivity. Hub nodes are highly connected nodes in the network. We can find different types of hubs: (i) provincial hubs connecting nodes inside a module and (ii) connector hubs connecting several modules within the network.

The combined use of both anatomical connectivity and dynamic

models of neural activity to relate both SC and FC has grown over recent years [54, 26, 41, 74, 101, 106]. It seems clear that neural dynamics and any associated functions are necessarily constrained by the underlying wiring structure [39], although the precise relationship between SC and FC networks is still far from clear. One key problem when attempting to define such a relationship is that structure-function matching is actually a one-to-many mapping, meaning that for a given fixed anatomy, the functional repertoire needs to be vast in order to facilitate perception, action, memory, cognition and complex behaviours. Thus, bridging the gap between structure and function, and understanding how such a huge repertoire of functional brain states can emerge out from a fixed structure is one of the fundamental challenges in neuroscience (see e.g. [118] and references therein).

As a first step in this direction, several works have analyzed functional connectivity in the resting state, i.e. when the brain being monitored is not involved in any goal-oriented tasks. These analyses revealed consistent and robust"resting state" functional connectivity (rsFC) patterns across subjects [127, 52, 123]. Functional pairwise correlations turn out to be relatively strong between structurally connected nodes [84, 72, 70, 79, 77, 139, 159], yet more surprisingly, strong functional connections also appear commonly between distant regions that lack direct structural connections [70, 77], revealing the existence of strong indirect effects. To overcome this limitation, the authors in [77] first made a suitable selection of brain regions to calculate the correlation on individual links in those masks, showing an enhancement of SC-rsFC correlations. This observation suggests that over and beyond direct node-to-node and link-to-link pairwise comparisons, more collective or systemic analyses will be necessary to shed light on the relationships between SC and rsFC networks.

We propose here, following recent work adopting the same strategy [144, 14, 85], to shift attention to groups of nodes, and to contrast structural and functional networks by exploiting their hierarchical modular organization. More specifically, by employing the template of hierarchical modular organization derived from structural data to represent the resting state functional one and vice versa, we search for

the optimal common partition shared by structure and function by maximizing a novel quantity, that we dub "cross-modularity". Our hypothesis is that, if we assume that segregated functions are associated with distinct structural moduli, visualizing the rsFC data in terms of the natural structural moduli derived solely from network architecture (i.e. the SC) should help define and highlight how strongly structure constraints function. Conversely, the functional hierarchical-modular organization can be employed to visualize structural data. As such, these two complementary approaches should shed light on the intricate relationships between structure and function, and in particular, this procedure allows the extraction of an optimal partition illustrating that structure and function are much more tightly correlated than previously thought. The novel partition that we uncover here divides the brain into disjointed regions that we refer to as common "structure-function modules" (SFMs), representing a coarse-grained skeleton of the brain, which is largely shared by structure and function.

The obtained hierarchical atlas and the code to compute "cross-modularity" can be downloaded from:

`http://www.nitrc.org/projects/biocr_hcatlas/`

3.1 Subjects and data pre-processing

This work was approved by the Ethics Committee at the Cruces University Hospital; all the methods were carried out in accordance to approved guidelines. A population of n=12 (6 males) healthy subjects, aged between 24 and 46 (33.5±8.7), provided information consent forms before the magnetic resonance imaging session. For all the participants, we acquired same-subject structure-function data with a Philips Achieva 1.5T Nova scanner. The total scan time for each session was less than 30 minutes. For more details about scanning protocol refer to [45].

To analyze the diffusion weighted images we first applied the eddy current correction to overcome artifacts produced by changes in the gradient field directions of the MR scanner and subject head move-

ment. Using the corrected data, a local fitting of the diffusion tensor was applied to compute the diffusion tensor model at each voxel. Subsequently, a FACT (fibre assignment by continuous tracking) deterministic tractography algorithm [110] was employed to reconstruct white matter pathways in the brain (connecting grey matter regions).

The first volumes of functional MRI data were discarded for correction of the magnetic saturation effect, and the remaining volumes were first movement corrected and next slice-time corrected for temporal alignment. All voxels were spatially smoothed with a 6mm FWHM isotropic Gaussian kernel and after intensity normalization, a band pass filter was applied between 0.01 and 0.08Hz [33] , which was followed by the removal of linear and quadratic trends. We next regressed out the motion time courses, the average CSF signal, the average white matter signal and the average global signal. Finally, the functional data was spatially normalized to the MNI152 brain template. For more detailed explanation of the pre-procesing steps refer to Appendix A.

3.2 SC and FC networks

As defined in Chapter 1 the first step towards constructing a brain graph is to select the brain regions of interest. Using all the brain voxels to compute the graph is computationally very expensive. We decided to parcellate the brain based on the similarity of the functional activity of the voxels. We applied the method of spatially constrained clustering to functional data over the subjects (n=12) in order to extract the regions of interest (ROI), as explained in [37] and allowing for the generation of common ROIs. A spatial constraint is imposed to ensure that the resulting ROIs are spatially coherent and clustering was performed based on temporal correlations between voxel time-series. To cluster at the group level, a 2nd−level approach was applied in which the single subject data was first clustered and then all the subjects data were combined to perform a second clustering. After the spatially constrained clustering, we obtained a parcellation of 2514 ROIs including both cortical and subcortical regions.

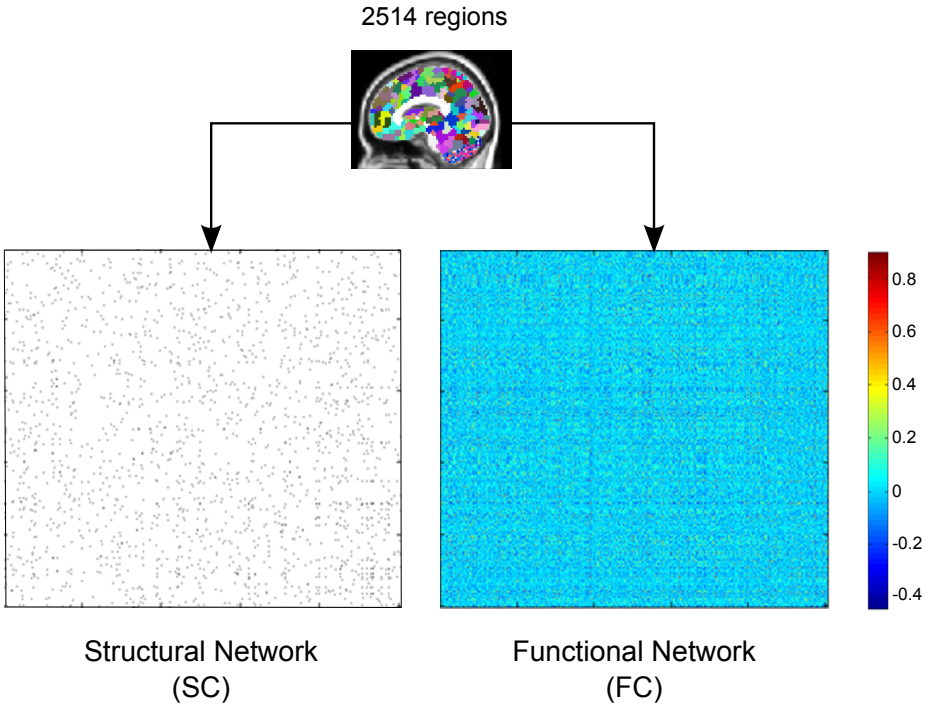

Figure 3.2: Using the 2514 brain regions of the resulting atlas we compute functional and structural matrices. SC matrix is represented in black and white; with each black dot representing the existence of at least one fibre connecting 2 regions. Functional connectivity matrices are displayed in color according to the strength of the functional connection between 2 regions (standard correlation).

This atlas was applied to obtain a 2514x2514 structural and functional matrix per subject (Figure 3.2).

Although the two datasets are acquired from the same subject, it is noteworthy that the two (FC and SC) networks are obtained independently, and they constitute two separate and autonomous datasets correlated to different physical and physiological mechanisms, and corresponding to distinct measures acquired and post-processed in a different manner. To focus on generic aspects and not on indi-

vidual singularities, we obtained the mean SC and FC networks by averaging the individual matrices of the subjects.

As a preliminary analysis, following standard approaches, we measured the Pearson correlation coefficient (r) between the averaged structural and functional matrices [72, 79]. This provided a link-to-link comparison between the two networks and gave an overall value of about r=0.2, indicative of a rather weak correlation between SC and FC matrices. By restricting the measurement to existing physical links, this value increased to a moderate value of r=0.3 and it can be augmented a little further by comparing only pairs of nodes within (but not between) structural moduli (see below for a proper definition and evaluation of moduli).

3.3 Hierarchical modularity

Modularity is one graph measure designed to quantify the performance of a network division into modules (also called groups, clusters or communities). If we compute the modules and reorder the adjacency matrices we can observe how the brain is organized in communities with similar profiles (Figure 3.3). Networks with high modularity have dense connections between the nodes within modules but sparse connections between nodes in different modules.

To detect these modules or communities we have to perform clustering to detect similar regions in the brain. To group the different regions of the brain in communities based on their similarity we need to define:

- **Brain region descriptor**. To determine if two brain regions are similar we need to compare some of their features. There are different features one can use to describe a brain region. For this work we decided to use how each region connects to the rest of the brain as a descriptor of the brain area. As a result of dividing the brain into 2514 regions, each region will be described by how it is connected to each of these 2514 regions.

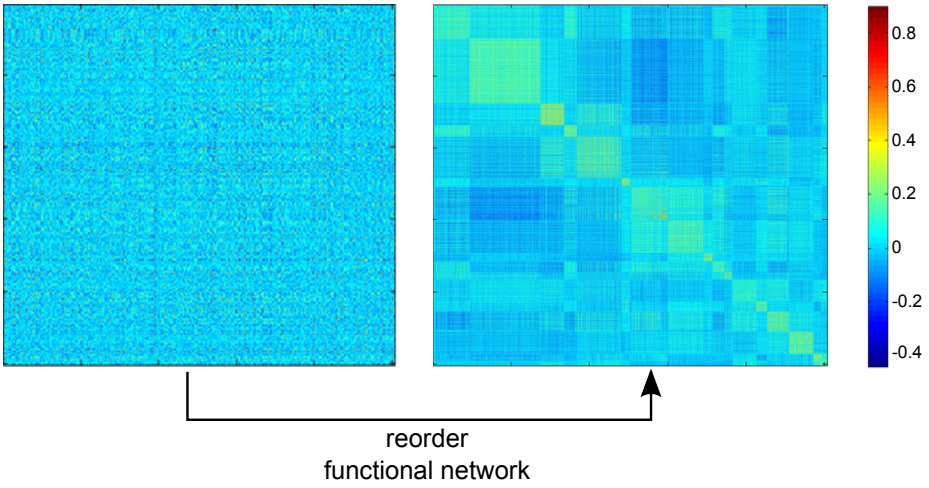

Figure 3.3: Reordering the FC based on similar regions we can observe how the brain organizes in to modules.

- **Similarity distance**. Once we decided the descriptor that defines each brain region we need a similarity measure to define how similar the different regions are. For small values of connectivity, the cosine distance, measuring the cosine of the angle between the 2 vectors, is a good choice for measuring the similarity.

Once we define the descriptor and the distance we can apply different clustering algorithms; we decided to use standard hierarchical agglomerative clustering (HAC) [133, 107, 50]. Normally clustering algorithms do not provide the optimal number of clusters in our data, so in our case we computed clustering for different numbers of communities and we evaluated which was the optimal one. As a result of having a 2514 ROIs partition we computed different partitions ranging from 1 to 2514 communities.

To find functional communities we used the FC matrix for the clustering. After the first step of applying hierarchical clustering, the similarity between all the 2514 regions is calculated and the most

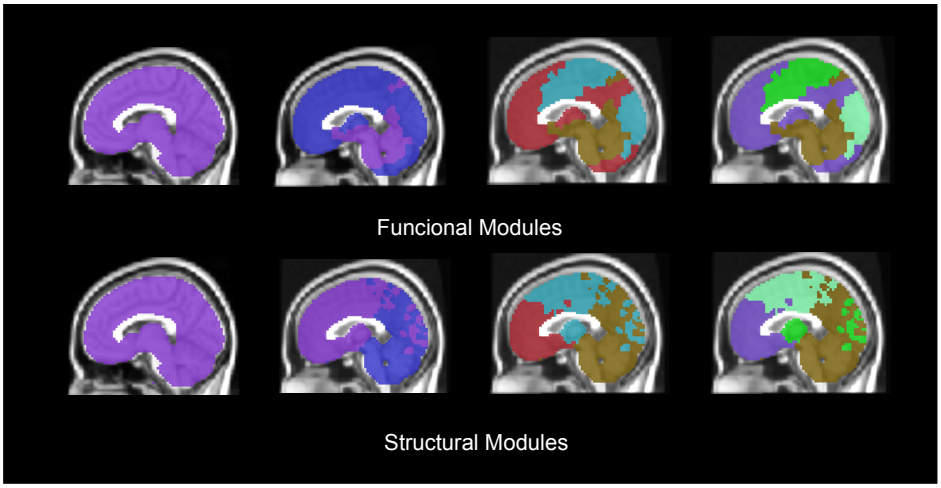

Figure 3.4: Hierarchical clustering of FC and SC data.

similar 2 regions are merged, resulting in a parcellation of 2513 regions. Next, after second step, the similarity between the remaining 2513 regions is calculated and again the most similar 2 communities are merged, obtaining a parcellation of 2512 regions. This procedure continues until the level of an individual ROI. During this process, we save all the intermediate parcellations of the hierarchical tree. This approach enables a hierarchical tree or dendrogram to be constructed in which nodes are progressively merged together into modules following a nested hierarchy of similarity. Cutting this tree at any arbitrary level leads to a pooling of the initial 2514 ROIs into a finite number of modules (M) that can be tuned by varying the depth of the cut. In Figure 3.4 we can see the brain as a unique module, then divided in 2 modules (the 2 most different modules in the brain regarding to their connectivity). The first row shows the first 4 levels of the tree of functional data and the second row for the structural parcellation. This hierarchical division of the brain allows us to study the brain at different levels where the lower part of the tree (smaller regions) perform individual tasks and they interconnect in higher levels of the tree to form more complex tasks.

3.4 SC-FC similarity at module level

A partition inferred exclusively from functional measurements leads to an excellent ordering of the structural/wiring data, allowing for a good organization and visualization of structural moduli (Figure 3.5). Conversely, employing an optimal partition for the SC network (i.e. the one with maximal Newmans modularity Q) entails quite a large modularity for the averaged FC matrix.

This simple observation constitutes an important finding: both FC and SC networks display high modularity (as already acknowledged) but with a previously unnoticed yet excellent match between functionally and structurally identified modules. As an example to illustrate the excellent matching between structure and function see Figure 3.6 showing a single module; it consists of different functionally correlated subregions (marked in red) which apparently are physically far from each other; however, they can be observed to be wired together by fibre bundles, forming a coherent, though de-localized module.

This observation, structural modules matching functional ones, implies that most of the aforementioned indirect effects observed in the resting-state reflect functional correlations that stem from the existence of modules. That is, most of the functional pairwise node-to-node correlations that cannot be explained by direct structural connectivity can be accounted for by their corresponding nodes lying in structurally connected moduli, even if the specific nodes lack direct wiring.

3.5 Cross-modularity index

To quantify the striking observation that a common partition into modules or communities describes both the FC and SC data remarkably well (Figure 3.5), we introduced an index X called "cross-modularity". The cross-modularity is based on:

- **SC-FC Similarity**: For each module of a given partition, the similarity between the corresponding sub-networks of SC and

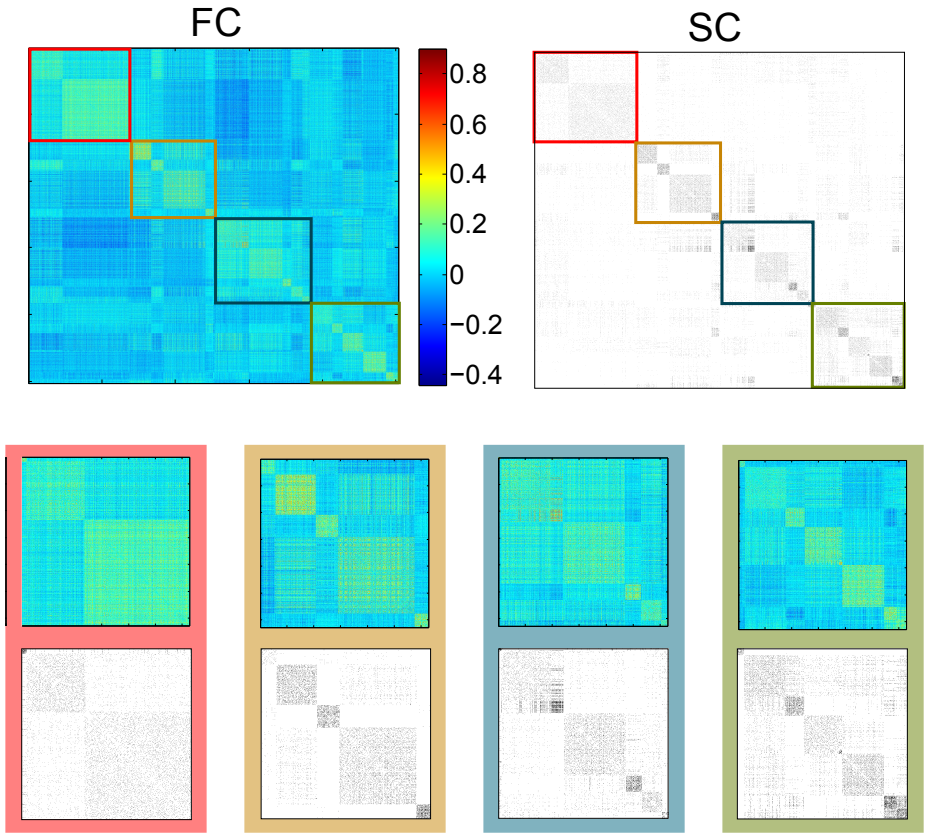

Figure 3.5: FC and SC matrix reordered to show the 20 modules found clustering functional data. To better appreciate the similarities between SC and FC different zooms of the top matrices of these regions are shown.

FC was calculated using the Sorensen index [148]. The Sorensen index accounts for the similarity between two binary networks (it is defined as twice the number of common edges shared by the two modules divided by the total number of edges in the two modules). To compare if SC and FC have the same links in each module we need to binarize both FC and SC. We can observe

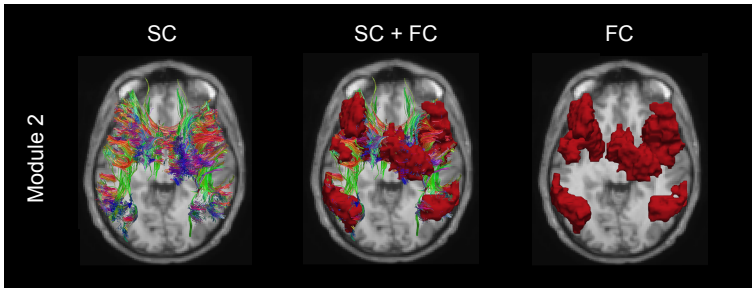

Figure 3.6: Brain regions corresponding to module 2 are shown in red. These sparse regions are connected by the underlying structure of the brain. To see the fibre bundles and the regions of the rest of the modules refer to [45].

in Figure 3.5 that the SC matrix is very sparse while the FC is almost fully connected. To make FC more sparse to be comparable with SC, we searched for a appropriate threshold to decide which links to remove. We chose the threshold that maximizes the Sorensen similarity between SC and FC. First we took the absolute value of FC matrix and we normalized the SC to values between zero and one. Next, we introduced two thresholds ranging from [0,1], α for FC and β for SC, to binarize each FC or SC matrix according to whether a value was higher than the threshold, in this case the matrix element was equal to one (zero otherwise). For each module we then calculated the Sorensen index as a function of α and β. Figure 3.7 represent the similarity for the different partitions maximizing α and β (typical values were about $\alpha = 0.45$ and β very close to zero). Finally, we calculated the mean similarity across all modules. Notice that it is possible to address two different similarity values: i) computing HAC in FC data and accordingly reordering the SC (blue line in Figure 3.7). Looking to the modules defined by the functional connectivity and after searching if those clusters lead to structural modules in the SC data. ii) computing HAC in SC and reordering the FC, is represented by the red line in Figure 3.7.

- **Modularity**: The Newman algorithm [111] was used to address modularity for a given brain partition. If M is the number of modules in the partition, modularity was calculated by $Q = \sum_{i=1}^{M}(e_{ii} - a_i^2)$, where e_{ii} is the fraction of links connecting two ROIs that belong to the same module and a_i is the fraction of links that connect a ROI from module i to other modules (Figure 3.7). Thus, partitions maximizing the within-module links and minimizing the between-modules links have high modularity values.

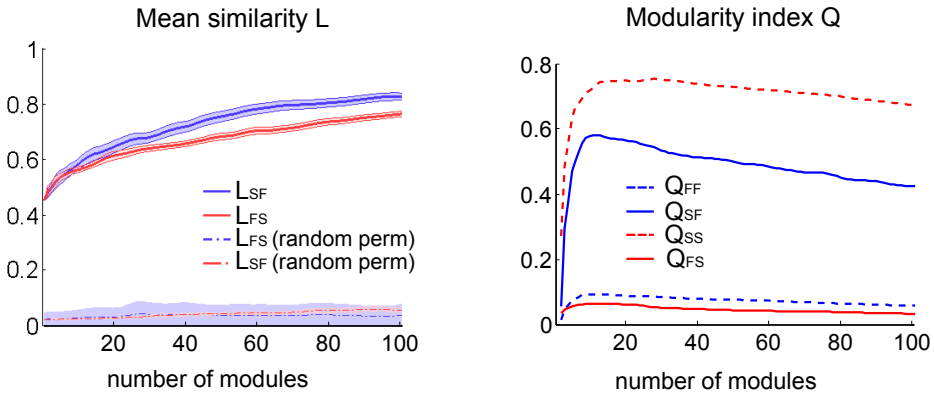

Figure 3.7: Similarity (L) and Modularity (Q) between FC and SC.

We introduced the cross-modularity X to quantify both the topological similarity between FC and SC, and the individual modularities in FC and SC. Taking the HAC ordering in FC and reordering the SC, we defined cross-modularity between SC and FC as

$$X_{SF} = (Q_{FF}Q_{SF}\overline{L_{SF}})^{\frac{1}{3}}$$

where $\overline{L_{SF}}$ is the mean similarity for all modules of the given partition, and Q_{FF} and Q_{SF} are the modularities of FC and SC, respectively (previously ordered with the HAC ordering of FC). Similarly, taking the HAC ordering of SC and reordering the rsFC, the

cross-modularity is:

$$X_{FS} = (Q_{SS}Q_{FS}\overline{L_{FS}})^{\frac{1}{3}}$$

The cross-modularity is large for a given partition if the corresponding Newmans modularities of the two matrices under comparison are large and there is also a large within-module similarity between both divisions (i.e. a large fraction of existing intra-module links are shared by both networks). Thus, a large cross-modularity value indicates that, using a given common partition, both matrices are highly modular and, at the same time, the moduli are internally wired in a similar way.

3.6 Structure-Function modules

A maximization of the cross-modularity X across possible partitions allows the finding of an optimal structure-function brain partition. Indeed, through this novel index, we found that the partition into 20 moduli derived from FC data (as portrayed in Figure 3.5) is optimal (Figure 3.8), although similar quality partitions can be obtained in the range of M from 10 to 30. The reason why the cross-modularity index is almost constant in this interval is that there is an overall balance between two opposing effects, both of them occurring when M increases: (i) the increase in the similarity between SC and FC (see Figure 3.7) and (ii) the decrease in Newman's modularity produced by an increase of inter-module connections and a decrease of intra-module connections (Figure 3.7).

The modular decomposition of the brain proposed here is quite robust across subjects: evaluating the corresponding cross-modularity, using each individual SC, leads to similar patterns to those obtained using the SC averaged over the the N=12 subjects. Moreover, it was also notable that slightly larger cross-modularity values (about 4% higher) were obtained using moduli derived from the FC to study the SC than vice versa and thus we focus on the first choice.

The brain partition for M=20 is described anatomically in [45], illustrated in figures 3.9 and 3.10. When looking at the spatial dis-

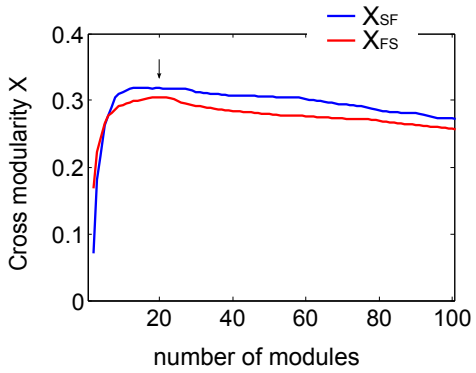

Figure 3.8: Cross-modularity for brain partitions of different sizes, varying from 1 (the entire brain) to 100 modules. The cross-modularity increases when either the topological moduli-similarity between FC and SC increases or if the individual modularity in FC or SC does. A stronger cross-modularity between FC and SC was achieved by applying the HAC to the FC data (blue curve XSF) rather than to the SC (red curve XFS). The arrow at M=20 indicates that at that point, both the blue and red curves are well represented in the hierarchical agglomerative clustering, with an optimal cross-modularity index.

tribution of SFMs, a high degree of symmetry exists between the two hemispheres in most of the modules (e.g. modules 3, 6 and 12). Observe, for example, in Figure 3.6, that moduli composed of segregated islands -characterized by correlated functional activity– have always structural connections bridging them, thus providing the possibility of functional cohesion.

Remarkably, the agreement between FC and SC was systematically better when the averaged across-subject matrices were used rather than those obtained on single subjects, which nevertheless remained high. This illustrates the robustness of the obtained partition, which is preserved despite of the existence of individual specific traits.

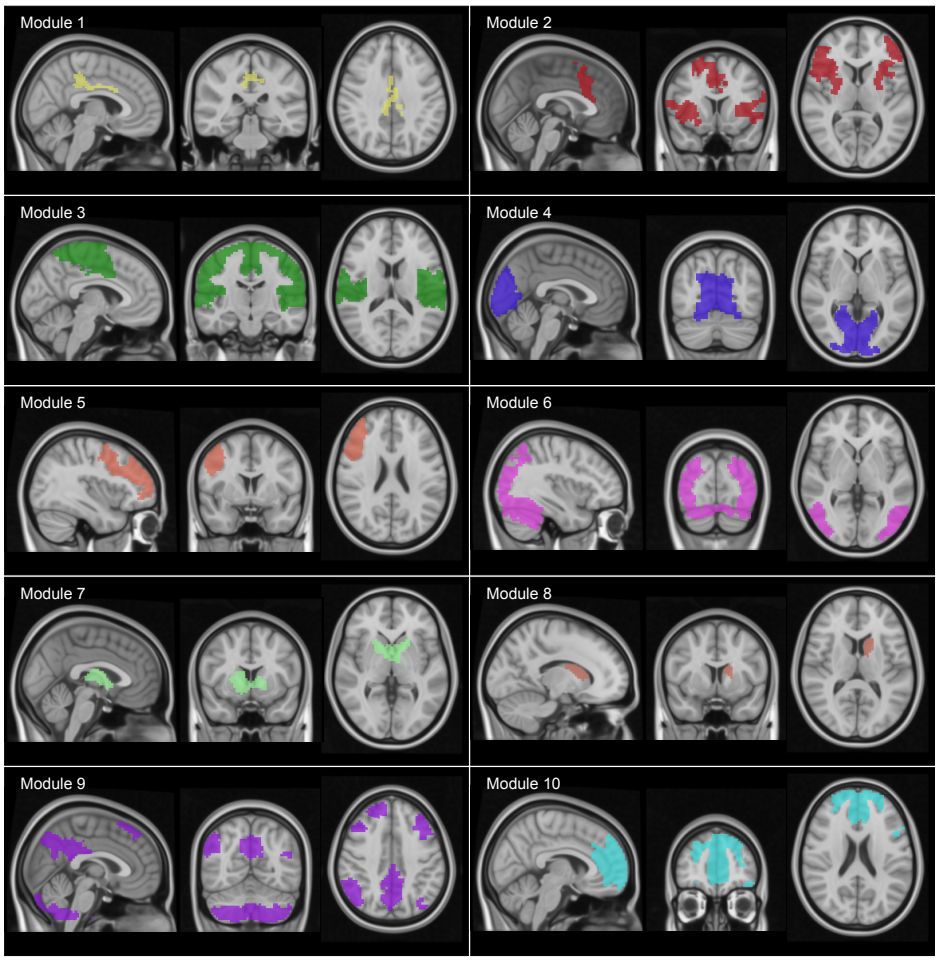

Figure 3.9: A brain atlas of 20 SFMs that maximizes the cross-modularity index (here only represented modules from 1 to 10, and similarly, Figure 3.10 showing modules from 11 to 20). These networks were obtained by identifying the 20 modules in the FC matrix. Note that some of the modules are composed of spatially separated brain regions (e.g. number 2, 9 in Figure 3.9 and 12, 14, 16, 17 and 18 in Figure 3.10).

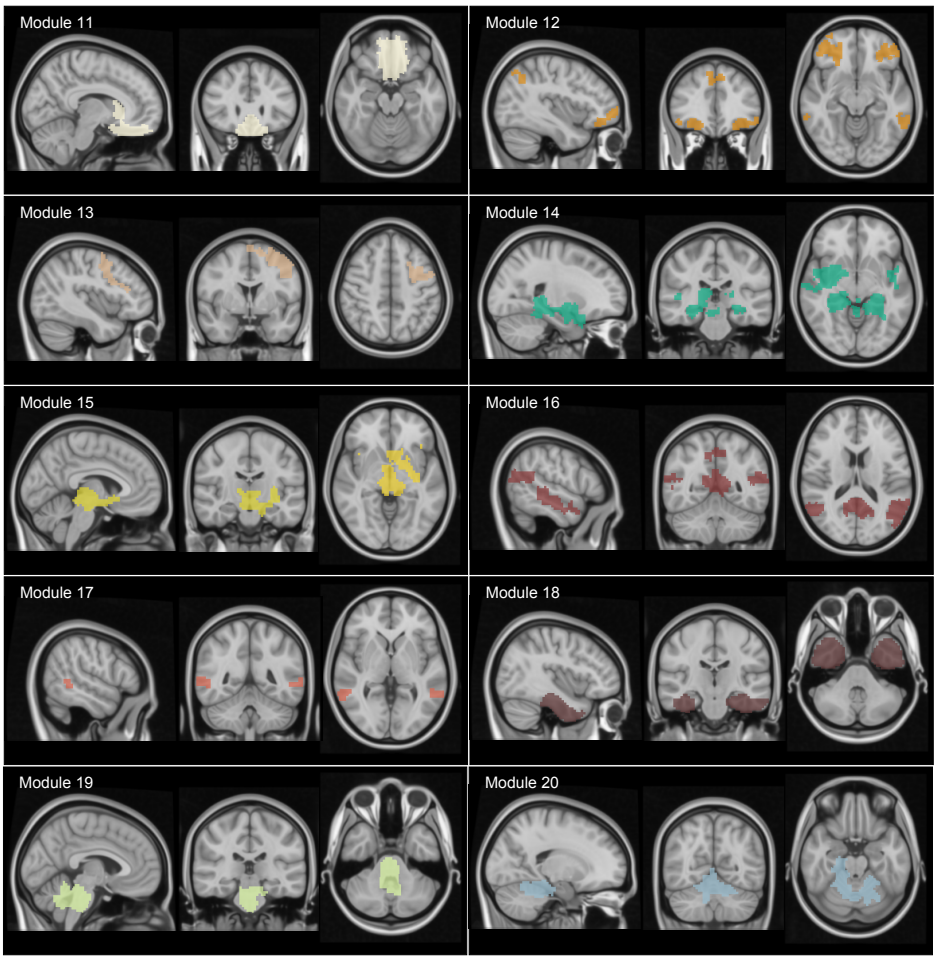

Figure 3.10: A brain atlas of 20 SFMs that maximizes the cross-modularity index (here only represented modules from 11 to 20, and similarly, Figure 3.9 showing modules from 11 to 20). These networks were obtained by identifying the 20 modules in the FC matrix. Note that some of the modules are composed of spatially separated brain regions (e.g. number 2, 9 in Figure 3.9 and 12, 14, 16, 17 and 18 in Figure 3.10).

3.7 Anticorrelations in SFMs

Whilst all the moduli in SFMs appear to be internally correlated, strong inter-module anti-correlations also exist with a pronounced modular structure. This observation becomes even more evident when plotting just the sign of the functional correlation in SFMs (see Figure 3.11: red for positive correlations; blue for anti-correlations; and green for values close to zero, i.e. ranging between -0.1 and 0.1). This not only reveals that all SFM resting-state moduli are internally correlated but many of them tend to be anti-correlated with others. In particular, our results showed that modules 9 and 10 are positively correlated with one another, and that both modules are strongly anti-correlated with module 3 (and more weakly with other modules), which is a module that strongly overlaps with the sensory-motor task-related network (see Figure 3.12). Whilst the existence of anti-correlations in resting state networks (over and above processing artifacts) has been the subject of some debate [79], it is now well-established that anti-correlations are inherent to resting state functional networks. In particular, it has been shown that the strongest anti-correlations are mediated by the default mode network (DMN), particularly with task performing areas [53]. This is indeed consistent with our results, as modules 9 and 10 (those with the strongest anti-correlations) overlap significantly with the DMN (see Figure 3.12).

3.8 SFMs and common brain partitions

We asked whether SFMs bore any resemblance (measured as percentage overlap) with other macro-scale brain parcellations commonly found in literature, which typically are based solely either on function or on structure (whilst SFMs aim at describing both). The percentage overlapping was addressed using the Sorensen index as defined previously for similarity. Statistical significance was addressed by generating 100 random permutations of a given brain partition and the p-values were calculated by the cumulative distribution of the

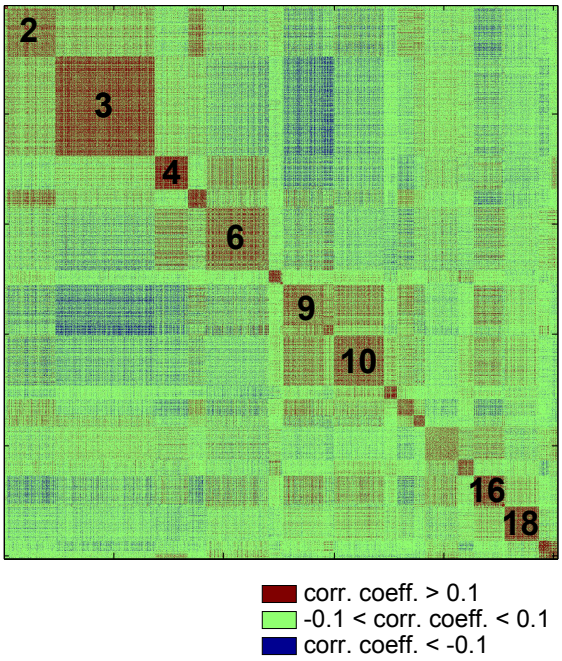

Figure 3.11: The figure shows that SFMs are internally correlated (red) and that many of them tended to be anti-correlated with others (blue). Black numbers are indicating SFM number for reference purposes.

Gaussian distribution. Only similarity values with a p-value less than 0.05 were considered.

3.8.1 Overlap between SFMs and AAL brain partition

First, we analyzed the overlap between SFMs and the brain regions belonging to a structural atlas, the automated anatomical labeling (AAL) [161], assessing the results for the 45 AAL homologue areas and for our 20 modules partition (i.e. SFMs, figures 3.12). Examining the overlap between SFMs and AAL brain areas, we found that different anatomical areas are included in a single SFM (i.e. a column

of the matrix), clearly highlighting how SFMs (that underlie different brain states at resting conditions) simultaneously recruit distinct brain circuits. Conversely, the same area of the AAL (the row of the matrix in Figure 3.12) might be included in several SFMs, highlighting the anatomical overlap of the latter. Such observations do not depend significantly on the number of modules composing the partition, since the overlap between a single AAL area and a single SFM never approaches a unitary value (Figure 3.12). Some AAL areas evidently have a strong overlap with the M=20 modules (e.g. SFM 11 and the Rectus gyrus, or SFM 16 and the Temporal middle gyrus, Figure 3.12), indicating that such anatomical areas might have a much more relevant functional role than previously believed in comparison to other AAL areas. Moreover, both the Rectus gyrus and Middle temporal gyrus seem to be functionally represented on a smaller scale as the overlap between them remains high as the number of modules increases (Figure 3.11). Other areas are also functionally represented on a smaller scale (e.g. the Thalamus, approx. M=40 onwards).

3.8.2 Overlap between SFMs and RSNs

In a similar way, we compared the well studied Resting State Networks (RSNs), a brain functional atlas constructed using independent component analysis of functional data [127, 52, 123, 10], to the M=20 brain partition of SFMs (Figure 3.12). Two RSNs display a strong overlap (>0.5) with two distinct SFMs, the "Sensory motor" with SFM 3 and"Medial visual" with SFM 4, while the other RSNs overlap with more than one SFM. Irrespective of the number of modules imposed on the FC matrix (Figure 3.12), we did not observe a complete overlap between RSNs and SFMs, in part due to the fact that SFMs are distinct to RSNs but also, to the large inter-subject variability that exists in the shape of each individual RSN.

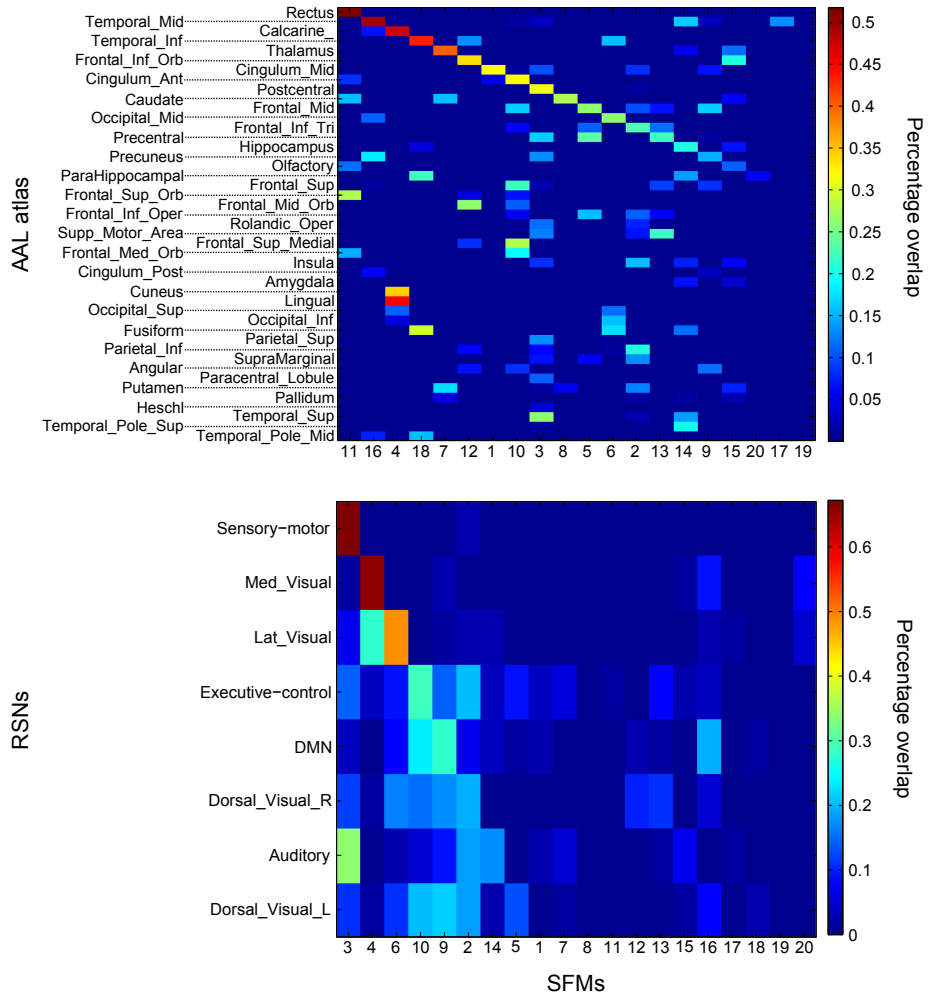

Figure 3.12: Percentage overlap of SFMs with the anatomical brain partition described in the AAL atlas and the Resting State Networks.

3.8.3 Overlap between SFMs and Broadmann areas

Similar results to those for the AAL and RSNs were also observed but for Brodmann areas, characterized by known neuro-psychological

functions based mainly on lession / post mortem studies, Figure 3.13. Indeed, Brodmann area number 18 is well-characterized by SFM 4 and Brodmann area 20 matches to SFM 18. Moreover, when the number of the modules in the partition increases, Broadmann areas 18, 20, 11, 10, 19 and 21 are represented by SFMs.

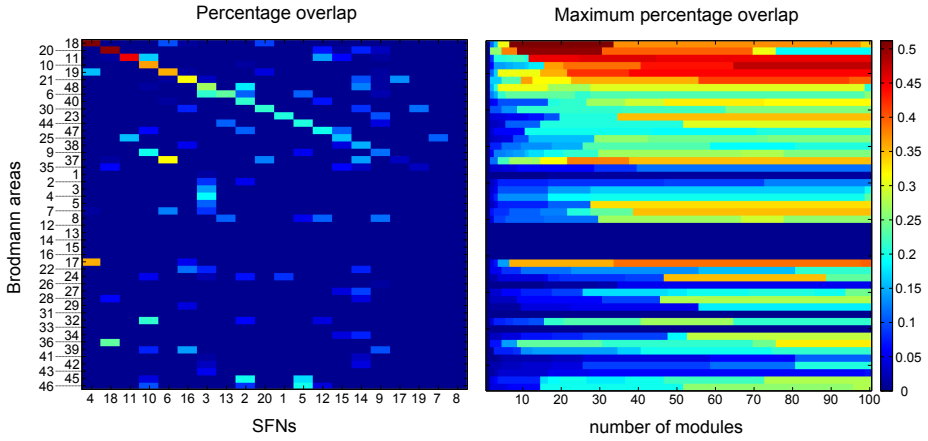

Figure 3.13: Percentage overlap of SFMs and the Broadmann areas.

3.9 SFMs: Final considerations

SFMs (i) represent a distinct brain partition from those previously described in literature; (ii) incorporate distinct both structural and functional brain regions into a single operative network/unit; and (iii) can overlap and share both anatomical and functional brain regions. In the same way as alterations in resting state networks have been reported in several brain pathologies and diseases, we expect that the use of the new brain partition represented by SFMs, with simultaneous focus on structure and function, might help also in diagnosing disease.

We hypothesize that since we are looking at the same entity, i.e. the brain, it is reasonable to expect that a brain partition (common

to both structure and function) might exist, but to the best of our knowledge, such partition has not yet been found. Indeed, different authors [54, 26, 41, 74, 101, 106, 72, 70, 79] have shown that brain activity cannot be simply inferred from the underlying structural network of interconnections, i.e. that functional and structural networks are very different objects. On the other hand, recent studies suggest a stronger relationship between the structural and functional network. For instance, both of them have been found to share a strong rich-club structure, meaning that moduli are interconnected through some local hub connectors and that such hubs are highly connected among themselves [163]. Another recent work has emphasized that resting-brain functional connectivity can be predicted by analytic measures of network shortest communication pathways [66], which strongly support that SC and FC are highly related to one another.

The partition we have elucidated here is the one maximizing the values of cross-modularity; however, there is a band with nearly constant values of the cross-modularity such that all the partitions within it are also plausible. Thus, in that plateau slightly different partitions (with 10 to 30 moduli) can be inferred, all of them describing similarly the structure-function interplay.

In our analysis, the asymmetry between the two strategies, structure following function (SF) and function following structure (FS), comes from the intrinsic differences between the two data sets (e.g. the structural network is sparse, whilst the functional network is dense). A more integrated method, considering both sources of recording together, would deal with the general problem of developing effective algorithms to optimize cross-modularity (e.g. by modifications of existing methods for modularity optimization). Although we are aware this is a challenging and interesting problem, it is beyond the aim of the current work.

It is important to emphasize that here, we have applied a data-driven approach, and no further assumptions have been made to obtain the novel brain partition. Two reasons might justify the differences we found in comparison with other existing partitions. First, and more importantly, most of the previous approaches considered

the number of subcortical regions either absent or accounting for less than 20% of all ROIs, see [38] and references therein. Here, we have incorporated both FC and SC data belonging to all subcortical structures (including amygdala, hippocampus and cerebellum). Second, all previous partitions were obtained looking solely at either SC or FC data but we, for the first time, have integrated the two data sets to force modules in the brain partition to be relevant to both structure and function.

In summary, our results show that when trying to correlate brain structure with function, a clear structure-function matching emerges when applying a hierarchical modular approach; that is, pooling brain regions of interest into more densely connected modules rather than scrutinizing the similarity at the level of individual links.

3.10 Future work: Localising neurosurgery targets

In this chapter functional and structural connectivity properties have been used to localize different brain regions. This technique might have an important impact for the localization of neurosurgery targets for presurgery planing. Several works have use functional connectivity analyses for neurosurgery, neurooncology, epilepsy surgery and deep brain stimulation [86].

As suggested by [86], resting state functional connectivity analysis may be used preoperatively to localize areas of eloquent cortex, to provide prognostic information by suggesting the degree of morbidity resulting from removal of specific areas of brain tissue and to inform surgeon of safe maximal resection boundaries.

In those cases where the patient can not perform a task inside the scanner additionally functional connectivity in resting state can identify high relevance areas in the brain for surgical planing. We can extract auditory and fronto-parietal left networks with high relevance in language function, the Default Mode Network and sensorymotor network.

Structural connectivity has also proven an important role for detecting neurosurgical targets. For example in [122] individualized thalamic structural connectivity was used for targeting a patient-specific therapeutic thalamic target for the treatment of tremor. This novel thalamic targeting approach is based on identifying the thalamic region with the highest probability of connectivity with premotor and supplementary motor cortices. This approach may prove to be advantageous over traditional preoperative methods of indirect targeting, providing patient-specific targets that could improve the precision, efficacy, and efficiency of deep brain stimulation surgery.

Chapter 4

Information flow between Resting State Networks in Alzheimer Disease

In Chapter 2 we extracted the activity in a given region computing the mean activity of all the voxels within that region. Computing the mean functional activity of a specific region can lead to a loss of information of the activities performed by this region. In this chapter we will use Principal Component Analysis to analyse more components of the brain within a given region and we will compute a new measure of information flow that uses these extra components. This technique will be used to study the information flow between Resting State Networks of the Brain in Alzheimer's Disease (AD).

The overall brain dynamics generated at rest can be decomposed as a superposition of multiple activation patterns, the so-called Resting State Networks (RSNs). Becoming a fundamental characteristic of brain function, RSNs are a pivotal element for understanding the dynamics and organization of the brain basal activity in health and disease [127, 52, 123, 124, 126]. RSNs emerge from the correlation in signal fluctuations across brain regions during resting state, a condition defined by the absence of goal-directed behavior or salient stimuli. Despite the simplicity of the context in which these brain activity patterns are generated, RSNs dynamics is rich and complex. Differ-

ent RSNs have been associated to specific cognitive networks (Figure 4.1) e.g. there are visual networks, sensory-motor networks, auditory networks, default mode networks, executive control networks, and some others (for further details see for instance [10] and references therein).

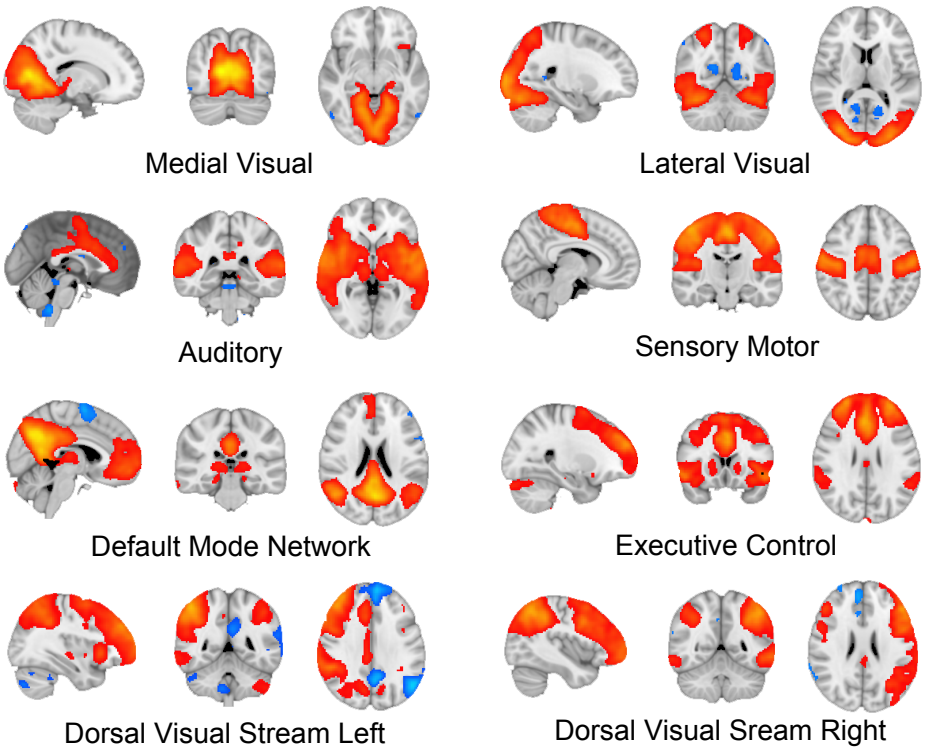

Figure 4.1: Eight Resting State Networks associated with specific cognitive networks.

Currently, it is well-established that a number of techniques, like Region-Of-Interest approach (ROI; seed-based), Independent Component Analysis (ICA) and Partial Least Squares (PLS), can decompose the resting state functional magnetic resonance images (rs-fMRI) to provide such RSNs [12, 11, 10, 103, 168]. Using these techniques, altered functional connectivity in specific RSNs has been described in

brain pathological conditions such as in patients with deficit of consciousness after traumatic brain injury [21, 113, 76, 98], schizophrenia [165, 83] and epilepsy [94]. In the particular case of Alzheimer's Disease (AD), the pathology we have addressed here, starting from the pioneer contribution showing alterations in fMRI [91], has been reported a decrease of functional connectivity in the Default Mode Network (DMN, a RSN related to memory function) and in the salience network at both early and advanced stages of the AD [69, 131, 15, 143].

Despite this emphasis on specific networks, it is important to realize that the RSNs functional-division into separate systems does not imply that the brain activity is composed of functional networks working in isolation [40]. Contrarily, the brain regions underlying the inter-RSNs relations have their independent organization and have a different function from the specific ones that each individual RSN has (for recent reviews see [51, 147]). These interactions between brain regions belonging to different RSNs have been described by means of whole-brain connectivity analysis techniques like graph analysis [149, 128, 154, 24], and more recently, where connectivity was also analyzed during different cognitive task conditions [104].

However, the analysis and interpretation of information flow (IF) between the RSNs remains an open question and has given rise to two contrasting theories attempting to interpret the resting brain activity. The functional integration theory (for review, see [168]) proposes that brain activity during resting-state requires the coordinated activity of all brain RSNs to support the reconstruction, analysis and simulation of experiences or possible scenarios to provide adaptive behavioral advantage. On the other hand, the functional segregation theory states that modality-specific mental activity (e.g. image- or language-based thoughts) is related to functional disconnection between the brain networks active during rest [42]. Therefore, resting activity would be maintained by functionally segregated inner-oriented and sensory-related cognition and the respective intrinsic and extrinsic brain networks they depend on.

The question of how different RSNs speak to each other is particularly relevant as the existence of disease-driven changes in func-

tional connectivity between different brain networks has been reported [134, 136]. Importantly, as the disease progresses, responsible RSNs are in turn affected, and this gradual loss of functional connectivity within networks is accompanied by a loss of functional correlation between them [23]. This indicates that altered functional activity induced by a local dysfunction might influence the functioning of additional brain regions, leading to the spread of changes in brain activity beyond the network originally affected and in turn the whole-brain functional connectivity pattern [134].

Here we propose a new method to study RSNs inter communication. The method is based on the inference of IF in terms of Transfer Entropy (TE) to study Directed Functional Connectivity (DFC) between RSNs[1]. To show one potential application of this method, we apply it to a dataset of AD patients from the Alzheimer's Disease Neuroimaging Initiative (ADNI) and compared the results of inter-RSNs communication with a group of healthy subjects (remark that the method is general and can be applied to any other disease).

4.1 Subjects and data pre-processing

4.1.1 ADNI

Data used in the preparation of this work were obtained from the ADNI database (adni.loni.ucla.edu). ADNI was launched in 2003 by the National Institute on Aging (NIA), the National Institute of Biomedical Imaging and Bioengineering (NIBIB), the Food and

[1]For brain connectivity studies, there exist different approaches for DFC [67, 137, 59, 120, 130, 8, 99, 58, 22, 57]: Dynamic Causal Modelling (DCM), addressing how the activity in one brain area is affected by the activity in another area using explicit models of effective connectivity (for details see [59, 120]). Alternatively, data-driven approaches for DFC work directly with the time-series, and not any further assumption have to be taken, neither about the hemodynamic response, nor about the biophysics from individual neuron to Blood Oxygen Level Dependent (BOLD) level. Two popular data-driven methods for calculating DFC are Granger causality (GC) [67] and transfer entropy (TE) [137]; for the Gaussian approximation the two methods are equivalent [8].

Drug Administration (FDA), private pharmaceutical companies and non-profit organizations, as a $60 million, 5-year public-private partnership. The primary goal of ADNI has been to test whether serial MRI, PET, other biological markers, and clinical and neuropsychological assessment can be combined to measure the progression of Mild Cognitive Impairment (MCI) and early AD. Determination of sensitive and specific markers of very early AD progression is intended to aid researchers and clinicians to develop new treatments and monitor their effectiveness, as well as lessen the time and cost of clinical trials.

The Principal Investigator of this initiative is Michael W. Weiner, MD, VA Medical Center and University of California - San Francisco. ADNI is the result of efforts of many co-investigators from a broad range of academic institutions and private corporations, and subjects have been recruited from over 50 sites across the U.S. and Canada. The initial goal of ADNI was to recruit 800 subjects but ADNI has been followed by ADNI- GO and ADNI-2. To date, these three protocols have recruited over 1500 adults, ages 55 to 90, to participate in the research, consisting of cognitively normal older individuals, people with early or late MCI, and people with early AD. The follow up duration of each group is specified in the protocols for ADNI-1, ADNI-2 and ADNI-GO. Subjects originally recruited for ADNI-1 and ADNI-GO had the option to be followed in ADNI-2. For up-to-date information, see www.adni-info.org.

4.1.2 Subjects and data pre-processing

The analysis was performed on n = 10 healthy subjects as control (5 males, 5 females, 73.70 ± 1.16 years old) and n = 10 AD patients (5 males, 5 females, 73.40 ± 1.08 years old) and both data sets were downloaded from the ADNI database.

Notice that rather than increasing the population size to a very large number, we preferred to select two small populations but choosing them the most balanced as possible with regard to age and gender. Demographic data (including the ADNI identifier) are given in Tables 4.1.

Resting State Functional Magnetic Resonance and anatomical

Table 4.1: Demographic data

AD Patients			**Healthy Subjects**		
ADNI ID	sex	age	ADNI ID	sex	age
002_S_5018	M	73	006_S_4485	M	73
006_S_4867	M	75	006_S_4150	M	75
018_S_4696	F	73	002_S_4262	F	73
018_S_5074	F	75	002_S_4270	F	75
100_S_5106	M	74	012_S_4026	M	74
130_S_4641	F	74	002_S_4264	F	74
130_S_4984	F	73	018_S_4349	F	73
130_S_5059	M	73	018_S_4400	M	72
136_S_4993	F	72	031_S_4032	F	72
006_S_4546	M	72	002_S_4225	M	72

scans were acquired (for more information about scanning protocol refer to [46]).

Data were motion corrected and smoothed using a Gaussian Kernel of 6 mm FWHM. After intensity normalization, a low-pass filter was applied within the slow fluctuations range of (0.01-0.1 Hz) that characterizes the resting state BOLD activity. Next, linear and quadratic trends were removed. Finally motion time courses, white matter signal, cerebrospinal fluid (CSF) signal and global signal were regressed out from the data.

4.2 Interaction between RSNs

4.2.1 ROIs definition from RSNs masks

The first step is to select the regions of interest to be studied. In this work we defined each ROI as the voxels belonging to each RSN, by using the masks reported in [10] and illustrated in Figure 4.1. Notice that we are not dealing with the independent components per se, but

with the multivariate activity of all the voxels time-series localized within the masks. Similar approaches, considering the RSNs masks rather the independent components per se, have been used before in previous work [155, 31, 74, 156]. Specifically, we have used the following eight RSNs: medial visual, lateral visual, auditory, sensory-motor, default mode, executive control, dorsal visual right, dorsal visual left (Figure 4.1). Once we defined the ROIs we extracted all the rs-fMRI time-series belonging to all the voxels in each RSNs.

4.2.2 HRF blind deconvolution

As pointed out in Chapter 1, fMRI measures the hemodynamic response in the brain, an indirect measure of the neural activity, but for computing information flow between regions the neural information works better if we transform the hemodynamic signals to neural activity. We know that fMRI signals are shaped by Hemodynamic Response Function (Chapter 1) and that the response to a continuous neural activity is the sum of the hemodynamic signals translated in time (linear and time invariant system). Thus, computing the deconvolution we can extract the neural activity from fMRI signals removing the effect of the Hemodynamic Response Function (HRF).

We individuated point processes corresponding to signal fluctuations with a given signature and extracted a voxel-specific HRF to be used for deconvolution, after following an alignment procedure. The parameters for blind deconvolution were chosen with a physiological meaning, according to [166]: for a TR equal to 3s, the threshold was fixed to 1 SD (standard deviation) and the maximum time lag varying from 3 to 5 TR, but results did not change. Results in the manuscript have been done for maximum time lag equal to 5 TR. For further details on the complete HRF blind deconvolution method and the different parameters to be used, see [166]. All the time-series extracted from the RSNs regions were HRF blind deconvolution and the resulting time-series were used for the calculation of the IF.

Table 4.2: Number of voxels in each RSN

RSN	Number of Voxels
medial visual	5649
lateral visual	8470
auditory	10894
sensory-motor	7668
default mode	8201
executive control	15209
dorsal visual right	12197
dorsal visual left	10524

4.2.3 Principal Component Analysis and multivariate Transfer Entropy

Let us consider two RSNs A and B. We have used TE to estimate IF from A to B and vice-versa. The standard method to compute the IF between 2 ROIs is to compute the mean fMRI signal on each ROI and then compute TE using these two time-series. Computing the mean time-series of a region simplifies what this brain region is doing (a brain region is not involved only in one activity) and important information is missed about the activity.

For each ROI we have different number of time-series, each time-series describing the activity of an individual voxel within that ROI. Table 4.2 illustrates the number of voxels (time-series) for each ROI. Simplifying more than 5.000 different time-series that each ROI has in a single time-series (its average) can lead to a poor description of the ROI activity. Indeed, taking the mean signal of all these time-series accounts for about 12% of the explained variance of each of these regions (we are missing 88% of the explained variance).

Thus, to take one representative signal of the brain is not enough, but to use all the voxels time-series is computationally very expensive. We also must have in mind that usually neighbouring voxels have similar activity so is convenient to reduce the number of different

activities within a region. To reduce the number of time-series, but at the same time, study the most representative activities of a given ROI, we can use Principal Component Analysis (PCA).

PCA is a statistical procedure that uses an orthogonal transformation to convert a set of observations of possibly correlated variables into a set of values of linearly uncorrelated variables called principal components. These principal components maximize the variance explained in the data and often a small number of components can be used to reconstruct (or approximate) a given set of data.

To understand better what PCA does, let's simplify the problem, imaging that our region has only 2 voxels and a single time point (2-dimensions). Figure 4.2.a represents an example data set where each circle represents the activity of voxel 1 and voxel 2 for a different subject. The colors represent 2 different groups, for example healthy subjects (blue) and disease (red).

PCA translates the data to a new coordinate system in which the biggest variance is captured by the first axis, the second highest variance in the second axis, similarly occurs for higher dimensions. Figure 4.2.a shows two arrows identifying the new axis. The largest arrow corresponds to the axis of the first component and the other one to the second component. Figure 4.2.a shows the data projected into the first component, while Figure 4.2.b shows the representation of the 2 components. We can see that the variance of the first component is higher, representing the 88.9% of the data variance, while the second component represents the 11.1%. In this example this first component is enough to see differences between the groups (first component > 0 for disease and < 0 for healthy subjects). In such a way the data dimensionality is reduced and instead of using 2 time-series, just one represents the region with the 88.9% of the explained variance.

Finally, the data is projected into the new coordinate system wth the projection coefficients defininf the PCA decomposition. As illustrated in Figure 4.3 when 2 voxels have the same activity or are highly correlated, just one component is enough to represent that activity, reducing the dimensionality of the data. In fMRI data, many neigh-

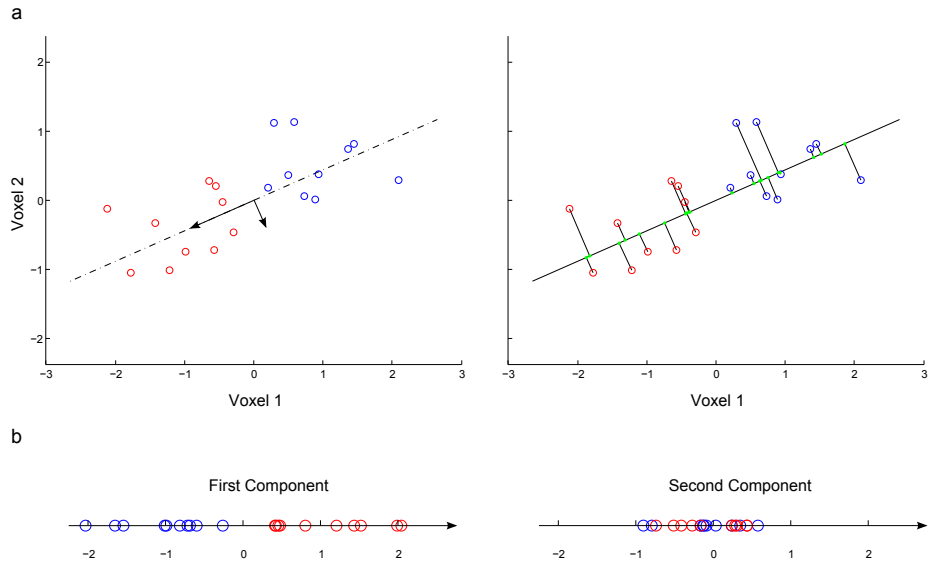

Figure 4.2: PCA translates the data to a new coordinate system. The left panel in a) shows the new coordinate system computed with PCA. This points are projected to the first component coordinate system as illustrated in the right panel of a). Finally the projected data into the first and second component is shown in b).

bouring voxels are highly correlated so PCA performs well in reducing the dimensionality of a given region.

However, for more heterogeneous regions, not always the first component can discriminate between two groups. Figure 4.4 represents an example where the second component is the one that can account for differences between healthy and controls.

In a real case, regions of interest have more than 2 voxels and have more than one time point, but the aim to reduce the data dimensionality is the same as the simplified example illustrated before.

In the Alzheimer's dataset, after averaging between subjects, about 60% of total variability was captured by the first 10 components (k=10) (Figure 4.5) and 99% of total variability was captured for

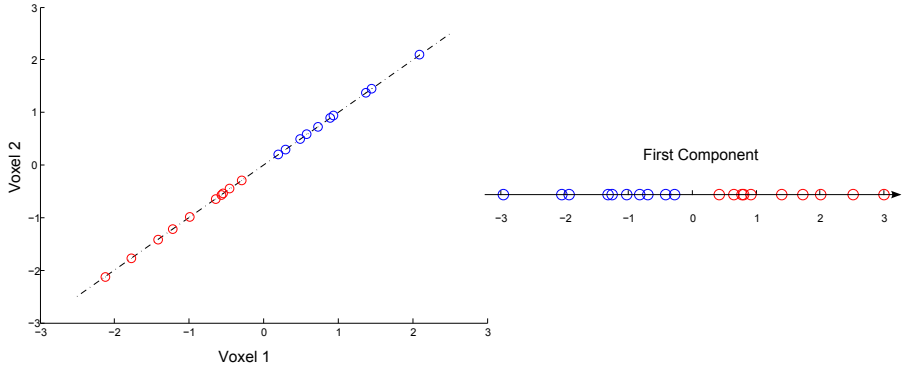

Figure 4.3: Just one component is sufficient to represent highly correlated data.

k=72. No statistically significant differences were found in the amount of variability between control and AD, indicating that the data representation in the different principal components were disease independent. Therefore, the reader should not be confused and be aware that differences in IF are not related to these percentages.

4.2.4 Information Flow between RSNs

Instead of using the standard procedure using the mean signal of each region, we decided to describe each ROI using more components for a given region. We computed the differences in the IF between RSNs for different number of components ranging from $k = 1$ to $k = 15$. Imagine, for instance, we want to compute IF from RSN A to RNS B for $k = 5$ components. For both regions A and B we will extract 5 time-series using PCA and take the 5 time-series of the region A and compute the multivariate transfer entropy to each of the 5 time-series describing region B. This method is univariate for the target and multivariate for the driver. This will lead to 5 transfer entropy values for each of the components in region B. Then we sum these TE values to account for all the contributions of these 5 components describing B which are statistically significant according to Bonferroni

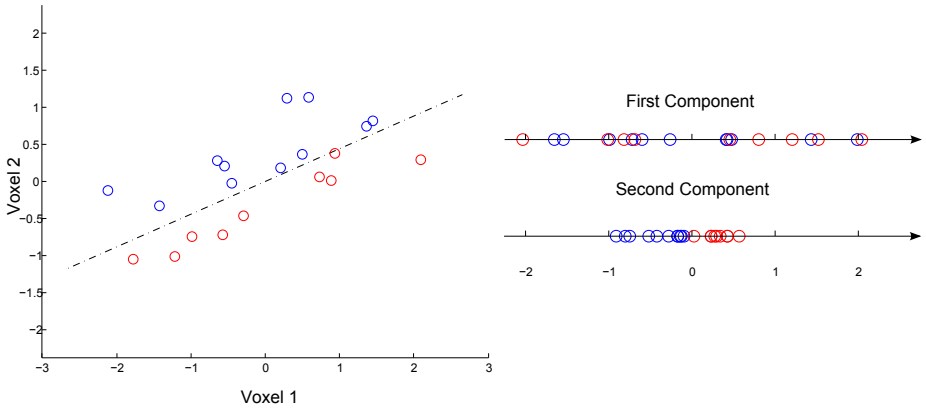

Figure 4.4: Not always the components with highest variance are the ones that will show differences between groups.

criterion($p < 0.05$). The complexity of the model is thus controlled by statistical testing, i.e. accepting only significant interactions (a similar strategy to control complexity is used in [100]).

For more details and formulas to compute the information flow refer to Appendix A.

To perform statistical significance between groups in Figures 4.6-4.8, a non-parametric Wilcoxon rank sum test was used to validate the hypothesis that two data distributions have equal medians. This was implemented in Matlab, The Mathworks, Inc., with the function ranksum at $p = 0.05$ with Bonferroni correction.

The average IF between the different RSNs is represented in Figure 4.6. Systematically, we recomputed IF with a different number of principal components (maintaining the same for all RSNs) from $k = 1$ up to $k = 15$. The case $k = 1$ is equivalent to calculating IF between the average voxel activities for each RSN. The case $k > 1$ corresponds to a multivariate situation. For visualization purposes, Figure 4.6 shows results up to $k = 11$ as for $k \geq 10$ the information was zero. Notice that having a zero IF is possible because, according to IF formula (refer to equation A.7 in Appendix A), the quantity

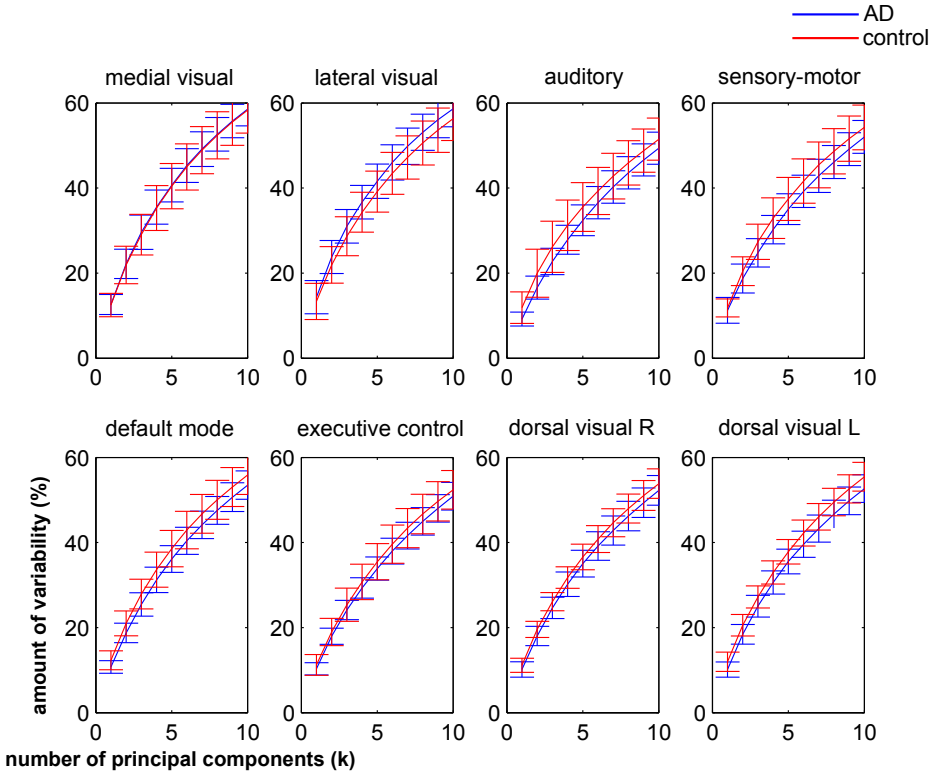

Figure 4.5: Amount of data variability captured for different principal components, from k=1 to k=10

IF is averaged over all the components. Thus, if adding a new component does not provide new independent information, the term in the denominator will eventually decrease the average IF. To represent Figure 4.6, notice that as we were dealing with $n = 10$ healthy subjects and $n = 10$ AD patients, we first obtained for each subject a matrix of IFs in which the element (i, j) indicated IF from the ith RSN to the jth one. Next, we pooled together all the matrices belonging to the same group (control and AD) and represented the average IF among all possible pairs; for 8 RSNs, the total number of pairs is 8 x ($8-1$) = 56, which is equal to the number of pairs minus

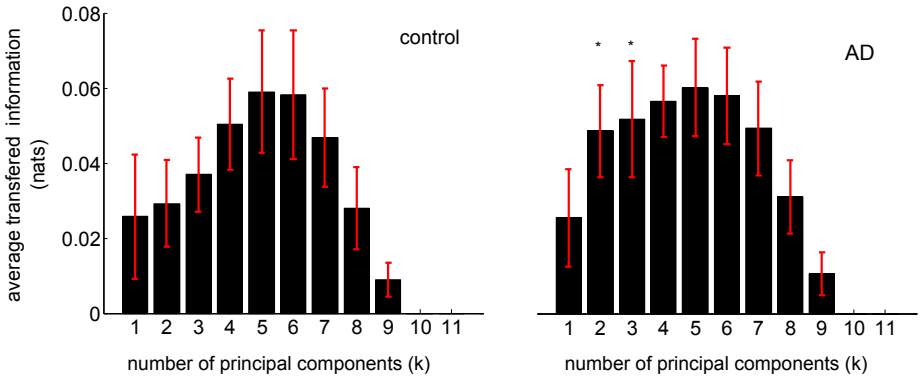

Figure 4.6: **Average transferred information between all RSNs as a function of the number of principal components**. Control (left) vs AD (right). The pattern of transferred information is the same for the two conditions; it increases from $k = 1$ up to the maximum at $k = 5$ to start to decrease up to zero information for $k \geq 10$. This means that the $k = 5$, multivariate, IF between the different RSNs is most informative than in any other dimension. Asterisks (*) represent statistical differences between control and Alzheimer, $p = 0.05$ (Bonferroni correction). Standard error (depicted in red) has been calculated across subjects for each group, control (n=10) vs Alzheimer ($n = 10$). Information has been calculated in nats (i.e. Shannon entropies have been calculated in natural logarithms); but to transform to information bits we have to multiply the value in nats by 1.44.

the elements in the principal diagonal. The profile of average information as a function of the number of principal components (used for calculation of the IF) is the same for control and AD: starting to increase from $k = 1$ up to the maximum at $k = 5$ to monotonically begin to decrease. Therefore we conclude that for dimensions bigger than $k = 5$, a higher dimension does not provide more IF. Statistically significant differences for the average IF between control and AD occurred for $k = 2$ and $k = 3$. Interestingly, the average inter-RSNs

IF is higher in AD than in controls.

Figure 4.7 shows all possible values of IF between all RSNs. Here, the number of principal components was fixed to $k = 2$ (the one with biggest statistical difference in Figure 4.6), but similar graphs were obtained for each value of k. Unlike correlations, TE measures directed functional connectivity and as such Figure 4.7 represents for each condition control and AD the two directions in IF (ie., for two generic RSNs A and B, if in the top panel we represented IF from A to B, then in bottom panel we depicted IF from B to A). In other words, the average value among all the flows in Figure 4.7 is the one plotted in Figure 4.6. It is important to remark that all RSNs are communicating with each other, and, as it is shown Figure 4.6, in average, the AD condition had higher information flowing between RSNs in comparison to control.

Next, we addressed IF arriving to and originating from each specific RSN. Figure 4.8 shows the outward information in blue and the inward information in red. The negativity in all the bars (obtained by subtracting the information in control minus the corresponding one in AD) confirmed that within all RSNs there existed an increase of the information for AD in both the outward and the inward directions.

4.2.5 Anatomical localization in brain differences: control vs AD

Finally, we performed a non-parametric two-sample unpaired t-test to localize the differences between AD and control for the $k = 2$ component in the brain. Using a General Linear Model we computed the contribution of each voxel of the brain to the $k = 2$ component, to obtain a subject-specific spatial map (more details in Appendix A). Next, to search for the group differences (control vs AD) in the spatial maps we performed a permutation-based nonparametric inference as implemented in the function randomise in FSL, option Threshold-Free Cluster Enhancement (TFCE) with FWE-Corrected $p = 0.05$.

Results are shown in Figure 4.9; the differences are plotted in

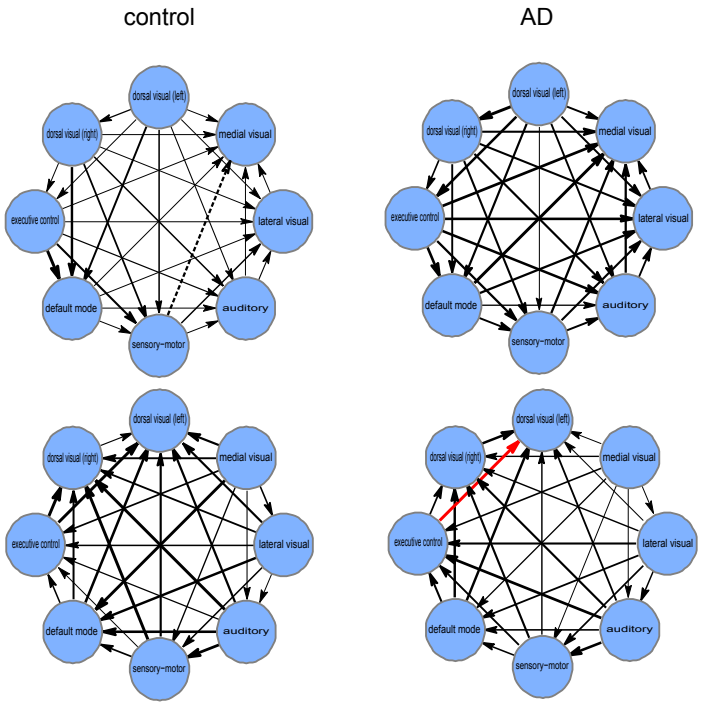

Figure 4.7: **Networks of IF between the different RSNs**. For $k = 2$ (where the biggest difference between control and AD in Figure 4.6 occurs), we have represented the multivariate IF between the different RSNs. Note Control (left) vs AD (right) for the two directions of IF (top and bottom). IF values are proportional to arrow thickness. Values represented in Figure 4.6 are the average among all the arrows represented in this figure taking into account the two flow directions (top and bottom). Only for visualization purposes, values of IF have been normalized to the common maximum (marked with the red arrow), corresponding to $TE = 0.078$ nats from the executive control network to the medial visual (left) in the AD condition. Dashed arrow from the sensory-motor network to the medial visual corresponds to the minimum value, which before normalization was $TE = 0.006$, and after normalization was fixed to zero.

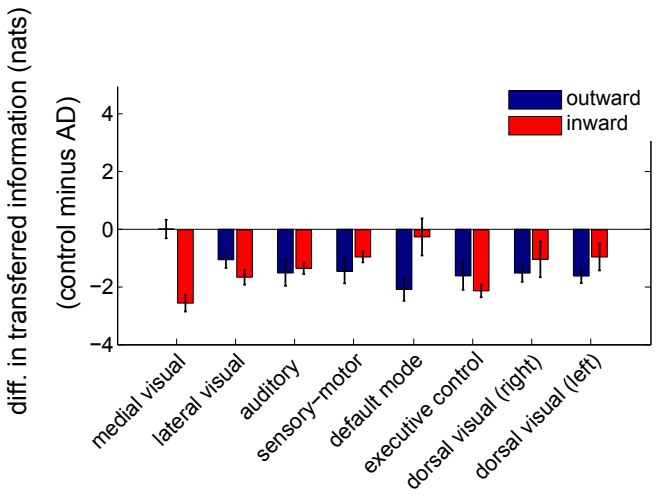

Figure 4.8: **Control minus AD differences in the total IF per RSN**. Note outward information (blue) and inward information (red) from/to each different RSN. Error bars have been calculated across subjects for each group. Notice that values in this figure are much higher than those in Figure 4.6 due to two reasons. First, values in Figure 4.6 correspond to the average value of IF, taking off principal diagonal elements. This implied dividing each IF value by a factor of 56. Second, to calculate both outward and inward information, we sum over columns and rows respectively. This means multiplying each IF value by a factor 6 (not including the self-node information, neither the element in the principal diagonal). Thus, values in this figure might be even up to 336 times bigger.

two colours: blue for the activity existing in control but nonexistent in Alzheimer and in red, vice versa, activated areas belonging to Alzheimer but not to control.

To localize the spatial maps plotted in Figure 4.9, we overlapped these maps with the Automated Anatomical Labeling (AAL) atlas [161] to get the anatomical regions underlying such differences. In particular, we calculated the overlapping percentage between all voxels in each spatial map and each of the 45 homologue brain areas

Table 4.3: Localization of brain differences in AD vs control using the AAL parcellation

RSN	Regions in AD but not in control (red in Figure 4.9)	Regions in control but not in AD (blue in Figure 4.9)
Medial Visual	Calcarine sulcus, Cuneus, Lingual Gyrus	Paracentral Lobule
Lateral Visual	Middle Occipital Gyrus	Superior Occipital Gyrus, Middle Occipital Gyrus
Auditory	Thalamus	Superior Temporal Gyrus
Sensory-Motor	Rolandic Operculum, Heschl's Gyrus, Superior Temporal Gyrus	Precentral
Default Mode	Medial Frontal Gyrus, Thalamus	Midcingulate Area, Cuneus, Angular Gyrus
Executive Control	Supramarginal Gyrus	Superior Frontal Gyrus, Middle Frontal Gyrus
Dorsal Visual Right	Inferior Parietal Lobule, Angular Gyrus	Inferior Frontal Gyrus, Pars Triangularis, Insula
Dorsal Visual Left	Angular Gyrus	–none upper 15% overlapping–

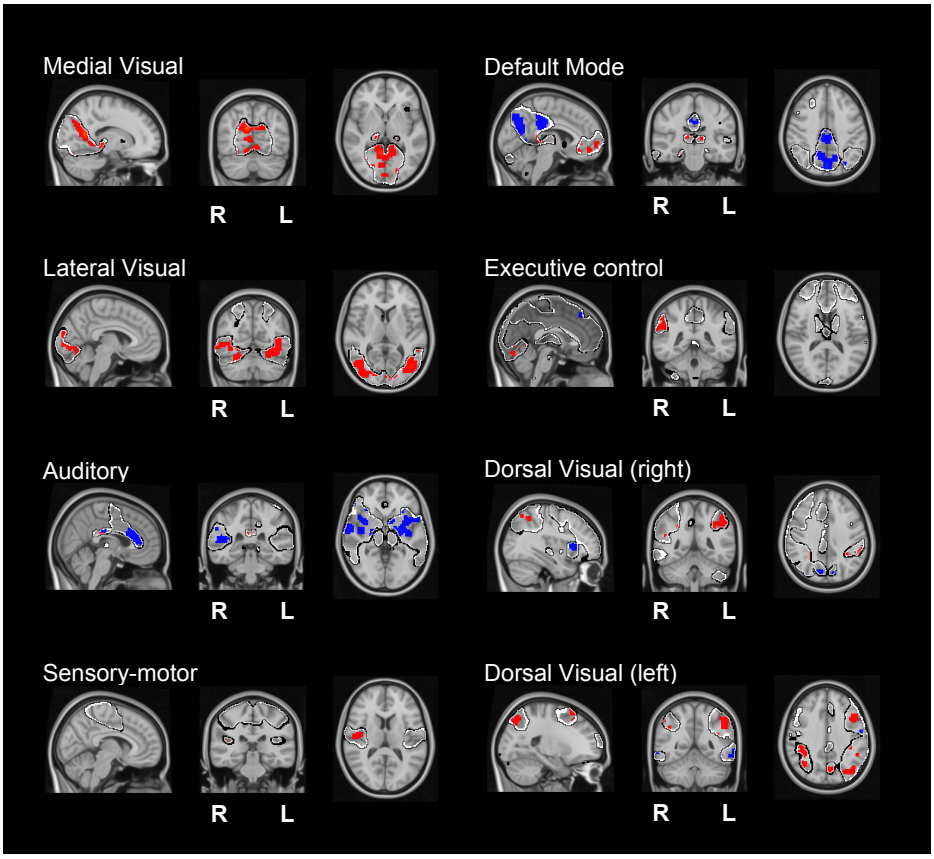

Figure 4.9: **Brain maps of statistical significance localizing the $k = 2$ component within each RSN**. After a two-sample unpaired t-test, we are representing two possible contrasts: in red, the figure shows the significant activity existing in AD but nonexistent in control. In blue, vice versa, differences which exist in control but not in AD.

existing in the AAL parcellation. Although the RSNs are widespread across the whole brain, our localization criteria only considered percentage of voxels in each spatial map to be bigger than 15% (with respect to the total spatial map size), results given in Table 4.3.

4.3 Final Considerations

RSNs are chiefly characterized by their universal emergence, meaning that, beyond individual subject differences, RSNs are ubiquitous in healthy brains. Whilst the emergence of RSNs in healthy subjects is a well-known fact, how these RSNs speak to each other is not fully understood yet. In our approach, instead of applying ICA to each subject separately to get their specific RSNs, we used templates provided in [10] for all subjects. The use of the same templates for all the subjects is indeed assuming that the spatial structure of all RSNs is universal. Our main hypothesis here is that the breakdown of this assumption might differentiate healthy subjects and AD patients, but the same method can be applied to any other disease. Searching for such differences might provide further insights about the alteration patterns of IF in the pathological brain. In other words, we were interested in providing an answer to the following question: what are the different features in healthy vs pathological brains under the hypothesis that the same templates characterize RSNs? To this end, we introduced a novel method that calculates IF between all the different RSNs.

We applied this methodology to AD datasets and compared these results to control. The interesting answer is that such assumption led –for the particular situation of AD– to differences in the information related to the second and third principal components and not to the first one (which is coincident with the average activity over all voxels per RSN). Thus, when we say that AD vs. control differences are associated to $k = 2$, we mean a multivariate driver having into account the two time-series $k = 1$ and $k = 2$. Therefore, as long as the average time-series of each ROI is concerned, no differences between the patterns of healthy and AD patients emerged. Performing a paired t-test to spatially localize the $k = 2$ component, we found the regions which were underlying those differences.

Some approaches have represented each ROI using more than one time-series, either using PCA [169] or cluster analysis [135]. The approach we are presenting here is rooted on principal component analysis and its novelty is based on two points: first, we preprocessed

the time-series corresponding to each individual voxel by HRF blind deconvolution and second, instead of fixing the number of components according to a prescribed fraction of the data variance, as it is usually done, we have analyzed IF as the number of components increases, including more details of the ROIs dynamics.

Recently, the point process analysis described in [155] showed that the relevant information in resting-state fMRI can be obtained by looking into discrete events resulting in relatively large amplitude BOLD signal peaks. Following this idea, we have considered the preprocessed resting fMRI time-series to be spontaneous event-related and individuated point processes corresponding to signal fluctuations with a given signature, extracting a voxel-specific HRF to be used for deconvolution.

We want to remark that the use the HRF deconvolution, apart from being conceptually mandatory in our opinion, is also crucial for our results. Indeed we repeated our analysis while omitting the deconvolution stage, and we found a clearly different pattern of IF between RSNs. In particular, IF differences were only significant for $k = 1$ and AD showed a decreased IF w.r.t. healthy subjects. We also verified that, in general, the use of HRF de-convolution increased the IF for all subjects in comparison to not using the de-convolution. Thus, if we had omitted the HRF deconvolution stage, we would not have observed the relevant role of the second and the third principal components in shaping the differences of IF in AD and controls.

Previous work has addressed DFC between the different RSNs; for instance, the authors in [43] ICA-extracted the time-courses of spatially independent components and found differences in DFC between schizophrenia and control conditions. It is worth mentioning that a method for effective connectivity inference, combining PCA and GC, was proposed in [169]. The main differences between our method (tailored to analyze the IF between RSNs) and the one developed in [169] are the blind deconvolution with HRF and the fact that we use the number of components as a parameter to be systematically increased (up to finding statistically significant different causalities), and both driver and target ROIs are described with the same num-

ber of components. In [169], instead, all voxels in the activated brain regions were taken as target and the PCA analysis was applied only to the driver region and not to the target one.

Following previous work extending the use of DFC to the multivariate situation [8, 44, 9, 93], we have applied here a multivariate DFC approach to the study of the interaction between RSNs. Specifically to AD, causal interactions among the different RSNs were addressed in [95] by a multivariate Granger causality. The authors found an increase in IF between RSNs in relation to the default mode network and the executive control one, which is in agreement with the increase of IF reported here, possibly suggesting compensatory processes in the brain networks underlying AD. Similarly and more recent, an increase of connectivity in the default mode network was found by other authors in [92] in amnesic Mild Cognitive Impairment by using GC.

The main result of the present study is the finding that the AD condition had higher IF between RSNs in comparison to control. This is apparently in contradiction to a recent paper [90] where a Bayesian network approach reported a general decrease in connectivity strength for AD. Moreover, the authors in [90] found an increase in connectivity between the default mode network and the dorsal attention network when using the average voxels activity, which in our approach is equivalent to considering $k = 1$. Here, if we apply the HRF deconvolution preprocessing, we find no significant differences between controls and AD at $k = 1$; but, if no deconvolution is applied, $k = 1$ for AD shows a significantly decreased IF w.r.t. healthy subjects, in full agreement with [90]. Moreover, for $k = 1$ we find an increase of the interaction from the default mode network to the dorsal visual (left) network and this is also consistent with the findings in [90]. It follows that the results in the paper [90] are consistent with the application of our method when just one component is considered and the HRF deconvolution is omitted. Our findings suggest that in AD the second (and, to a lesser extent, the third) components of the signals within RSNs are responsible of the increased IF. Approximating each RSN by a single signal is not enough to put in evidence these

phenomena.

The IF increase found in AD might have different causes; perhaps, due to a compensatory re-organization of brain circuits triggered by synaptic plasticity [1], or due to the fact that AD patients might fail in ignoring irrelevant inputs when integrating information to performing particular cognitive tasks [129], or due the reduction in inhibitory modulatory influence across the whole-brain network in AD [4, 13, 132], but the exact mechanism producing an increase of IF in AD needs further investigation.

The small population size included in this study only allows for a limited interpretation of the details of connectivity changes between networks. However, a conservative approach to this analysis indicates that the IF implicated in sensory processing networks and the DMN is relatively increased in AD compared to controls. Both reductions as well as increments in functional connectivity have been previously reported between brain regions in early AD. Interestingly, most of the regional connectivity increments have been described in the frontal regions, overlapping with regions belonging to the executive control network, DMN and frontal regions of the dorsal visual processing stream [134].

Chapter 5

Brain reorganization in Traumatic Axonal Injury

In Chapter 3 we obtained a data driven brain partition of 20 modules that were both functionally and structurally connected. In this chapter we will use this parcellation to study how the brain is reorganized in patients with traumatic axonal injury. As performed in Chapter 4 we will also use more components to describe the activity in each of the modules.

Traumatic Axonal Injury (TAI) produces a non-focal axonal lesion due to rapid head movement (in either acceleration or rotation of the brain) which as a consequence disrupts structural brain networks – the graph of white matter tracts connecting different brain regions –. Due to this network disruption, many studies on TAI were successfully approached by using brain networks methods [20, 75, 27, 97, 141, 29, 28, 142, 7]. In the attempt to try to correlate network topology with behavior, it was recently suggested that the cognitive impairment triggered by TAI might be originated by disconnection of network hubs [48].

Following previous studies [162, 47, 30], we focus here in studying how the brain is capable to reorganize after TAI. In spite of great achievements, it is not clear what is the structural correlate/substrate of the brain functional reorganization occurring after TAI.

We provide here further insights by exploiting the atlas decom-

position reported in Chapter 3 and find co-localized reorganization in both functional and structural networks. The use of this atlas is justified by our main hypothesis here: if structural networks reorganize and become more connected at some location, such a structural reorganization should be accompanied by an increase of activity in the corresponding functional networks, and vice versa, as the relation between brain structure and function is a closed-loop relationship [39, 118, 45].

Using structural and functional data we found that both structural and functional networks reorganize at the frontal lobe of the brain, a region highly studied in TAI patients and associated to deficits in cognitive control and executive function [89, 108, 65].

5.1 Subjects and data pre-processing

A total of 41 young participants were included in the study: 14 of them had a traumatic axonal injury (TAI) ranging from moderate to severe (age: 13.14 ± 3.25 years, 6 males, 8 females) and the remaining 27 subjects were used as the control group, an age-matched typically developing group (age: 15.04 ± 2.26 years, 12 males, 15 females). The average age at the moment of the injury was 10 ± 2.26 years and the time interval between the injury and the MRI session was in average 3.5 years. Exclusion criteria was based on pre-existing developmental disorders, central neurological disorders, intellectual disabilities and musculoskeletal disease. The demographic and clinical descriptors of the TAI group are given in Tables 5.1 and 5.2.

The study was approved by the KU Leuven Ethics Committee for biomedical research. Patients were recruited from several rehabilitation centers in Belgium. In all of them, written informed consents were obtained from either participants or patients first-degree relatives, according to the Declaration of Helsinki.

The scanning was performed on a Siemens 3T Magnetom Trio MRI scanner (Siemens) with a 12-channel matrix head coil and structural, diffusion and fMRI data were acquired.

Using the same preprocessing steps used in Chapter 3 for diffusion

Table 5.1: Demographic table of TAI patients. TA = Traffic Accident; C = Coma; NA = Information not available; GCS = Glasgow Coma Scale score; M = male; F = female

ID	Age	Gender (y)	Cause of injury	Age at injury (y)	Time since injury (y)	GCS/coma duration
T01	8.6	M	TA	7.9	0.7	C: 5days
T02	18.1	F	TA	15.6	2.5	C: 5days
T03	9.3	F	TA	7.9	1.4	C: 2weeks
T04	16.5	F	TA	7.2	9.3	NA
T05	14.2	F	TA	7.7	6.5	NA
T06	13.4	M	TA	12.5	0.8	NA
T07	19.0	F	Fall	12.5	6.5	NA
T08	15.6	M	TA	12.5	3.2	C: 10days
T09	13.9	M	TA	13.5	0.3	GCS: 3
T10	8.5	F	TA	7.7	0.8	NA
T11	11.4	M	Sport injury	9.8	1.5	NA
T12	13.3	M	TA	12.1	1.2	NA
T13	16.0	F	NA	NA	NA	NA
T14	13.8	F	Object Impact	3.0	10.8	NA

data we compute the 2514x2514 structural connectivity matrices for each subject.

The functional MRI data was pre-processed with FSL (FMRIB Software Library v5.0) and AFNI (http://afni.nimh.nih.gov/afni/). At the first stage, the fMRI dataset was aligned to the middle volume to correct for head-motion artifacts. Next, the slice-time correction was applied for temporal alignment of the slices. All voxels were spatially smoothed with a 6mm full width at half maximum (FWHM) isotropic Gaussian kernel and after intensity normalization, a band pass filter was applied between 0.01 and 0.08 Hz [33], which was followed by the removal of linear and quadratic trends. We next regressed out the motion time courses, the average cerebrospinal fluid (CSF) signal, the average white-matter signal and the average global

Table 5.2: Clinical data table of TAI patients.

ID	Acute MRI scan within 24 h after injury lesion location/pathology	MRI scan at test session lesion location/pathology
T01	Subdural hematoma R FL/PL/TL; cortical contusion R FL/PL; DAI in R FL	Microbleeding R centrum semiovale and CC
T02	Subdural hematoma/hemorragic contusion TL/FL; injuries R FL, thalamus, R cerebral peduncle, L mesencephalon; cortical and subcortical hemorrhagic areas in PL/TL	Injuries surrounding drain trajectory in RH (superior frontal gyrus, head nucleus caudatus, crus anterius of internal capsule, thalamus, and pons)
T03	DAI in L TL/FL, R TL/FL/PL	Contusion: R anterior temporal pole and R orbitofrontal cortex; Injuries and atrophy in CC (body and splenium); Atrophy of R pons; Hemosiderin deposits in L cerebellar hemisphere, R nucleus entiformis, L/R FL, L/R PL and R PL
T04	Epidural hematoma R FL/TL; shift midline	Injuries in R medial frontal gyrus
T05	NA	Injuries in R medial frontal gyrus Atrophy of the cerebellum; injuries at the level of L FL, premotor cortex, medial frontal gyrus, cingulum, orbitofrontal cortex (L ¿ R); contusion anterior temporal pole (R¿ L); hemosiderin deposits in CC, L thalamus, striatum (R ¿ L)
T06	Hemorrhagic contusion L TL; brain edema	Hemosiderosis; DAI PL (superior and inferior), R cerebellum, L superior frontal gyrus
T07	Subdural hematoma L FL/TL/PL	Hemosiderin deposits R cerebellar vermis
T08	DAI R TL, internal capsule, supra-orbital R FL, L FL WM (anterior corona radiata), L middle cerebellar peduncle	Atrophy cerebellum; Contusion R FL WM
T09	DAI FL, TL, L OL (hemorrhagic injury), cerebellum, CC, external capsule, R globus pallidus, L thalamus, R cerebral peduncle, R mesencephalon	DAI L FL, periventricular WM, body and genu CC, L thalamus, R external capsule, anterior TL (L ¿ R), cerebellum; Limited atrophy cerebellum
T10	NA	Enlarged fourth ventricle, atrophy of cerebellar vermis, contusion R cerebellar vermis, hypotrophy of middle cerebellar peduncle and L pons; contusion L TL; hemosiderin deposits R FL, L TL, CC; ventricle drain
T11	Contusion L FL/TL; enlarged, asymmetric ventricle (temporal horn)	DAI splenium CC; ventricular drain
T12	DAI in genu and splenium CC, L FL	Hemosiderin deposits L FL, genu CC
T13	NA	Mild atrophy in cerebellum and cerebrum, more pronounced atrophy in frontal cortices, enlarged ventrikels; contusion L/R anterior temporal pole and L/R orbitofrontal cortex. Hemosiderin deposits in cerebellum, R FL
T14	Hemorrhagic contusion L FL, atrophy L FL	Contusion: L anterior middle frontal gyrus and L anterior superior frontal gyrus

*WM=whitematter; RH=right hemisphere; LH=left hemisphere; FL=frontal lobe; TL=temporal lobe; PL=parietal lobe; OL=occipital lobe; CC=corpus callosum; R = right; L = left. Other codes: y = years;

signal. Finally, the functional data was spatially normalized to the MNI152 brain template.

5.2 Structural data reorganization

Figure 5.1 shows the sketch followed in this study for finding TAI alterations in both functional and structural networks.

To search for structural changes we computed group differences in both intra-region and inter-region degree. The degree is a graph properties that defines the number of links (connections) of each node. We want to find changes to a smaller scale than the 20 region atlas defined in Chapter 3 so we search for a structural partition where the global degree measure give significant differences ($p < 0.05$) between TAI and Controls (Figure 5.2).

For *intra-region differences* we accounted for all the connections in 2514×2514 structural network belonging to a given region in the hierarchical atlas with $M = 120$ regions, the level at the hierarchical partition in which global group differences started to be significant (marked with an arrow in Figure 5.2).

For *inter-region differences*, we counted to all the connections starting from each of the $M = 120$ regions and finalizing in a different one (Figure 5.3).

A one-way anova test was used to search for significant alterations for both intra and inter-region degree (pvalue < 0.05).

Figure 5.3, with the red scale indicating control >TAI degree and the blue scale TAI >control, shows that TAI patients had a global decreased in the intra-module structural connectivity (first row in Figure 5.3). In particular, control >TAI connectivity occurred in the the frontal superior orbital, the rectus, the left parietal inferior, the left posterior central, the left parietal superior, the superior motor area, the right cingulum middle, the paracentral lobule, the right hippocampus, the right parahippocampus, the right amygdala, the right putamen, the right insula, the right frontal inferior orbital, the right thalamus, the right pallidum, the right temporal pole superior, the cerebellum and the brainsteam. TAI >control intra-region con-

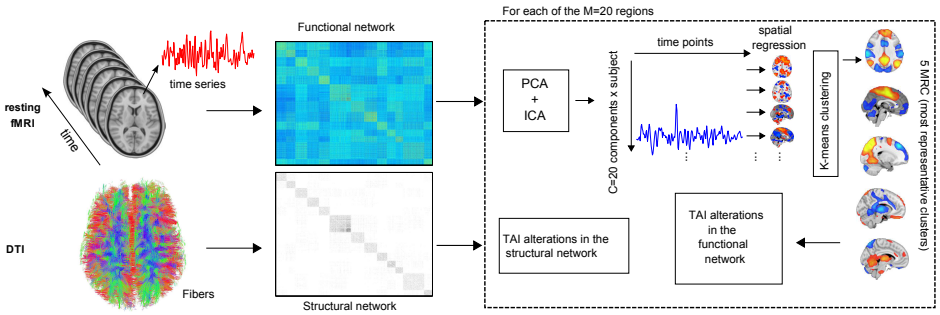

Figure 5.1: **Methodological sketch.** After pre-processing data, we used a brain partition of 2514 ROIs to generate a functional network (extracted from resting state time-series) and a structural one (counting the number of fibres connecting any two regions). The 2514 ROIs where further clustered in M=20 regions using the hierarchical atlas reported in [45]. Differences between TAI and control were evaluated in both functional and structural networks. TAI alterations in the functional network were obtained by extracting the time-series belonging to each of the $M = 20$ regions and computing PCA+ICA to obtain $C = 20$ components in each region. Next, these components were used in a spatial regression model to identify which voxels outside the region were interacting the most with each component, i.e. to obtain the spatial map for each component. Finally, all the spatial maps where clustered using K-means clustering. These results the 5 MRC (most representative clusters), which are the networks that each of the M=20 regions use to interact with the rest of the brain. TAI alterations in the structural network were evaluated by comparing intra-region and inter-region connectivities (i.e. fibre number connectivity) using regions in the hierarchical atlas.

nectvity was found only at a small part of the precuneus and at the cuneus.

With regard to differences in inter-region connectivity, control >TAI were found at the cerebellum, the brainsteam, the left hippocampus, the left parahippocampus, the left fusiform, the letf tem-

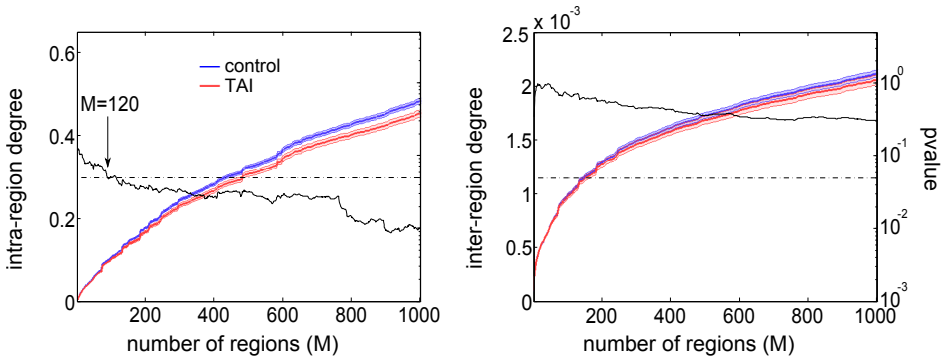

Figure 5.2: **Control (blue) vs TAI (red) differences between intra-region and inter-region degree across number of regions in the hierarchical partition**. At $M = 120$ regions (marked with an arrow) the global intra-region degree starts to be different between TAI and control ($pvalue = 0.05$, marked with a dashed straight line). Notice that in general, TAI disrupts structural connectivity as TAI has less intra and inter connectivity across different number of regions in the hierarchical partition. Both intra-region and inter-region connectivities were normalized just dividing the number of connections in each case by the total number of possible connections.

poral pole, the left temporal middle, the left temporal inferior, the left frontal middle orbital, the left insula, the left putamen, the left frontal inferior opercular. TAI >control inter-region connectivity was found at the rectus, the frontal superior-inferior orbital, the olfactory cortex and the precentral and the left postcentral.

5.3 Functional data reorganization

5.3.1 Differences in functional dynamic patterns

Using the $M = 20$ modules described in Chapter 3, we measured group differences between Control and TAI by looking to different

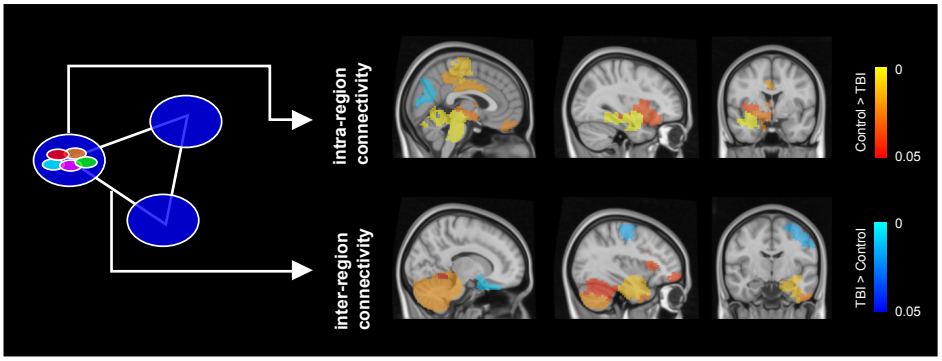

Figure 5.3: Structural network alterations.

dynamical patterns in the time-series of the most representative component of each module. For all the voxels belonging to each of the $M = 20$ regions in each subject we applied a general linear model to identify the time-series components that better describe the activity of each region and subject.

Next, we computed different descriptors from the time-series associated to this component. In particular, we focused on the second moment of the time-series (i.e. the variance), the third moment (skewness) and the forth moment (kurtosis), both skewness and kurtosis accounting for deviations from Gaussianity. Another descriptor was the number of points in the time-series which had a value above a certain threshold; here, the threshold was equal to the mean value plus one times the standard deviation, i.e. the so-called Point Process Analysis, PPA [155].

For each region in the $M = 20$ regions atlas and for each of the four different descriptors of this component (variance, skewness, kurtosis and number of points after PPA) we applied a one-way anova test to evaluate significant differences between TAI and control (pvalue < 0.05). This is illustrated in Figure 5.4. Only the two regions 10 and 11 of the hierarchical atlas presented functional differences in TAI with respect to control. This was confirmed by three different descriptors: the variance, the kurtosis and the number of points after

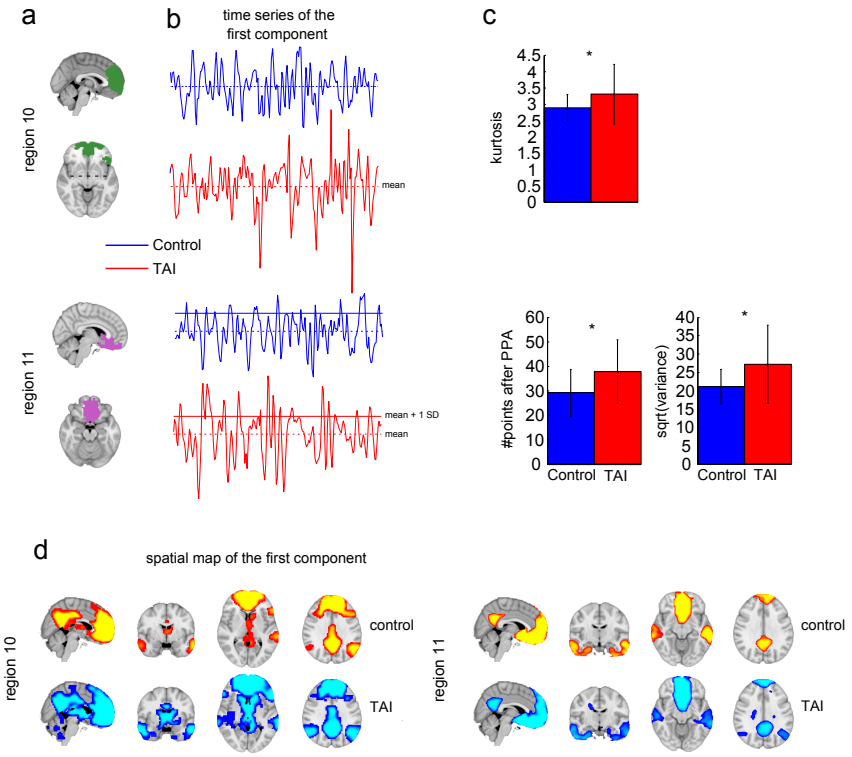

Figure 5.4: **Functional network alterations within regions in the hierarchical atlas. a:** Only two regions showed differences between TAI and control: regions 10 and 11, both localized at the frontal lobe of the brain. **b:** Time-series of the most representative component. Dashed lines represent the mean value of the time-series, and solid lines represent the threshold used for PPA, here equals to the mean + 1 SD. **c:** For region 10, only kurtosis showed differences between TAI and control. For region 11, the number of points after PPA and the variance of the first component (plotted here its square root, i.e. the standard deviation) showed differences between TAI and control. **d:** Plot of the spatial map of the first component in each region.

PPA, but no differences was found when comparing the skewness in the two groups. Interestingly, for the three descriptors (variance, kurtosis and number of points after PPA) the TAI patients had an increase of activity in comparison to control.

5.3.2 Interacting networks: Most representative clusters

It is important to emphasize that, unlike it occurs for structural networks, the functional interactions that a given region has with the entire brain are highly dynamical and vary in a very short time scale (even in a few of milliseconds). Here, to quantify the interactions that each of the $M = 20$ regions had with the entire brain we followed a procedure which was motivated by [146] and is illustrated in Figure 5.1. This procedure uses Independent Component Analysis (ICA) to extract different components in the brain.

ICA was developed to solve the problem of detecting unknown signals in a dataset, sometimes called the blind source separation problem [121]. To describe this problem is often used the example of cocktail party problem. Imagine a party with a large number o people talking in a room with different microphones. The recording of each microphone reflects a mixture of all the different speakers, weighted by their distance to the microphone etc. The goal is to separate out the speech stream of each person speaking using the recordings of the microphones. If we translate this problem to the brain using ICA we can compute the different neural processes occurring in the brain.

As we see in Chapter 4 PCA is also used to extract components in the data. PCA is sensitive only to signals that follow a Gaussian distribution and although some signals in fMRI datafollow such a distribution, there are many signals which do not. Thus, when computing PCA some components of interest will be mixed together by PCA because they do not follow a Gaussian distribution. In this case, independent components analysis is a more appropriate technique.

For ICA we will assume that the components in the brain are statistically independent. Statistical independence of two signals A

and B obtains when the joint probability is equal to the product of the individual probabilities: P(A,B) = P(A)P(B). When A and B are independent, then knowing the value of one does not provide any information about the value of the other. In the case of sources being not independent, ICA finds a space where they are "maximally" independents. Independence is different from orthogonality (or uncorrelatedness); it is possible that two variables can be statistically dependent even been orthogonal, which occurs when the data do not follow a Gaussian distribution. Since ICA searches for non-Gaussian signals, we can use first PCA for dimensionality reduction and for whiten the data.

In particular, to reduce data dimensionality and find uncorrelated components, we used a principal component analysis (PCA) to obtain the first 20 principal components for each of the $M = 20$ regions. Next, we applied independent component analysis (ICA) and obtained the $C = 20$ independent components for each of the $M = 20$ regions. Finally, for each of the $C = 20$ independent components per region we applied a spatial regression method to obtain the contribution that each voxel has on each component (i.e. we obtained the spatial map for each component). Unlike [146] instead of computing ICA to the whole brain data we only compute ICA to the region of interest.

When computing ICA the resulting component do not have a natural ordering and there is not a simple way to match these components between different subjects. We need a clustering or correlation analysis allowing us to match the 20 components of individual subjects. Observing these components, three important issues were present: 1. It occurred that several components from each region interacted with the same spatial map, 2. Typically, the spatial maps resulting from each component were noisy, and 3. It occurred that the inter-subject variability was also high. To match components between subjects and to overcome these limitations, we clustered all spatial maps data by applying the k-means clustering algorithm using the spatial correlation as the distance-to-grouping measure [16]. In such a way, we obtained the 5 most representative clusters (MRC)

for each region in the atlas and subject. Indeed, the MRC represent to which extent a given region in the atlas functionally interacts at the large scale with the rest of the brain or how this region interacts with a specific neural process.

Next, we computed group differences for each region and MRC by applying a t-test implemented in *randomise*, a FSL's tool for non-parametric permutation inference on neuroimaging data using a threshold-free enhancement (TFCE) and a family-wise error (FWE) corrected value of $p < 0.05$. Figure 5.5 shows the interaction pattern of different regions of the brain with a neural process composed by subcortical structures, the thalamus, the temporal superior area and the frontal inferior triangularis area. Three classes of statistical maps for each MRC and region in the atlas were shown: 1. The mean activation in control (corresponding to the contrast [1 0]), 2. The mean activation in TAI (contrast [0 1]), and 3. The differences between TAI and control (by applying the two different contrasts [1 -1] and [-1 1]).

The first row in Figure 5.5 is associated to regions 3, 14 and 15; corresponding with the motor network, the basal ganglia, the hippocampus, the amygdala and the insula. When these regions interacts with subcortical structures neural process TAI patients employed a higher activation in the frontal lobe (contrast [-1 1] in the randomise test).

The second row in Figure 5.5 is associated to regions 18, 19 and 20, regions which being spatially located in the temporal poles, the cerebellum and the brainstem. These regions when interacting with neural processes in subcortical structures also showed an increase connectivity in TAI at frontal regions together with a decrease of connectivity at supramarginal regions. Figure 5.6 shows increased frontal connectivity with the interaction of subcortical and frontal regions.

Figure 5.7 shows the functional reorganization of regions 1, 4, 5, 12, 14 and 15 when they interact with dorsal attention network. A greater frontal connectivity was observed again for TAI patients.

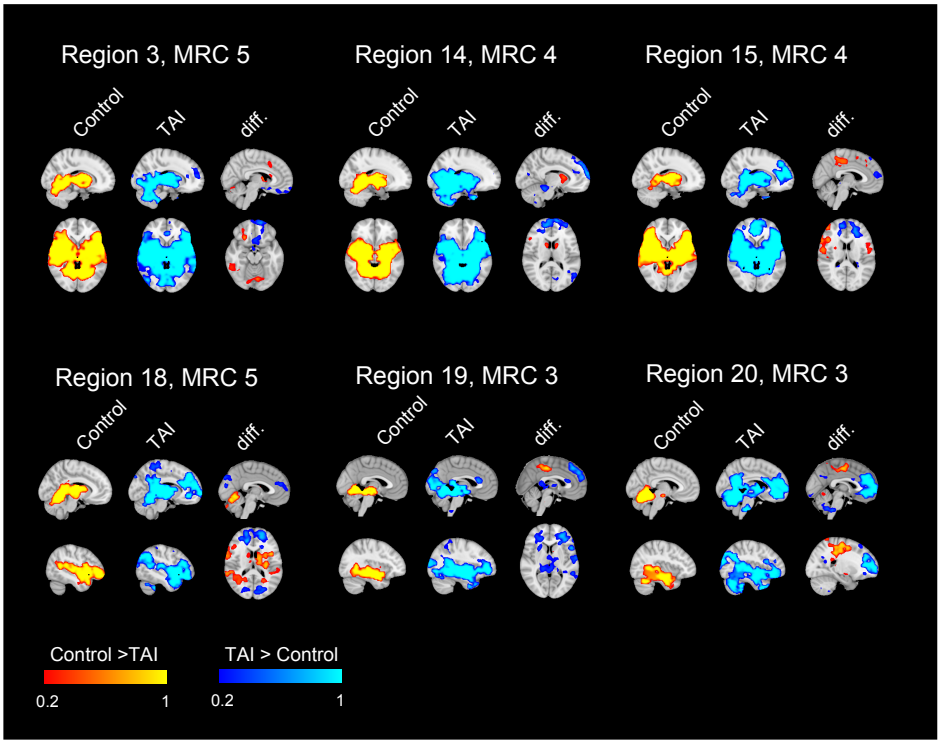

Figure 5.5: **Functional network reorganization when interacting with neural processes of subcortical structures.** The figure is showing significant regions after using different contrasts: Column 1, label "Control", contrast [1 0]; Column 2, label "TAI", contrast [0 1]; Column 3, label "diff.", contrasts [1 -1] and [-1 1], respectively, in red and blue colors. That is, the red color is representing regions with activity is greater in controls, and the blue one, greater in TAI. For both cases, the scales correspond to 1 minus the pvalue. Regions 3, 14 and 15 (top row) are associated to MRCs extracted from the motor network, the basal ganglia, the hippocampus, the amygdala and the insula. Regions 18, 19 and 20 (bottom row) are associatted to MRCs extracted from the cerebellum the brain stem and the temporal poles.

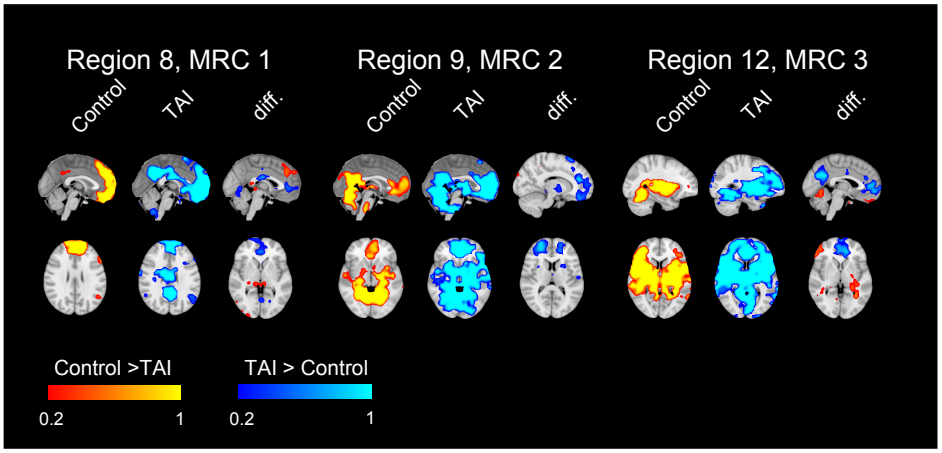

Figure 5.6: **Increased functional connectivity during subcortical-frontal regions interaction.** The left panel shows an increased frontal connectivity when caudate and putamen regions (region 8) interact with frontal regions. The same occurs when the DMN part (region 9) interacts with a subcortical region (middle panel). The right panel shows increased frontal connectivity when frontal regions interact with subcortical structures.

5.4 Final Considerations

TAI patients had a decreased structural connectivity in motor areas, brainstem, cingulum, cerebellum, temporal poles and subcortical areas, all areas which have been typically associated to motor skills, balance control and memory.

A decrease of structural connectivity after TAI was widely reported to occur in the brainstem, the corpus callosum and the subcortical parasagittal connectivity, affecting connections of the basal ganglia, the thalamus and the cerebellum [63, 167, 81]. Other studies using voxel-based morphometry found decreased grey matter density in the frontal and temporal cortices, cingulate gyrus, subcortical grey matter and cerebellum in patients with chronic traumatic injury [60].

Thus, our study shows that TAI patients had (as already acknow-

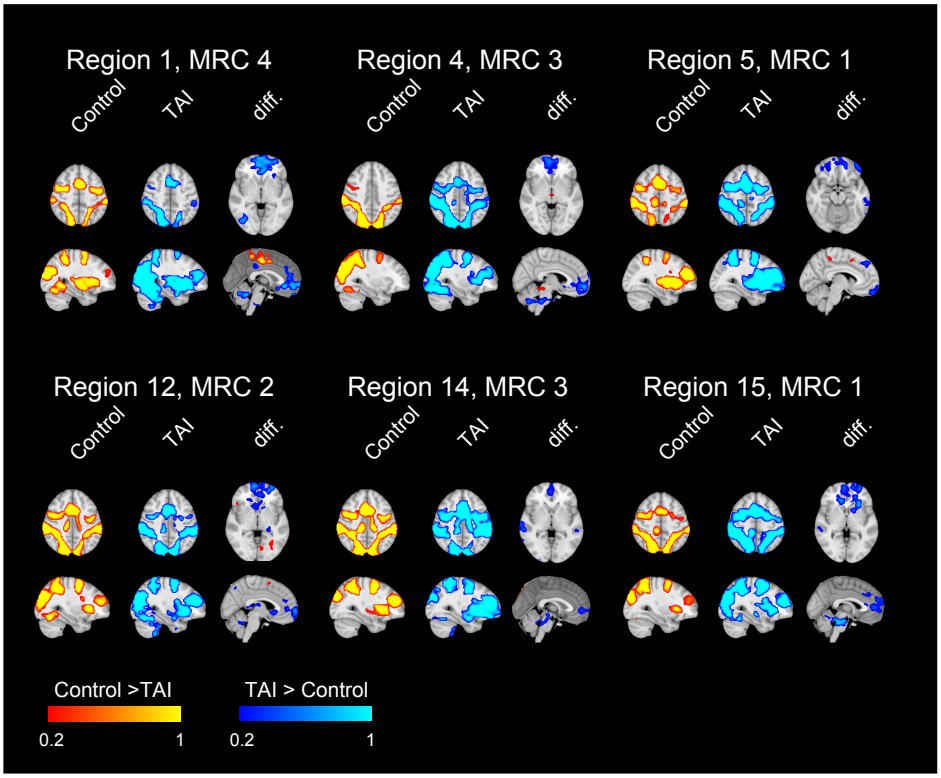

Figure 5.7: **Functional network reorganisation between regions in the hierarchical atlas and the dorsal attention network.** Similar to Figure 5.5, but different regions. Region 1: the posterior cingulate; region 4: the medial visual; region 5: the medial frontal gyrus; region 12: the inferior parietal and temporal gyrus, the lateral frontal orbital gyrus, the rostral pars of the middle frontal gyrus and the pars orbitalis and triangularis; regions 14 and 15: subcortical structures.

ledged) a global decrease in their structural connectivity but, much less reported, a increase in their brain functional connectivity in the frontal brain when some of the regions in the hierarchical atlas interact with subcortical regions and/or the dorsal attention network.

Similar to previous studies, we paid special interest to mechanisms of reorganization/compensation in brain networks after TAI. Using a working memory paradigm, the authors in [102] found that patients after TAI required compensatory activation of the contralateral prefrontal region to perform the tasks in comparison healthy controls. Different authors found more activity in the resting activity of TAI patients at frontal regions [115], an activity which was correlated with cognitive performance. Voxel-based morphometry also found that gray matter volume increased in the prefrontal cortex, and this increase of gray matter was positive-correlated with subject's performance [157].

Our approach looked to the interaction between the regions in the hierarchical atlas and the rest of the brain and found that increased frontal activity in TAI patients occurred mainly when interacting with subcortical structures and the dorsal attention network.

It is important to remark that the increase of activation occurring when analyzing the functional networks, was corresponding with an increase of connectivity in the structural network from the frontal regions to subcortical ones, thus showing the existence of new structural circuits capable to accomplish the new functional nets. Figure 5.8 illustrates the structural and functional reorganization together. In particular, Figure 5.8 shows an increase of structural connectivity when interacting with subcortical structures and the dorsal attention network. The structural network goes from the frontal orbital region (purple node in the graph) to frontal superior and medium orbital, the insula, the amygdala and the striatum (represented by red circles in the graph)

The frontal cortex does not work in isolation; interactions from the frontal to the basal ganglia were reported to play a key role in movement control [2, 109, 5, 78, 35, 36]. Furthermore, executive function was shown to depend on a more complex network involving the frontal cortex, the basal ganglia and the thalamus [55].

There is evidence that the connectivity reduction in the fronto-striato-thalamic circuit is correlated with the reduction in subcortical volume and task performance after traumatic brain injury [87, 88].

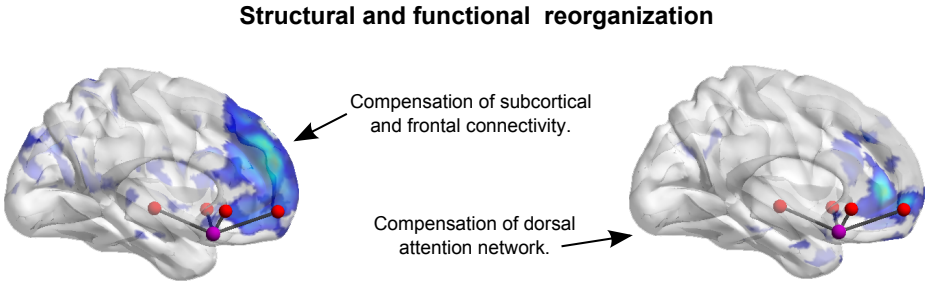

Figure 5.8: **Functional reorganization together with the structural one.** Reorganization in two networks, the one accounting for the frontal interaction with subcortical regions (left panel) and the dorsal attention (right panel). For both panels, the maps in the brain surface represent the functional connectivity resulting from averaging all spatial maps with contrast [-1 1] in Figure 5.5 (left panel) and Figure 5.7 (right panel). The two panels also include the structural network, represented by a graph between the frontal orbital region (the purple node in the graph) and the frontal superior and medium orbital, the insula, the amygdala and the striatum (represented by red circles in the graph).

Even more, it has been shown that white matter connectivity and subcortical gray matter volume continued decreasing up to 4 years post-injury [49], what might lead to, as previously suggested, a reorganization in the frontal regions of the brain to compensate the damage in the fronto-striato-thalamic circuit [87, 88].

With regard to the analysis of functional networks, we have shown that TAI patients increased their interaction with the areas of the frontal part of the default mode network (DMN). Increased DMN connectivity has been found in patients with moderate to severe brain injury and a suggested mechanism was that the loss of structural connectivity produced by the damage of the cingulum tract triggered an increase of functional connectivity in the frontal part of the DMN [141, 115].

In summary, we have made use the hierarchical atlas from Chapter

3 in which regions are relevant to both structure and function to show that TAI patients increased both structural and functional connectivity in frontal regions to overcome deficits in cerebellum and subcortical connections.

Chapter 6

General Conclusion

In this thesis, mainly methodological, I have presented the use of new neuroimaging methods to study disease and neurological disorders; in particular, the thesis focuses on brain connectivity methods to approach healthy brains, patients with deficit of consciousness, Alzheimer's disease and traumatic axonal injury. Because each chapter has its own conclusions, here, we briefly mention general aspects covering the entire scope of the thesis.

Magnetic resonance imaging is to the date the only modality to large-scale imaging the human brain. After image postprocessing methods, MRI provides functional and structural networks, brain areas connected respectively functionally or structurally. In the following lines, I would like to mention some facts that are not intuitive but are the result of applying a brain network analysis:

In Chapter 2, resting activity of patients with disorder of consciousness (DOC), even for those patients in a deep coma stage, have a slightly similar brain dynamics than the one in healthy subjects (described by the BOLD signal time series). In particular, DOC patients present similar functional connectivity values intra-hemispherically than healthy subjects. However, the connectivity between homologue left-right hemisphere areas has a strong breakdown in comparison to control. Thus, it is the coherence (ie., the similarity) between the left and right hemisphere dynamics the one that characterizes the strength of disorder of consciousness. We also have seen that, the

fact that the connectivity between left-right hemispheres is high, it is a mechanism for having a high information flow within (but not between) hemispheres, thus facilitating intra-hemispherical segregation.

In Chapter 4, we have seen that when comparing Alzheimer's disease (AD) with a healthy population with regard to the information flow (IF) between the most fundamental resting state networks (RSNs), the average activity (roughly coincident with the first principal component) within ROIs does not provide significant differences in IF between disease and control. However, it is the second component and to a lesser extent the third, the ones that can differentiate the IF between disease and control. In other words, differences are found when looking to IF beyond average ROI activity, as curiously, it is usually done in neuroimaging. Furthermore, we have seen that when dealing with ROIs with high number of voxels (in the order of a thousand voxels), as it is standard in ROIs analysis, the more number of voxels we use to describe the ROI dynamics, it is not the better, as IF saturates and upper a certain dimension (specifically for the dataset we have used here, k=10), IF goes to zero. Finally, AD showed bigger IF in comparison to control, meaning that, RSNs speak more each other in AD in comparison to control.

In Chapter 3, we have addressed the relation between structural and functional networks, two data sets acquired at a different session, each data set having different physiological correlates (structure, white matter diffusion, function, BOLD signal variations). We have shown that, when comparing the two networks at the level of individual link (that means, looking in ROI pais if the value of the the structural link is in somehow similar to the similarity between the two ROI dynamics), functional and structural networks are hardly similar. However, when comparing the two networks at the module level (that means, when looking to cluster of ROIs rather than pairs), high similarity between brain structure and function emerges. We have provided the best brain partition (in crossmodularity sense) that occurs for M=20 different regions. One region in this partition guarantees that the dynamics within is homogeneous and, at the same

time, is highly integrated by white-matter fibers. As a consequence, alterations in these regions can tackle both functional and structural dysfunction at the same time.

Indeed, Chapter 5 shows that this is the case. We have made use of the M=20 brain partition to show that, after traumatic axonal injury, there exists a frontal-lobe reorganization in these patients when interacting with subcortical regions and/or with the dorsal attention network, and this is revealed by an increase of both functional and structurally connectivity.

Finally, a reflection more than a fact, albeit we are aware than clinical practice is beyond the use of brain networks to approach disease, I believe that clinical practice should move forward in this direction as diseases are not the result of a failure in a single-anatomical area; rather, a focal lesion affecting one area will propagate to the entire brain functioning. Clinical practice needs for new methods than can quantify these alterations occurring in brain networks. However, we also are aware that brain networks lack of simple descriptors, easy to be measured, allowing to follow an individual patient across disease's progression. With this thesis, I want to shed some light in this direction.

Euskaraz

Kapitulua 7

Sarrera

Garuna, tresna elektroniko ugari baino txikiagoa izan arren, existitzen den gailu konputazional konplexu eta dotoreena da. Izan ere, errendimendu handiko informatika laborategi aurreratuenak ere ez dira burmuinaren prozesamendu gaitasunak erreproduzitzeko gai izan [71][96][105]. Burmuinak, informazio sentsorial ugari jaso eta interpretatzen du, oinarrizko portaera konplexu zein sinpleak kontrolatzen ditu, erabaki konplexuak hartzeko gai da, sormenez pentsatu dezake eta sentimenak izan ditzake [164].

2006-garren urtean, Munduko Osasun Erakundeak egindako estimazioaren arabera, gaitz neurologikoek eta haien ondorioek milaka milioi gizakiengan eragiten dute. Arazo neurologiko hauek agertzearen arrazoiak natura desberdinetakoak izan daitezke, hala nola: gaitz genetikoak, jaiotze arazoak, infekzioak, bizimodu edo ingurumen osasun arazoak (malnutrizioa barne), burmuin / bizkarrezur / nerbioen lesioak, arazo zerebrobaskularrak burmuin lesioak garatuz etab. Munduan, 6.8 milioi pertsona inguru hil egiten dira urtero gaitz neurologikoak direla eta, 50 milioi pertsona baino gehiagori epilepsia sortzen diete, 35.6 milioi pertsonek dementzia jasaten dute (7.7 milioi kasu berri agertzen direlarik urtero eta Alzheimer gaitza ohikoena izanik) populazioaren ehuneko hamarrak baino gehiagok buruko mina jasaten dute; hauek denak, gaixotasun neurologikoen ondorioak dira. Europan bakarrik, gaitz neurologikoen inguruko gastu ekonomikoa 139 mila milioi eurokoa izan zen 2004an eta hirugarren milurteko ha-

sieran eskuratutako datuek ez dute adierazten egoera hobetuko denik. Populazioa zaharkitzearekin batera, garun arazoen pertsonen ehunekoak gora egiten jarraitzen du, eta ondorioz, tratamendu berri eta eraginkorrak lortzeko asmoarekin, burmuinaren ezagupen sakonagoa sustatzen duten ikerketak bultzatu behar dira.

Gaur egun, ikerketa ugari gaixotasun zehatz batzuek garunean eragiten dituzten aldaketei azalpena ematen hasi dira burmuin egituran, funtzionamenduan edo bien arteko korrelazioan oinarrituta. Nahiz eta zientziaren aurrerapenak azkar joan, garunaren funtzionamenduaren inguruan ezjakintasun handia dago oraindik.

Tesi honetan, gaitz neurologiko desberdinek garunaren estruktura eta funtzionamenduan duten eragina aztertzeko metodo berriak garatu dira. Metodo hauek, garuneko lesio traumatiko hedatsuak, Alzheimer eta kontzientzia gaitzak ikertzeko erabili dira. Neurozientzia, izatez jakintza alor anitzeko esparrua da non Neurologoek, Ingeniariek, Biologoek, Fisikoek eta beste hainbat arloek batera lan egiten duten. Hori dela eta, diziplina desberdinetako ikerlari guztiek idatzitakoa uler dezaten, tesi hau idazterako orduan, detaile matematikoak saihestu eta xehetasun metodologiko ugari sinple mantentzen saiatu naiz; nahi izatekotan, garapen matematikoak eta informazio zehatzagoa A Eranskinean aurki daiteke. Era berean, bertan garatutako informazioa, tesi honen garapenaren igarotzean idatzitako artikulu zientifikoetan aurki daiteke (ikusi 231 orria artikulu zerrenda kontsultatu nahi izatekotan).

7.1 Garunaren Oinarrizko Anatomia

Garuna, tresna konputazional eraginkor bat bihurtzen da elkar konektatuta dauden neuronen propietate estruktural eta funtzionalei esker. Neurona hauek, burmuinaren oinarrizko langile unitateak dira; seinale elektrikoen eta kimikoen bidez informazioa prozesatu eta transmititzeko diseinatutako zelula espezializatuak hain zuzen ere.

7.1 Irudiak ugaztun baten neurona erakusten du. Neuronak, honako atal hauetaz daude osaturik:

- **Gorputz zelularra**: neuronaren lantegia da, zelularen nukleoa

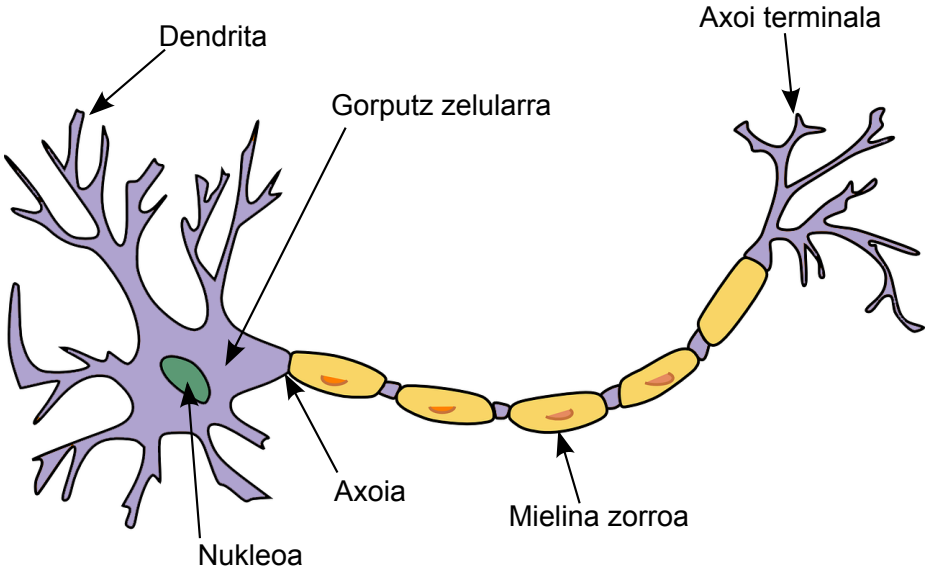

Irudia 7.1: Ohizko ugaztunen neurona baten egitura.

eta zitoplasma bere barne dituena.

- **Axoiak**: gorputz zelularretik irteten dira beste neuronetara mezuak transmitituz. Neuronek bultzada elektrikoak transmititzen dituzte bere axoietatik. Hauek zentimetro baten frakzio batetik metro bat edo gehiagora luzatu daitezke. Gorputz zelular batetik axoi bakar bat ateratzen da beti, nahiz eta axoiak, milioika adar izan ditzakeen bukatu baino lehen. Axoi ugari, mielinaz osatutako azal batekin estalita daude eta mielina estalki hauek, seinale elektrikoak axoian zehar azkarrago transmititzearen eragileak dira. Glia izena dute mielina azala sortzen duten zelula espezializatuak.

- **Dendritak**: beste neuronetatik gorputz zelularrean mezuak jasotzeko erabiltzen diren adarrak dira. Gorputz zelularrak dendrita ugari ditu neurona askotatik mezuak jaso ahal izateko. Neuronen arteko “kontaktua” gertatzen den tokia sinapsi izena

dauka. Sinapsia, neurona baten axoi batek eta beste neurona baten dendritek sortzen dute..

Axoien eta dendriten helburu nagusia neuronak konektatzea da neurona sareak osatzeko. Neurona hauek, gai gris eta gai zurian antolatzen dira. Gai grisa gorputz zelular ugariz eta mielinatutako axoi gutxiz osatuta dagoen bitartean, gai zuria mielinatutako axoi luze ugariz eta gorputz zelular gutxiz osatuta dago (7.2 Irudia). Bi substantzia hauetaz gain, burmuinean likido zerebroespinala aurkitu dezakegu. Likido honek burmuinaren kortex-arengan indargetzaile bezala lan egiten du, oinarrizko babes mekaniko eta immunologiakoa ematen dio burmuinari garezurraren barruan eta funtzio garrantzitsua du burmuinaren odol jarioaren auto-erregulazioan.

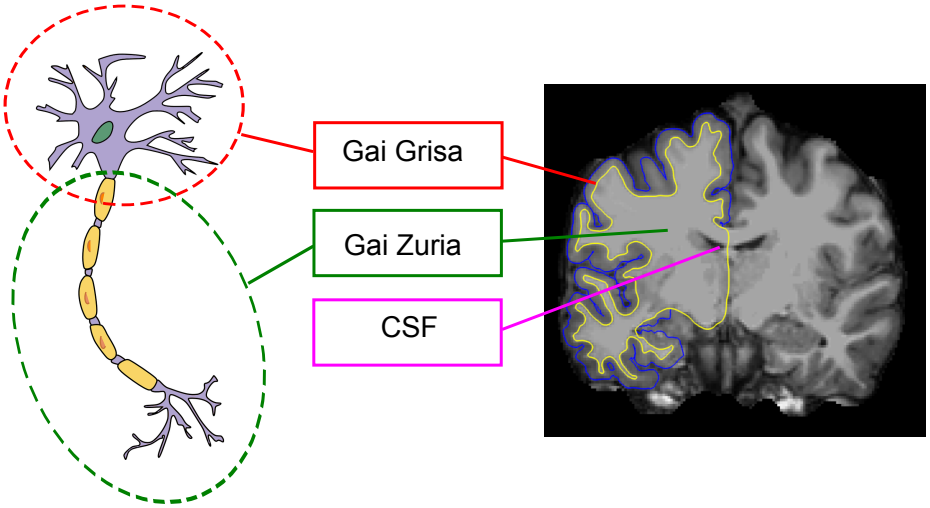

Irudia 7.2: Irudi honetan gai gris, zuri eta likido zerebroespinala ikus daitezke (ebaki koronala).

Gizaki baten garunak, 1400 zentimetro kubikoko bolumen batean 10^{11} neurona inguru ditu, non neurona bakoitzak ehun milaka sipnapsi dituen. Neurona eta sinapsi hauek, konexio zelularren sare dentso bat osatu egiten dute, oraindik mapeatu gabe dagoena [153].

Kontuan izan beharra dago, giza burmuina gorputzaren pisuaren %2a bakarrik izan harren, gorputz osoaren %20-ko energia behar duela eta ikerlariek uste dute energia honen %60tik %80ra neuronen eta haien zelulen artean komunikazioa mantentzeko erabiltzen dela. Bestalde, momentuko eskaerak (zeregin batetik sortutako neuronen aktibitatea) bakarrik energiaren %0.5 eta 1 artean behar du [125].

7.2 Garun datuak eskuratzen

Garuna ikertzeko datuak eskuratzeko teknika desberdinak daude. Teknika hauek talde desberdinetan sailkatu daitezke erresoluzio espaziala kontuan hartuz [151]:

- **Mikroeskala**: Neurona eta konexio sinaptikoak neurtzeko eskala.
- **Mesoeskala**: Neurona taldeak neurtzen ditu, ehunka mikrometroko erresoluzio espaziala izanda.
- **Makroeskala**: Neurona talde handiak hartzen ditu barne. Neurona hauek burmuinaren area desberdinak sortzen dituzte interkonektatuta dauden bideen bidez.

Tesi honetan erresonantzia magnetiko bidezko irudigintza (MRI-*Magnetic Resonace Imaginig*) delakoarekin lorturiko datuekin lan egingo da. Neuroirudi teknika honek, makroeskalan hartzen ditu irudiak.

MRI teknika, prozedura ez-inbaditzailea da eta biztanleria osasuntsuaren garunaren ezaugarri funtzionalak eta estrukturalak argitzeko trebetasuna duela erakutsi du. Beraz teknika honek oso erabilgarria den informazioa ematen du gaitz neurologiko desberdinetan agertzen diren aldaketa estruktural eta funtzionalak ikertzeko. Irudi hauen bidez garun kaltetuetan aurkitutako aldaketak biomarkatzaile bezala proposatu dira gaitz neurologiko desberdinetan diagnostiko espezifikoagoa eta azkarragoa sustatzeko, pronostiko zehatzagoa emateko eta terapia neurobabesle berriak garatzeko.

MRI-ak aplikazio ugari ditu diagnosi medikoan haren bidez garunaren irudi desberdinak eskuratu ditzakeelako. Tesi honetan egindako ikerketetan hiru irudi mota desberdin erabili dira: irudi estrukturala, difusio irudia eta irudi funtzionala (7.3 Irudia). Irudi hauek hiru dimentsio dituzte eta *voxel*-ez osaturik daude, 3 dimentsioko sareta baten balioa (alegia, *pixel*-aren 3 dimentsioko baliokidea). Irudi hauen *voxel* tamaina 1 eta 5mm artekoa da normalean bista bakoitzean (bista: sagitala, koronala, axiala).

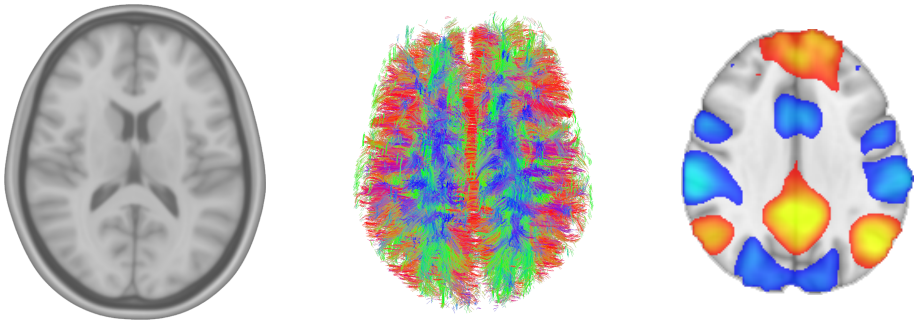

Irudia 7.3: Garun irudi estrukturala, garun-zuntzak eta sare funtzionalak.

7.2.1 Irudi estrukturalak

Kalitate altuko irudi estrukturalak, garunaren gai grisa eta zuria osatutako estruktura desberdinen forma, tamaina eta narriadura kuantitatiboki zein kualitatiboki ikertzeko aproposenak dira. Neuroirudi-teknikak erabiltzen dituzten lan guztietan irudi estrukturalak erreferentzia anatomiko bat izateko, garunaren toki interesgarriak aurkitzeko, irudi mota desberdinak bateratzeko edota talde analisia egiteko erabiltzen dira. Garun funtzioa estrukturaren ondorioz aldatu daitekenez, irudi estrukturalak erabiliz ehun galera edo kalteak seinale funtzionaletan izan ditzaketen eragina ikertu daiteke.

7.2.2 Difusio irudiak

Difusio MRIak, ur molekulen mugimendu termikoa (bai magnitudea eta bai norabidea) neurtzen du *voxel* bakoitzean. Ur molekulak libreki mugitzen dira norabide guztietan zero absolutua baino tenperatura altuagoetan ($>-273°$), mugimendua galarazten duen estrukturarik ez egotekotan. Gai grisean eta likido zerebroespinalean hedapen isotropikoa aurkitu daiteke, hau da, ur molekulak berdinki mugitzen direla norabide guztietan. Baina gai zurian hedapena mugatua dago eta ur molekulek axoien norabidea jarraitzen dute (mugimendu anisotropikoa) 7.4 irudian ikusi ahal den bezala.

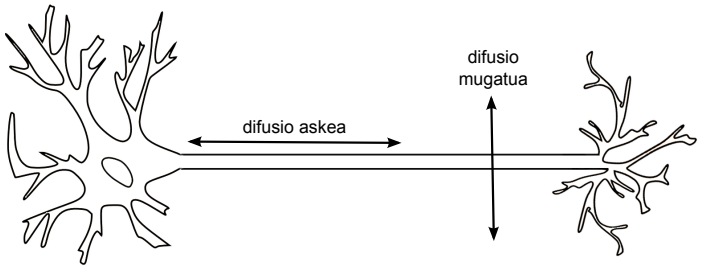

Irudia 7.4: Ur molekulen mugimendua mugatua dago axoietan.

Difusioa, ur molekulen mugimendua, hiru dimentsioko prozesua da, non molekulak norabide desberdinetan mugitzen diren. Hiru dimentsioko mugimendu hau esfera formakoa da. Mugimendu hau deskribatzeko era egokiena tentsore bat erabiltzea da (7.5 Irudia): 3 bektore tentsorearen norabideak deskribatuz eta 3 mugimendu ratio, bat norabide bakoitzeko.

Behin *voxel* bakoitzeko zuntz bakoitzaren orientazioa ezagututa, hauek lotu eta jarraitu daitezke burmuinaren bideak berregiteko, zuntz-grafikoa izeneko prozesuan. Era sinple batean azalduta; puntu batetik hasi eta zuntza jarraitzen da lehentasunezko norabidea jarraituz gai grisera heldu arte edo bi *voxel* tarteko kurba muga batera heldu arte ($45°$ normalean). Teknika sinple honen izena zuntz-grafiko determinista da eta 7.6 irudian ikusi dezakegu azalduta.

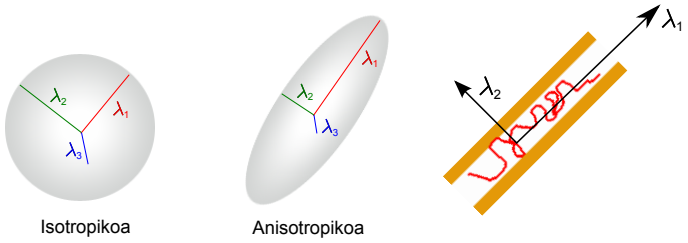

Irudia 7.5: Forma esferikoko tentsorearen mugimendu isotropikoa eta anisotropikoa eta zuntz baten 2D proiekzioa eta difusioaren mugimendua (Ezkerretik eskumara).

Zuntz-grafikoaren edo traktografiaren zuntzak ez dira benetako axoiak. Axoien diametroa 1μm da baina gure *voxel*-ak normalean 1-5mm eskalan daude. Ondorioz, milaka axoi izan ditzakegu *voxel* bakoitzean eta gainera ez dute zertan norabide berdinean joan behar. Zorionez, garun zati desberdinak lotzen dituzten konexioak, sorta luzeetan antolatuak daude non ehunka mila axoi antolatuak ageri dira. Garrantzitsua da ohartzea ez gaudela axoi bakoitzaren bideak lortzen baizik eta burmuineko estruktura makroskopikoki lortzen ari garela.

Voxel batek konexio ugari izan ditzake, haien artean zuntz sorta ugari zeharkatzen egonik. Honek askotan arazoak sortzen ditu zuntz-grafiko deterministarekin lan egiterakoan, bertan *voxel* bakoitzak bakarrik konexio bat izan dezakeelako, baina teknika berriek arazo hauei erantzun bat emateko gai dira. Teknika probabilistikoek adibidez, *voxel* bakoitzean zuntzen norabide probableena eta zuntz hauek beste norabideetan egoteko probabilitate kalkulatzen dituzte. Ondoren, konexioak milaka alditan trazatzen dira, aldi bakoitzean euren norabidea pixka bat eraldatuz (haien probabilitatea kontuan hartuta) eta horrela *voxel* bakoitza zeharkatzen duten zuntzen sorta lortzen dugu.

Zuntz grafikoa edo traktografia, ebakidurarik egin gabe, zuntz bideak irakurtzeko modu bakarra da. *Voxel* bakoitzean difusio tentsorea kalkulatzeko haztatutako irudi desberdinak hartu behar dira no-

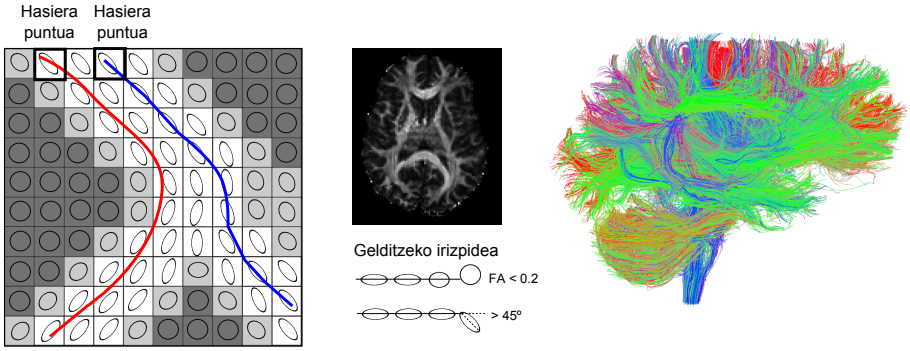

Irudia 7.6: Zuntzak berregiten hasiera puntu desberdinetan hasiz. *Fractional Anisotropy* delakoa deskribatzen duen ebaki axial-ean gai grisak intentsitate balio txikiak dituela ikusi daiteke <0.2 (zuntzen amaiera). Ez da onartzen 45° baino gehiagoko kurbatura duen zuntzik.

rabide gradiente desberdinak erabiliz eskanerrean. Tentsorea kalkulatzeko gutxienez sei norabide gradiente eskuratu beharko dira, baina hobe izango litzateke gehiago erabili ahalko balira, zuntzen tarteen erresoluzio hobeagoa izango baikenuke (nahiz eta norabide gehiago eskuratzeak eskaner barruan denbora gehiago egotea suposatuko lukeela gaixoarentzat eta hau normalean nekagarria izaten da). Irudi mota hauek, Difusio Tentsore Irudiak (DTI) izena dute. DTI neurketa onartua izan da beste metodo inbasiboekin lortutako konexio estrukturala konparatzean; adibidez garun baten post-mortem egindako disekzioaren ondorioz [32] , nahiz eta azken hau DTIak baino erresoluzio handiagoa eman.

Datu hauek prozesatzeko xehetasun gehiago ikusteko irakurri A Eranskina.

7.2.3 Irudi funtzionalak

Erresonantzia magnetiko bidezko irudigintza funtzionala (fMRI), teknika ez inbaditzailea da eta jarduera neuronalaren ondorioz agertzen

den garunaren portaera hemodinamikoa neurtzen du. Jarduera neurologikoak gora egiten duenean, honek energi eskaera bat eragiten du garunean eta odolak oxigeno gehiago askatzen du, prozesu honi erantzun hemodinamikoa deitzen zaio. Honek oxyhemoglobina eta deoxyemoglobina maila erlatiboak aldatzea eragiten du (odol oxigenatu edo deoxigenatua) eta seinale magnetikoaren aldaketa bat eragiten du, MRI eskanerra erabiliz antzeman ahal dena.

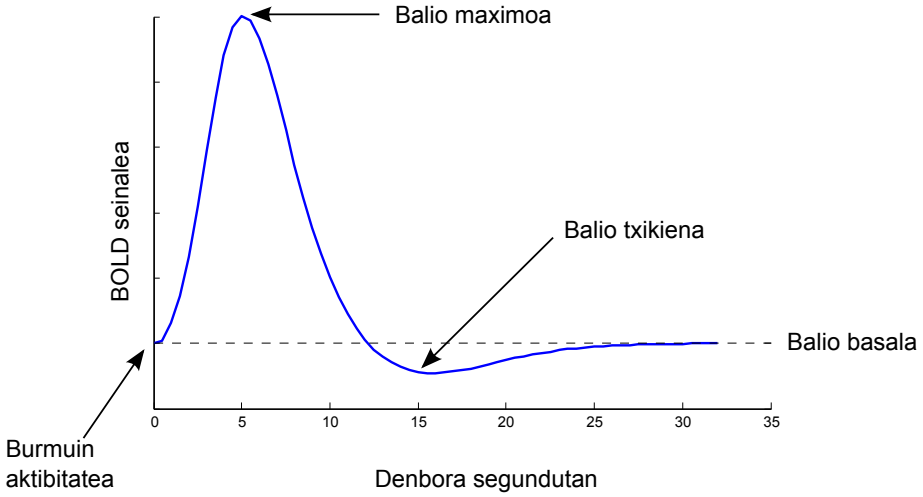

Irudia 7.7: Erantzun hemodinamikoa erakusten duen funtzioa.

Jarduera neuronala milisegundoetan gertatzen den bitartean, erantzun hemodinamikoa mekanismo motelagoa da. Azken kasu honetan, 5 segundo behar ditu balio altuenera heltzeko eta hasieratik 15 segundo pasatuko dira balio txikienera heltzen denerarte. 7.7 irudian jarduera neuronalak sortutako erantzun hemodinamiko tipikoa ikusi dezakegu. Erantzun hemodinamiko hau pertsonaren eta aztertutako burmuin zatiaren arabera aldatu ahal da.

Erantzun hemodinamikoak sistema linealak eta denboran aldaezinak izango balira bezala tratatuko ditugu (jarduera neuronal jarrai baten erantzuna denboran birkokatutako seinale hemodinamikoen batura baita).

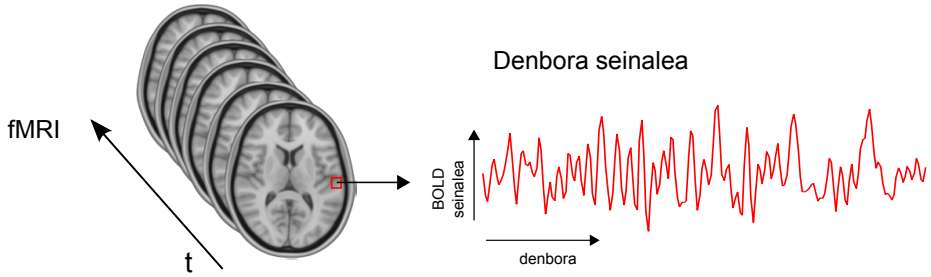

Irudia 7.8: BOLD denbora serie bat daukagu garunaren *voxel* bakoitzeko.

fMRI irudiek denbora serie desberdinak neurtzen dituzte *voxel* bakoitzeko, odoleko oxigenoaren mailaren menpeko efektua neurtuz (*blood-oxygen-level dependent*, BOLD efektua)(7.8 Irudia). Normalean denbora serie hauek 1-5mm tamainako *voxel*-etatik hartzen dira. fMRI seinalearen denbora-puntu bakoitza 1-3 segunduoro eskuratzen da (denbora erresoluzio baxua) eta normalean 200 denbora-puntu eskuratzen dira (10 minutu MRI eskanerrean).

Orokorrean, fMRI seinaleak bi modutan neurtu daitezke: gaixoa jarduera bat egiten hari denean (task-fMRI) edo atsedenean dagoenean (rs-fMRI). Task fMRI-an gaixoaren garun aktibitatea neurtzen da (erresonantzia eskaner barruan) bai estimulu bati erantzuten ari den bitartean edota jarduera konkretu bat egiten ari denean, efektu funtzionalak edo garuneko zirkuituak nola aldatzen diren ikertzeko asmoz. Bestetik, burmuinean aktibitatea ere aurkezten denez, nahiz eta jarduera bat ez egin, interesgarria izanen da egoera honetan neurketak egitea (garunaren ezaugarri hau klinikoentzat oso baliagarria da). Rs-fMRI-an gaixoen seinaleak neurtu egiten dira jarduerarik egiten ez dagoenen edota estimulurik jasotzen ez duenean. Azken kasu honetan, seinalea hartzen ari garen bitartean gaixoak ezin duela ezer konkretutan pentsatu ezta ezin dela lo geratu ere seinalatzea garrantzitsua da .

Garrantzitsua da gogoratzea denbora serie hauek, odoleko oxigenoaren mailaren menpeko (BOLD) efektua neurtzen dutela, ez dute

beraz garunaren aktibitate elektrikoa edo metabolikoa kalkulatzen baizik eta zeharkako aktibitate neuronala. Lortutako denbora seriak oso zaratatsuak dira eta prozesatze pauso desberdinak behar dituzte beste edozein analisiren bat egin baino lehen. Prozesamendu pausoen xehetasun gehiagori buruz irakurtzeko joan A Eranskinera.

Lortutako denbora serieetan osagai independenteen analisia (ICA) erabiliz, garunean atsedenan egoeran sortutako dinamikak deskonposatu daitezke aktibazio patroiak gainezarpen gisa, eta osagai hauei atseden egoera sareak (RSN) deitzen zaie. RSN-ak burmuinaren funtzionamenduaren ezaugarri garrantzitsu bat bihurtu dira eta gaur egun elementu beharrezkoak dira oinarrizko burmuin dinamikak eta antolakuntza ulertzeko bai pertsona osasunetan eta bai gaixoetan [127, 52, 123, 124]. RSN-ak garunaren leku desberdinetako seinaleen gorabeheren korrelazioek sortzen dituzte. Nahiz eta burmuin aktibitate seinale hauek testuinguru sinple batean sortu, euren dinamikak oso aberatsak eta konplexuak dira. Loturak aurkitu dira RSN eta jarduera kognitibo desberdinen artean: ikusmen jarduerak, motorzentzumen jarduerak, entzumenezko jarduerak, lehenespen jarduera, kontrol exekutibo jarduerak eta beste batzuk [10] (informazio gehiago 4 atalean aurki daiteke). RSN hauek, pertsona osasuntsu guztietan agertzen dira eta ikerketa ugarik gaixotasunekin hauek aldatzen direla ikusi dute.

7.3 Garun sareak

Konektibitatea aztertzeko garuna sare bat bezala erabiltzen da normalean. Sareek sistema biologiko konplexuak (garuna barne) aztertzeko potentzial izugarria dute eta hauek erabiliz, garunaren oinarrizko arkitektura eta funtzio nagusiak azaltzen hasi dira. Sareak deskribatzen eta kuantifikatzen dituen hizkuntza matematikoari Grafo teoria deritzogu.

Grafoak hizkuntza egoki bat eskaintzen dute burmuin osoaren patroiak eta elkarreraginak deskribatzeko (7.9 Irudia). Grafo bat sare baten irudikapen matematikoa da, erpin eta ertz mugatuez osaturik dagoena:

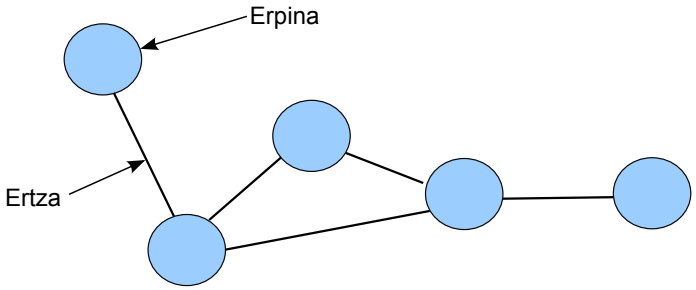

Irudia 7.9: Grafo bat erpinez eta ertzez osaturik dago.

- **Erpinak**: Garunaren leku interesgarriak dira. Hauek era egoki batean aukeratzeak eragin handia izan dezake sortutako sarean.

- **Ertzak**: Garunaren leku desberdin (erpinen) arteko konektibitatea azaltzen dute.

Grafo teoria eta ikasketa automatikoa nahastea ezin hobea da gaitz neurologikoen diagnosia eta pronostikoarentzat burmuin sareak gaixotasunekin kaltetzen direlako eta beraz, biomarkatzaile bezala erabil ditzakegu. Nahiz eta grafoek potentzial handia izan gaixotasunak ezaugarritzeko, gaur egun ez dira praktika klinikoaren tresnatzat onartzen oraindik.

Garun grafo bat eraikitzeko lehengo pausua erpinak edo garunaren leku interesgarriak aukeratzea da. *Voxel*-ak erpinetan bihurtzeko aukera desberdinak daude:

- ***Voxel*-etan oinarritutakoak**: Irudiaren *voxel* bakoitza erpintzat erabiltzen da. Grafo honekin egin beharreko azterketaren arabera, aukera hau konputazionalki oso garestia izan daiteke. Grafo algoritmo hoberenek erpin gutxi (ehunka erpinetik milaka erpinera gehienez) dituzten grafoei bakarrik aurre egin diezaiekete, beraz metodo hau ez da konputazionalki eraginkorra eta hau izango da teknika ez erabiltzearen arrazoia.

- **Atlasetan oinarritutakoak**: Hil ondoren egindako ikerketen ondorioz sortutako jakintza anatomikoa atlas ugari sortzera eraman gaituzte (identifikatu den burmuinaren leku bakoitza erpin bat izango da). Hau da gehien erabiltzen den metodoa burmuinaren grafoa egiteko eta aztertzeko.

- **Datuetan oinarritutakoak**: Datuetan oinarritutako algoritmoak, osagai independenteen analisia (ICA) edo multzokatze teknikak, erabiltzen dira gaixo espezifiko baten burmuin leku funtzional edo estruktural desberdinak aurkitzeko. Kasu hauetan erpin bat aurkitzen da burmuinaren leku bakoitzarentzat, baina kasu honetan *voxel* bat burmuineko leku bat baino gehiagora egokitu daiteke. Teknika honi buruzko xehetasun gehiago 9 atalean ikusiko dira.

Behin erpinak aukeratuta, gure garun-grafoa eraikitzeko hurrengo pausua erpin hauen artean konektibitatea definitzea da. Hiru konektibitate modu nagusi daude [151, 19]:

- **Konektibitate estrukturala**: konexio anatomikoak kodetzen ditu garun leku desberdinen artean [149], normalean difusio irudietako gai zuriko zatietatik ateratako zuntzak [38]. Gai zuriaren (des)konektibitatea gaixotasun neurologiko eta psikiatriko ugariren kausa dela pentsatzen da.

- **Konektibitate funtzionala**: populazio neuronal desberdin artean azaltzen diren aktibazioak eta mendekotasunak dira [56]. Garuneko antzeko bi gunek aktibazio funtzionala badute, konektibitate balio sendoa izango dute bi erregio horien artean (7.10 Irudia). Zaila da mendekotasunak kalkulatzea erpinen zenbakia handia denean denbora puntuen kopuruarekin konparatuz.

- **Konektibitate efektiboa**: Elkarreragin kausalak edo informazio fluxua identifikatzen ditu [58].

Konexio hauek ezin bestekoak dira gure burmuinaren funtzionamendua ulertzeko (Data estrukturaletik, burmuinaren leku urrutien

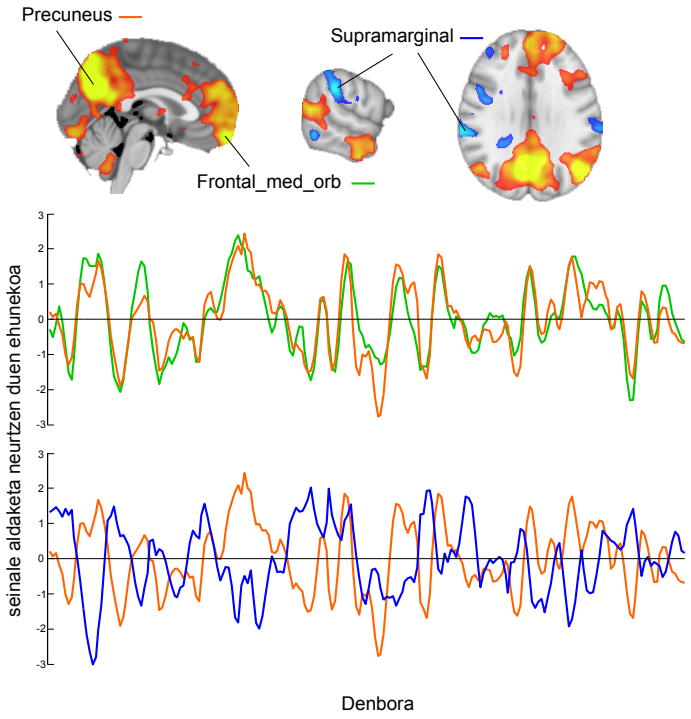

Irudia 7.10: Prekuneoko voxel bateko serie denbora bat hartura, gainontzeko garunaren *voxel*-en serieekin konparatzen badugu, euren arteko korrelazioa ikusi dezakegu. Garunean, korrelazio positiboa duten erregioak kolore gorriz irudikatuta daude. Korrelazio negatiboak ordea, kolore urdinetan ikusi ditzazkegu. Prekuneoko aktibitatearen seinale denborala kolore laranjaz irudikatuta dago eta garuneko aurreko partea kolore berdez. Irudian behatu daitekeenez, bi erregio hauen artean korrelazioa handia da eta bi denbora seinaleak oso antzekoak dira. Supramarginal erregioa ordea (denbora seinale urdina), haurreko biekin antikorrelazionatuta dago. Prekuneo aktibatuta dagoenean supramarginal area ez da aktibaturik egongo eta alderantziz.

arteko informazio transferentziara). *Voxel* bakoitzeko analisi bakarra egin beharrean, burmuinaren *voxel*-en arteko elkarrekintza ikasteko garun sareak garrantzia irabazten ari dira.

Taula 7.1: Mota desberdineko konektibitate sareak lor daitezke algoritmo desberdinak erabiltzen.

Konektibitate Estrukturala	**Konektibitate Funztionala**	**Konektibitate Efektiboa**
Zuntz kopurua	Pearson Korrelazioa	Granger-kausalitatea
Bolumena	Korrelazio partziala	Entropia transferentzia
Dentsitatea	Elkarrekiko informazioa	Zuzeneko kausal eredua
Zuntz luzera	Koherentzia	Estruktural ekuazio eredua
Fractional Anisotropy	Fase sinkronizazioa	
Mean Diffusivity	Sinkronizazio lineal orokorra	
Radial Diffusivity		
Axial Diffusivity		

Erpinak konektatzen dituzten ertzak noranzkorik gabeak edo noranzdunak izan daitezke. Noranzko ertzek norabide jakin bat dute eta beraien ondokoetan eragin bat dute (bi erpinak ondokoak dira beraien ertzetatik konektatuta daudenean), baina ez beste norabidean. Beste aldetik, noranzkorik gabeko ertzeetan A-B erpinen arteko eragina eta B-A erpinen arteko eragina berdina da. Grafoa sortzerakoan, Konektibitate estruktural edo funtzionaletatik noranzkorik gabeko sareak lortzen ditugun bitartean, konektibitate efektiboa kalkulatzerakoan noranzdun sareak lortzen ditugu. 7.1 taulak sare hauek ze algoritmoekin sor daitezkeen erakusten du.

Hurrengo ataletan grafoak sortzeko eta hauek gaixotasunak ikertzeko nola erabiltzen diren azalduko da.

7.4 Tesiaren ikuspuntu orokorra

Tesi honetan garun sareak erabili dira patroi funtzionalak eta estrukturalak burmuin osasuntsuetan aztertzeko eta hauek gaitz neurologikoekin nola aldatzen diren ikertzeko.

Bigarren atalean sareak sortzeko emandako pausuak xehetasun

gehiagorekin azaltzen dira. Ondoren, kontzientzia gaitzen biomarkatzaile berriak bilatu egin dira sare funtzionalak eta efektiboak erabiliz. Azkenik, biomarmatzaile hauek praktika klinikoan erabiltzen diren proba desberdinekin konparatu dira.

Hirugarren atalean sare funtzionalak eta estrukturalak bateratuz, garun atlas berri bat sortu da (bai estruktura eta funtzioa kontuan hartzen dituena). Era berean, Modularitate gurutzatua deskribatu egiten da, garun partizio hoberena aukeratzeko aurkezten den metodo berria. Lortutako garun zatiketa atlas anatomiko eta funtzional desberdinekin konparatu ditugu.

Laugarren atalean, osagai nagusien analisia erabilita, atsedenean agertzen diren sareetatik informazio gehiago lortu da informazio-fluxu metodo berri bat garatzeko (osagai gehiago erabiliz). Metodo berri hau, Alzheimer gaitza jasaten duten pertsonetan atseden sare desberdinak bilatzeko erabili da eta desberdintasunak ez direla beti osagai nagusian gertatzen frogatu dugu (normalean informazio-fluxua kalkulatzeko metodoetan erabiltzen dena).

Bostgarren atalean, 9-garren atalean sortutako atlas-a erabili da axoietan kalte duten gaixoen burmuin berrantolaketa ikertzeko (berrantolaketa funtzionala eta estrukturala). Era berean, garun zati desberdinetatik osagai gehiago erabiliz (4-garren atalean bezala), kalteak dituzten garunetan bere zati desberdinen elkarreraginak espezifikoak aztertzeko teknika berri bat garatu da.

Tesi honi bukaera emateko, azken atal bat garatu da non ikerketarekin lortutako ondorioak azaltzen diren.

Era osagarrian, BioCruces Ikerketa Institutuan egindako lana oinarritzat hartuz, Web plataforma berri bat ezarri dugu Gurutzetako Unibertsitate Ospitaleko neuroirudi datuak automatikoki prozesatzeko. Ospitaleko profesionalek zituzten beharrei erantzuna emateko izan da Web plataforma eraikitzearen arrazoia. Plataforma buruzko informazio gehiago ikusteko B Eranskina irakurri.

Kapitulua 8

Kontzientzia gaitzen garun funtzio aldaketak

Kapitulu honetan sare funtzional eta efektiboak nola sortu daitezkeen ikusiko da kontzientzia gaitzetan garrantzitsuak diren biomarkatzaileak aurkitzeko asmoz.

Azken urteotan frogaturik geratu da fMRI-ren bidez eskuratutako irudiak erabiliz lortzen diren garun sareak kontzientzia gaitzen (DOC) ondorioz aldatu egiten direla [113, 76]. DOC-a, burmuinaren lesio larri baten ondorioz gerta daiteke eta gaitz hau duten gaixoek, bi ezaugarri desberdin izan ditzakete: alde batetik loaren zikloa eten egin daiteke eta beste aldetik, norbera eta bere ingurunearen ezaguera galdu dezakete.

Egoera kliniko ugari daude DOC izenaren azpian, lo zikloa eta norberaren ezagueraren arabera sailkatzen direnak , hala nola, koma egoera (non lo zikloa eten egiten den eta gaixoak ez diren esnatzen), egoera begetatiboa (-VS-, non lo zikloa ez den kaltetzen baina norberaren eta inguruaren ezaguera galdu egiten den), kontzientzia minimoa (-MCS-, gaixo hauek ez dira komunikazio fidagarri bat edukitzeko gai baina haien existentziaren ezaguera dutela erakusten dute) edota gatibu sindromea (-lock-in sindromea edo LI -, non pertsonak guztiz kontzienteak diren baina mugitu ezinik daudenak, begi mugimenduak kenduta).

DOC gaixoen pronostiko maila neurtzeko, praktika klinikoetan

Glasgow Coma Scale (GCS) [158] erabiltzen da. Atal honetan eskala alternatibo bat erabili da, *JFK Coma Recovery Scale-Revised (CSR-R)* [64] hain zuzen ere, eskala honek egoera neurologikoa eta norberaren ezaguera hartzen baititu kontuan. 0-23 tarteko balioko eskala da non 0 koma egoera sakonena den eta 23 guztiz berreskuratuta gaixoa deskribatzen duen.

Nahiz eta eskala hauek praktika klinikoan egunero erabiltzen diren, neuroiruidietan oinarritutako metodo fidagarriagoak behar dira DOC gaixoen garun aldaketa funtzionalak era egokian deskribatzeko gai izateko. Koma egoera ulertu eta gaixoen eboluzioa zein izango den aurresateko metodo berriak diseinatzea beharrezkoa da. Irakurlea ohartu beharra dago, DOC gaixoetatik lortutako neuroirudiak "atsedenen egoeran" lortutakoak izango direla, gaitz hauek jasaten dituzten pertsonek ezin baitute jarduera espezifikorik egin.

Atal honetan fMRI seinaletatik lortutako konektibitate funtzional eta efektiboa kontzientzia gaitzen ondorioz aldatzen den aztertuko da. Ikerketa garatzeko, bi subjektu talde desberdinen informazioa aztertu da: heldu osasuntsuak alde batetik eta DOC gaixoak bestetik. Desberdintasun nabarmenak aurkitu dira bi taldeen artean ikerketa burutzerako orduan eta hurrengo azpiataletan azalduko dira.

8.1 Subjektuak eta datuen aurre prozesamendua

Lehen azterketa honetan, hamazazpi heldu osasuntsu (Kontrol Taldea), 25 ± 5 urte tartean dauden eta arazo neurologiko eta psikiatrikorik gabekoak, parte hartu zuten. *Edingburdg Handedness Inventory* erabili izan zen subjektuak eskuinak edo ezkerrak ziren aztertzeko [114]. 13 subjektu eskuinak ziren eta 4 ezkerrak.

Aldiz, DOC taldea 11 DOC gaixok osatu zuten. Euren adin tartea 17-44 urtekoa izan zen eta 6 gizon eta 5 emakumek osatzen zuten talde. Irakurlea ohartu beharra dago bi gaixoren informazioa baztertu behar izan zela eskaner barruan asko mugitzen baitziren. Gaixo bakoitzaren koma eskala *Revised Coma Recovery Scale* (CRS-R, [64])

Taula 8.1: DOC gaixoen ezaugarri klinikoak. TSI: istripua gertatu zenetik pasatutako denbora; VS: egoera begetatiboa ; MCS: norberaren existentziaren ezaguera minimoa; C: kontzientea; EMCS: MCS-tik azaleratuak (MCS eta C arteko egoera); *: bigarren eskaner aurretik kontzientzia berreskuratu zuten gaixoak

Gaixoaren kodea	Adina	TSI (hilabetetan)	1 eskanerrean egoera	Eskanerren arteko denbora (hilabetetan)	2 eskanerrean egoera
P1	34	2	VS	5	VS
P2*	18	4	MCS	4	C
P3*	44	2	MCS	3	C
P4	17	6	VS	6	MCS
P5	26	4	VS	3	MCS
P6*	26	4	EMCS	4	C
P7	29	4	MCS	3	MCS
P8	41	2	VS	6	VS
P9*	34	5	VS	5	C

erabiliz neurtu zen, non bere eskala, lehen esan bezala, 0-tik (koma egoera sakonena) 23-ra (berreskurapen osoa) doan. Gaixoak bi aldiz eskaneatu ziren: lehenengoa, 2-6 hilabete igarota burmuinaren lesioa gertatu ondoren eta bigarrena 3-6 hilabete pasa zirenean(8.1 taula). 4 DOC gaixok (Berreskurapen Taldea) kontzientzia berreskuratu zuten bigarren eskanerra egin baino lehen (izartxo baten bidez adierazi dira 8.1 taulan).

Ikerketaren protokoloa *Insitute of Neurological Research - FLENI*-ren etika batzordea onartu zuen eta parte hartzaileen informatutako baimena osasuntzuetatik eta gaixoen senidu hurbilenetik jasoa izan zen.

Pertsonekin lan egiten den ikerketetan, ikerketa protokolo bat onartu behar da eta gaixoek euren datu medikoak ikerketarako erabiltzea onartu behar dute, azterlana aurrera eraman ahal izateko. Kasu honetan, ikerketaren protokoloa *Insitute of Neurological Research - FLENI*-ren etika batzordeak onartu zuen eta parte hartzaileen informatutako baimena pertsona osasuntsuetatik eta gaixoen senide hurbilenetik jaso zen.

fMRI datuak 3 Tesladun Signa HDxt GE eskaner bat erabiliz lortu ziren. Subjektuak atsedenean zeudela erresonantzia magnetikoaren bidezko irudi funtzional eta anatomikoak lortu ziren (erresonantzia irudiak egiteko erabili ziren protokolo xehetasunak aztertu nahi izatekotan [97] erreferentzia irakurri). Erresonantzia magnetikoaren bidezko irudi funtzionala lortzeko, subjektuek 7 minutu igaro behar izan zituzten eskaner barruan etzanda, mugitu eta hitz egin gabe.

7 minutuetan hartutako irudi funtzionalak lerrokatu ondoren, eskaner barruan buruarekin egindako mugimenduaren efektuak zuzentzen dira. Lortutako irudiak garun estandar baten formara transformatu behar dira (Montreal Neurological Institutoak sortutako garun irudi estandarrera hain zuzen ere), talde konparazioak egiteko [6]. Normalizatutako irudiak 4 x 4 x 4 mm^3 tamainako *voxel*-ez osatuta daude. Hauek 8-mm FWHHM kernel isotropiko bat etabiliz prozesatzen dira. Ondoren, fMRI seinalearen joera lineala kendu ostean 0.01Hz - 0.08Hz artean dauden seinaleak hartzen dira. Aurreprozesuaren detaile gehiago ikusteko A Eranskina irakurtzea gomendatzen diogu irakurleari.

8.2 Konektibitate funtzionalean aurkitutako aldaketak

Sare teoria erabiliz sare funtzionalak eta estrukturalak burmuinaren dinamika aztertuz lortu daitezke. Datu hauek garun zati garrantzitsuak aurkitu eta hauen sinkronizazio mekanismoak zehaztu ditzakete. Lehengo atalean definitu den bezala, grafo funtzionalak populazio neuronal desberdinen artean azaltzen diren aktibazioak eta mendekotasunak dira.

90 interes erregio (ROI) definitu ziren *Automatic Anatomical Labeling atlas*-ean (AAL) oinarrituz [161], (ikusi 8.1a, 8.1b eta 8.1d irudiak). Burmuinaren area bakoitza bi ROI-ez azalduta ageri da, bat ezkerreko hemisferioan eta beste eskuinekoan (adb. ezkerreko hipokanpoa, eskuineko hipokanpoa, ezkerreko amigdala, eskuinako amigdala etab). Beraz, AAL atlasa 45 burmuin zati ditu 90 ROI

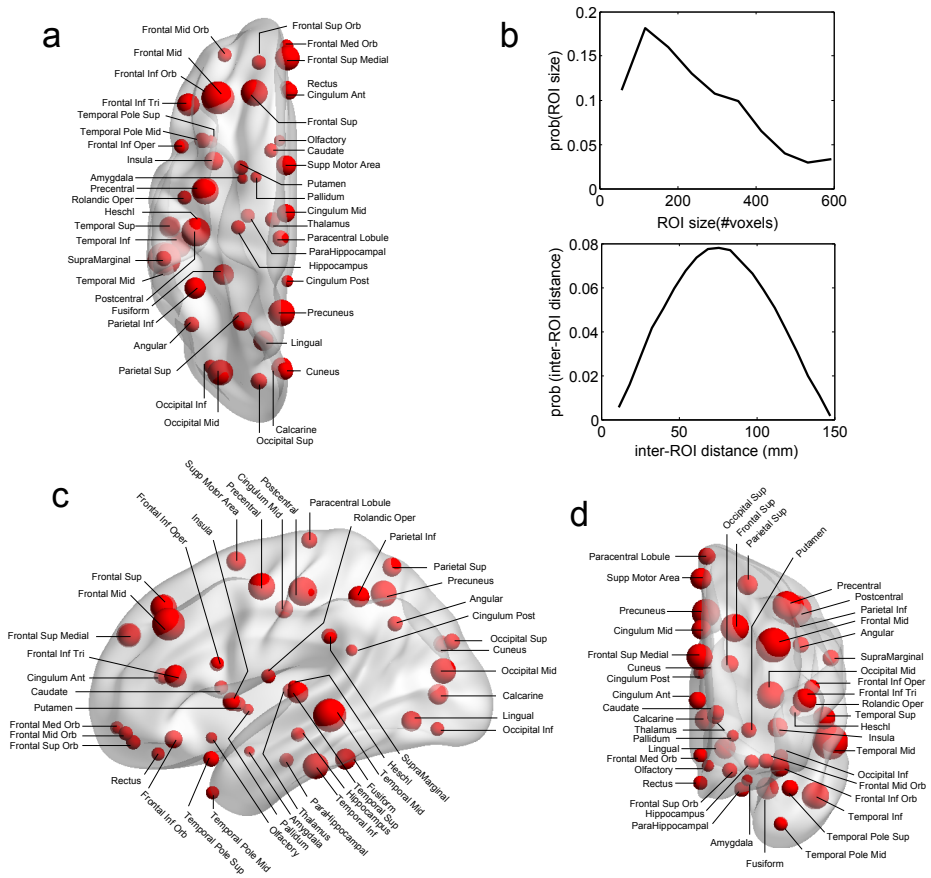

Irudia 8.1: **Garun zatiketa anatomikoa.** Bista: **a**: Axiala, **c**: Sagitala , **d**: Koronala. Esfera gorriak burmuin zati desberdinak adierazten dituzte. Esferen diametroak burmuin zatien tamainarekiko proportzionalak dira. Atlas honek garun zati kortikalak eta subkortikalak ditu. **b**: Zatien tamaina eta zatien arteko distantziaren distribuzioak. *Voxel* bakoitzak 4 milimetro kubiko inguru ditu eta garun zati bakoitzak ≈ 150 *voxel* ditu bataz beste. Garun zati handienak ≈ 600 *voxel* inguru ditu.

desberdinez osatuta. AAL atlasa zati kortikalak eta subkortikalak hartzen ditu bere barne, eta horregatik DOC gaixoak ikertzeko aukeratua izan zen.

Enpirikoki, ROI bakoitzak osatutako *voxel* guztien denbora seinaleen batezbestekoa egin ondoren fMRI denbora-seinale bakar bat lortzen da. Denbora-seinale honek ROI honen aktibitatea deskribatuko du (8.1 irudiak burmuineko ROI-en banaketa erakusten du). ROI bakoitzaren erdialdeko koordenatuak euren arteko distantzia kalkulatzeko erabiltzen da (8.1b Irudia). Modu desberdinak daude ROI baten aktibitatea kalkulatzeko; informazio gehiago nahi izatekotan, irakurlea A Eranskinera jo dezake. Tesi honetan denbora-seinaleen batezbestekoa erabili da adierazi den bezala.

Burmuinaren *voxel* desberdinen aktibitate funtzionala ikusmiratzen bada, pareko portaera duten zonaldeak aurkitu daitezke (7.10 irudia). Garuneko bi zona desberdin momentu berdinean aktibatzen badira, horrek zihurrenik elkar lan egiten dutela esan nahiko du seguru aski, hau da, nolabait konektatuta daudela. Bi gune desberdin hauen aktibitatean oinarrituz erregioen arteko konexioaren pisua kalkulatzeko aukera dago. Garunean zonalde antikorrelatuak daudela esango da, zona bat aktiboa dagoen bitartean bestea ez-aktibo egoeran dagoenean (7.10 irudia).

Konektibitate funtzionala matrize baten antzera irudikatzen da, non matrizearen gai edo elementu bakoitzak garunaren 2 gune desberdinen arteko konexiotzat deskribatzen du. Bi 90 x 90 konektibitate matrizeak ikusi ditzazkegu 8.3 Irudian. Matrizearen lehenengo lerroak AAL atlasaren lehengo zatiaren (*Precentral Left*) konektibitatea azaltzen du. Lerro honetako zutabe bakoitzak burmuin zona honek burmuineko beste zona guztiekin duen konektibitatea irudikatzen du (balore negatiboak antikorrelazioak adierazten dituztelarik). Matrize honen diagonala 1 zenbakiaz osaturik dago, 8.3 irudian ikusten den bezala . Honek, burmuinaren zati bakoitza berarekin korrelazionatuta dagoela esan nahi du. Konektibitate funtzionala matrize simetriko bat da, Ak Brekin duen konexio balioa Bk Arekin duen balio berbera da.

Konektibitate funtzionala lortzeko era ohikoena fMRI denbora-

seinaleen arteko korrelazioa kalkulatzea da [17]. Bi bumuin gune desberdin korrelazio balio altua badute, hiru egoera eman daitezke: zuzenki konektatuta egotea, zeharki konektatuta egotea edota konexiorik izan gabe (baina) sarrera berdina edukitzea (8.2 Irudia).

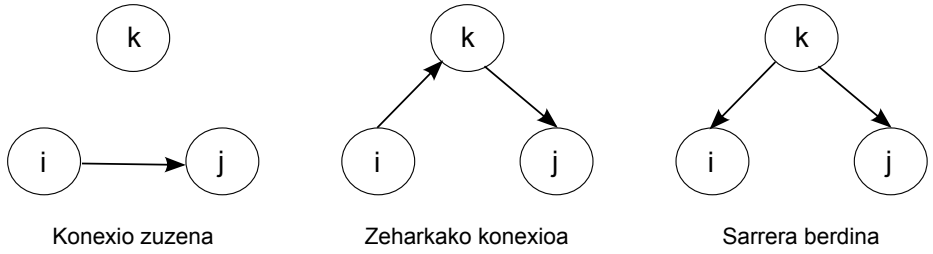

Irudia 8.2: Garunaren bi zona korrelazio balio handia izan dezakete hiru egoera hauetan: bi zati hauek konexio zuzena dutenean (ezkerreko irudia), zeharkako konexioa dutenean (erdiko irudia) edo sarrera berdina dutenean (eskuineko irudia).

Pearson korrelazioa kalkulatu ondoren burmuin zati guztiak korrelaturik daudela ikusi daiteke (8.3 irudia). Korrelazio mota honek ez ditu zuzenki edo partekatuta dauden konexioak elkarren artean desberdintzen.

Atal honetan korrelazio partziala (PC) erabili dugu sare funtzionalak denbora-seinaleetatik sortzeko. PC zeharkako efektuak ezabatzen ditu (Pearson korrelazioa eta korrelazio partziala nola kalkulatzen diren, A Eranskinean aurkitu daiteke). Talde lan honek egindako beste aurreko ikerketa batean [3], PC eta konektibitate estrukturala (zuntz grafikotik ateratakoak) oso antzekoak zirela frogatu zen, Pearson korrelazioa baino antzekoagoak hain zuzen ere.

8.4 irudiak kontrol eta DOC taldeko bi subjektuen konektibitate matrizeak erakusten ditu. Diagonal nagusiarekin paralelo dauden bi lerro diagonal ikus daitezke kontrol matrizean. Bi diagonal hauek, DOC matrizean desagertu egiten dira. Lerro diagonal hauek, burmuinaren hemisferio arteko area kideen konektibitatea erakusten dute. 2 taldeen arteko desberdintasun hau biomarkadore bezala erabili dai-

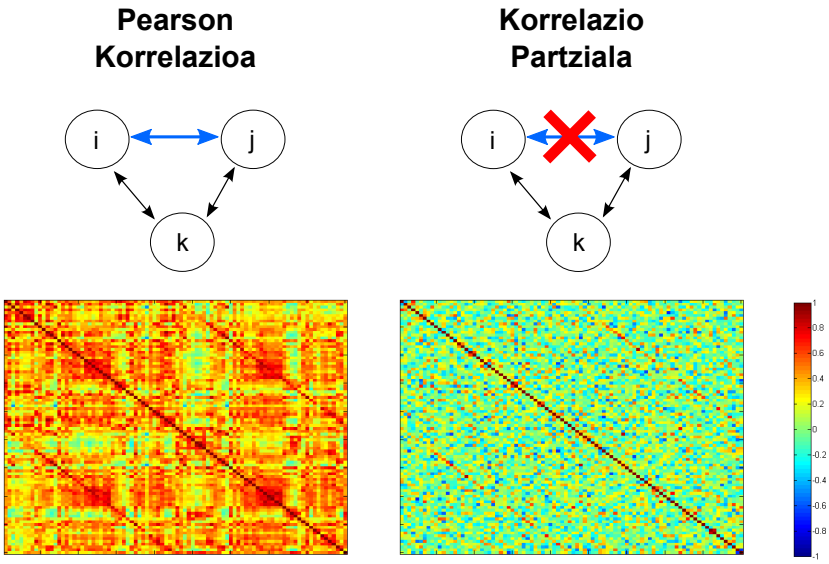

Irudia 8.3: Pearson korrelazioak konexio zuzenak eta zeharkakoak (lerro urdina) kalkulatzen ditu. i k-ra konektatuta badago eta k j-ra, orduan i eta k konektatuta egongo dira. Korrelazio partzialak zeharkako efektua ezabatzen du eta konexio zuzenak erakusten ditu soilik.

teke DOC gaixoetan.

Pearson korrelazioa erabiliz lortutako emaitzak berdinak dira, nahiz eta korrelazio mota honek zeharkako konexioak eduki.

Ikerketaren joatean, subjektu bakoitzarentzat PC matrizea kalkulatu zen. PC balioak talde desberdinetan sailkatu ziren hurrengo klasifikazioa erabiliz : inter-hemisferikoa (ezkerreko area bat eskuineko hemisferioan dauden area guztiekin duen konexioa, edo alderantzizkoa), inter-hemisferio homologoak (ezkerreko area bat eskuineko hemisferioan dagoen area berberarekin, edo alderantzizkoa),eskuin intra-hemisferikoa, ezker intra-hemisferikoa eta guztiak batera.

Prozesuan zehar, lehenik eta behin kalkulatutako PC konexioak begiratu ziren (ikusi 8.2 taula). Bariantza-analisiak konexio patroi desberdinak aurkitu zituen konexio taldeen artean ($p<0.001$). Konexio talde hauek Kontrol taldearekin eta DOC taldearekin artean

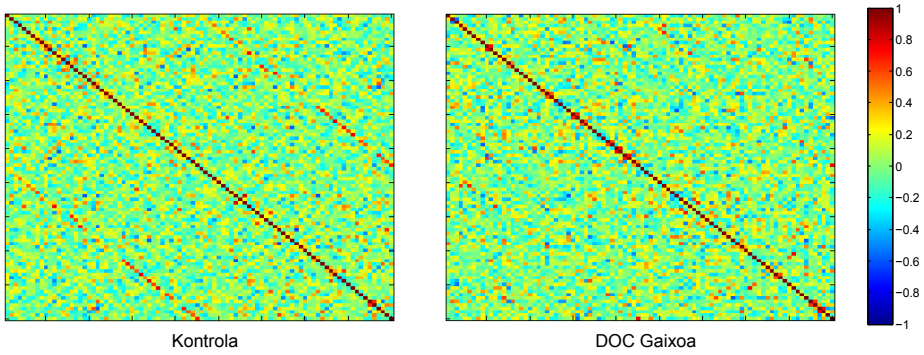

Irudia 8.4: Kontrol eta DOC pertsona baten matrize funtzionalak. Hemisferio arteko kidetasun konexioak desagertzen dira DOC gaixoetan.

konparatuz honako desberdintasunak ikus daitezke ($p<0.001$):

- Kontrolen batezbesteko PC balioa gaixoena baino baxuago zen ($p<0.001$).
- Konexio desberdinak begiratzen badira, konexio inter-hemisferiko homologoak handienak dira konexio intra-hemisferiko eta inter-hemisferikoekin konparatuz ($p<0.001$).

Taula 8.2: PC balioen laburpena (batazbeste ± desbidaratze estandarra) . **Kontrolak eta DOC balio desberdinak dituzte; p<0.05.*

Korrelazio Partziala	Kontrolak	DOC	Berreskuratuak
inter-hemisferiokoa	0.11±0.01	0.12±0.01	0.12±0.01
inter-hemisferio homologoak	0.4±0.03	0.24±0.03*	0.26±0.04*
ezker intra-hemisferiokoa	0.13±0.01	0.15±0.01	0.15±0.01
eskuin intra-hemisferiokoa	0.13±0.01	0.15±0.01	0.15±0.01
Guztiak	0.12±0.01	0.13±0.01*	0.13±0.01*

- Intra-hemisferio konexioak inter-hemisferio konexioak baino altuagoak dira ($p<0.001$).
- Inter-hemisferio homologoko konexioak Kontroletan altuagoak dira ($p<0.001$).

Seinale hauetatik kalkulatutako konexio inter-hemisferikoek zentzumen kortexeko datu elektrofisiologikoekin korrelazio haundia dute [112], gamma erritmoekin batez ere. Datu guzti hauek beraz, DOC gaixoek dituzten konexio inter-hemisferiko baxuek datu elektrofisilogikoen gama erritmoen koherentzian aldaketa bat gertatuko dela adierazten dute.

Koma egoeratik berreskuratutako gaixoen taldea kontrol taldearekin konparatzen baditugu, konexioen arteko desberdintasunak mantentzen direla ikus daiteke, hain nabarmenak ez diren arren ($p=0.002$). Konexio mota desberdinen arteko efektuak berdin mantentzen dira. Inter-hemisferio homologoko konexioak Kontrol taldearenak baino txikiagoak dira ($p<0.001$). Garun konexio guztiak kontuan hartzen badira, orduan bai desberdintasunak ikus daitezkeela kontrol eta gaixoen taldeen artean ($p=0.018$). Datu hauek 8.2 taulan eta 8.5 irudian ikus daitezke.

Konexio inter-hemisferiko homologoen artean, konektibitate patroi desberdinak ikus daitezke; hurbilago dauden konexioek korrelazio balio handiagoak dituzte urrunago daudenak baino. Distantziaren araberako konexioen portaera ikertzeko, garun zati desberdinen arteko distantzia Euklideoa neurtu zen. Kontrol taldean konexio hauek balio altuak dituztela antzeman zen, beti ere 20mm baino hurbilago egotekotan. 20mm baino urrunago dauden garun zatiak korrelazio baxuagoak dituzte. Portaera hau, DOC gaixoekin mantendu egiten da. 20mm baino hurbilago dauden garun zatietan konexio altuagoak aurkitzen dira eta ez dira kontrol eta DOC taldeen artean desberdintasunik ikusi. Bestalde, 20mm baino urrunago dauden garun zatiak konexio balio baxuagoak dituzte DOC taldean ($pval=10^{-6}$). Era berean, distantzia handiagoak hartzen badira desberdintasunak ere handiagoak dira (>40mm $pval=10^{-14}$). Koma batetik berreskuratu diren subjektuetan urrun dauden konexioak DOC gaixoek dituztenak baino balio altuagoak dituzte (8.6 Irudia).

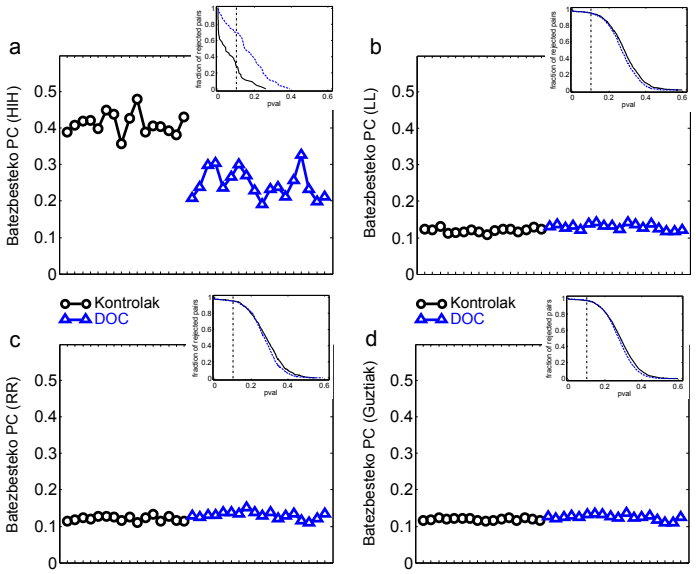

Irudia 8.5: **Subjektu bakoitzaren batezbesteko PC balioak**. **a**: HIH (konexio inter-hemisferiko homologoak); **b**: LL (ezker intra-hemisferiko konexioak); **c**: RR (eskuin intra-hemisferiko konexioak); **d**: Guztiak. Adierazgarriak ez ziren konexio guztiak ikusi ahal dira irudian, hauek analisietatik kanpo geratu ziren. Zirkulu beltzak kontrolak dira; Triangelu urdinak DOC gaixoak dira: Kontrol eta DOC gaixoen artean HIH konexioak oso desberdinak dira. Hau ez da beste konexio motetan gertatzen (LL eta RR). Balio hauek miatzeko, 8.2 taulara jo.

Laburbilduz, korrelazio partziala erabiliz, kontrol, DOC eta koma batetik berreskuratu diren gaixoen artean desberdintasunak ikusi daitezkeela esan dezakegu. Zehazki, inter-hemisferikoki konektibitate baxuagoak eta intra-hemisferikoki konektibitate altuagoak ageriko dira DOC gaixoetan.

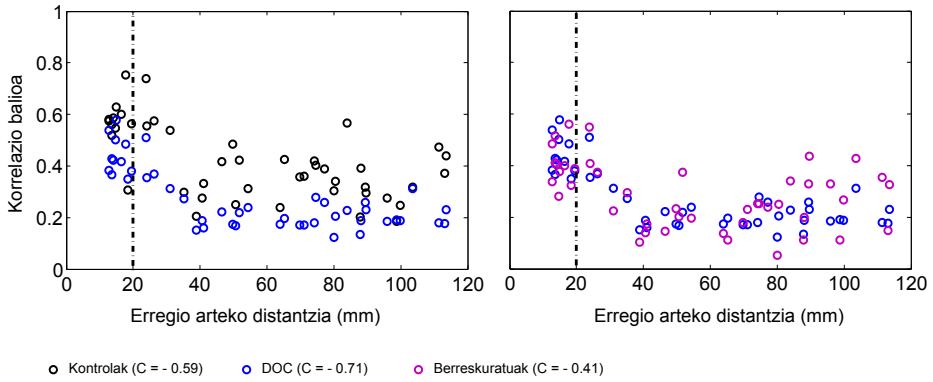

Irudia 8.6: **Konexio inter-hemisferiko homologoen batuketa**. Garun zatien arteko konexioa behera egiten du beraien arteko distantzia handiagoa denean. Antzeko portaera ikusi daiteke hiru taldeetan: Kontrolak, DOC eta Berreskuratuak.

8.3 Konektibitate efektiboan aurkitutako aldaketak

Konektibitate efektiboak, elkarreragin kausalak edo informazio fluxua identifikatzen ditu. Informazio teoriaren bidez definitutako metodoak erabiltzen dira konektibitate hauek kalkulatzeko.

Informazio teoria Shannon-ren entropian oinarrituta dago, azken honek zorizko aldagaren batazbesteko ziurgabetasuna neurtzen duelarik. Bi aldagaien arteko elkarreagina neurtzeko, aldagai bat ezagututa beste aldagaiaren ziurgabetasuna zenbat murrizten den kalkulatzen da [82, 34]. Azken hamarkadan, transferentzi entropia (TE) metodoa erabiltzen hasi da denbora-seinale desberdinen arteko elkarreragina kalkulatzeko, [137] ikerketan ikusten den bezala. Ikerketa honen gaiarekin erlazionatzen badugu, transferentzi entropia erabiliz garunaren konektibitate efektiboa kalkulatu daiteke (era berean elkarreragin ez linealak ere neurtzeko gai da). Kasu honetan konektibitate matrizeek norabideak izango dituzte (eta matrizea ez da simetrikoa izango). A-tik B-ra eragindako elkarreragina ez da B-tik A-ra

dagoen elkarreragin berdina. TE kalkulatzeko informazio gehiago A Eranskinean aurkitu daiteke. TE-ak, ROI baten etorkizuneko aktibitateak eta beste ROI baten aktibitateak (lehenengo ROI-a kondizio duelarik) duten elkarrekiko informazioa neurtzen du zehazki. Datu gaussiarrak edukitzeko kasuan, TE eta Granger kausalitate metodoak erabiliz, balio berdinak lortuko [8].

Lortutako datuek denbora puntu gutxi dituztenean TE-ak *bias* bat aurkeztuko du [117, 116, 18]. Kasu honetan Kontrol eta DOC gaixo taldeek denbora puntu berdinak dituzte, beraz *bias* hau bi taldeetan egongo da eta konparazioak arazorik gabe egin ahal izango dira.

Subjektu bakoitzarentzat TE matrize bat kalkulatu da ikerketa honetan. Lortutako TE balioak talde desberdinetan banatu egin direlarik, hala nola, konexio inter-hemisferikoak (ezkerreko area batek eskuineko hemisferioan dauden area guztiekin duen konexioa, edo alderantziz), konexio inter-hemisferiko homologoak (ezkerreko area batek eskuineko hemisferioan dagoen area berberarekin, edo alderantziz), eskuin intra-hemisferikoak, ezker intra-hemisferikoak eta burmuin guztiko konexioak.

Kalkulatutako TE balioekin bariantza analisia egitea da hurrengo pausua. Analisi honetan, taldeen artean ($p=0.0025$) eta konexio desberdinen artean ($p<0.001$) desberdintasunak aurkitzea da helburua eta TE konexio inter-hemisferiko homologoak eta beste konexioen artean desberdintasuna handia dela aurkitu egin da kontrol subjektuetan. Zehazki, TE konexio homologoak konexio intra-hemisferiko eta inter-hesmiferikoak baino baxuagoak dira (ezkerrekoak: $p<0.005$. eskuinekoak: $p<0.025$). Ezkerreko TE konexio intra-hemisferikoak, ezkerretik eskuinerako TE konexio inter-hemisferikoak eta garun guztienak; TE-k balio desberdinak hartzen dituela aurkitu da kontrol eta gaixo dauden subjektuak konparatzerako orduan.

Bestalde, bariantza analisia DOC gaixoen eta Kontrolen artean kalkulatzean diferentziak ikusi dira baita ere ($p<0.001$), TE konexio mota desberdinen artekoekin batera ($p<0.001$). Kontrol taldeak eskuin eta ezker aldeko TE intra-hemisferikoetan balio handiagoak erakusten dituzte ($p<0.05$) eta ezkerretik eskuinera doazen TE inter-

Taula 8.3: TE balioen laburpena (batezbestea ± desbideratze estandarra). **Kontrolek eta DOC-ek balio desberdinak dituzte; p<0.05.* HLR: ezkerretik eskuinera dauden konexio inter-hemisferiko homologoak; HRL: eskumatik ezkerrera dauden konexio inter-hemisferiko homologoak; LL: ezkerreko konexio intra-hemisferikoak; RR: eskuineko konexio intra-hemisferikoak; LR: ezkerretik eskuinera dauden konexio inter-hemisferikoak; RL: eskuinetik ezkerrera dauden konexio inter-hemisferikoak

TE	Kontrolak	DOC	Berreskuratuak
HLR	0.009±0.027	0.006±0.015	0.017±0.030
HRL	0.011±0.020	0.02±0.049	0.019± 0.032
LL	0.04±0.021	0.017±0.016*	0.04±0.003
RR	0.039±0.020	0.027±0.039	0.065±0.050
LR	0.043±0.024	0.021±0.021*	0.047±0.017
RL	0.043±0.021	0.031±0.045	0.066±0.049
Guztira	0.041±0.018	0.024±0.026*	0.054±0.028

hemisferikoak altuagoak dituzte (p=0.001).

TE balioak 8.3 taulan ikusi daitezke. Bi denbora seinalek korrelazio handia badute beraien arteko TE balioa baxua izango da (zero inguruan). Bi denbora seinalek korrelazio baxua izatekotan eta bat beste seinale batean eraginen bat izatekotan, TE-k balio handia izango du norabide batean eta baxua bestean. Datu hauetan, TE-k erregio homologoen artean balio baxuak ditu korrelazio handietako konexioak direlako.

Subjektu gaixoen kasuan, TE intra-hemisferikoek balio baxuagoak dituzte eta hori dela eta korrelazio handiagoak dituzte. Berreskuratutako subjektu taldeen batezbesteko TE-ren balioak *bias*-a aurkezten du, talde honetako gaixo batek TE balio oso altuak aurkeztu baititu.

TE grafoa aztertzerakoan, DOC eta kontrolen arteko batezteste-ko balioetan (8.3 taulan) desberdintasunak aurkitu ditzakegu, baita grafoan zenbat konexio dauden zenbatzerakoan ere (8.7 irudian ma-

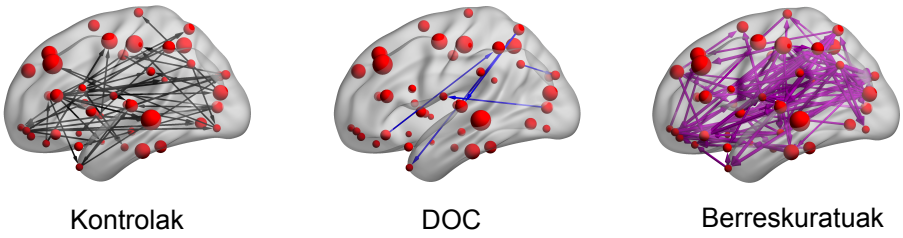

Irudia 8.7: **Ezkerreko hemisferio barruko TE konexioak**. Hiru talde desberdinen ezkerreko hemisferio barruko TE konexioak ikusi ahal dira irudi honetan. Gezien lodiera TE balioen arabera irudikatu da (gezi lodiagoak TE altuak dituzten konexioetan aurkitzen dira). Irudi argiagoa izateko bakarrik 0.2 baino handiagoak dituzten TE konexioak irudikatu dira.

rraztutako gezi zenbakia). Kontrol gaixoek, DOC gaixoek baino 9 aldiz konexio gehiago dituzte (Kontrolek 47 konexio eta DOC-ek 5 konexio). Berreskuratutako taldean 99 konexio aurkitu ziren, kontrol taldean baino konexio gehiago. Efektu hau, garuna kontzientzia gabe egon ondoren behin-behineko konpentsazio baten ondorioa izan daiteke. Anil Seth eta bere lankideek kontzientzia neurtzeko garuneko area bakoitza zenbat Granger kausalitate konexio zituzten zenbatu zuten [140]. Antzeko efektua ikusi da anestesiatik esnatzen diren subjektuetan eta kontroletan baino konexio handiagoa ikusten da [80].

Laburbilduz, TE grafoak aztertu direnean, DOC eta kontrol gaixo taldeen artean desberdintasunak agertu egin dira. Hemisferio barruko konexioek eta hemisferioen arteko konexioek TE balio txikiagoak dituzte gaixoengan (ez ziren area homologoetan desberdintasunik ikusi). Kasu honetan ez dira burmuinaren guneen arteko distantziaren araberako desberdintasunik aurkitu, nahiz eta ezker intra-hemisferiko konexioek balio txikiagoak izan.

8.4 DOC neuro irudi biomarkatzaileak eta CRS-R frogaren arteko korrelazioa

Atal honetan, kontzientzia gaitzak grafo funtzionalak nola aldatzen dituzten ikusiko da. Garun aktibitatea errepresentantzen dituen denbora seinaleetatik, grafo funtzionalak aztertu dira korrelazio partziala eta transferentzia entropia erabiliz. Ondoren, bi taldeen grafo funtzionalak konparatu dira: Kontrol taldea eta DOC gaixoen taldea. Analisi hau egiteko garuna 90 erregio anatomikoetan zatitu da, AAL atlas-a erabiliz. Erregio hauen arteko konexioak inter-hemisferiko homologo, inter-hemisrferiko, intra hemisferiko eta konexio guztietan sailkatu dira. Grafo konexioak aztertu ondoren 2 biomarkatzaile aurkitu dira: hemisferio desberdinen arteko erregio homologoen PC balioak eta ezkerreko hemisferio barruko TE balioak.

Hemisferio desberdinen arteko erregio homologoen arteko PC balioak Kontrol taldean handiagoak direla ikusi da (DOC eta berreskuratutako gaixoen kasuan ematen direnak baino handiagoak). Garuneko konexio guztien batezbestekoa konparatzerako orduan ez da desberdintasunik aurkitu. Esan beharra dago, grafo analisi hauetan oso garrantzitsua dela garun osoko konexioen artean, desberdinak diren konexioak aurkitzea.

Garun osoko TE batezbesteko balioa kalkulatzen bada ez da DOC eta kontrolen artean desberdintasunik ikusten. Baina hemisferio bakoitzeko barruko konexioak begiratzen badira desberdintasun nabarmenak antzeman daitezke.

Bi seinale denboralen artean korrelazio handia izatea eta TE balio handia izatea gauza desberdinak direla kontuan izan behar du irakurleak. Bi seinale denboralek korrelazio handia badute beraien arteko TE-a zero izango da, 2 denbora seinale berdinak badira, batek ez diolako besteari informazio berria emango. Hori dela eta, erregio homologoen arteko PC balio handiek bi hemisferioen arteko informazio-fluxua isolatzen dute. Bi hemisferioen barruko TE konexioak handiak dira, bi hemisferioen arteko informazio-fluxua baino handiagoa.

Emaitza hauetan oinarrituta DOC gaixoak ebaluatzeko biomar-

katzaile hoberenak hemisferio desberdinen arteko erregio homologoen arteko PC-ak (8.5 Irudia) eta ezkerreko hemisferio barruko TE konexioak (8.7 Irudia) direla esan daiteke.

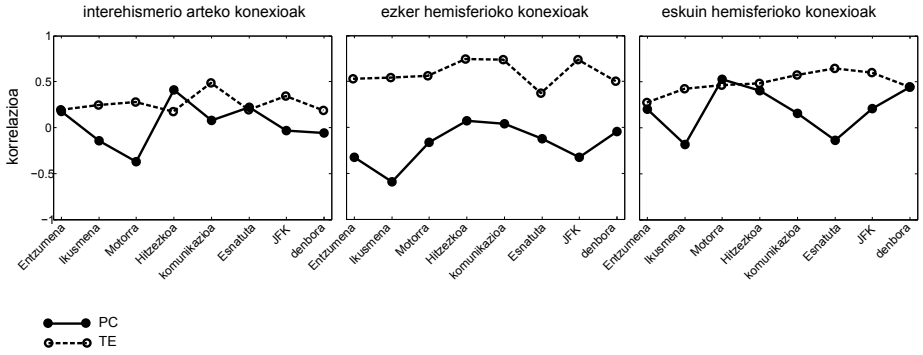

Irudia 8.8: **Hemisferio desberdinen arteko erregio homologoen arteko PC-ak eta ezkerreko hemisferio barruko TE konexioak**. PC (lerro zuzena) eta TE (lerro etena) biomarkatzaileak eta CRS-R eskala funtzional desberdinen arteko korrelazioa kalkulatu da. Eskala hauek funtzio desberdinak neurtzen dituzte: entzumena, ikusmena, motorra, hitzezkoa, komunikazioa, esnatutako eskala eta eskala guztien arteko batuketa. Istripua gertatu denetik pasa den denbora ere erabili da biomarkatzaileekin korrelazioak bilatzeko. HIH-ko PC balioak, (HLR+HRL)/2 TE balioak, LL TE balioak eta RR balioak erabili dira korrelazioak bilatzeko.

Ondoren, kalkulatutako grafoen biomarkatzaileak, jokabidearen eskala eta eskala nerologikoekin (CRS-S eskala) korrelazioak dituen edo ez kalkulatu da. Emaitzak 8.8 irudian ikusi daitezke. Hemisferio desberdinen arteko konexio homologoetako TE balioak, korrelazio handia du komunikazio eskalarekin. Ezkerreko hemisferio barruko TE konexioak 0.73-ko korrelazioa du hitzezko eskalarekin, komunikazio eskalarekin eta guztien batuketarekin (8.8 irudian “JFK”).

8.5 Etorkizunerako lana: DOC gaixoetan gertatutako kalteak garun eremu desberdinetan

Analisi honen helburua ez da gaixo bakoitzak dituen desberdintasunak adieraztea, DOC taldeek dituzten patroi berdinak aztertzea baizik dira. Ez dugu oraindik garuneko leku espezifikoetan DOC efektua ikertu. Grafo konplexuen teknika desberdinak erabiliz PC eta TE grafoetan garun erregio desberdinak ikertu ahal dira. Planteamendu hau posiblea dela erakusteko area desberdinen PC balioak erabiliz de-korrelazio indize bat kalkulatu dugu DOC-ak eta kontrolak konparatzeko (balio hauek 8.9 Irudian ikus daitezke). Area bakoitzaren de-korrelazio indizea hurrengo formula erabiliz kalkulatu zen: (corrKontrol-corrDOC)/corrKontrol. Urdin koloreak, garunaren 5 erregio desberdinenak identifikatzen ditu (*Fusiform, Insula, Parietal Superior, Precentral* eta *Temporal Superior*). Area hauetan DOC gaitzek efektu handiagoak dituzte. Kaltekatuta dauden bost area txikienak *Cingulum Anterior, Cingulum Middle, Frontal Superior Orbital, Superior Motor Area* eta *Temporal Inferior* dira.

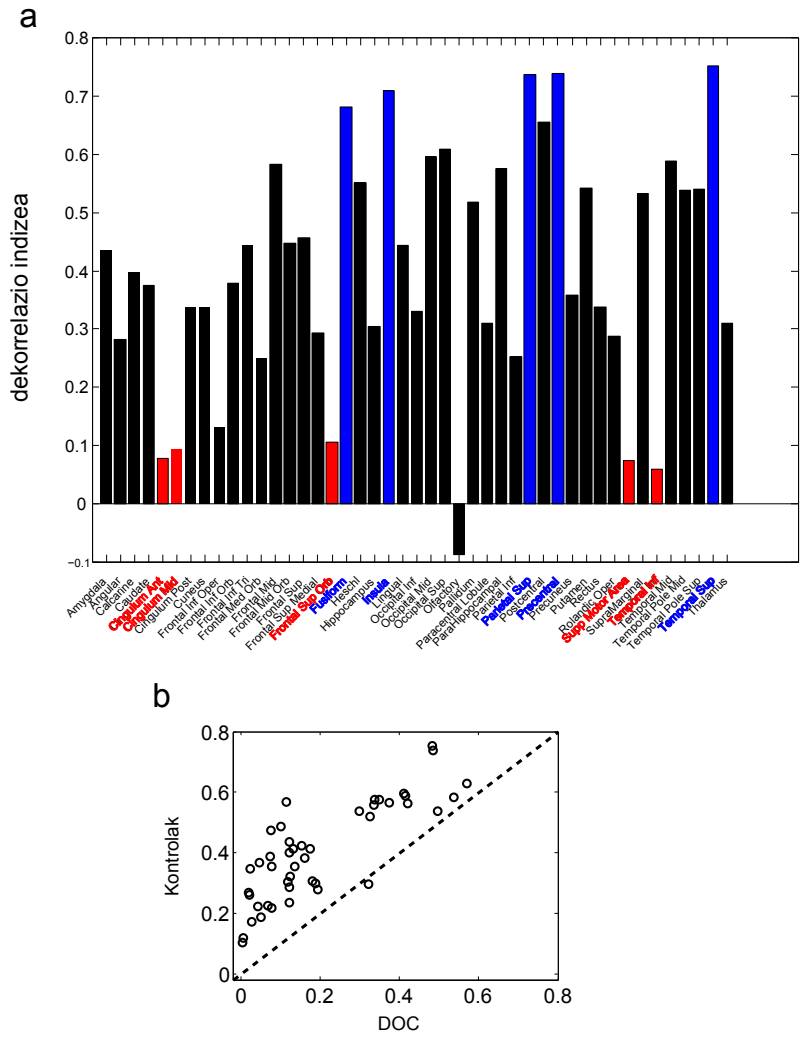

Irudia 8.9: AAL erregioetan desberdintasunak ikusteko de-korrelazio indizea erabili dugu. Barra urdinak desberdinago diren areak dira eta gorriak gutxiago kaltetutako areak. b irudiak, DOC eta kontrol arteko taldeen korrelazioa irudikatzen du. Diagonaletik hurbil dauden erregioak kalte gutxiagoak dituzte urrun daudenak baino.

Kapitulua 9

Estruktura eta funtzio artean partekatutako eskeletoa

Aurreko atalean, grafo funtzionalak kalkulatzen eta nola hauek kontrol eta gaixo taldeen artean desberdintasunak aurkitzeko erabili ahal diren ikusi da. Atal honetan ordea, ohiko garun atlas bat erabili beharrean, datu estrukturalak eta funtzionalak erabiliz atlas berri bat sortuko da. Datu hauek erabiliz, atlas berri honen erregioak estrukturalki eta funtzionalki koherenteak izango dira. Datuetatik sortutako atlas berria gaur egun erabiltzen diren atlas anatomiko eta funtzional desberdinen artean konparatu egingo da. Behin hau eginda, hurrengo ataletan eta ikerketa osoan zehar, atlas berri hau erabiliko da gaixoen garun berrantolaketa ikertzeko.

Garunaren funtzionamendua aztertzerako orduan, bi printzipio osagarri aurki daitezke [160]: segregazioa eta integrazioa.

- **Segregazioa:** Garunak, jasotzen duen informazioa prozesatzeko eta jarduera desberdinak aldi berean egiteko, funtzionalki espezializatutako areak behar ditueneko egoera da.

- **Integrazioa:** Garun area desberdinen aktibazioarekin erlazionatutako egoera da zeinetan aktibazio koordinatua beharrez-

koa den jarduera eta portaera kognitibo koherenteak edukitzeko [68, 25].

Segregazio eta integrazioaren arteko oreka optimoa ulertzeko, garunaren konexio arkitektura argitzea beharrezkoa da. Arazo hau, gaur egun Neurozientziak duen erronka garrantzitsu bat da.

Grafo analisi konplexu desberdin ugari erabili dira garunaren arkitektura eta bere dinamikaren xehetasunak ikasteko [153]. Analisi hauek garunaren estruktura eta funtzio konektibitateek (SC eta FC) antolamendu hierarkikoa dutela frogatu dute. Honela, garuna, modulu (edo area) desberdinetan banatzen da eta *hub* konektoreen bidez modulu hauek komunikatu egiten dira elkarren artean [150, 152, 73]. Garunaren antolakuntza hierarkikoa ezin bestekoa da segregazioa gerta dadin eta *hub* konektoreak beharrezkoak dira bereizita dauden moduluen artean integrazioa mantendu dadin [152, 61](9.1 Irudia).

SC-a eta FC-a erlazionatzeko ahaleginetan, azken urteotan konektibitate anatomikoa eta garun aktibitatearen modelo dinamikoen analisi anitz egin dira [54, 26, 41, 74, 101, 106]. Zuzena dirudi ondorioztatzea beraz, garun aktibitatearen dinamikak, garunaren zuntz estrukturalak kondizionatzen duela [39], baina oraindik SC-aren eta FC-aren arteko harremana ez dago guztiz argi. Harreman hau bilatzen saiatzerakoan, arazo batekin topatzen gara ikerlariok: estruktura anatomiko bakar batentzako funtzio-grafo desberdinak aurkitu daitezke. Funtzio-grafo desberdin asko daude burmuinean pertzepzioa, ekintza, memoria, ezagutza eta jokabide konplexuak errazteko. Hau dela eta, garun estruktura eta funtzioaren arteko harremana ulertzea Neurozientziaren erroka handienetako bat da [118].

Erroka honi azalpena bilatzeko analisi ugariren lehenengo urratsak, aztertutako subjektuak atseden egoeran egonda, lortutako fMRI seinaleak erabiliz eman dira. Seinale hauek erabiliz, konektibitate sare funtzional berdinak lortzen zirela pertsona osasun desberdinen artean behatu egin zen [127, 52, 123]. Gainera, estrukturalki konektaturik dauden garun area desberdinen artean, normalean konektibitate funtzional handia dagoela aurkitu egin zen [84, 72, 70, 79, 77, 139, 159]. Baina, era berean, garunean estrukturalki konektatuta ez dauden erregio ugarik konektibitate funtzional handia izan

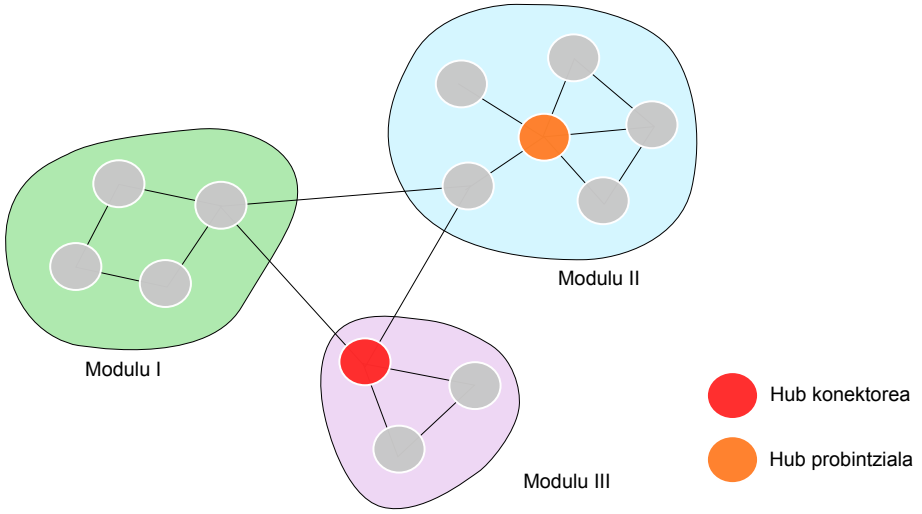

Irudia 9.1: Sareak osatutako moduluak erpin azpimultzo batez osatuta daude. Erpin azpimultzo hauek beraien artean konexio ugari dituzten bitartean, beste moduluek osatzen dituzten erpinekin aldiz konexio gutxi dituzte. *Hub* erpinak, sarean konexio ugari dituzten erpinak dira. *Hub* mota desberdinak aurkitu ditzakegu: (i) *hub* probintzialak modulu barruan dauden erpinak konektatzen eta (ii) *hub* konektoreak modulu desberdinak osatzen dituzten erpinak konektatzen.

dezakete [70, 77]. Honek garunean zeharkako efektu handiak daudela adierazten du. Arazo honi aurre egiteko [77] sare erpin egokiak aukeratu behar dira SF-FC artean korrelazioa handitzeko. Era berean, SC-aren eta FC-aren arteko harremana argitzeko beste analisi mota batzuk behar dira.

Atal honetan, beste lan ugarik erabili zuten metodologia oinarritzat hartuz [144, 14, 85], erpin taldeei arreta ematea erabaki zen, analisi hierarkikoa erabiliz. Datu estrukturaletan antolaketa modular hierarkikoa erabiliz, baita funtzionala ere, garun zatiketa optimoa bilatu zen *cross-modularity* (ikerketa honen garapenenan sortutako metodo berria) erabiliz. Gure hipotesiaren arabera, funtzio segrega-

tuak estrukturatik aurkitutako modulu desberdinekin lotuta egongo lirateke. Hipotesia frogatzen saiatzerako orduan, aurkitutako modulu estrukturalak konexio funtzioarekin batera irudikatzean, SC eta FC moduluetan berdintasunak ikusi ziren. Era berean, aurkitutako modulu funtzionalek konexio estrukturarekin antzekotasunak zituztela ikusi zen. Bi planteamendu hauek funtzio eta estrukturaren arteko antzekotasunak argitzeko erabili ziren, metodo hauen bidez garun zatiketa berri bat lortuz. Garun zatiketa honek garun estrukturak eta funtzioak iraganean uste zen baino antzekotasun handiagoa dutela frogatzeko balio izan zuen. Aurkitutako zatiketak garuna modulu funtzional-estrukturaletan (SFMs) banatzen ditu, garunaren eskeletoa osatuz.

Lortutako atlas hierarkikoa eta *cross-modularity* kalkulatzeko kodea hurrengo web orritik deskargatu daiteke: `http://www.nitrc.org/projects/biocr_hcatlas/`

9.1 Subjektuak eta datuen aurre prozesamendua

Atal honetan azalduko den ikerketa lanak Gurutzetako Unibertsitate Ospitaleko etika batzordeak onartu zuen, metodo guztiak onartutako jarraibideetan oinarrituz garatu zirelarik. 12 pertsona osasuntsuk (6 gizon), 24-45 urte artean (33.5±8.7), bere idatzitako baimena eman zuten erresonantzia saio bat egiteko. Subjektu guztien datu funtzionalak eta estrukturalak lortu ziren *Philips Achieva 1.5T Nova* eskanerra erabiliz. Subjektuak 30 minutu baino gutxiago egon ziren eskaner barruan. Eskanerraren protokoloaren xehetasun gehiago [45] artikuluan aurkitu daitezke.

Difusio irudiak aztertu baino lehen aurre-prozesamendu pauso ugari egin behar izan dira informazio erabilgarria lortu ahal izateko. Lehenik eta behin, eskanerrak ekoiztutako *Eddy* korronteen efektua eta subjektuaren buruaren mugimenduak sortutako artefaktuak zuzendu ziren. Bigarrenik, *voxel* bakoitzeko tentsore bat kalkulatu zen. Azkenik *FACT* izeneko algoritmoa eraili zen zuntz grafikoa eraiki-

tzeko [110]. Pausu hauek guztiak jarraituz, garunaren gai gris zati desberdinek konektatzen dituzten zuntzak atera ziren.

Era berean, fMRI datuek ere aurre-prozesamendu pauso desberdinak behar dituzte. fMRI-ak osatutako lehenengo irudiak ezabatu ziren saturazio magnetikoaren efektuagatik. Eskaner barruan buruarekin egindako mugimenduaren efektuak zuzendu ondoren, irudiak lerrokatu egin ziren. Lortutako irudiak 8-mm FWHHM kernel isotropiko bat erabiliz prozesatu ziren eta bere intentsitate balioak normalizatu ziren. Ondoren, 0.01Hz - 0.08Hz artean dauden seinaleak hartu ziren [33] eta hauen jokaera lineala zuzendu zen. Azkenik, lortutako seinaleei buru mugimendua, gai zuriaren seinalea, CSF seinalea eta garun seinale orokorraren efektua ezabatu ondoren garuna MNI152 garun estandarrera transformatu zen. Aurreprozesuaren detaile gehiago ikusteko A Eranskina irakurri.

9.2 SC eta FC sareak

Lehenengo atalean azaldu den bezala, sare bat eraikitzeko egin behar den lehenengo pausua intereseko garun erregioak aukeratzea da. *Voxel* guztiak erabiltzea garun sarea egiteko konputazionalki oso garestia da, beraz, garuna funtzio berdina duten erregio txikietan zatitzea erabaki zen. *Spatially constrained clustering* izeneko algoritmoa erabili zen 12 subjektuen zatiketa funtzionala egiteko [37]. Lortutako zatiak espazialki koherenteak zirela ziurtatu zen (alegia, (*voxel* guztiak erregio berdinean zeudela). Garun (*voxel*-ak erregio berdinekoak ziren edo ez erabakitzeko, denbora seinaleen arteko korrelazioa erabili zen. Subjektu guztien zatiketa multzokatzeko bigarren mailako klustering metodoa erabili zen. Azkenik, 2514 erregio desberdinetako garun zatiketa lortu genuen. Zatiketa honek garunaren erregio kortikalez eta subkorlikalez osaturik zegoelarik.

Zatiketa hau subjektu bakoitzeko 2514 x 2514 sare funtzionalak eta estrukturalak eraikitzeko erabili zen (3.2 irudia).

Nahiz eta pertsona berdinaren datu estrukturalak eta funtzionalak izan, datu hauek mekanismo fisiko eta fisiologiko desberdinak neurtzen lortu ziren eta ondorioz, datu hauen prozesamendua ere desber-

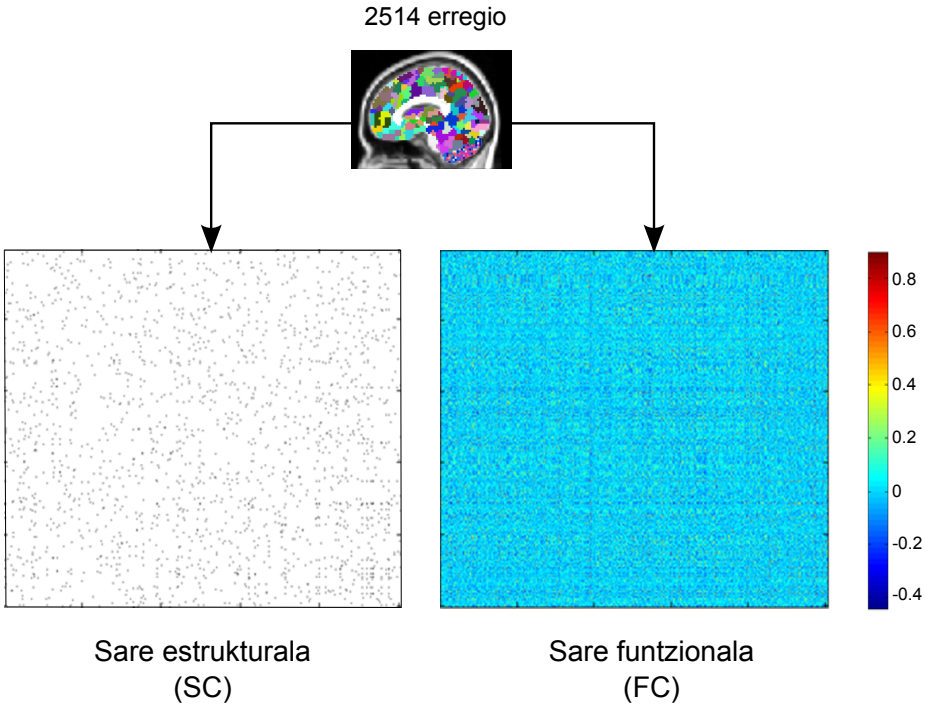

Irudia 9.2: Lortutako 2514 erregiodun atlasa erabiliz sare funtzionalak eta estrukturalak kalkulatu ziren. SC sarea zuri beltzez irudikatuta dago (puntu beltzak bi erregioen artean gutxienez zuntz bat dagoela adierazten du). FC sarea konexioaren indarraren arabera koloretu dira (Pearson korrelazioa).

dina izan zen. FC-aren eta SC-aren arteko harremana ikertzeko 12 subjektuen batezbesteko FC eta SC sareak kalkulatu ziren, horrela banakako aldakortasuna murrizteko.

Aurreko analisian egin den moduan, eta beste ikerketa askotan egin den bezala, funtzio eta estruktura sareen arteko Pearson korrelazioa (r) neurtu zen [72, 79]. Analisi honetan ausazko bi erregioren arteko konektibitatea konparatuz r=0.2 lortu zen (FC eta SC artean korrelazio baxua). Konparaketa hau haien arteko zuntzen bidez konektatutako erregioen informazioa erabiltzean r=0.3 lortu zen. Ko-

rrelazio balio hau, zeozer gehiago handitu daiteke bakarrik modulu barruan dauden konexioak aztertzen.

9.3 Modularitate hierarkikoa

Modularitatea grafoen neurri bat da, honen moduluen (talde, kluster edo komunitateen) jarduera neurtzeko. Grafo bat hartuta bere moduluak bilatu ahal dira eta matrizeak berrantolatuz garuna komunitate desberdinetan antolatzen dela ikus daiteke (9.3 Irudia). Modularitate handia duten sareek konexio asko dituzte modulu barruko erpinen artean eta konexio gutxi modulu desberdinen artean.

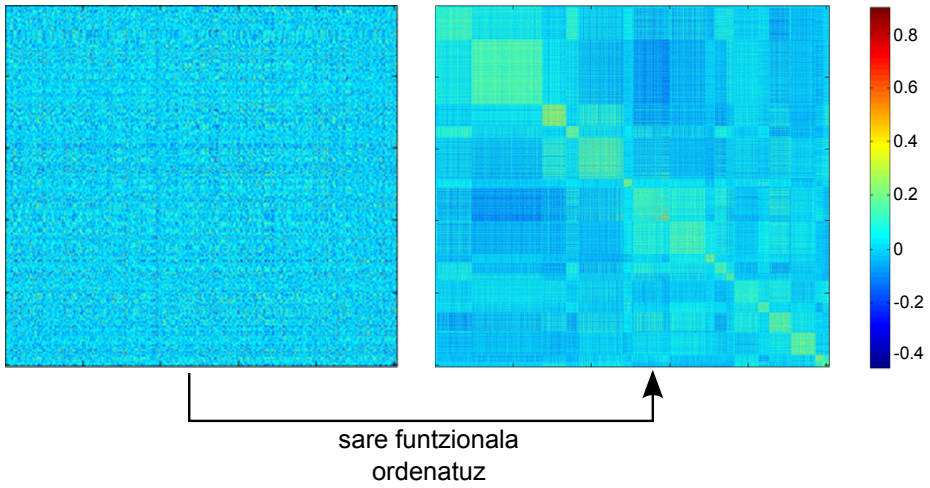

Irudia 9.3: FC sarea, garun moduluak ikusteko ordena daiteke erpinen antzekotasuna erabiliz.

Modulu hauek aurkitzeko, multzokatze teknikak erabiltzen dira antzekoak diren erpin taldeak aurkitzeko. Erpin desberdinak taldeetan antolatzeko honako bi terminoak deskribatzea beharrezkoa da:

- **Garun erregioak deskribatzen dituzten aldagaiak**. Bi garun erregio berdinak diren jakiteko hauek deskribatzen dituz-

ten aldagaiak behar dira. Aldagai desberdin askok garunaren erregioak deskriba ditzakete. Atal honetan, erregio bakoitza garuneko beste 2513 erregioekin nola konektatzen den erabili da aldagai moduan. Garuna 2514 aldiz zatitu zenez erregio bakoitza nola konektatzen den beste 2513 erregioekindeskribatzen du.

- **Antzekotasuna neurtzeko metodoa**. Erregio bakoitzak deskribatzen duen aldagaia aukeratu ondoren, deskribatzaile hauen antzekotasuna neurtu behar da. Konektibitate balioek balio txikiak dituztenez, bi deskribatzaileak osatzen duten bektoreen arteko kosinua erabili da hauen antzekotasuna neurtzeko.

Erregioa deskribatzeko aldagaiak aukeratuta eta beraien artean antzekotasunak bilatzeko metodoa aukeratuta daudelarik, multzokatze teknika desberdinak erabili daitezke moduluak aurkitzeko. Kasu honetan *Hierarchical Agglomerative clustering* (HAC) izeneko teknika erabili egin da ikerketa honetan [133, 107, 50]. Multzokatze teknikek ez dute normalean zenbat modulu dauden kalkulatzen. Hori dela eta, modulu kopuru desberdinekin frogatzea beharrezkoa izan da eta hauen artean zatiketa hoberena bilatu egin da. 2514 erregio edukita, modulu kopurua 1tik -2514ra arteko kopuruguztiekin frogatu da.

Komunitate funtzionalak lortzeko FC sarea erabili da. Multzokatze hierarkikoaren lehen pausua 2514 erregioen arteko antzekotasuna neurtzea izan da. Antzekotasun handiena dituzten bi erregioak batu ondoren 2513 erregioko garun zatiketa lortu da. Berriro ere 2513 erregioen artean antzekotasuna neurtu da ondoren, antzekotasun handienak dituzten bi erregioak batzeko. Prozedura hau jarraituz,modulu bakarra lortzen da bukaeran, tarteko garun zatiketa guztiak gordez. Prozesu honen ondorioz zuhaitz hierarkikoa edo dendrograma bat sortzen da non pausu bakoitzean bi erregio batzen diren modulu berri bat osatuz. Zuhaitz hau nahi dugun maila M-an moztean 2514 erregioko garuna M modulu finituetan antolatuta egongo da. 9.4 irudian, garuna modulu bakar bat bezala ikusi dezakegu. Ondoren, honen garuna bi zati desberdinetan zatitzen da etab. Lehenengo lerroak, datu funtzionalekin lortutako zuhaitzaren lehen 4 mailak erakusten ditu.

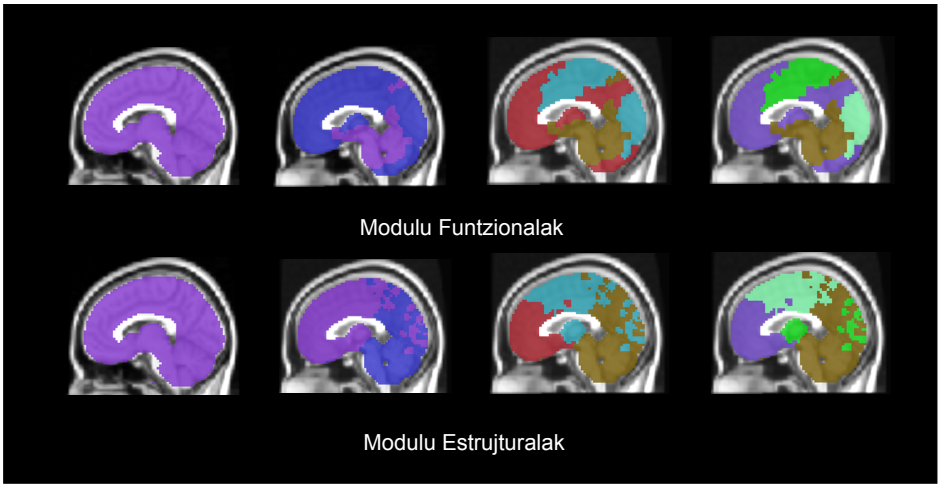

Irudia 9.4: FC eta SC sareen multzokatze hierarkikoa.

Bigarren lerroak ordea, datu estrukturalak erabiliz lortutako zuhaitza erakusten du. Zatiketa hierarkiko honi esker, garuna maila desberdinetan ikertu ahal da. Zuhaitzaren beheko aldea modulu txikienez osatuta dago eta hauek zuhaitzaren goiko mailetan konektatzen dira.

9.4 SC-FC modulu arteko antzekotasuna

Sare funtzionala erabiliz kalkulatutako garun zatiketa datu estrukturalak irudikatzeko erabiltzen bada, bien arteko antzekotasuna handia dela ikus daiteke (9.5 irudia). Era berean, sare estrukturala erabiltzen bada garun zatiketa kalkulatzeko eta datu funtzionalak irudikatzeko, antzekotasun handiak ikusi daitezke.

Behaketa sinple hau, aurkikuntza garrantzitsu bat da: FC eta SC sareak modularitate handia dute (jadanik frogatu egin den bezala) eta hauen artean antzekotasun izugarri handia dago (orain arte ikusi ez dena). Estruktura eta funtzioaren arteko antzekotasunaren adibide bat 9.6 irudian ikusi daiteke. Irudi honetan garun modulu bakar bat

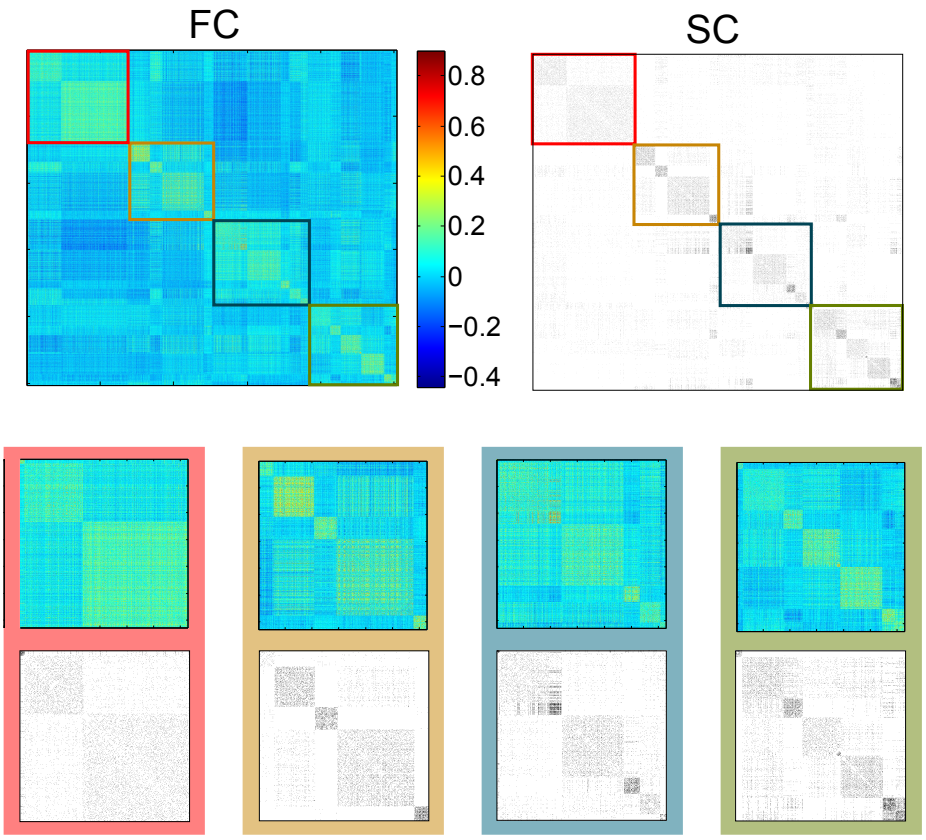

Irudia 9.5: Sare funtzionala erabiliz lortutako zatiketaren ondoren, FC eta SC matrizeak berriro ordenatzen dira modulu hauen arabera. Estruktura eta funtzioaren arteko antzekotasunak ikusteko bigarren lerroko goiko matrizeetan zoom egin da.

ikus daiteke, garun zati desberdinetan kokatutako erregioez osatua. Erregio hauek konektibitate funtzional handia dute eta irudian ikus daitekeenez zuntz ugariz konektaturik daude.

Estruktura eta funtzio arteko antzekotasun handi honek garun funtzioan ikusitako zeharkako efektu gehienak modulu barruan dauden korrelazio handiak sortzen dituztela adierazten du. Hau da, ko-

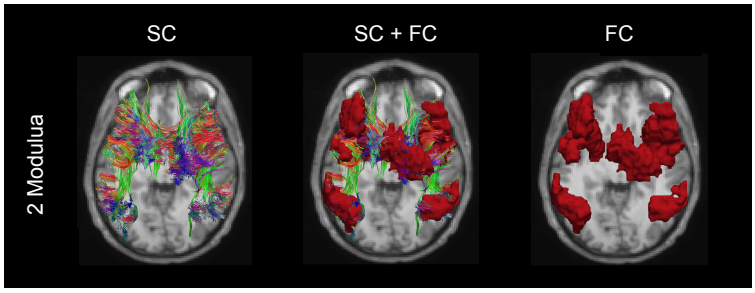

Irudia 9.6: Bigarren moduluak burmuineko erregio desberdinak lotzen ditu. Garun erregio desberdinak zuntzen bidez loturik daude. Beste moduluen zuntzak eta osatzen dituzten erregioak ikusteko [45] artikulua irakurri

nexio estrukturalak ez dauden lekuetan azaldu ezin diren konexio funtzional gehienak, konexio asko dituzten moduluetan daudelako ageri dira, nahiz eta hauek beraien artean zuntzik ez eduki.

9.5 Cross-modularity indizea

Garun zatiketa baten moduluak konexio funtzionalak eta estrukturalak ondo deskribatzen dituela zihurtatzeko (9.5 irudia) *cross-modularity* X indizea garatu dugu. *Cross-modularity* delakoa hurrengo neurrietan oinarrituta dago:

- **SC-FC arteko antzekotasuna**: Zatiketa baten modulu bakoitza hartu eta SC-aren eta FC-aren arteko antzekotasuna kalkulatu da Sorensen indizea erabiliz [148]. Sorensen indizeak bi sare bitarren arteko antzekotasunak neurtzen ditu (bi sareek dituzten konexio berdinak bider bi, zati bi sareen artean dituzten konexio guztien kopurua). SC-ak eta FC-ak konexio berdinak badituzte FC eta SC konparatzeko sareak binarizatu behar dira (sareen pisua desagertu egiten da, eta beraz orain garrantzitsua dena bi erreegioren artean konexioa dagoen edo ez da, hau da, 1 edo 0). 9.5 irudian ikusi daiteke SC matrizeak konexio gutxi dituela eta FC alderantziz ia guztiz konektatuta dagoela.

FC sarean konexioak erabatzi behar dira SC sarearekin konparatzeko. FC sareetan atals bat bilatu behar dugu sare hauek binarizatzeko. Atalase hau aurkitzeko, Sorensen indizea erabiliz FC eta SC arteko antzekotasuna maximizatzen duen balioa bilatu behar da. FC sareen balio absolutuak erabili dira honetarako eta SC sareen balioak normalizatu eginten dira bere balioak 0 eta 1 artean egoteko. Ondoren, atalase bat erabiltzen da [0,1] balioen artean (α FC sarearentzat eta β SC sarearentzat) sare hauek binarizatzeko. Konexioen balioa atalasea baino handiago izatekotan 1 jarri eta atalasea baino txikiagoa bada, 0 jarriz. Ondoren modulu bakoitzerako Sorensen indizea erabili da antzekotasuna neurtzeko α eta β erabiliz. 9.7 irudian FC eta SC sareen arteko antzekotasunak ikusi daitezke modulu kopuru desberdinentzat (α eta β maximizatzen). α balioa normalean 0.45 inguru dago eta β balioa 0 inguruan. Azkenik, modulu kopuru desberdinetarako batezbesteko antzekotasuna kalkulatu zen. Bi antzekotasun balio desberdin daude: i) HAC FC sarea erabiliz kalkulatutakoa (lerro urdina 9.7 irudian). Funtzio moduluak kalkulatu ondoren modulu hauen estrukturari begiratzen zaio. ii) HAC SC sarea erabiliz kalkulatutakoa eta modulu hauek dituen funtzioari begiratuz (lerro gorria 9.7 irudian).

- **Modularitatea**: Garun zatiketa baten modularitatea kalkulatzeko *Newman* algoritmoa [111] erabili da ikerketa honetan. M garun zatiketaren modulu kopurua bada, Modularitatea kalkulatzeko hurrengo formula erabili zen: $Q = \sum_{i=1}^{M}(e_{ii} - a_i^2)$. e_{ii} modulu barruan dauden konexioen frakzioa eta a_i i modulutik beste moduluetara dauden konexio frakzioak adierazten dutelarik (9.7 irudia). Modulu barruan konexio ugari eta modulu artean konexio gutxi dituzten zatiketek modularitate handia dutela esango dugu.

Cross-modularity X indizeak zatiketa baten FC eta SC arteko antzekotasun topologikoa eta sare hauen modularitatea neurtzen du. HAC FC sarea erabiliz eta honen ordena SC sarean erabiliz, *cross-*

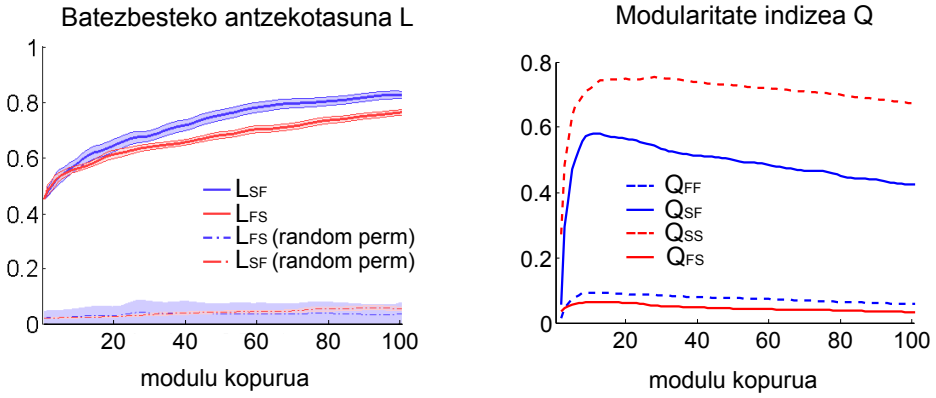

Irudia 9.7: FC eta SC arteko antzekotasuna (L) eta hauen modularitatea (Q).

modularity indizea FC eta SC sareen artean hurrengo formularekin neurtu daiteke:

$$X_{SF} = (Q_{FF}Q_{SF}\overline{L_{SF}})^{\frac{1}{3}}$$

$\overline{L_{SF}}$ batezbesteko antzekotasuna neurtzen du zatiketa bakoitzaren modulu guztientzat. Q_{FF} eta Q_{SF} FC eta SC sareen modularitatea neurtzen du (HAC FC sarearekin lortutako ordena erabiliz). SC sarea erabiltzen bada HAC algoritmoarekin moduluak aurkitzeko orduan *cross-modularity* indizea hurrengoa izango da:

$$X_{FS} = (Q_{SS}Q_{FS}\overline{L_{FS}})^{\frac{1}{3}}$$

Garun zatiketa batek *cross-modularity* balio handia izango du baldin eta SC eta FC sareak modularitate handiak badute eta beraien moduluen konexio funtzionalak eta estrukturalak antzekoak badira. Beraz, *cross-modularity* balio handiek, estrukturak eta funtzioak modularitate handia dutela eta beraien artean konexio berdinak dituztela adierazten du.

9.6 Modulu Funtzio-Estrukturalak

Garun zatiketaren modulu kopuruaren arabera *cross-modularity* balioak kalkulatu dira. Balio hau maximizatzean garuneko modulu kopuru hoberena zein den kalkulatu egiten da. 20 modulu funtzionaletan zatitutako garunak cross-modularity balio handiena lortu duela aurkitu dugu (9.5era 9.8 irudiak). 10 eta 30 modulu kopuruen arteko zatiketek ere antzeko *cross-modularity* balioak dutela antzeman egin da. *cross-modularity* balioak modulu kopuru tarte honetan berdin irauten du bi efektu desberdinen orekaren ondorioz. Modulu kopurua handitzean: (i) SC eta FC sareen arteko antzekotasuna handitu (9.7 irudia) eta (ii) *Newman* modularitatea txikitu egiten dira (9.7 irudia).

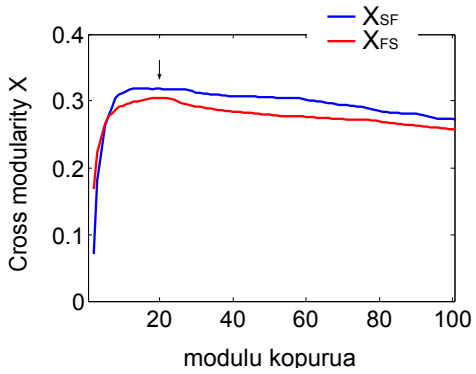

Irudia 9.8: Garun zatiketen *cross-modularity* balioak modulu kopuruen arabera. Irudi honetan modulu kopuruak 1 (garun osoa) - 100 tartean ikusi daitezke. *Cross-modularity* balioa handitu egiten da moduluen arteko FC-SC sareak antzekoak direnean edo FC edo SC sareak modularitate handia badute. *Cross-modularity* balio handiagoak lortu dira FC eta SC artean HAC FC sarearekin erabiltzen denean (XSF, marra urdina). HAC SC sarearekin erabiltzen denean (XFS, marra gorria) balio baxuagoak ikusi daitezke. M=20 moduluan dagoen geziaren zatiketa honek FC eta SC ordena erabiltzean *cross-modularity* balio hoberenak lortzen direla adierazten du.

Proposatutako garun zatiketa hau egonkorra da subjektu desber-

dinen artean: subjektu bakoitzeko SC sareak erabiliz edo batezbesteko SC sarea erabiliz *cross-modularity* balioak kalkulatzean antzeko balioak ditugu. Azpimarratzekoa da FC sareekin kalkulatutako *cross-modularity* balioak SC sareak erabiliz baino handiagoak direla, %4 inguruan.

M=20 moduluak osatzen duen garun atlas hau [45] artikuluan anatomikoki deskribatuta dago. Atlas hau 9.9 eta 9.10 irudietan ikus daiteke. SFM desberdinen kokapen espaziala begiratzerakoan modulu batzuek bi hemisferioen artean simetria handia daukatela antzematen da (adibidez 3, 5 eta 12 moduluek). 9.6 irudian garun erregio desberdinak dituen modulu bat ikusi dezakegu. Erregio hauek konexio funtzional handiak dituzte eta beraien artean zuntz ugari aurkitu daitezke.

FC eta SC sareen arteko antzekotasuna nabarmenagoa da subjektuen arteko batezbesteko sareak erabiltzerakoan, subjektu bakoitzaren sareak erabili beharrean. Nahiz eta subjektu bakoitzaren datuak erabiliz antzekotasuna ere oso nabarmena izan. Honek esan nahi du metodo hau sendoa dela garun zatiketak bilatzeko eta subjektu bakoitzaren aldakortasuna handia izan arren, beti modulu antzeko hauek aurkitu ahal izan dira.

9.7 SFM eta Antikorrelazioak

SFM-z osatutako modulu bakoitzaren barruko konexio funtzionalak oso korrelazionatuak egon arren, modulu desberdin batzuen arteko konexioek balio antikorrelazionatuak dituzte (korrelazio balio negatiboak). Funtzio sarea hiru koloretan irudikatzen badugu korrelazio eta antikorrelazioen arabera, efektu hau hobeto ikusi daiteke (9.11 irudia: kolore gorria korrelazio positiboak dira; kolore urdinak antikorrelazioak irudikatzen ditu; kolore berdea korrelazio baxuak dira -0.1 eta 0.1 artean). Irudi honetan SFM modulu guztien barneko konexioak positiboak dira baina modulu batzuk beste batzuekin dituzten konexioak negatiboak dira. 9 eta 10 moduluen arteko korrelazioak positiboak dira eta bi modulu hauek hirugarren moduluarekin antikorrelazionatuta daude (hirugarren modulua zentzumen eta motor

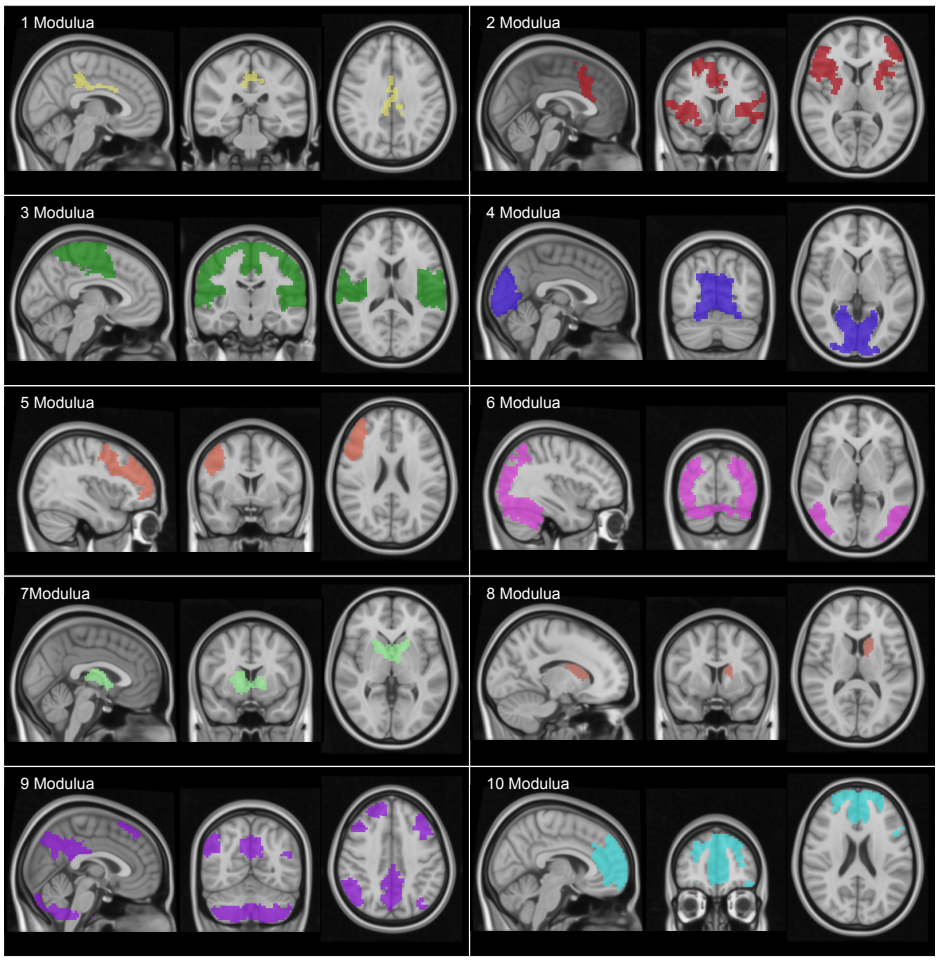

Irudia 9.9: 20 SFMs osatutako garun atlasa. Atlas honek *cross-modularity* indizea maximizatzen du. Irudi honetan lehenengo 10 moduluak ikusi daitezke eta 9.10 irudian beste 10 moduluak). Garun erregio hauen FC sarean kalkulatutako moduluak garunean irudikatzea lortu da. Irakurlea ohartarazi nahi dugu nola modulu batzuk espazialki banatutako garun erregioak osatzen dituztela (adibidez 2 eta 9 moduluak 9.9 irudian eta 12, 14, 16, 17 eta 18 9.10 irudian).

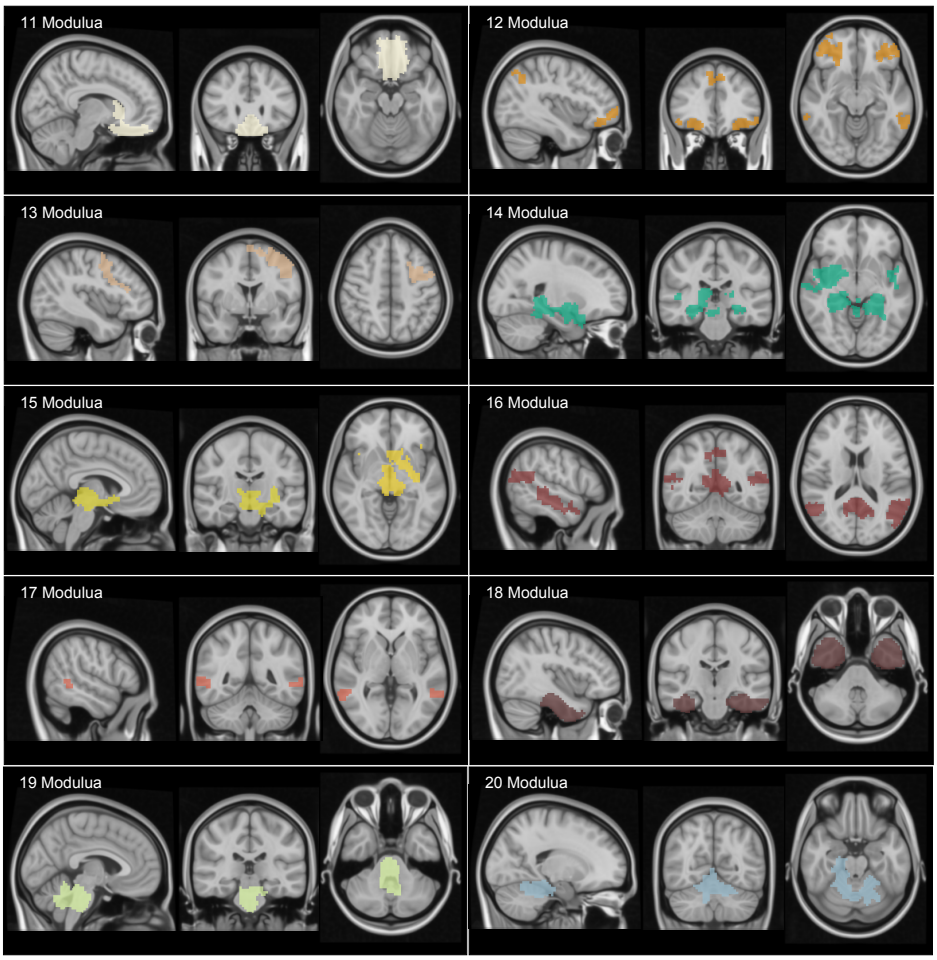

Irudia 9.10: 20 SFMs osatutako garun atlasa. Atlas hau *cross-modularity* indizea maximizatzen. Irudi honetan azken 10 moduluak ikusi daitezke eta 9.9 irudian beste 10 moduluak) . Garun erregio hauen FC sarean kalkulatutako moduluak garunean irudikatzen lortu da. Ohar ezazu modulu batzuk espazialki banatutako garun erregioak osatzen dituztela (adibidez 2 eta 9 moduluak 9.9 irudian eta 12, 14, 16, 17 eta 18 9.10 irudian).

jarduerekin erlazionatuta dago, ikusi 9.12 irudia). Atsedenean lortutako fMRI seinaleen arteko anti-korrelazio balioak eztabaida batzuk sortu ditu [79]. Anti korrelazio handienak DMN izeneko osagaiak eta sentsori-motor osagaiak ikusi dira beste lan batzuetan [53]. Ikerketa honetan lortutako emaitzak aurreko lanetan lortutakoekin koherenteak direla ikusi da. Gure 9 eta 10 moduluek DMN osagaia osatzen dute eta 3garren modulua osagai sentsori-motorea da (ikusi 9.12 irudia).

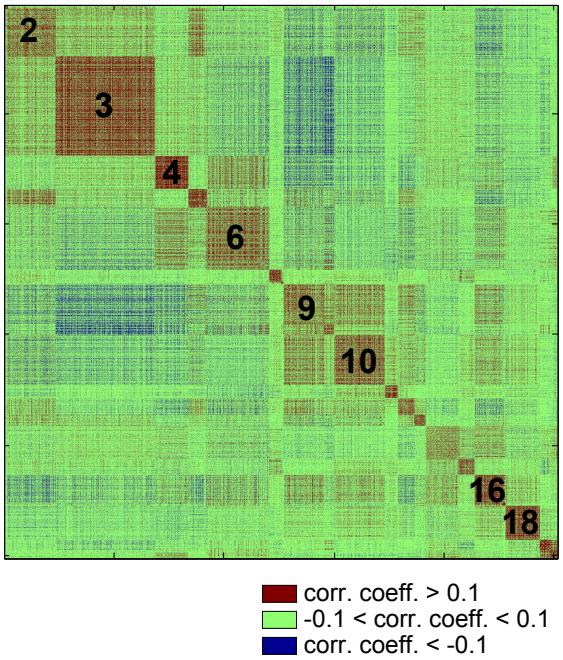

Irudia 9.11: Irudi honetan SFM moduluak osatutako barne konexioak positiboki (kolore gorria) korrelazionatuta daudela ikusi dezakegu. Modulu desberdinen arteko konexio negatiboak ere ageri dira (urdin kolorea). Zenbaki beltzak sare barruan moduluak identifikatzeko erabili dira.

9.8 SFM eta garun atlas arruntak

SFM moduluek beste garun atlas desberdinekin dituzten antzekotasunak begiratu dira atal honetan. Normalean literaturan aurkitutako atlas desberdinak garunaren anatomian edo funtzioan oinarrituta daude. Lan honetan sortutako atlas berria garunaren anatomian eta funtzioan batera oinarrituta dago. Sortutako atlas-a eta beste atlas-ekiko antzekotasunak neurtzeko gainjartze ehunekoa kalkulatu da Sorensen indizea erabiliz (aurrez aldetik definitu duguna). Garun atlas bakoitzeko 100 ausazko truke egin dira p-balioak kalkulatzeko. 0.05 baino txikiagoak diren p-balioak bakarrik kontsideratu dira.

9.8.1 SFM eta AAL atlasen arteko gainjartzea

Lehenik eta behin SFM eta AAL (*automated anatomical labeling*) [161] atlas anatomikoen arteko gainjartzea kalkulatu egin da. 9.12 irudian SFM 20 moduluen eta AAL atlasaren 45 erregio homologoen arteko gainjartzea ikus daiteke. Irudi hau aztertzerakoan, erregio anatomiko desberdinak SFM modulu bakarrean barne daudela ikusten da. Honek garun funtzio desberdinak burmuineko area anatomiko desberdinen aktibazioa behar duela adierazten du. AAL atlas-aren area anatomiko batzuk ere SFM modulu desberdinetan banatuta zeuden (9.12 irudiko lerroak). Nahiz eta modulu kopurua desberdina izan, ez da inoiz modulu eta area anatomiko bat guztiz berdinak izatea lortu (9.12 irudia). Uste zen bezala AAL area eta modulu batzuk oso antzekoak dira (SFM 11 eta *rectus gyrus* edo SFM 15 eta *temporal middle gyrus* adibidez, 9.12 irudia). Area anatomiko hauek garunaren funtzioan pentsatzen zena baino rol garrantzitsuagoa izan dezakete, AAL-ak deskribatutako beste area ugari baino. *Rectus gyrus* eta *temporal middle gyrus* hierarkiaren maila txikiago batean hobe irudikatuta aurkitu ahal dira. Gainjartzea handia mantentzen da modulu kopurua handitzean (9.11 irudia). Beste garun area asko zuhaitz hierarkikoan aurkitu ditzakegu modulu gehiago hartzen badira (Talamoa adibidez M=40 modulurekin).

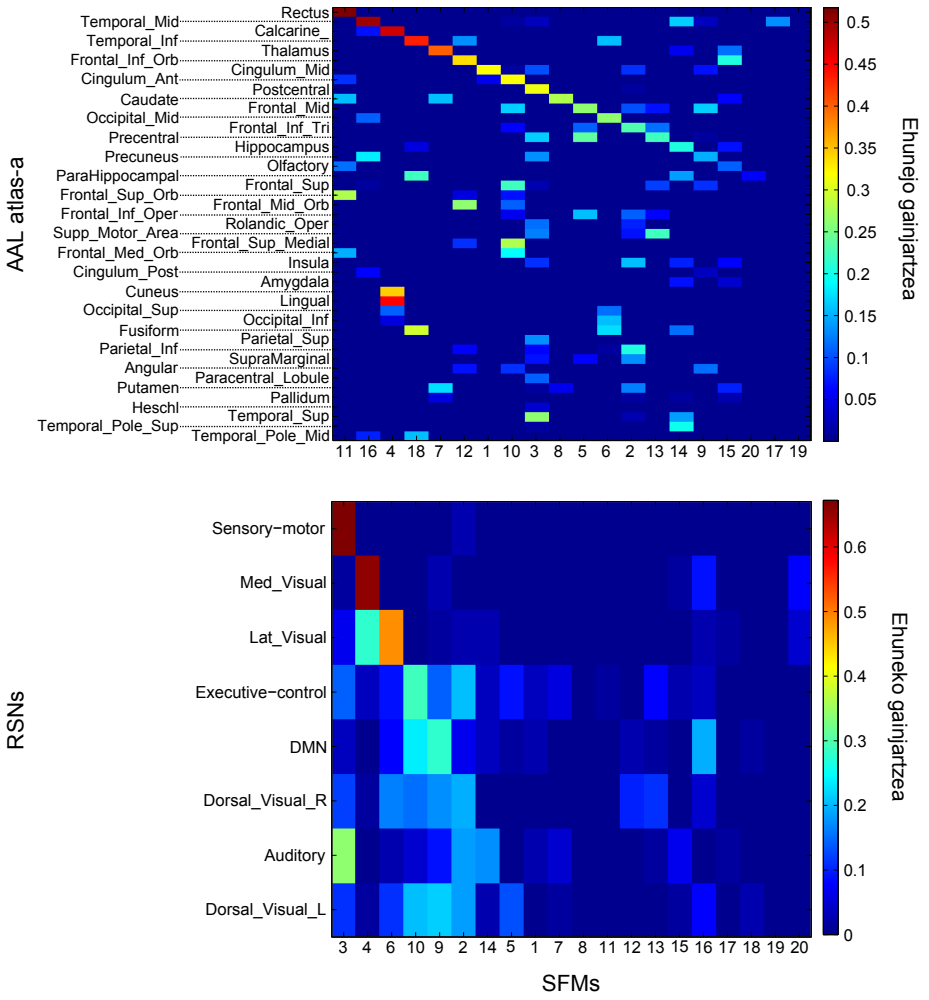

Irudia 9.12: SFM eta AAL atlas anatomiko erregioen arteko gainjartze ehunekoa ikusi daiteke. SFM eta RSN osagai funtzionalen arteko gainjartze ehunekoa ere ikusi daiteke.

9.8.2 SFM eta RSN osagaien arteko gainjartzea

Era berean, SFM moduluen eta asko erabiltzen diren RSN osagaien arteko gainjartzea kalkulatu da (9.12 irudia). RSN osagaiak, datu

funtzionaletan osagai independente analisia (ICA) erabiltzen kalkulatzen dira [127, 52, 123, 10]. Bi RSN osagaiek eta 2 moduluk antzekotasun handia dute: *Sensory motor* eta SFM-3-k eta *Medial visual* eta SFM-4-k. Beste RSN osagaiak SFM bat baino gehiagorekin gainjartzen dira. Nahiz eta modulu kopurua aldatu, ez dira lortu RSN osagai berberak (9.12 irudia). Honakoa, SFM-ak eta RSN-ak desberdinak direlako eta subjektu desberdinen arteko RSN osagaien forma aldakortasun handia duelako eman da.

9.8.3 SFM eta Broadmann area arteko gainjartzea

Azkeneko bi atlasen modura Broadmann atlas eta SFM arteko gainjartzea kalkulatu da (9.13 irudia). Broadmann areak *post-morten* eta lesioen bidez garatutako atlas bat da. Atlas honek funtzio neurofisiologiko desberdinetan oinarrituta dago. Broadmann 18 area eta SFM 4 modulua antzekoak dira, baita Broadmann 20 eta SFM 18 areak. Modulu gehiago erabiltzen badira, Broadman 18, 20, 11 ,10, 19 eta 21 antzekotasun handiak dituzte SFM modulu desberdinekin.

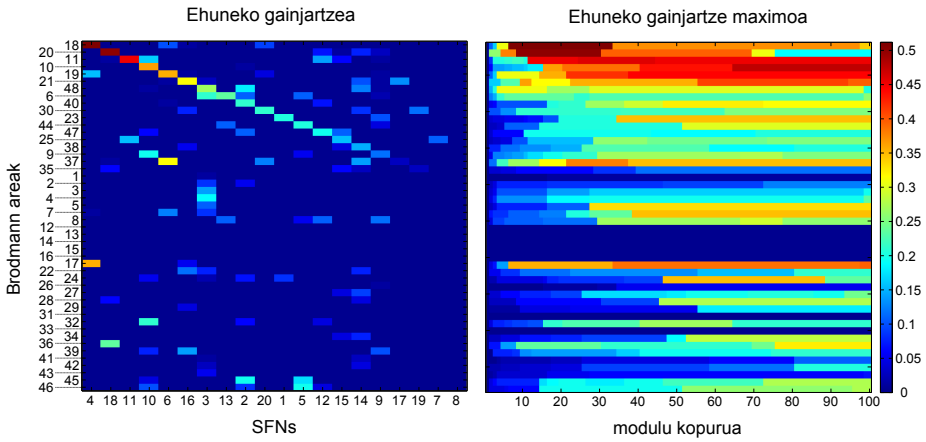

Irudia 9.13: SFM eta Broadmann area arteko gainjartzea.

9.9 SFMs: Azken oharrak

SFM-k (i) literaturan erabiltzen diren garun atlas berri bat aurkezten du; (ii) garun erregio estrukturalak eta funtzionalak sare/unitate batean batzen ditu; eta (iii) garun anatomia eta funtzioak errepresentatzen dituzten moduluak gainjartzen ditu. RSN osagaiak, gaitz neurologiko desberdinetan aldatzen direla ikusi da. Era berean, SFM moduluek gaixotasunak aztertzeko potentzial handia izatea espero da. Gainera, metodo honek ez du garunaren funtzioa soilik aztertzen baizik eta nola funtzioa eta estrukturaren arteko harremana aldatzen den.

Garuna aztertzerako orduan, logikoa ematen du garun zatiketa bat estruktura eta funtzioaren araberakoa dena existitzea, baina orain arte ez da zatiketa hau aurkitu. Egindako analisi ugariren ondorioz [54, 26, 41, 74, 101, 106, 72, 70, 79] ikusi da garunaren aktibitate funtzionala ezin dela datu estrukturaletatik inferitu, sare estrukturalak eta funtzionalak gauza desberdinak baitira. Bestetik, analisi berrietan estruktura eta funtzio sareen artean harreman handia dagoela ikusi da. Bi sare hauek grafo teorian definitutako *rich-club* estruktura dutela nabaritu da. Honek ezan nahi du garuneko modulu desberdinak beraien artean *hub* konektoreen bidez konektaturik daudela eta aldi berean *hub* hauek beraien artean oso konektatuta daudela [163]. Lan berri batek hurbil dauden areak konektatzen dituzten bideak begiratuz konektibitate funtzionala aurreikusi ahal dela azpimarratu du [66]. Honek SC-ak eta FC-ak beraien artean harreman handia dutela esan nahi du.

Atal honetan sortutako atlas berriak *cross-modularity* balioa maximizatzen du; baina modulu kopuruaren arabera tarte bat existitzen da non *cross-modularity* balioa mantendu egiten den. Tarte honetan (10 eta 30 modulu tartean) modulu desberdinak lortu ditzakegu, guztiak estrukturarekiko eta funtzioarekiko harreman handia izanik.

Atal honetan atlasa osatzeko funtzioa (SF) edo estruktura (FS) erabilia izan da eta gero beste modalitateekiko duen antzekotasuna begiratu da. Bien arteko desberdintasunak datu desberdinak direlako ematen da (datu estrukturalek oso konexio gutxi dituzte eta funtzionalek aldiz konexio asko ditu). Bi sare hauek batzeko metodo berriak

balio handia du *cross-modularity* balioa optimizatzeko. Nahiz eta metodo berri hau bilatzeak emaitza hobeak jasotzeko potentziala izan, lan honen helburutik kanpo geratu da.

Lan honetan lortutako garun zatiketak soilik garun datuak erabiltzen lortu dela azpimarratzea garrantzitsua da. Ez ziren hipotesirik erabili. SFM moduluak beste garun atlasekin konparatzerakoan aurkitutako desberdintasunek bi arrazoi desberdin izan ditzakete; Lehenengoa eta garrantzitsuena, erabiltzen diren beste atlas ugarik garuneko erregio subkortikalak ez dituztelako aztertzen edo erregio guztien %20 baino gutxiago errepresentatzen dituztelako [38]. Kasu honetan estruktura subkortikalak erabili ditugu gure analisian. Bigarrenik, existitzen diren beste atlasak estruktura edo funtziora begiratzen sortu dira. Beraz, esan daiteke biak aldi berean kontuan artzen dituen garun zatiketa bat sortu dela lehenengo aldiz.

Laburbilduz, garun estrukturaren eta funtzioaren arteko antzekotasunak bilatzerakoan, analisi hierarkiko bat eginez eta garun moduluak ateratzen oso antzekoak diren moduluak ikusi daitezke. Antzekotasun hau ikusteko garun moduluei begiratu behar zaie eta ez sare konexio guztiak konparatu.

9.10 Etorkizunerako lana: Neurokirurgiarako garun erregioak aurkitzen

Atal honetan konektibitate funtzionala eta estrukturala erabili dira garun erregio desberdinak aurkitzeko. Teknika honek inpaktu handia izan dezake burmuinean kirurgia egin beharreko momentuan kaltetutako garun erregioa aurkitzeko. Lan ugarik konektibitate funtzionala erabili dute neurokirurgia, neuro-onkologia, epilepsia kirurgia eta garun sakonean egindako estimulazioan prestatzeko [86].

Atsedenean egindako konektibitate analisi funtzionala, kirurgia hobeto prestatzeko adierazgarriak diren kortex erregioak aurkitzeko erabili daiteke. Era berean, analisi hau kirurgia ondorengoko informazio pronostikoa emateko erabili ahal izango da (garun zati bat kendu ondoren gaixoak izango duen morbidotasun maila) eta baita

neurokirurgia erresekzio muga seguruak identifikatzeko erabili ahal izango da.

Gaixoak ezin duenen eskaner barruan jarduerarik egin atsedenean lortutako funtzio seinaleak erabiliko dira kirurgia prestatzeko area garrantzitsuak identifikatzeko. Analisi honekin garunak hizkuntza prozesatzen duen area (entzunezko erregioa eta ezkerreko frontoparietal erregioa), DMN area eta zentzumen-motor area aurkitu ditzake.

Datu estrukturaletatik lortutako konektibitateak ere potentzial handia du neurokirurgiarako. Gaixo bati dardara kentzeko talamoaren zein zatitan estimulatu behar zaion kalkulatu daiteke [122]. Metodo honek, talamotik garuneko *premotor* eta *supplementary motor* konexio gehien dituen zatia bilatzen du. Metodo hauek metodo tradizionalak baino askoz hobeak dira, pertsona guztien burmuina desberdina baita eta beraz, estruktura hauek ez dira burmuin guztietan leku berberean egoten. Hori dela eta, oso garrantzitsua da gaixo bakoitzarentzat erregio hauek bilatzea eta ez eredu orokorrak erabiltzea.

Appendix A

MRI data pre-processing

MRI data from the scanner requires a number of preprocessing operations to prepare the data for the analysis [121]. The goal of Appendix A is to provide further insights into the techniques used for processing and the analysis of MRI data.

A.1 Functional data pre-processing

fMRI is a sequence of 3D brain volumes where each voxel intensity is the measure of the blood oxigenation level in a specific time point. The time period between each volume acquisition is defined as the Temporal Resolution (TR, typically between 1 and 3 seconds). Resting state fMRI usually is recorded for a period of 7 minutes (the acquired number of volumes will depend on the TR, typically about 200).

The first acquired volumes have to be deleted until the scanner measures reach the steady state (usually the first 2 or 3 volumes). During this period the acquired images have higher intensity values. Some scanners automatically remove these dummy scans.

A.1.1 Motion correction

All subjects inside the scanner slightly move their heads (due to swallowing etc), what introduces artifacts. In particular, the head movement results in a mismatch of the location of subsequent images (a voxel must have the same brain coordinates in all the acquired volumes). The goal of motion correction or realignment is to reduce this misalignment.

The first step is to choose an image reference to realign all the images to this one (a good choice is to use the middle volume of the acquisition). We assume a rigid motion, where head position can translate or rotate but head size does not change, and estimate the motion of each time point volume with respect to the reference volume. To estimate the translation and rotation of each volume, a gradient descent method is used with a normalized correlation cost function. When large amounts of activation are present, it is better to use the mutual information instead of the normalized correlation. The estimated head motion is saved for further processing steps (3 translation values and 3 rotation values).

Once the head motion is estimated we need to apply a transformation to all the volumes to realign them to the reference volume. Typically the computed transformation is applied with a trilinear interpolation to estimate the intensity values in each voxel (there exist better interpolation methods but they are computationally more expensive and due to the smoothing step, do not provide better results).

Head motion can produce large effects on the brain edges due to the fact that large intensity changes can occur when a voxel off the brain tissue, after movement, becomes located within brain tissue.

A.1.2 Slice Time correction

fMRI data are acquired through a collection of several 2-dimensional slices, each slice acquired at a different time. The slices can be captured in different orders: ascending, descending, interleaved (odd slices followed by even slices), etc. In any case, each slice is acquired at different time and this is why slice time correction has to

be applied (i.e. to have all the events in all the slices occurring at the same time). A reference slice is chosen and after, the data from other slices are interpolated to match the timing in the reference slice.

When slice time correction is used, artifacts in one image can be propagated throughout the time-series due to interpolation. This fact makes not everyone using this pre-processing step. If we acquired volumes with a small TR ($< 2seg$) with interleaved acquisition, there is no need to compute slice time correction (as the error is very small).

A.1.3 Spatial smoothing

fMRI acquisitions are noisy and smoothing removes part of this noise. In particular, spatial smoothing of a volume removes high-frequency information (small changes in the image). Most of the activations in the brain extend across many voxels and smoothing increases the signal-to-noise ratio in these regions.

When performing group analysis, data are combined across individuals (each individual brain is transformed to a template brain), but individual variability in the spatial location of functional regions is high. Spatial smoothing is used to reduce this variability.

For spatial smoothing of fMRI data, a convolution with a three-dimensional Gaussian filter is used. The amount of smoothing is determined by the width of the distribution described by the full width at half-maximum (or FWHM, the width of the distribution at the point where it is at half of its maximum).

The smoothing filter must be smaller than the activation signal to be detected, otherwise the activation of this area could be attenuated by smoothing. Usually, it gives good results to apply a little smoothing of about 2 times the size of a voxel.

A.1.4 Intensity normalization

A problem when analyzing raw fMRI data is that the level of the signal may substantially differ between voxels caused by non-controled reasons. This is a problem when comparing effect sizes across voxels and for multi-subject analysis. To overcome the varying intensities

between voxels and subjects, a grand mean scaling is often used. In particular, we scale all time-series of the voxels to have a median intensity value of 10000. Scaling to the median value is chosen instead of the mean value because the former is less sensitive to outliers.

A.1.5 Temporal filtering

Due to the poor temporal resolution of fMRI, time-series data contain little high-frequency noise and contain very slow frequency fluctuations that may be unrelated to the signal of interest.

Low-frequency noise has typically been found between 0.0-0.015 Hz due in part to scanner instabilities [145]. Other factors contributing to noise in a time-series are cardiac and respiratory effects, which will often show up as noise around 0.15 and 0.34 Hz, respectively.

Low frequency signals characterising the resting state BOLD activity have been found between 0.01-0.1 Hz [33, 62, 170, 138]. So after intensity normalization, a low-pass filter is applied within the slow fluctuations range of (0.01-0.08 Hz).

A.1.6 Detrend

We apply detrend to remove linear and quadratic trends of the signal from voxels time-series using linear least squares (each voxel is treated independently).

A.1.7 Regress out of Covariate signals

The brain activity can be perturbed with head motion, white matter signal or CSF signal effects. To remove the effect of these variables we use a General Linear Model (GLM). The GLM relates a single continuous dependent, or response, variable to one or more continuous or categorical independent variables, or predictors.

Let's assume that our measured time-series (Y) in a voxel is composed of:

$$Y = \beta_0 + \beta_1 X + \beta_2 M + \beta_3 W + \beta_3 C + \epsilon$$

where X represents the neural signal, M represents the head motion, W the white matter effect and C the CSF effect. We are interested in X, that represents the fMRI signal without the effects of head motion, white matter and CSF. The goal is to create a model that fits the data, and estimates the contribution of each variable to finally compute X. Y is a measured signal with some degree of error. To account for this error we add an ϵ term and we assume that it is normally distributed with mean of 0 and a variance of σ^2. The parameter β_i provides the contribution of each variable to the model.

Head motion signals are estimated in the motion correction step. For white matter and CSF signals we extract the mean signal of the voxels belonging to these regions. Usually some prior maps are used, accounting for the most probable regions of the white matter and CSF signals.

To estimate the parameters β_i, a least squares estimation is used, which minimizes the squared difference between the data and the estimates.

Once the parameters have been estimated we can easily compute X from the equation, which represents the fMRI signal without the effect of the covariates.

A.1.8 Spatial maps of brain components

The GLM can be also used to know the contribution of each voxel to a specific component, represented by its time-series. In this case, the measured fMRI signal Y is a linear combination of the time-series and a residual. i.e.

$$Y = \beta_0 + \beta_1 X + \beta_2 V + \epsilon$$

where V represents the time-series and X the fMRI signal without the effect of the time-series. β_2 provides how much the time-series contributes to every voxel in the brain. As explained before, using least square minimization of the squared difference between the data and the estimates allows to commpute β_2.

A.1.9 Spatial normalization to the MNI152 Template

The preprocessed data are represented in the functional space for each subject. Because individual brains are unique and different each other we need to transform all subjects brains to a common template to after perform group analysis. Spatial normalization is also required to use an atlas to define ROIS.

To perform normalization to a common template, first a mean fMRI signal is computed with all the time points of the acquisition. This mean volume is used to compute the transformation with the template before the the analysis. The first step is to compute a transformation from the mean fMRI image and the individual subject's structural image. For this transformation we need to estimate 12 degrees of freedom and a normalized correlation for cost function. The next step is to compute a transformation from the subject's structural image to the template structural image (again 12 degrees of freedom and a normalized correlation for cost function is used). The most used template is the MNI152 Template. Finally we can concatenate the two transformations to transform fMRI data to MNI152 template.

A.1.10 Time-series extraction from regions within an atlas

The next step is to extract the functional activity of the defined regions. A ROI is composed from many voxels, each one with a different hemodynamic activity (usually voxels that are close to each other have similar functional activity). They are 2 main approaches used in the literature for obtaining the characteristic hemodynamic activity of a given region:

- Temporal mean timecourse of all the voxels activity within a region.
- First component after PCA of the voxels activity within a region. Applying Principal Component Analysis to this time-

series we extract the functional activity that maximizes the explained variance, the predominant functional activity in this region, that is,the one that most of the voxels in this ROI are contributing to.

A.1.11 Functional connectivity network

The functional networks represents the activation profiles and dependencies among distinct neuronal populations. To calculate those dependencies, in this thesis we have used both Pearson's and partial correlation. Both connectivity matrices are symmetric (a region A interacts with another B in the same way as B interacts with A).

Pearson's Correlation

Pearson's correlation refers to one of the possible manners for calculating statistical relationships between variables. The correlation is obtained by dividing the covariance of the two variables by the product of their standard deviations:

$$\mathrm{C(x,y)} = \frac{E[(X-\mu_x)(Y-\mu_y)]}{\sigma_x \sigma_y} \tag{A.1}$$

The Partial Correlation

Partial correlation measures the degree of association between two random variables, eliminating the effect of the rest of variables.

Let C be a non-singular correlation matrix, then each element of the PC matrix is given by

$$\mathrm{PC}_{ij} = -\frac{P_{ij}}{\sqrt{P_{ii}P_{jj}}} \tag{A.2}$$

where $P \equiv C^{-1}$ is the inverse of the correlation matrix (ie., the precision matrix).

A.1.12 Effective connectivity networks

To create a network that identifies causal interactions underlying temporally ordered activation we have used Transfer Entropy. In this thesis we also developed a new method to compute Information Flow for the multivariate case (Chapter 4).

Transfer Entropy

Transfer Entropy quantifies the *directed* interaction between any two ROIs. To compute it, let define i^F as the future of the time-series of the ROI i. Similarly, i^P and j^P represent the pasts of ROIs i and j. Then, the TE from j to i is defined as

$$\mathrm{TE}_{ji} = H(i^F|i^P) - H(i^F|i^P, j^P) \tag{A.3}$$

with $H(i^F|i^P) = H(i^F, i^P) - H(i^P)$ representing the conditional Shanon entropy of i^F conditioning on i^P (for details, see [34]). Similarly, $H(i^F|i^P, j^P) = H(i^F, i^P, j^P) - H(i^P, j^P)$ is the conditional Shanon entropy of i^F conditioning on i^P and j^P. The TE is a non-symmetrical measure, i.e. $\mathrm{TE}_{ij} \neq \mathrm{TE}_{ji}$.

The Shanon Entropy (average uncertainty) of the random variable X is defined as $H(X) = -\sum_x \mathrm{prob}(x)\log\ \mathrm{prob}(x)$, where x represents a possible state in variable X [34]. For base 2 logarithm (as we have done in this thesis), the Information is computed in information bits.

In Chapter 2 we did not performed binning; alternatively, we just rounded each value in the time-series to its nearest integer and computed probabilities (number of time points in a given state divided by the total time-series length). The conditional entropies have been calculated with the function *condentropy* developed by Hanchuan Peng in C++ and plugged into MATLAB via mex. The code is available for download at [119].

The past of the time-series were the original time-series. The future of time-series were built by shifting the time-series in MATLAB with the function *circshift* with a lag value of l time points.

The statistical significance of the TE values were obtained by shuffling the time-series of the target ROI (for the calculation of the

TE from j to i, hereafter j will be referred as the source and i as the target). The time-series is shuffled just to remove the temporal information in the target variable. Next, the TE value is calculated for many repetitions of this shuffling procedure to obtain the distribution of values under the null hypothesis of zero values of TE (zero uncertainty reduction from source j to target i).

In the Chapter 4, we have developed a new method to calculate the multivariate TE, a measure providing the information flow. Let region A be described by N_A continuous time-series $\{x_\alpha^A(t)\}_{\alpha=1,...,N_A}$ (ie. set of voxels belonging to region A), and B described by N_B continuous time-series $\{x_\alpha^B(t)\}_{\alpha=1,...,N_B}$. All the time-series have been de-convolved by the HRF. Fixing the number k of the principal components the same for A and B, we represent the dynamics for A as $\{y_i^A(t)\}_{i=1,...,k}$ and the one for B as $\{y_i^B(t)\}_{i=1,...,k}$. Note that these components are statistically independent in the Gaussian approximation, the case considered in Chapter 4. Given the order m (the number of past points to be included in the state vector) and the lag parameter δ, we denote for the ith-component the state vector

$$Y_i^A(t) = (y_i^A(t-\delta)...y_i^A(t-\delta-m)) \tag{A.4}$$

and the corresponding one for B

$$Y_i^B(t) = (y_i^B(t-\delta)...y_i^B(t-\delta-m)) \tag{A.5}$$

According to Akaike information criterion, we use $m = 1$. The calculation of IF from A to B depends on the used lag δ. In order to evaluate the IF from A to B, we first calculate the IF from A to the ith-component of B, ie.,

$$t(A \to B^i) = H(y_i^B|\{y_j^B\}_{j=1,..,k}) - H(y_i^B|\{y_j^B\}_{j=1,..,k}; \{y_j^A\}_{j=1,..,k}) \tag{A.6}$$

where H is the conditional Shannon entropy, evaluated over the empirical distribution of samples at hand under the assumption of gaussianity, see [8]. Remark two important issues from eq. A.6: first, that the two conditioned states $\{y_j^B\}_{j=1,...,k}$ and $\{y_j^A\}_{j=1,...,k}$ are

accounting for lagged interactions, i.e. the two depend on the δ parameter appearing in eqs. A.4,A.5, but the term y_i^B is not lagged. Second, that the interaction given by eq. A.6 is univariate for the target and multivariate for the driver.

Next, repeating the same as in eq. A.6 for each of the components in B, ie., $i = 1, ..., k$ and denoting π_i as the probability of $t(A \to B^i)$ under the null hypothesis of the absence of influence, both π_i and $t(A \to B^i)$ can be calculated analytically in the Gaussian approximation (cf. eq. (12) in paper [8]). Finally, IF is then estimated as the average over all components in B, i.e.

$$IF(A \to B) = \frac{1}{k} \sum_{i=1}^{k} \theta(\frac{\tau}{k} - \pi_i) t(A \to B^i) \tag{A.7}$$

where θ is the Heaviside function, what makes the sum to account for all the contributions which are statistically significant according to Bonferroni criterion, i.e. those with $\pi_i < \tau/k$ where τ is the statistical significance (we use 0.05 here).

The complexity of the model is thus controlled by statistical testing, i.e. accepting only significant interactions (a similar strategy to control complexity is used in [100]).

A.2 Diffusion Tensor data pre-processing

DTI acquisition is a sequence of 3D brain volumes with different diffusion directions. This acquisition also generates parameters of the diffusion (direction vectors and b-values) that are used to reconstruct the fibre bundles of the brain.

A.2.1 Eddy current correction

The application of strong field gradients to acquire tensor imaging (DTI) can lead to eddy currents, which results in artifacts in the brain image. These distortions are different for different gradient directions. These artifacts may include stretches, shear, false fibre

tracking, enhanced background, image intensity loss and image blurring. Eddy Current Correction corrects for these distortions, and for simple head motion, using affine registration to a reference volume.

A.2.2 Calculation of the Diffusion Tensor

Using the corrected data, a local fitting of the diffusion tensor is applied to compute the diffusion tensor model at each voxel as explained in Chapter 1. Once the diffusion tensor is computed using the obtained eigenvectors and eigenvalues in each voxel we can compute Fractional Anisotropy (FA) map, that represents the eigenvalue variance (normalized between 0 and 1):

$$FA = \sqrt{\frac{3\sum_{i=1}^{3}(\lambda_i - \overline{\lambda})^2}{2\sum_{i=1}^{3}\lambda_i^2}} \tag{A.8}$$

This map is used for the tracking of the fibres in the brain.

A.2.3 Streamline Tractography

Once we know the orientation of fibres (i.e. the tensor eigenvectors) at every voxel in the brain, we can join and follow these directions and reconstruct entire pathways and brain connections in a process called tractography. In its simplest form, we start at a seed location and track the individual fibres by connecting the voxel where the fibre is initiated with the adjacent one towards the fibre direction (as determined by the leading local eigenvector of the diffusion tensor), and by iterating this procedure until it is terminated according to the criterion that the fibre arrives to a grey matter region (as identified by a fractional anisotropy index equal to 0.1, characteristic of grey matter) or that the fibre has a sharp curvature greater than 45 degrees from a given voxel to the following one (for further technical details on the employed tractography algorithm see [110].

A.2.4 Structural Network

The nodes defining the regions of the network need to be represented in a standard space (MNI Template), but the tractography is calculated in the subject's space. After the transformation to standard space the tractography is in the MNI space and we can count the number of fibres connecting each two ROIS of the chosen atlas.

Appendix B

Translational product: the BISCAY Platform

During this thesis, I also developed a new Neuroimaging platform for clinical practice. This platform is currently patent-pending.

In recent years, the development of new imaging techniques (Magnetic Resonance Imaging, CT, PET ...) has revolutionized modern medicine. Every day hundreds of images are acquired in hospitals that are used by clinicians in their diagnostics, evaluations, patient monitoring, surgical planning, etc. In parallel to this, new algorithms are developed every day, allowing for a very efficient manipulation and inferring key information from all these images. Unfortunately, most of these algorithms are not used in clinical practice due (mainly) to several reasons:

- Clinicians lack knowledge in image processing, limiting their practice to the available options incorporated in the proprietary software they usually work with. But current technology and methods allow for more complex algorithms to find small patterns that are imperceptible to the naked eye.
- Clinical software is expensive and difficult to use. Sometimes, because of its complexity, software is not used correctly.
- Hospital equipment has limited computing resources.

They goal of BISCAY (Brain ImageS CArtographY) platform is to provide the newest image processing techniques in a simple and user-friendly way for hospital clinicians. The processing is done in the BioCruces Supercomputing Lab (thus, there is no need for acquiring new high computing devices in the hospitals) with a simple platform that makes the use of tools and algorithms transparent to the user.

Cloud Computing Solution

Clinicians access the platform via a web browser to process all images in the cloud. Thus, the BISCAY platform, located in the Biocruces Supercomputing Lab, is used for advanced processing of medical images in a simple and user-friendly environment, and as such, does not require image-processing expertise. These techniques do not aim to diagnose, but to provide new and more precise information to help clinicians improving their decisions.

All the available services have been designed based on real needs defined by clinicians from the Cruces University Hospital. Platform users (i.e. clinicians) decide via a web browser the analysis they want to perform to a chosen patient (there is no need to install any software because everything is done in the web browser). The images are sent to the Biocruces Supercomputing Lab, where the core analysis is done. Final reports and images are sent back to clinicians.

This solution allows hospitals to centralize all different image processing software in just a single platform; thus, avoiding the need for searching new software and buying and maintaining all different licences.

The BISCAY platform has been implemented to interact with Picture Archiving and Communication Systems (PACS) in hospitals, so it can communicate with the different image storage machines and access the patient images database.

Finally, it is important to emphasize that these type of algorithms that are not usually used in clinical practice have been widely used in research for the evaluation of different clinical treatments or to study disease progression, providing promising results to be used in clinical practice.

Services

We have developed some initial services and continue working to incorporate new ones into the platform.

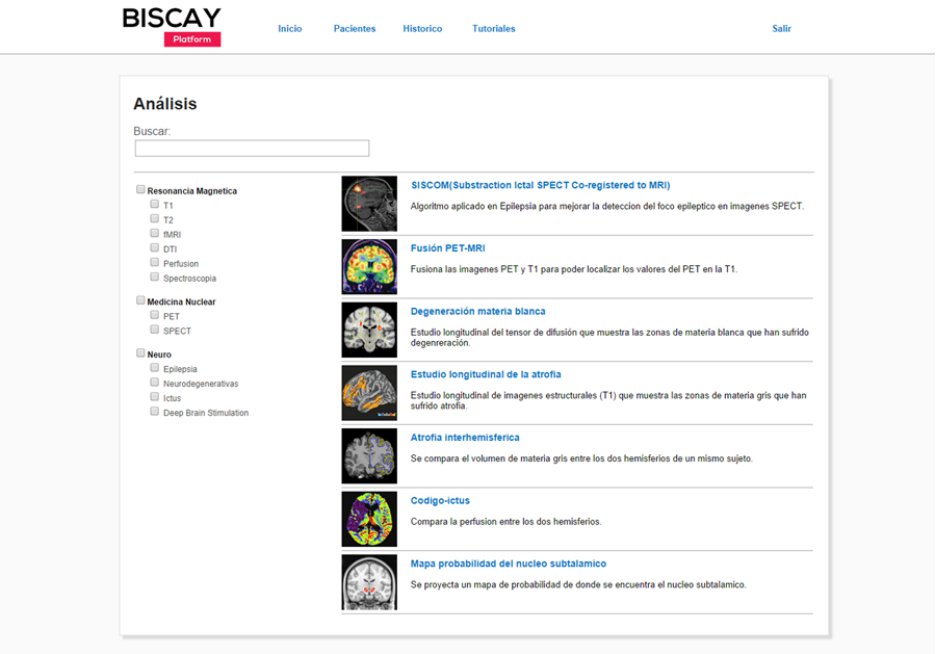

Figure B.1: BISCAY service list.

So far, here we list a few examples of some of the available services in BISCAY platform:

- SISCOM (Subtraction ictal SPECT co-registered to MRI): this algorithm is applied in epileptic patients for localization of the epileptic focus.
- PET-MRI fusion: two different type image modalities are fused allowing positron emission tomography (PET) images to be co-registered with structural images, thus improving areas localization beyond typical information obtained from solely a PET image.

- Longitudinal white matter degeneration: to study degeneration of the brain's fibre tracts (useful for instance in neurodeneration diseases, dementia or aging).

- Atrophy longitudinal analysis: to identify the cortical areas where the grey matter is losing volume.

- Sub-thalamic nucleus probabilistic map: some basal ganglia structures in the brain are not seen in conventional MRI images but using a probabilistic map created with the position of the sub-thalamic nucleus of 30 patients, BISCAY platform provides a probabilistic map for localization of each region for neurosurgery planning, e.g. in deep brain stimulation.

As we can observe in Figure B.1, clinicians can choose the service to be processed in the BISCAY platform's menu, and after providing the necessary images required for each choice, BISCAY platform does the job. It is important to remark that available menus have been adapted to specific users and to each particular service; for example, for epileptic patients clinicians can choose the "Epilepsy filter", and only those services associated to that disease are appearing (thus for instance not offering the possibility of neurodegeneration services in that case).

Once a service is requested to the BISCAY platform, this process is added to the processing queue. In a clinical environment, there are different priority classes for each specific query. BISCAY platform also allows sending the analysis to a priority queue for the cases where a fast analysis is needed.

To examine the images, a web based medical image viewer has been implemented (Figure B.2) allowing to see all these images from any computer of the hospital without installing any software (a big advantage because hospital computers have many limitations when installing software).

BISCAY platform has customization tools that allow the administrator to create new platform users, add hospital PACS to read stored images, specify the clinicians email where to receive the notifications once a service has finished, etc.

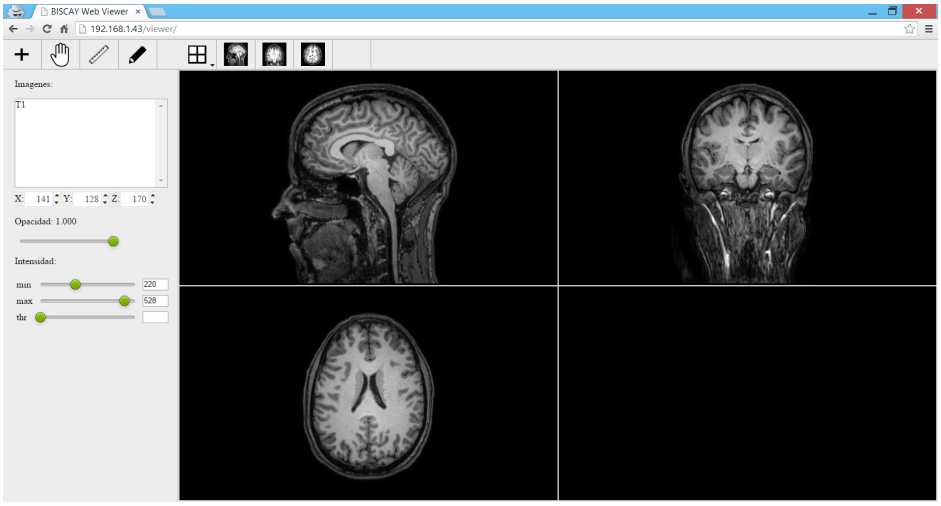

Figure B.2: BISCAY visualization tool.

Albeit the available services are easy to use and do not require image processing knowledge at all, there is an available tutorial for clinicians, providing further details for each specific service and the algorithm employed in question.

Users

It is expected that the BioCruces SuperComputing Lab will be configured November 2015, inside the Osakideza network (Basque Health System), allowing all the computers connected to Osakidetza's network to use the platform. In a second stage we will consider allowing other hospitals to use the platform. For this stage, we developed a electronic device that can be connected to any hospital outside Osakidetza's network to give access to the platform's services. The electronic device also anonymizes all the patient's information and generate an encrypted connection with the BioCruces Supercomputing Lab to provide all the available services to users outside Osakidetza.

Bibliography

[1] IM Adams. Structural plasticity of synapses in alzheimer's disease. *Mol. Neurobiol*, 5:411419, 1991.

[2] G.E. Alexander, M.D. Crutcher, and M.R. DeLong. Basal gangliathalamocortical circuits: Parallel substrates for motor, oculomotor, "prefrontal" and "limbic" functions. *Prog Brain Res*, 85:119146, 1990.

[3] C. Alonso-Montes, I. Diez, L. Remaki, I. Escudero, B. Mateos, Y. Rosseel, D. Marinazzo, S. Stramaglia, and J.M. Cortes. Lagged and instantaneous dynamical influences related to brain structural connectivity. *Front Psychol*, 6:1024, 2015.

[4] H Amieva, LH Phillips, S Della Sala, and JD Henry. Inhibitory functioning in alzheimer's disease. *Brain*, 127:949–964, 2004.

[5] A.R. Aron and R.A. Poldrack. Cortical and subcortical contributions to stop signal response inhibition: role of the subthalamic nucleus. *J Neurosci*, 26:2424e2433, 2006.

[6] J. Ashburner and K.J. Friston. Nonlinear spatial normalization using basis functions. *Hum Brain Mapp*, 7:254–266, 1999.

[7] A. Barbey, A. Belli, A. Logan, R. Rubin, M. Zamroziewicz, and J. Operskalski. Network topology and dynamics in traumatic brain injury. *Curr Opin Behav Sci*, 4:92–102, 2015.

[8] L. Barnett, A.B. Barrett, and A.K. Seth. Granger causality and transfer entropy are equivalent for Gaussian variables. *Phys Rev Lett*, 103:238701, 2009.

[9] A.B. Barrett, L. Barnett, and A.K. Seth. Multivariate Granger causality and generalized variance. *Phys Rev E*, 81:041907, 2010.

[10] C.F. Beckmann, M. DeLuca, J.T. Devlin, and S.M. Smith. Investigations into resting-state connectivity using independent component analysis. *Philos. Trans. R. Soc. Lond. B. Biol. Sci*, 360:10011013, 2005.

[11] C.F. Beckmann and S.M. Smith. Probabilistic independent component analysis for functional magnetic resonance imaging. *IEEE Trans Med Imaging*, pages 137–152, 2004.

[12] A.J. Bell and T.J. Sejnowski. An information-maximization approach to blind separation and blind deconvolution. *Neural Comput*, 7:11291159, 1995.

[13] P. Bentley, J. Driver, and R.J. Dolan. Cholinesterase inhibition modulates visual and attentional brain responses in alzheimer's disease and health. *Brain*, 131:409–424, 2008.

[14] R.F Betzel, A. Griffa, A. Avena-Koenigsberger, J. GOI, J.P. Thiran, P. Hagmamm, and O. Sporns. Multi-scale community organization of the human structural connectome and its relationship with resting-state functional connectivity. *Network Science*, 1:353373, 2013.

[15] M.A. Binnewijzend, M.M. Schoonheim, E. Sanz-Arigita, A.M. Wink, W.M. van der Flier, N. Tolboom, S.M. Adriaanseand, J.S. Damoiseaux, P. Scheltensand, B.N. van Berckel, and F. Barkhof. Resting-state fmri changes in alzheimers disease and mild cognitive impairment. *Neurobiol Aging*, 33:20182028, 2012.

[16] CM Bishop. *Pattern recognition and machine learning*. Springer, 2006.

[17] B. Biswal, F.Z. Yetkin, V.M. Haughton, and J.S. Hyde. Functional connectivity in the motor cortex of resting human brain using echo-planar MRI. *Magn. Reson. Med.*, 34:537541, 1995.

[18] J.A. Bonachela, H. Hinrichsen, and M.A. Mu noz. Entropy estimates of small data sets. *J Phys A: Math Theor*, 41:202001, 2008.

[19] P. Bonifazi, M. Goldin, M.A. Picardo, I. Jorquera, A. Cattani, G. Bianconi, A. Represa, Y. Ben-Ari, and R. Cossart. The human connectome: A structural description of the human brain. *Science*, 326:14191424, 2009.

[20] V. Bonnelle, R. Leech, K. Kinnunen, T. Ham, C. Beckmann, X. D. Boissezon, R. Greenwood, and D. Sharp. Default mode network connectivity predicts sustained attention deficits after traumatic brain injury. *J Neurosci*, 31:1344213451, 2011.

[21] P. Boveroux, A. Vanhaudenhuyse, M.A. Brun, Q. Noirhomme, S. Lauwick, A. Luxen, C. Degueldre, A. Plenevau, C. Schnakers, C. Phillips, J.F. Brichant, V. Bonhomme, P. Maquet, M.D. Greicius, S. Laureys, and M. Boly. Breakdown of within- and between- network resting state functional magnetic resonance imaging connectivity. *Anesthesiology*, 113:10381053, 2010.

[22] S.L. Bressler and A.K. Seth. Wiener-granger causality: a well-established methodology. *Neuroimage*, 58:323329, 2011.

[23] M.R. Brier, J.B. Thomasand, A.Z. Snyder, T.L. Benzinger, D. Zhang, M.E. Raichle, D.M. Holtzman, J.C. Morris, and B.M. Ances. Loss of intranetwork and internetwork resting state functional connections with alzheimers disease progression. *J Neurosci*, 32:88908898, 2012.

[24] E. Bullmore and O. Sporns. Complex brain networks: graph theoretical analysis of structural and functional systems. *Nat Rev Neurosci*, 10:186198, 2009.

[25] G. Buzsaki. *Rhythms of the Brain.* Oxford University Press, 2006.

[26] J. Cabral, E. Hugues, O. Sporns, and G. Deco. Role of local network oscillations in resting-state functional connectivity. *Neuroimage*, 57:130139, 2011.

[27] K. Caeyenberghs, A. Leemans, M. Heitger, I. Leunissen, T. Dhollander, S. Sunaert, P. Dupont, and S. Swinnen. Graph analysis of functional brain networks for cognitive control of action in traumatic brain injury. *Brain*, 135:12931307, 2012.

[28] K. Caeyenberghs, A. Leemans, I. Leunissen, J. Gooijers, K. Michiels, S. Sunaert, and S. Swinnen. Altered structural networks and executive deficits in traumatic brain injury patients. *Brain Struct Funct*, 219:193209, 2014.

[29] K. Caeyenberghs, A. Leemans, I. Leunissen, K. Michiels, and S. Swinnen. Topological correlations of structural and functional networks in patients with traumatic brain injury. *Front Hum Neurosci*, 7:726, 2013.

[30] K. Caeyenberghs, R. Siugzdaite, D. Drijkoningen, D. Marinazzo, and S. Swinnen. Functional connectivity density and balance in young patients with traumatic axonal injury. *Brain Connect*, 2014.

[31] R.L. Carhart-Harris, R. Leech, P.J. Hellyer, M. Shanahan, A. Feilding, E. Tagliazucchi, D.R. Chialvo, and D. Nutt. The entropic brain: A theory of conscious states informed by neuroimaging research with psychedelic drugs. *Frontiers in Human Neuroscience*, 8:20, 2014.

[32] M. Catani, R.J. Howard, S. Pajevic, and D.K. Jones. Virtual in vivo interactive dissection of white matter fasciculi in the human brain. *Neuroimage*, 17:7794, 2002.

[33] D. Cordes, V.M. Haughton, K. Arfanakis, J.D. Carew, P.A Turski, C.H. Moritz, M.A. Quigley, and M.E. Meyerand. Frequencies contributing to functional connectivity in the cerebral cortex in resting-state data. *Am. J. Neuroradiol*, 22:13261333, 2001.

[34] T.M. Cover and J.A. Thomas. *Elements of Information Theory*. John Wiley & Sons, Inc, 2006.

[35] J.P. Coxon, D.J. Goble, I.A. Van, V.J. De, N. Wenderoth, and S. Swinnen. Reduced basal ganglia function when elderly switch between coordinated movement patterns. *Cereb Cortex*, 20:2368e2379, 2010.

[36] J.P. Coxon, A. Van Impe, N. Wenderoth, and S.P. Swinnen. Aging and inhibitory control of action: cortico-subthalamic connection strength predicts stopping performance. *J Neurosci*, 32:8401e8412, 2012.

[37] R.C. Craddock, G.A. James, P.E. Holtzheimer, X.P. Hu, and H.S. Mayberg. A whole brain fmri atlas generated via spatially constrained spectral clustering. *Hum. Brain Mapp*, 33:19141928, 2012.

[38] R.C. Craddock, S. Jbabdi, C.G. Yan, J.T. Vogelstein, F.X. Castellanos, A. Di Martino, C. Kelly, K. Heberlein, S. Colcombe, and M.P. Milham. Imaging human connectomes at the macroscale. *Nat. Methods*, 10:524539, 2013.

[39] J.S. Damoiseaux and M.D. Greicius. Greater than the sum of its parts: a review of studies combining structural connectivity and resting-state functional connectivity. *Brain Struct. Funct*, 213:525533, 2009.

[40] J.S. Damoiseaux, S.A. Rombouts, F. Barkhof, P. Scheltens, C.J. Stam, S.M. Smith, and C.F. Beckmann. Consistent resting-state networks across healthy subjects. *Proc Natl Acad Sci USA*, 103:13848, 2006.

[41] G. Deco, V.K. Jirsa, and A.R. McIntosh. Emerging concepts for the dynamical organization of resting-state activity in the brain. *Nat. Rev. Neurosci*, 12:4356, 2011.

[42] P. Delamillieure, G. Doucet, B. Mazoyer, M.R. Turbelin, N. Delcroix, E. Mellet, L. Zago, F. Crivello, L. Petit, N. Tzourio-Mazoyer, and M. Joliot. The resting state questionnaire: An introspective questionnaire for evaluation of inner experience during the conscious resting state. *Brain Res. Bull*, 81:565573, 2010.

[43] O. Demirci, M.C. Stevens, N.C. Andreasen, A. Michael, J. Liu, T. White, G.D. Pearlson, V.P. Clark, and V.D. Calhoun. Investigation of relationships between fmri brain networks in the spectral domain using ica and granger causality reveals distinct differences between schizophrenia patients and healthy controls. *Neuroimage*, 46:419–431, 2009.

[44] O. Demirci, M.C. Stevens, N.C. Andreasen, A. Michael, J. Liu, T. White, G.D. Pearlson, V.P. Clark, and V.D. Calhoun. Multivariate granger causality analysis of fmri data. *Hum Brain Mapp*, 30:13611373, 2009.

[45] I. Diez, P. Bonifazi, I. Escudero, B. Mateos, M.A. Muoz MA, S. Stramaglia, and J.M Cortes. A novel brain partition highlights the modular skeleton shared by structure and function. *Sci Rep*, 5:10532, 2015.

[46] I. Diez, A. Erramuzpe, I. Escudero, B. Mateos, A. Cabrera, D. Marinazzo, E.J. Sanz-Arigita, S. Stramaglia, and J.M. Cortes. Information flow between resting-state networks. *Brain Connect*, 2015.

[47] D. Drijkoningen, K. Caeyenberghs, I. Leunissen, C. Linden, S. Sunaert, J. Duysens, and S. Swinnen. Training-induced improvements in postural control are accompanied by alterations in cerebellar white matter in brain injured patients. *Neuroimage Clin*, 7:240251, 2015.

[48] E. Fagerholm, P. Hellyer, G. Scott, R. Leech, and D. Sharp. Disconnection of network hubs and cognitive impairment after traumatic brain injury. *Brain*, 138:16961709, 2015.

[49] K.D. Farbota, A. Sodhi, B.B. Bendlin, D.G. McLaren, G. Xu, H.A. Rowley, and S.C. Johnson. Longitudinal volumetric changes following traumatic brain injury: a tensor-based morphometry study. *Neuropsychol Soc*, 18:1006e1018, 2012.

[50] L. Ferrarini, I.M. Veer, E. Baerends, M.J. van Tol, R.J. Renken, N.J. van der Wee, D.J. Veltman, A. Aleman, F.G. Zitman, B.W. Penninx, M.A. van Buchem, J.H. Reiber, S.A. Rombouts, and J. Milles. Hierarchical functional modularity in the resting-state human brain. *Hum. Brain Mapp*, 30:22202231, 2009.

[51] A. Fornito, A. Zalesky, and M. Breakspear. Graph analysis of the human connectome: Promise, progress, and pitfalls. *Neuroimage*, 80:426444, 2013.

[52] M.D. Fox, A.Z. Snyder, J.L. Vincent, M. Corbetta, D.C. Van Essen, and M.E.A.G. Raichle. The human brain is intrinsically organized into dynamic, anticorrelated functional networks. *Proc Natl Acad Sci USA*, 102:9673–9678, 2005.

[53] M.D. Fox, D. Zhang, A.Z. Snyder, and M.E. Raichle. The global signal and observed anticorrelated resting state brain networks. *J. Neurophysiol*, 101:32703283, 2009.

[54] F. Fraiman, P. Balenzuela, J. Foss, and D.R Chialvo. Ising-like dynamics in large-scale functional brain networks. *Phys. Rev. E*, 79:061922, 2009.

[55] M.J. Frank, A. Scheres, and S.J. Sherman. Understanding decision-making deficits in neurological conditions: insights from models of natural action selection. *Phil Trans R Soc B Biol Sci*, 362:1641e1654, 2007.

[56] K.J. Friston. Functional and effective connectivity in neuroimaging: A synthesis. *Hum. Brain. Mapp*, 2:5678, 1994.

[57] K.J. Friston. Causal modelling and brain connectivity in functional magnetic resonance imaging. *PLoS Biol*, 7:e33, 2009.

[58] K.J. Friston. Functional and effective connectivity: a review. *Brain Connect*, 1:1336, 2011.

[59] K.J. Friston, L. Harrison, and W. Penny. Dynamic causal modelling. *Neuroimage*, 19:12731302, 2003.

[60] S.D. Gale, L. Baxter, N. Roundy N., and S.C. Johnson. Traumatic brain injury and grey matter concentration: a preliminary voxel based morphometry study. *J Neurol Neurosurg Psych*, 76:9848, 2005.

[61] L.K. Gallos, H.A. Makse, and M. Sigman. A small world of weak ties provides optimal global integration of self-similar modules in functional brain networks. *Proc. Natl. Acad. Sci. USA*, 109:28252830, 2012.

[62] D.G. Gee, B.B. Biswal, C. Kelly, D.E. Stark, D.S. Margulies, Z. Shehzad, L.Q. Uddin, D.F. Klein, M.T. Banich, F.X. Castellanos, and M.P. Milham. Low frequency fluctuations reveal integrated and segregated processing among the cerebral hemispheres. *Neuroimage*, 54:517527, 2011.

[63] L.R. Gentry, J.C. Godersky, and B. Thompson. MR imaging of head trauma: review of the distribution and radiopathologic features of traumatic lesions. *AJR Am J Roentgenol*, 150:663e672, 1988.

[64] J.T. Giacino, K. Kalmar, and J.G. Whyte. The jfk coma recovery scale-revised: measurement characteristics and diagnostic utility. *Arch Phys Med Rehabil*, 85:2020–2029, 2004.

[65] O. Godefroy. Frontal syndrome and disorders of executive functions. *J Neurol*, 250:1–6, 2003.

[66] J. Goi, M.P. van den Heuvel, A. Avena-Koenigsberger, N. Velez de Mendizabal, R.F. Betzel, A. Griffa, P. Hagmann, B. Corominas-Murtra, J.P. Thiran, and O. Sporns. Resting-brain functional connectivity predicted by analytic measures of network communication. *Proc Natl Acad Sci USA*, 111:833838, 2014.

[67] C.W.J. Granger. Investigating causal relations by econometric models and cross-spectral methods. *Econometrica*, 37:424438, 1969.

[68] C.M. Gray and W. Singer. Stimulus-specific neuronal oscillations in orientation columns of cat visual cortex. *Proc. Natl. Acad. Sci. USA*, 86:16981702, 1989.

[69] M.D. Greicius, C. Srivastava, A.L. Reiss, and V. Menon. Default-mode network activity distinguishes alzheimers disease from healthy aging: Evidence from functional mri. *Proc Natl Acad Sci USA*, 101:46374642, 2004.

[70] M.D. Greicius, K. Supekar, V. Menon, and R.F. Dougherty. Resting-state functional connectivity reflects structural connectivity in the default mode network. *Cereb. Cortex*, 19:7278, 2009.

[71] Markram H. The blue brain project. *Nat. Rev. Neurosci*, 7:153–160, 2006.

[72] P. Hagmann, L. Cammoun, X. Gigandet, R. Meuli, C.J. Honey, V.J. Wedeen, and O. Sporns. Mapping the Structural Core of Human Cerebral Cortex. *PLoS Biol*, 6:e159, 2008.

[73] P. Hagmann, M. Kurant, X. Gigandet, P. Thiran, V.J. Wedeen, R. Meuli, and J.P. Thiran. Mapping Human Whole-Brain Structural Networks with Diffusion MRI. *PLoS ONE*, 2:e597, 2007.

[74] A. Haimovici, E. Tagliazucchi, P. Balenzuela, and D.R. Chialvo. Brain Organization into Resting State Networks Emerges at Criticality on a Model of the Human Connectome. *Phys. Rev. Lett*, 110:178101, 2013.

[75] T. Ham and D. Sharp. How can investigation of network function inform rehabilitation after traumatic brain injury? *Curr Opin Neurol*, 25:662669, 2012.

[76] L. Heine, A. Soddu, F. Gomez, A. Vanhaudenhuyse, L. Tshibanda, M. Thonnard, V. Charland-Verville, M. Kirsch, S. Laureys, and A. Demertzi. Resting state networks and consciousness: alterations of multiple resting state network connectivity in physiological, pharmacological, and pathological consciousness states. *Front Psychol*, 3:295, 2012.

[77] A.M. Hermundstad, D.S. Bassett, K.S. Brown, E.M. Aminoff, D. Clewett, S. Freeman, A. Frithsen, A. Johnson, C.M. Tipper, M.B. Miller, S.T. Grafton, and J.M. Carlson. Structural foundations of resting-state and task-based functional connectivity in the human brain. *Proc. Natl. Acad. Sci. USA*, 110:61696174, 2013.

[78] O. Hikosaka and M. Isoda. Switching from automatic to controlled behavior: cortico-basal ganglia mechanisms. *Trends Cogn Sci*, 14:154e161, 2010.

[79] C.J. Honey, O. Sporns, L. Cammoun, X. Gigandet, J.P. Thiran, R. Meuli, and P. Hagmann. Predicting human resting-state functional connectivity from structural connectivity. *Proc. Natl. Acad. Sci. USA*, 106:20352040, 2009.

[80] A.G. Hudetz. General anesthesia and human brain connectivity. *Brain Connect*, 2:291–302, 2012.

[81] M.B. Hulkower, D.B. Poliak, S.B. Rosenbaum, M.E. Zimmerman, and M.L. Lipton. A decade of dti in traumatic brain injury: 10 years and 100 articles later. *AJR Am J Roentgenol*, 34:2064–74, 2013.

[82] E.T. Jaynes. Information Theory and Statistical Mechanics. *Phys Rev 106*, 106:620630, 1957.

[83] H. Karbasforoushan and N.D. Woodward. Resting-state networks in schizophrenia. *Curr Top Med Chem*, 12:24042414, 2012.

[84] M.A. Koch, D.G. Norris, and M. Hund-Georgiadis. An investigation of functional and anatomical connectivity using magnetic resonance imaging. *Neuroimage*, 16:241250, 2002.

[85] A. Kolchinsky, M.P. van den Heuvel, A. Griffa, P. Hagmann, L.M. Rocha, O. Sporns, and J. Goi. Multi-scale integration and predictability in resting state brain activity. *Front. Neuroinform*, 8:66, 2014.

[86] S. Lang, N Duncan, and G. Northoff. Resting-state functional magnetic resonance imaging: review of neurosurgical applications. *Neurosurgery*, 74:453–64, 2014.

[87] I. Leunissen, J.P. Coxon, K. Caeyenberghs, K. Michiels, S. Sunaert, and S. Swinnen. Subcortical volume analysis in traumatic brain injury: the importance of the fronto-striato-thalamic circuit in task switching. *Cortex*, 51:67–81, 2014.

[88] I. Leunissen, J.P. Coxon, K. Caeyenberghs, K. Michiels, S. Sunaert, and S. Swinnen. Task switching in traumatic brain injury relates to cortico-subcortical integrity. *Hum Brain Mapp*, 25:2459–69, 2014.

[89] H. Levin and M. Kraus. The frontal lobes and traumatic brain injury. *J Neuropsychiatry Clin Neurosci*, 6:443454, 1994.

[90] R Li, X Wu, K Chen, AS Fleisher, EM Reiman, and L Yao. Alterations of directional connectivity among resting-state networks in alzheimer disease. *AJNR Am J Neuroradiol*, 34:340–345, 2013.

[91] S.J. Li, Z. Li, G. Wu, M.J. Zhang, M. Franczak, and P.G. Antuono. Alzheimers disease: Evaluation of a functional mr imaging index as a marker. *Radiology*, 225:253259, 2002.

[92] P Liang, Z Li, G Deshpande, Z Wang, X Hu, and K Li. Altered causal connectivity of resting state brain networks in amnesic mci. *PLoS One*, 9:e88476, 2014.

[93] W Liao, J Ding, D Marinazzo, Q Xu, Z Wang, C Yuan, Z Zhang, G Lu, and H Chen. Small-world directed networks in the human brain: multivariate granger causality analysis of resting-state fmri. *Neuroimage*, 14:26832694, 2011.

[94] W. Liao, Z. Zhang, Z. Pan, D. Mantini, J. Ding, X. Duan, C. Luo, G. Lu, and H. Chen. Altered functional connectivity and small-world in mesial temporal lobe epilepsy. *PLoS One*, 5:e8525, 2010.

[95] Z Liu, Y Zhang, L Bai, H Yan, R Dai, C Zhong, H Wang, W Wei, T Xue, Y Feng, Y You, and J Tian. Investigation of the effective connectivity of resting state networks in alzheimers disease: a functional mri study combining independent components analysis and multivariate granger causality analysis. *NMR Biomed*, 25:1311–1320, 2012.

[96] Waldrop MA. Brain in a box. *Nature — News Feature*, 2012.

[97] V. Maki-Marttunen, I. Diez, J.M. Cortes, D.R. Chialvo, and M. Villarreal. Disruption of transfer entropy and inter-hemispheric brain functional connectivity in patients with dis-

order of consciousness. *Frontiers in Neuroinformatics*, 7:24, 2013.

[98] V. Maki-Marttunen, I. Diez, J.M. Cortes, D.R. Chialvo, and M. Villarreal. Disruption of transfer entropy and inter-hemispheric brain functional connectivity in patients with disorder of consciousness. *Front Neuroinform*, 7:24, 2013.

[99] D. Marinazzo, W. Liao, H. Chen, and S. Stramaglia. Nonlinear connectivity by granger causality. *Neuroimage*, 58:330338, 2011.

[100] D. Marinazzo, M. Pellicoro, and S. Stramaglia. Kernel method for nonlinear granger causality. *Phys Rev Lett*, 100:144103, 2008.

[101] D. Marinazzo, M. Pellicoro, G. Wu, L. Angelini, J.M Cortes, and S. Stramaglia. Information transfer and criticality in the ising model on the human connectome. *PLoS One*, 9:1e93616, 2014.

[102] M. Maruishi, M. Miyatani, T. Nakao, and H. Muranaka. Compensatory cortical activation during performance of an attention task by patients with diffuse axonal injury: a functional magnetic resonance imaging study. *J Neurol Neurosurg Psychiatry*, 78(2):168173, 2007.

[103] A.R. McIntosh and N.J. Lobaugh. Partial least squares analysis of neuroimaging data: applications and advances. *Neuroimage*, 23:S250263, 2004.

[104] D.G. McLaren, R.A. Sperling, and A. Atri. Flexible modulation of network connectivity related to cognition in alzheimer's disease. *Neuroimage*, 15:544–557, 2014.

[105] P.A. Merolla, J.V. Arthur, R. Alvarez-Icaza, A.S. Cassidy, J. Sawada, F. Akopyan, B.L. Jackson, N. Imam, C. Guo, Y. Nakamura, B. Brezzo, I. Vo, S.K. Esser, R. Appuswamy,

B. Taba, A. Amir, M.D. Flickner, W.P. Risk, R. Manohar, and DS Modha. Artificial brains. a million spiking-neuron integrated circuit with a scalable communication network and interface. *Science*, 245:668–673, 2014.

[106] A. Messe, D. Rudrauf, H. Benali, and C. Marrelec. Relating Structure and Function in the Human Brain: Relative Contributions of Anatomy, Stationary Dynamics, and Non-stationarities. *PLoS Comput. Biol*, 10:e1003530, 2014.

[107] D. Meunier, R. Lambiotte, A. Fornito, K. Ersche, and E.T. Bullmore. Hierarchical modularity in human brain functional networks. *Front. Neuroinform*, 3:37, 2009.

[108] E. Miller. The prefrontal cortex and cognitive control. *Nat Rev Neurosci*, 1:5965, 2000.

[109] J.W. Mink. The basal ganglia: focused selection and inhibition of competing motor programs. *Prog Neurobiol*, 50:381e425, 1996.

[110] S. Mori, B.J. Crain, V.P. Chacko, and P.C. van Zijl. Three-dimensional tracking of axonal projections in the brain by magnetic resonance imaging. *Ann. Neurol*, 45:265269, 1999.

[111] M.E. Newman. Fast algorithm for detecting community structure in networks. *Phys. Rev. E*, 69:066133, 2004.

[112] Y. Nir, R. Mukamel, I. Dinstein, E. Privman, M. Harel, L. Fisch, H. Gelbard-Sagiv, S. Kipervasser, F. Andelman, M.Y. Neufeld, U. Kramer, A. Arieli, I. Fried, and R. Malach. Interhemispheric correlations of slow spontaneous neuronal fluctuations revealed in human sensory cortex. *Nat Neurosci*, 11:1100–1108, 2008.

[113] Q. Noirhomme, A. Soddu, R. Lehembre, A. Vanhaudenhuyse, P. Boveroux, M. Boly, and S. Laureys. Brain connectivity in pathological and pharmacological coma. *Front Syst Neurosci*, 4:160, 2010.

[114] R.C. Oldfield. The assessment and analysis of handedness: the edinburgh inventory. *Neuropsychologia*, 9:97–113, 1971.

[115] E.M. Palacios, R. Sala-Llonch, C. Junque, T. Roig, J.M. Tormos, N. Bargallo, and P. Vendrell. Resting-state functional magnetic resonance imaging activity and connectivity and cognitive outcome in traumatic brain injury. *JAMA Neurol*, 70(7):845–851, 2013.

[116] L. Paninski. Estimation of entropy and mutual information. *Neural Comp*, 15:1191–1254, 2003.

[117] S. Panzeri and A. Treves. Analytical estimates of limited sampling biases in different information measures. *Network: Comput Neural Syst*, 7:87–107, 1996.

[118] H.J. Park and K. Friston. Structural and functional brain networks: from connections to cognition. *Science*, 342:1238411, 2013.

[119] Hanchuan Peng. Mutual Information Toolbox. `http://home.penglab.com/software/Hanchuan_Peng_Software/software.html`.

[120] W.D. Penny, K.E. Stephan, A. Mechelli, and K.J. Friston. Modelling functional integration: a comparison of structural equation and dynamic causal models. *Neuroimage*, 23:264274, 2004.

[121] R.A. Poldrack, J.A. Mumford, and T.E. Nichols. *Handbook of Functional MRI Data Analysis*. Cambridge University Press, 1 edition, 2011.

[122] N. Pouratian, Z. Zheng, A.A. Bari, E. Behnke, W.J. Elias, and A.A. Desalles. Multi-institutional evaluation of deep brain stimulation targeting using probabilistic connectivity-based thalamic segmentation. *J Neurosurg*, 115:995–1004, 2011.

[123] M. Raichle and M. Mintum. Brain work and brain imaging. *Annu. Rev. Neurosci*, 29:449476, 2006.

[124] M. Raichle and A.Z. Snyder. A default mode of brain function: a brief history of an evolving idea. *Neuroimage*, 37:1083–1090, 2007.

[125] Marcus E. Raichle. The Brain's Dark Energy. *Neuroscience*, 314:1249–1250, 2006.

[126] M.E. Raichle. A paradigm shift in functional brain imaging. *J Neurosci*, 29:12729 12734, 2009.

[127] M.E. Raichle, A.M. MacLeod, A.Z. Snyder, W.J. Powers, D.A. Gusnard, and G.L. Shulman. A default mode of brain function. *Proc. Natl. Acad. Sci. USA*, 98:676682, 2001.

[128] J.C. Reijneveld, S.C. Ponten, H.W. Berendse, and C.J. Stam. The application of graph theoretical analysis to complex networks in the brain. *Clin Neurophysiol*, 118:2317 2331, 2007.

[129] E Rodriguez, N George, JP Lachaux, J Martinerie, B Renault, and FJ Varela. Perception's shadow: long-distance synchronization of human brain activity. *Nature*, 397:430–433, 1999.

[130] A. Roebroeck, E. Formisano, and R. Goebel. Mapping directed influence over the brain using granger causality and fmri. *Neuroimage*, 25:230242, 2005.

[131] S.A. Rombouts, F.F. Barkhof, R. Goekoop, C.J. Stam, and P. Scheltens. Altered resting state networks in mild cognitive impairment and mild alzheimers disease: an fmri study. *Hum Brain Mapp*, 26:231239, 2005.

[132] R Rytsar, E Fornari, RS Frackowiak, JA Ghika, and MG Knyazeva. Inhibition in early alzheimer's disease: an fmri-based study of effective connectivity. *Neuroimage*, 57:1131–1139, 2011.

[133] R. Salvador, J. Suckling, M.R. Coleman, J.D. Pickard, D. Menon, and E. Bullmore. Neurophysiological architecture of

functional magnetic resonance images of human brain. *Cereb. Cortex*, 15:13321342, 2005.

[134] E.J. Sanz-Arigita, M.M. Schoonheim, J.S. Damoiseaux, S.A. Rombouts, E. Maris, F. Barkhof, P. Scheltens, C.J., and Stam. Loss of small-world networks in Alzheimers disease: graph analysis of fMRI resting-state functional connectivity. *PLoS One*, 5:e13788, 2010.

[135] JR Sato, A Fujita, EF Cardoso, CE Thomaz, MJ Brammer, and E Amaro. Analyzing the connectivity between regions of interest: An approach based on cluster granger causality for fmri data analysis. *NeuroImage*, 52:14441455, 2010.

[136] M.M. Schoonheim, J.J. Geurts, D. Landi, L. Douw, M.L. van der Meer, H. Vrenken, C.H. Polman, F. Barkhof, and C.J. Stam. Functional connectivity changes in multiple sclerosis patients: a graph analytical study of meg resting state data. *Hum Brain Mapp*, 34:52–61, 2013.

[137] T. Schreiber. Measuring information transfer. *Phys Rev Lett*, 85:461–464, 2000.

[138] C.E. Schroeder and P. Lakatos. Low-frequency neuronal oscillations as instruments of sensory selection. *Trends in neurosciences*, 32:918, 2009.

[139] J.M. Segall, E.A. Allen, R.E. Jung, E.B. Erhardt, S.K. Arja, K. Kiehl, and V.D. Calhoun. Correspondence between structure and function in the human brain at rest. *Front. Neuroinform*, 6:10, 2012.

[140] A.K. Seth, E. Izhikevich, G.N. Reeke, and G.M. Edelman. Theories and measures of consciousness: An extended framework. *Proc Natl Acad Sci USA*, 103:1079910804, 2006.

[141] D. Sharp, C. Beckmann, R. Greenwood, K. Kinnunen, V. Bonnelle, X.D. Boissezon, J. Powell, S. Counsell, M. Patel, and

R. Leech. Default mode network functional and structural connectivity after traumatic brain injury. *Brain*, 134:22332247, 2011.

[142] D.J. Sharp and R. Leech. Network dysfunction after traumatic brain injury. *Nat Rev Neurol*, 10:156166, 2014.

[143] Y.I. Sheline and M.E. Raichle. Resting state functional connectivity in preclinical alzheimers disease. *Biol Psychiatry*, 74:340347, 2013.

[144] P. Skudlarski, K. Jagannathan, V.D. Calhoun, M. Hampson, B.A. Skudlarska, and G. Pearlson. Measuring brain connectivity: diffusion tensor imaging validates resting state temporal correlations. *Neuroimage*, 43:554561, 2008.

[145] A.M. Smith, B.K. Lewis, U.E. Ruttimann, F.Q. Ye, T.M. Sinnwell, Y. Yang, J.H. Duyn, and J.A. Frank. Investigation of low frequency drift in fmri signal. *Neuroimage*, 9:526533, 1999.

[146] S.M. Smith, P.T. Fox, K.L. Miller, D.C. Glahn, P.M. Fox, C.E. Mackay, N. Filippini, K.E. Watkins, R. Toro R, A.R. Laird, and C.F. Beckmann. Correspondence of the brains functional architecture during activation and rest. *Proc Natl Acad Sci USA*, 106:13040–13045, 2009.

[147] S.M. Smith, D. Vidaurre, C.F. Beckmann, M.F. Glasser, M. Jenkinson, K.L. Miller, T.E. Nichols, E.C. Robinson, G. Salimi-Khorshidi, M.W. Woolrich, D.M. Barch, K. Ugurbil, and D.C. Van Essen. Functional connectomics from resting-state fmri. *Trends Cogn Sci*, 17:666682, 2013.

[148] T. Sorensen. A method of establishing groups of equal amplitude in plant sociology based on similarity of species and its application to analyses of the vegetation on danish commons. *Kongelige Danske Videnskabernes Selskab*, 5:1–34, 1948.

[149] O. Sporns, D.R. Chialvo, M. Kaiser, and C.C. Hilgetag. Organization, development and function of complex brain networks. *Trends. Cogn. Sci*, 8:418425, 2004.

[150] O. Sporns, G. Tononi, and G.M. Edelman. Theoretical neuroanatomy: relating anatomical and functional connectivity in graphs and cortical connection matrices. *Cereb. Cortex*, 10:127141, 2000.

[151] O. Sporns, G. Tononi, and R. Kotter. The human connectome: A structural description of the human brain. *PLoS Comput. Biol*, 1:245251, 2005.

[152] O. Sporns and J.D. Zwi. The small world of the cerebral cortex. *Neuroinformatics*, 2:145162, 2004.

[153] Olaf Sporns. *Networks of the Brain*. The Mit Press, 1 edition, 2011.

[154] C.J. Stam and J.C. Reijneveld. Graph theoretical analysis of complex networks in the brain. *Nonlinear Biomed Phys*, 1:3, 2007.

[155] E. Tagliazucchi, P. Balenzuela, D. Fraiman, and D.R. Chialvo. Criticality in large-scale brain fmri dynamics unveiled by a novel point process analysis. *Front Physiol*, 3:15, 2012.

[156] E. Tagliazucchi, R. Carhart-Harris, R. Leech, D. Nutt, and D.R. Chialvo. Enhanced repertoire of brain dynamical states during the psychedelic experience. *Hum Brain Mapp*, 35:5442–5456, 2014.

[157] M. Taubert, B. Draganski, A. Anwander, K. Mller, A. Horstmann, A. Villringer, and P. Ragert. Dynamic properties of Human Brain Structure: Learning-Related Changes in Cortical Areas and Associated Fiber Connections. *J Neurosci*, 30:35, 2010.

[158] G. Teasdale and B. Jennett. Assessment of coma and impaired consciousness: A practical scale. *Lancet*, 2:81–84, 1974.

[159] P. Tewarie, A. Hillebrand, E. van Dellen, M.M. Schoonheim, F. Barkhof, C.H. Polman, C. Beaulieu, G. Gong, B.W. van Dijk, and C.J. Stam. Structural degree predicts functional network connectivity: a multimodal resting-state fMRI and MEG study. *Neuroimage*, 110:296307, 2014.

[160] G. Tononi, O. Sporns, and G.M. Edelman. A measure for brain complexity: Relating functional segregation and integration in the nervous system. *Proc. Natl. Acad. Sci. USA*, 91:50335037, 1994.

[161] N. Tzourio-Mazoyer, B. Landeau, D. Papathanassiou, F. Crivello, O. Etard, N. Delcroix, B. Mazoyer, and M. Joliot. Automated Anatomical Labeling of activations in SPM using a Macroscopic Anatomical Parcellation of the MNI MRI single-subject brain. *Neuroimage*, 15:273–289, 2002.

[162] A. Vakhtin, V. Calhoun, R. Jung, J. Prestopnik, P. Taylor, and C. Ford. Changes in intrinsic functional brain networks following blast-induced mild traumatic brain injury. *Brain Inj*, 27:13041310, 2013.

[163] M.P. van den Heuvel and O. Sporns. An anatomical substrate for integration among functional networks in human cortex. *Neurosci*, 33:1448914500, 2013.

[164] Sthephen G. Waxman. *Clinical Neuroanatomy*. Mc Graw Hill Education, 27 edition, 2013.

[165] N.D. Woodward, B. Rogers, and S. Heckers. Functional resting-state networks are differentially affected in schizophrenia. *Schizophr Res*, b130:8693, 2011.

[166] G.R. Wu, W. Liao, S. Stramaglia, J.R. Ding, H. Chen, and D. Marinazzo. A blind deconvolution approach to recover ef-

fective connectivity brain networks from resting state fmri data. *Med Image Anal*, 17:365374, 2013.

[167] G. Zappala, M. Thiebaut De Schotten, and P.J. Eslinger. Traumatic brain injury and the frontal lobes: what can we gain with diffusion tensor imaging? *Cortex*, 48:156e165, 2012.

[168] D. Zhang and M.E. Raichle. Disease and the brains dark energy. *Nat Rev. Neurol*, 6:15–28, 2010.

[169] Z. Zhou, Y. Chen, M. Ding, P. Wright, Z. Lu, and Y Liu. Analyzing brain networks with pca and conditional granger causality. *Hum Brain Mapp*, 30:21972206, 2009.

[170] X.-N. Zuo, A. Di Martino, C. Kelly, Z.E. Shehzad, D.G. Gee, D.F. Klein, F.X. Castellanos, B.B. Biswal, and M.P. Milham. The oscillating brain: complex and reliable. *Neuroimage*, 49:14321445, 2010.

List of Figures

List of publications

First author contributions

- **I. Diez***, P. Bonifazi*, I. Escudero, B. Mateos, M. A. Muoz, S. Stramaglia, J.M. Cortes (*Equal contribution). *A novel brain partition highlights the modular skeleton shared by structure and function.* Nature Scientific Report 5: 10532, 2015. IF: 5.578 Q1(Multidisciplinary Sciences): 5/56. Reference [45]

- **I. Diez***, A. Erramuzpe*, I. Escudero, B. Mateos, A. Cabrera, D. Marinazzo, EJ Sanz-Arigita, S. Stramaglia, J.M. Cortes (*Equal contribution). *Information flow between resting state networks.* Brain Connectivity, 2015. No IF yet (creation of journal in 2011). Reference [46]

- V. Maki-Marttunen*, **I. Diez***, J.M. Cortes, D.R. Chialvo, M. Villarreal (*Equal contribution). *Disruption of transfer entropy and inter-hemispheric brain functional connectivity in patients with disorder of consciousness* . Frontiers in Neuroinformatics 7: 24, 2013. IF: 3.261 Q1(Mathematical & computational biology): 7/56. Reference: [97]

Other JCR articles

- C. Alonso-Montes, **I. Diez**, L. Remaki, I. Escudero, B. Mateos, Y. Rosseel, D. Marianazzo, S. Stramaglia, J.M. Cortes. *Lagged and instantaneous dynamical influences related to brain structural connectivity.* Frontiers in Psychology, 2015. IF: 2.56

Q1(Psychology, multidisciplinary): 23/129. Reference [3].

- T.A. Amor, R. Russo, **I. Diez**, P. Mudnal, M. Zirovich, S. Stramaglia, J.M. Cortes, L. de Arcangelism, D.R. Chialvo. *Extreme brain events: Higher order statistics of brain resting activity and its relation with structural connectivity.* To appear in EPL, 2015. IF: 2.095 Q2(Physics, multidisciplinary): 20/78.

Other articles in review

- **I. Diez**, D. Drijkoningen, S. Stramaglia, P. Bonifazi, D. Marinazzo, S.P. Swinnen*, J.M. Cortes* (*Equal last-author contribution). *Reorganization in both structural and functional networks in young patients after traumatic axonal injury.* In review, 2015.

- J.M. Kroos, **I. Diez**, J.M. Cortes, S. Stramaglia, L. Gerardo Giorda. *Geometry shapes propagation: assessing the presence and absence of cortical symmetries through a computational model of cortical spreading depression.* In review, 2015.

In preparation

- **I. Diez**, I. Escudero, B. Mateos, S. Stramaglia, D. Marinazzo, J.M. Cortes . *New evidence for the default mode network having the highest contribution in integrating the large-scale brain functioning.*

- C. Alonso-Montes, **I. Diez**, L. Remaki,J.M. Cortes, S. Stramaglia. *Fractional anisotropy analysis across severity progression in Alzheimer's disease.*

Media Dissemination

2013

- El Pais - Un diagnóstico certero para el coma
- El Mundo Digital - Una investigación cuantifica por técnicas de Neuroimagen los daos en la función cerebral de trastornos de consciencia
- Telecinco - Una investigación cuantifica por técnicas de Neuroimagen los daos en la función cerebral de trastornos de consciencia
- EuropaPress - Una investigación cuantifica por técnicas de Neuroimagen los daos en la función cerebral de trastornos de consciencia
- 20Minutos - Una investigación cuantifica por técnicas de Neuroimagen los daos en la función cerebral de trastornos de consciencia
- El Economista- Una investigación cuantifica por técnicas de Neuroimagen los daos en la función cerebral de trastornos de consciencia
- Diario Medico - Miden la conectividad cerebral en el momento de despertar del coma

- Basque Research. Elhuyar Fundazioa ES - Cuantifican por técnicas de neuroimagen los daos cerebrales de trastornos de consciencia

- Basque Research. Elhuyar Fundazioa EN - Neuroimaging methods used to show disturbances of brain function in DOC patients

- Basque Research. Elhuyar Fundazioa EU - Neuroirudi-tekniken bidez kuantifikatu dituzte kontzientzia-asaldurak dituztenen kalte zerebralak

- Ikerbasque ES - Cuantifican por técnicas de neuroimagen los daos cerebrales de trastornos de consciencia

- Ikerbasque EN - Neuroimaging methods used to show disturbances of brain function in DOC patients

- Ikerbasque EU - Neuroirudiko tekniken bidez kontzientzia gaitzen garun-kaltea neurtu dute

- LaInformacion.com - Una investigación cuantifica por técnicas de Neuroimagen los daos en la función cerebral de trastornos de consciencia

- La Voz Libre - Una investigación cuantifica por técnicas de Neuroimagen los daos en la función cerebral de trastornos de consciencia

- Atencion Primaria de Salud - Miden la conectividad cerebral en el momento de despertar del coma

- Madrid + d - Un diagnóstico certero para el coma

- El Medico Interactivo - Una investigación con participación espaola descubre el aumento de la actividad cerebral tras salir del coma

- Portales Medicos - Una investigación consigue cuantificar por técnicas de neuroimagen los daos en la función cerebral de los trastornos de consciencia por TCE

2015

- Elmundo.es - Investigadores vascos publican en 'Nature' un inédito 'atlas cerebral'
- abc.es - Biocruces elabora un nuevo atlas del cerebro para estudiar sus patologías
- abc salud - Dibujan un nuevo atlas del cerebro clave para estudiar el alzhéimer o el párkinson.
- Deia - BioCruces crea un atlas del cerebro para estudiar el Alzheimer o el Parkinson
- El correo - Biocruces elabora un nuevo atlas del cerebro para estudiar sus patologías
- Cadena ser - Biocruces abre nuevas vías de estudio de patologías neurológicas
- Infosalus.com - BioCruces crea un atlas del cerebro que abre alternativas para estudiar patologías como Alzheimer o Parkinson
- euskadiactual.com - Un nuevo atlas del cerebro abre vías alternativas para estudiar sus patologías
- Redaccion médica - Un atlas cerebral de Biocruces abre nuevas alternativas para el alzheimer y el párkinson
- Actasanitaria.com - El Instituto BioCruces crea un atlas del cerebro con un patrón funcional y estructural común
- parkinsonsnewstoday.com - New 'Brain Atlas' To Focus On InterRelationship Between Anatomy And Physiology

- psypost.org - A new atlas of the brain opens up alternative means for studying brain disorders
- Sciencedaily.com - New atlas of the brain opens up alternative means for studying brain disorders
- berria - Eritasunak garaiz atzemateko bidean, garuneko atlas bat lagun
- Radio Euskadi. La mecánica del caracol: http://www.eitb.tv/es/radio/radio-euskadi/la-mecanica-del-caracol/2514856/3344754/atlas-del-cerebro-y-congreso-sobre-aislantes-topologicos/
- Radio Onda Vasca. http://www.ondavasca.com/2015/07/09/un-equipo-del-instituto-de-investigacion-sanitaria-biocruces-descubre-un-nuevo-atlas-del-cerebro/
- Radio Euskadi. Boulevard. http://www.eitb.eus/es/radio/radio-euskadi/ programas/boulevard/audios/detalle/3361714/cerebro-humanoradio-euskadi/